Petrology, geochemistry and geochronology of mafic lithologies at the Olympic Dam iron oxide Cu-U-Au-Ag deposit: implications for tectonic settings and ore-forming processes

By

Qiuyue Huang

(BSc. Peking University, 2012)

UNIVERSITY OF TASMANIA

CODES

ARC CENTRE OF EXCELLENCE IN ORE DEPOSITS

Submitted in fulfilment of the requirements for the Degree of
Doctor of Philosophy (Geology)

University of Tasmania

June, 2016

Declarations

This thesis contains no material which has been accepted for a degree or diploma by the University or any other institution, except by way of background information and duly acknowledged in the thesis, and to the best of my knowledge and belief no material previously published or written by another person except where due acknowledgement is made in the text of the thesis, nor does the thesis contain any material that infringes copyright.

The publisher *Precambrian Research* of the two papers comprising Chapter 3 and 4 holds the copyright for that content, and access to the material should be sought from the respective journal. The remaining non-published contents of the thesis may be made available for loan and limited copying and communication in accordance with the Copyright Act 1968.

Qiuyue Huang

University of Tasmania

June, 2016

Statement of Co-authorship

The following people and institutions contributed to the publication of work undertaken as part of this thesis:

Qiuyue Huang, University of Tasmania = Ph.D. candidate

Vadim S. Kamenetsky, University of Tasmania = Author 1

Jocelyn McPhie, University of Tasmania = Author 2

Kathy Ehrig, BHP Billiton = Author 3

Sebastien Meffre, University of Tasmania = Author 4

Roland Maas, University of Melbourne = Author 5

Jay Thompson, University of Tasmania = Author 6

Maya Kamenetsky, University of Tasmania = Author 7

Isabelle Chambefort, GNS Science, Wairakei Research Centre = Author 8

Olga Apukhtina, University of Tasmania = Author 9

Yongbin Hu, Guangzhou Institute of Geochemistry = Author 10

Published Paper 1, Neoproterozoic (ca. 820-830 Ma) mafic dykes at Olympic Dam, South Australia: Links with the Gairdner Large Igneous Province.

Located in Chapter 3.

Candidate was the primary author. Author 1, author 2 and author 3 contributed to the idea, its formalisation and development. Author 4 to 8 assisted with refinement and presentation. Author 9 and author 10 offered general laboratory assistance. A percentage estimate of the contribution made by each author can be seen in Appendix 1.

The following people and institutions contributed to the publication of work undertaken as part of this thesis:

Qiuyue Huang, University of Tasmania = Ph.D. candidate

Vadim S. Kamenetsky, University of Tasmania = Author 1

Kathy Ehrig, BHP Billiton = Author 2

Jocelyn McPhie, University of Tasmania = Author 3

Maya Kamenetsky, University of Tasmania = Author 4

Ken Cross, Terramin Australia Ltd = Author 5

Sebastien Meffre, University of Tasmania = Author 6

Andrea Agangi, Curtin University of Technology = Author 7

Isabelle Chambefort, GNS Science, Wairakei Research Centre = Author 8

Nicholas G. Direen, University of Tasmania = Author 9

Roland Maas, University of Melbourne = Author 10

Olga Apukhtina, University of Tasmania = Author 11

Published Paper 2, Olivine-phyric basalt in the Mesoproterozoic Gawler silicic large igneous province, South Australia: Examples at the Olympic Dam Iron Oxide Cu–U–Au–Ag deposit and other localities.

Located in Chapter4.

Candidate was the primary author. Author 1, author 2 and author 3 contributed to the idea, its formalisation and development. Author 4 to 9 assisted with refinement and presentation. Author 10 and 11 offered general laboratory assistance. A percentage estimate of the contribution made by each author can be seen in Appendix 1.

We the undersigned agree with the above stated "proportion of work undertaken" for each of the above published (or submitted) peer-reviewed manuscripts contributing to this thesis:

Signed:

Prof. Vadim (Dima) Kamenetsky

Primary Supervisor

School of Physical Sciences

University of Tasmania

Prof. John Dickey

Head of School

School of Physical Sciences

University of Tasmania

Date: June, 2016

Abstract

The Olympic Dam deposit, South Australia, is a supergiant iron oxide Cu-U-Au-Ag deposit currently containing the world's largest uranium, fifth largest copper, and third largest gold resource (10,100 Mt at 0.78% Cu, 0.25 kg/t U_3O_8, 0.30 g/t Au, 1 g/t Ag, BHP Billiton 2015 Annual Report). The exploration model leading to the discovery of the deposit in 1975 was source-oriented: altered mafic lithologies were considered as the potential source of copper and early exploration focused on defining and searching for these lithologies. Not surprisingly, drilling and underground mining at Olympic Dam have revealed the occurrence of more than one generation of mafic lithologies. Previous studies have considered these mafic lithologies to be closely related to brecciation, hydrothermal circulation (by providing heat), and mineralization at Olympic Dam. One suite of mafic rocks, inferred to belong to the ca. 1590 Ma Gawler Range Volcanics (GRV), has been proposed to be a major source of Cu (~50% of the contained Cu) found in the deposit.

However, at over forty years since discovery of the deposit, questions remain as to which groups the various mafic lithologies at Olympic Dam belong to regionally, as to what kinds of tectonic settings there were when the mafic lithologies were emplaced, and as to how the emplacement and alteration of the mafic lithologies were related to the ore-forming processes at Olympic Dam.

This study endeavours to provide answers to these issues. The presence of two generations of mafic lithologies at Olympic Dam has been confirmed by primary accessory apatite U-Pb dating. The first group is found to be correlated with the ca. 1590 Ma Gawler Range Volcanics and the Gawler silicic large igneous province (SLIP), consisting of intensely altered olivine-phyric basalt, and other mafic dykes of various textures (aphanitic, porphyritic, and doleritic). The second group comprises basaltic to mainly doleritic dykes (named the Olympic Dam dolerite), proved to belong to the ca. 820 Ma Gairdner Dyke Swarm and the Gairdner large igneous province (LIP).

The ca. 1590 Ma olivine-phyric basalt at Olympic Dam typically contains a higher abundance of former olivine phenocrysts (~20 vol.%) and is more intensely altered than

equivalent mafic GRV outside the deposit at Kokatha, Mount Gunson and Wirrda Well. Therefore, this suite of basalt represents the most ultramafic component in the GRV recognized thus far. Compositions of a large number of Cr-spinel inclusions within olivine pseudomorphs and olivine-phyric basalt samples of mafic GRV (including Olympic Dam samples) reveal different magma types and indicate derivation of mafic GRV from a heterogeneous mantle source that may have been modified by subduction, implying a setting proximally to a continental margin or in a back-arc. This inference is also compatible with the previous proposal that the formation of the Gawler SLIP was associated with the assembly of the Laurentian supercontinent. The ca. 820 Ma Olympic Dam dolerite shows similar petrographic features and comparable compositional variations to the regional Gairdner Dyke Swarm. The correlation of the Olympic Dam dolerite with the Gairdner Dyke Swarm thus extends the spatial distribution and the compositional spectrum of the latter. Geochemical comparisons among LIP and mafic suites in South Australia (including the Gairdner Dyke Swarm), South China and North America, associated with the break-up of the supercontinent Rodinia are in support of the "missing-link" model in which South China was situated on top of a mantle plume and South Australia (including Olympic Dam) was affected by the plume-induced rift magmatism at ca. 820 Ma. In conclusion, from the perspective of mafic magmatism, the evolution of the supergiant Olympic Dam deposit turned out to be linked to two supercontinent cycles: the assembly of Laurentia at ca. 1590 Ma, and the break-up of Rodinia at ca. 820 Ma.

Investigations of the alteration of the two generations of mafic lithologies at Olympic Dam have shown that they contain similar major secondary minerals (chlorite, sericite, and carbonate). Both are characterized by a mineral assemblage of magnetite-apatite ± chlorite ± quartz that is strikingly similar to the inferred early reduced iron oxide alteration present in the periphery and at depth of the Olympic Dam Breccia Complex that is the immediate host to ore. Secondary spongy apatite in the ca. 1590 Ma olivine-phyric basalt yielded an age that is broadly coeval with the basalt's emplacement. Sericite-altered basalt produced a post-primary Rb-Sr isochron age of ca. 1180 Ma, likely to indicate the most recent significant sericite alteration of these rocks. Extreme concentrations of some components (e.g. up to 26 wt.% CO_2, 50 wt.% of Fe_2O_3, and 6,000ppm of Cr) and extraordinary near linear positive correlations between Cr and

high field strength elements (e.g. Ti, Nb, and Zr) revealed in drill core assays of the basalt indicate significant whole-rock mass and/or volume loss due to hydrothermal alteration, in accordance with its previously proposed role as a major Cu source. Results obtained on the secondary apatite and titanite in the ca. 820 Ma Olympic Dam dolerite also confirmed hydrothermal activities associated with the emplacement of the younger dolerite. Pb isotope compositions of the dolerite as well as chalcopyrite and galena within the dolerite indicate derivation of radiogenic Pb from hydrothermal fluids circulating through the Olympic Dam Breccia Complex, implying that the dolerite was a part of the active hydrothermal system at Olympic Dam at ca. 820 Ma. Elevated Zn, Pb and depleted Cu concentrations of the ca. 820 Ma Olympic Dam dolerite compared to dolerite worldwide suggest that the dolerite can even be an additional Cu source to the Olympic Dam deposit. Moreover, the younger and less altered dolerite provides a better opportunity to envisage Cu depletion processes that may also be anticipated for the older olivine-phyric basalt, where such processes are no longer recognizable due to superimposition of multiple hydrothermal events on the basalt. At last and most importantly, magmatic-hydrothermal activities (ca. 1590 Ma, 1180 Ma, 820 Ma) recorded in both generations of mafic rocks can be correlated with ages (spanning from ca. 1590 Ma to 570 Ma) obtained on the Olympic Dam Breccia Complex. This advocates the existence of an all-encompassing, multi-stage, hydrothermal system at the supergiant Olympic Dam deposit.

Acknowledgments

This work was funded by BHP Billiton and the Australian Research Council. The author is indebted to his primary supervisor Prof. Dima Kamenetsky for providing him new ideas and different thinking now and then, for always being ready to read whatever he wrote, and for invaluable technical and intellectual support for all kinds of analyses. The author is grateful to his secondary supervisor, Prof. Jocelyn McPhie, who provided support for field work and carefully reviewed every manuscript contained in the thesis. Dr Kathy Ehrig helped with sample collection, preparation and analyses, kindly allowed use of drill core assays, and was always keen to review every manuscript. Olga Apukhtina and Dr Maya Kamenetsky provided help for a large number of analyses. Dr Karsten Goemann, Dr Sandrin Feig, Dr Sarah Gilbert, Dr Paul Olin, Katie McGoldrick have offered analytical assistance. Ben Cave, Teena Rusak and Stacey McAvaney introduced the SARIG database to the author. Dr Weidong Sun, Dr Mingxing Ling, Dr Yongbin Hu and Dr Hongzuo Wang helped with isotope analyses and were acknowledged here. The author benefited from discussions with Dr Sebastien Meffre, Dr Roland Maas, Jay Thompson, Dr Isabelle Chambefort, Dr Andrea Agangi, Dr Ken Cross, Dr Nicholas G. Direen. Finally, to my parents, who supported me immeasurably throughout my study.

Table of Contents

List of Figures

List of Tables

Chapter 1 Introduction

The Olympic Dam iron oxide Cu-U-Au-Ag deposit, South Australia, contains the world's largest uranium, fifth largest copper and third largest gold resource (10,100 Mt at 0.78% Cu, 0.25 kg/t U_3O_8, 0.30 g/t Au, 1 g/t Ag, BHP Billiton 2015 Annual Report). It was discovered by Western Mining Corporation in 1975 based on a sediment-hosted copper deposit model developed in Haynes (1972). This is a source-oriented model, in which altered mafic lithologies were considered the ultimate source of copper and sedimentary sequences on top of altered mafic lithologies were regarded as potential targets. In the early exploration of Olympic Dam, the copper depletion signature of one suite of Proterozoic basalt (i.e. Roopena Volcanics) in South Australia drew immediate attention to the Stuart Shelf which contains flat-lying upper Proterozoic sediments (Haynes, 2006). Geophysical investigation of the Stuart Shelf defined five geophysical (gravity and aeromagnetic) anomalies of interest, including the anomaly at Olympic Dam which had the shallowest interpreted depth to source (Haynes, 2006). Therefore, the anomaly at Olympic Dam was programmed for testing and the Stuart Shelf therein was drilled, but no mineralization was found. However, in the Gawler Craton basement beneath the Stuart Shelf, copper sulfides were discovered, in what is later referred to as the Olympic Dam Breccia Complex (ODBC) (Reeve et al., 1990). The ODBC occurs at the intersections of a number of fault sets and is the immediate host to the Olympic Dam deposit (Reeve et al., 1990; Ehrig et al., 2012). This complex is hosted within the Roxby Downs Granite, part of the ca. 1590 Ma Hiltaba Suite (Creaser, 1989).

Despite the success of the exploration model, no mafic lithologies were recognized during the discovery stage, even though mafic rocks occurred in RD6 (5^{th} drill hole at Olympic Dam). More mafic lithologies have been intersected by subsequent drilling. Two generations of mafic lithologies were considered to be present (Reeve et al., 1990; Ehrig et al., 2012): the first group was correlated with the ca. 1590 Ma Gawler Range Volcanics, consisting of intensely altered olivine-phyric basalt, and other mafic dykes of various textures (aphanitic, porphyritic, and doleritic); the second group comprises basaltic to mainly doleritic dykes (named OD dolerite), probably belonging to the ca. 820 Ma Gairdner Dyke Swarm.

1.1 Key research question one: tectonic evolution of the Olympic Dam deposit through time

The Olympic Dam deposit is the archetype of the iron oxide Cu and Au (IOCG)-type deposit (Hitzman et al., 1992; Groves et al., 2010). A key research question for this thesis is: what was the tectonic setting when the Olympic Dam deposit initiated to form? How did the tectonic setting of the Olympic Dam deposit evolve through time?

Mafic lithologies produced in different tectonic settings tend to show different compositional characteristics. Therefore, compositions (combined with distribution and volume) of mafic lithologies have been used for recognition of paleo-tectonic settings (Pearce, 1996). At Olympic Dam, the two generation of mafic lithologies may be correlated with the ca.1590 Ma Gawler silicic large igneous province, and the ca. 820 Ma Gairdner large igneous province, respectively.

Large igneous provinces (LIP) consist of voluminous lavas (>0.1 Mkm^3), sills and dyke swarms which are emplaced in short duration (>75% of the total volume of igneous rocks in ca. 1 to 5 Myr); the maximum lifespan duration is ca. 50 Myr (Coffin and Eldholm, 1994; Bryan and Ernst, 2008). Most LIP are mafic-dominated, consisting of flood basalt lavas, dyke swarms and layered intrusions (Bryan and Ferrari, 2013), composed of mantle-derived magmas. However, a wider range of magma compositions from basaltic to rhyolitic may be present in LIP, and silicic large igneous provinces (SLIP) have been defined, where silicic igneous rocks (>65 wt.% SiO_2) predominate (Bryan et al., 2002).

The formation of the ca. 1590 Ma Gawler SLIP (Allen et al., 2008), consisting of the Gawler Range Volcanics (GRV) and the Hiltaba Suite (HS), in South Australia, was probably associated with the assembly of the Laurentian supercontinent (Blissett et al., 1993; Creaser, 1995; Allen and McPhie, 2002; Payne et al., 2009). However, rare exposures of mafic units in the Gawler SLIP and the generally evolved character (clinopyroxene-plagioclase-phyric) of these units have hampered follow-up research into the petrogenesis (importantly, characteristics of mantle source) and any implications for the tectonic setting of the overlying crust at ca. 1590 Ma.

The ca. 820 Ma Gairdner LIP mainly consists of northwest-striking mafic dykes, including dominantly the Gairdner Dyke Swarm in the Gawler Craton, the Amata Dyke Swarm in the Musgrave Block and scattered dykes in Western Australia; the Wooltana Volcanics and Little Broken Hill Gabbro are additional components (Zhao et al., 1994; Claoue-Long and Hoatson, 2009). Igneous units generated during continental break-up may be separated and may exist as separate LIP on different continents (e.g. ca. 180 Ma Karoo LIP in Africa and Ferrar LIP in Antarctica, ca. 130 Ma Parana LIP in South America and Etendeka LIP in Africa, all associated with the break-up of Gondwana) (Veevers, 2004). The ca. 820 Ma Gairdner LIP (Australia), the ca. 820 Ma Guibei LIP and the ca. 780 Ma Kangding LIP (South China), and the ca. 780 Ma Gunbarrel mafic suite (North America) are thought to be associated with the break-up of the supercontinent Rodinia (Li et al., 2008).

Petrological, geochemical and geochronological investigations of the two generations of mafic lithologies, i.e. olivine-phyric basalt and basaltic to doleritic dykes, intersected by drilling at Olympic Dam, can help to 1) confirm their correlations with corresponding LIP, if at all, 2) to investigate the petrogenesis and tectonic settings of both generations of mafic lithologies, and further, 3) to provide constraints on the tectonic evolution of the deposit.

1.2 Key research question two: assessment of the link between the alteration of mafic lithologies and the ore-forming processes at Olympic Dam

Mafic lithologies, in particular, the inferred ca. 1590 Ma GRV at Olympic Dam have been considered to be closely related to the brecciation, hydrothermal circulation (by providing heat), and mineralization (Reeve et al., 1990; Johnson and Cross, 1995; Johnson and McCulloch, 1995; Ehrig et al., 2012). Moreover, geochronological results obtained on uraninite, iron oxides, and sulfides in the ODBC by previous studies (Trueman, 1986; Johnson, 1993; McInnes et al., 2008; Maas et al., 2011; Ciobanu et al., 2013) suggest that the Roxby Downs Granite, the ODBC and the mafic lithologies may have interacted with various hydrothermal fluids repeatedly over a period of hundreds of million years. The effects of alteration on the Roxby Downs Granite and ODBC have been characterized in Ehrig et al. (2012), and the elements that have been

added to the deposit from the granite versus those derived from the hydrothermal system have been determined.

Drill core assays and whole-rock analyses of both generations of mafic lithologies at Olympic Dam, combined with petrography, would allow us to conduct a detailed study of the invariably altered mafic lithologies and to assess how closely they are related to the ore-forming processes at the Olympic Dam deposit, if at all.

1.3 Thesis structure

This study has been written in a form of paper-based thesis. Chapter 2 (Literature review) provides the regional geological background of the Gawler Craton and local geology of the Olympic Dam deposit and other adjacent IOCG prospects and deposits. The younger Olympic Dam dolerite (basaltic to doleritic dykes) is characterized by its generally fresher appearance and better competency, as well as higher magnetic susceptibility, compared to other mafic facies. Therefore, Chapter 3 first focuses on describing the occurrence of these younger dykes and discussing the implications for petrogenesis and tectonic setting. Chapter 3 has been published in *Precambrian Research*. This chapter is re-formatted from the original published version to conform to thesis requirements. Chapter 4 reports the intensely altered older (ca. 1590 Ma) olivine-phyric basalt at Olympic Dam and compares it with other olivine-phyric rocks in the Gawler SLIP. Chapter 4 has been published in *Precambrian Research*. Chapter 5 is a detailed study of the alterations of both generations of mafic lithologies. Chapter 6 is a synthesis of the results of this study.

Chapter 2 Geology and literature review

2.1 Regional geology of the Gawler Craton

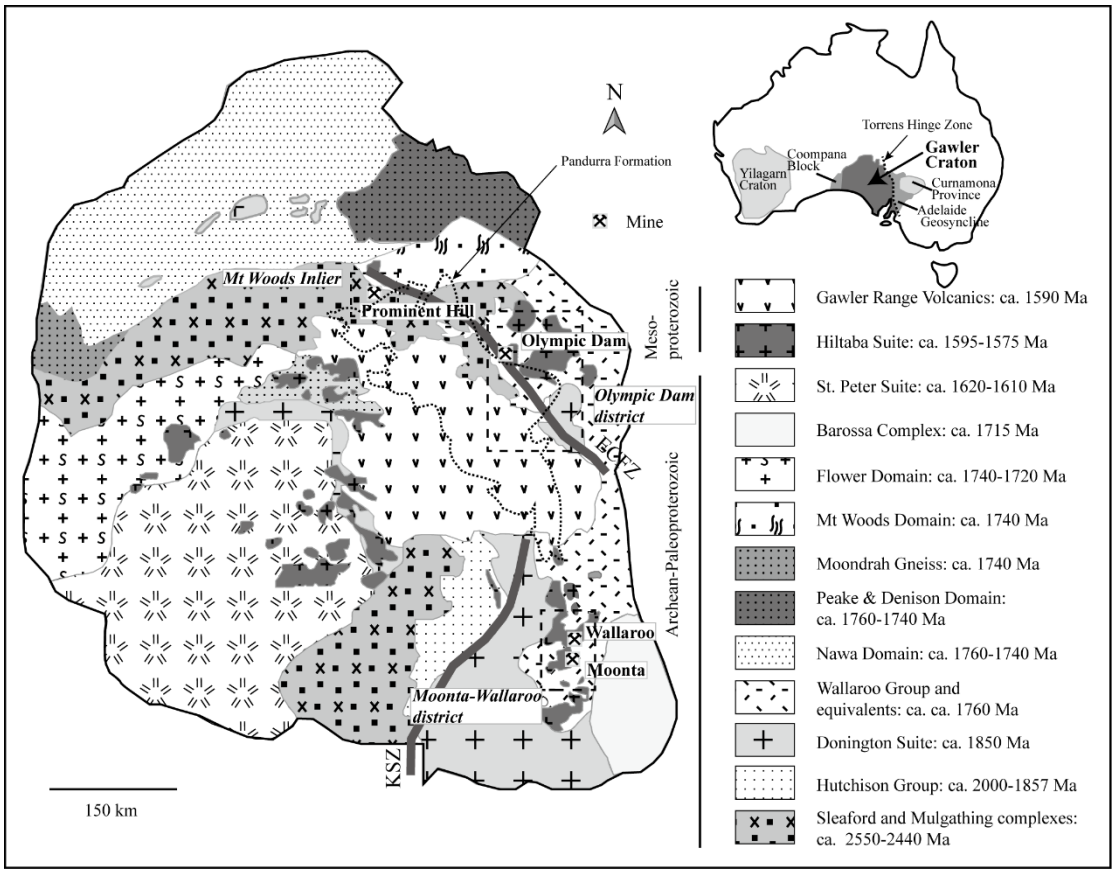

Figure 2.1 Interpreted crystalline basement geology of the Gawler Craton, South Australia, showing the location of major mineral deposits and prospects (simplified after Hand et al., 2007). KSZ, Kalinjala Shear Zone; ECFZ, Elizabeth Creek Fault Zone.

The Gawler Craton covers approximately 440,000 square kilometres of central South Australia. Its Precambrian crystalline basement (crust) was cratonised at ca. 1550-1450 Ma. Prior to 1550 Ma, the craton comprised a number of active Proterozoic orogenic belts extending back to at least 2450 Ma.

A major NS-trending structural feature, the Torrens Hinge Zone, forms both the eastern and north-eastern margin of the Gawler Craton, and the boundary between the Stuart Shelf and the Adelaide Geosyncline. The Gawler Craton records several cycles of magmatism, sedimentation, and orogenesis in its protracted evolution from the Meso-Archean to Mesoproterozoic. A brief introduction is presented here and further

details can be found in Drexel et al. (1993), Hand et al. (2007) and Reid and Hand (2012).

Late Archean rocks form a geographic nucleus of the Gawler Craton and have been divided into to the Sleaford Complex in the southern Gawler Craton and the Mulgathing Complex in the central-western part of the craton (Fig. 2.1, Hand et al., 2007). Geochemical, isotopic, and geochronological data suggests the Mulgathing and Sleaford complexes share a common history and are likely to represent portions of a single Late Archean belt (Swain et al., 2005; Fraser et al., 2010). These late Archean rocks of the Gawler Craton are dominated by (meta)sedimentary sequences including aluminous metasediment units interlayered with banded iron formation, carbonates, and siliceous rocks, and broadly coeval felsic and mafic-ultramafic volcanics, including komatiites which were deposited or erupted in the interval ca. 2560 to 2500 Ma (Hand et al., 2007). The Sleaford Complex is composed of banded iron formations, paragneiss and orthogneiss of the Carnot Gneiss, granulites, amphibolite facies paragneiss of the Wangary Gneiss, and weakly deformed granites of the Dutton Suite (Daly et al., 1998).

The Hutchison Group formed the largest basin sequence in the eastern Gawler Craton (Fig. 2.1) and was deposited after ca. 2000 Ma and most likely before ca. 1845 Ma on a passive margin to the east of the Archean core (Parker and Lemon, 1982; Hand et al., 2007). The basal sequence comprises quartzite and massive dolomite, which is overlain by the economically significant Middleback Subgroup consisting of carbonates, interlayered pelitic units, and iron ore-hosting formations (Parker and Lemon, 1982; Yeates, 1990). The upper part of the Hutchison Group consists of pelitic rock types and felsic volcanic and volcaniclastic units of the 1866 ± 10 Ma Bosanquet Formation (Fanning et al., 2007).

Voluminous syn-tectonic granitoids of the Donington Suite were emplaced between 1850 ± 3.5 and 1860 ± 4 Ma in the eastern Gawler Craton (Fig. 2.1) (Jagodzinski, 2005; Reid et al., 2008). Red K-feldspar-bearing arkosic metasedimentary rocks (Wandearah Formation?) were largely derived from and overlie, the Donington Suite in the Olympic Dam district (Jagodzinski, 2005). The Elizabeth Creek Fault Zone and Kalinjala Shear Zone are understood to be the boundaries

between the Archean nucleus to the west and Proterozoic sequences to the east (Direen and Lyons, 2007; Hayward and Skirrow, 2010).

The Wallaroo Group was deposited during the period ca. 1765 to 1740 Ma over much of the eastern margin of the Gawler Craton (Cowley et al., 2003) and is an important host sequence for several IOCG prospects (Fig. 2.1). The arkoses (Wandearah Formation?) noted above may form a lower unit of this group whereas the upper parts of the Wallaroo Group comprise thin–bedded feldspathic to biotite-rich or carbonaceous metasiltstones, metacarbonate rocks, metavolcanic rocks of greenschist to amphibolite facies, and minor banded iron formation (BIF). These rocks were deformed during the ca. 1740 Ma to 1700 Ma Kimban Orogeny (Daly et al., 1998; Dutch et al., 2008). The northern and western Gawler Craton (Nawa Domain, Fig. 2.1) contains poorly exposed Paleoproterozoic metasedimentary units including pelite, iron formations, and carbonates (Direen et al., 2005; Payne et al., 2006; Hand et al., 2008; Thomas et al., 2008). Granitoids of the St. Peter Suite in the southwestern Gawler Craton were emplaced at ca. 1620 Ma, and this suite has been interpreted to have formed in a magmatic arc setting (Swain et al., 2008; Symington et al., 2014).

The Gawler Range Volcanics (GRV)-Hiltaba Suite (HS) are a record of an intracontinental, Mesoproterozoic, dominantly silicic volcanic province (Fig. 2.1, Gawler silicic large igneous province, Gawler SLIP) that was generated during the Laurentian supercontinent assembly (Blissett et al., 1993; Creaser, 1995; Allen and McPhie, 2002). This event was associated with a major thermal and metallogenic episode that affected much of the Gawler Craton (Daly et al., 1998; Skirrow et al., 2002; Hand et al., 2007; Skirrow et al., 2007). According to Blissett et al. (1993) and Allen et al. (2003), the GRV have a maximum preserved thickness of ~1.5 km and are exposed over more than 25,000 km^2 across the central Gawler Craton. The GRV are a felsic-dominated bimodal sequence, with lower GRV consisting of variable assemblages ranging in composition from basalt and andesite to dacite, rhyodacite and rhyolite with a variable silica gap between the tholeiitic basalt-andesite series and the felsic series, and upper GRV represented by flat-lying sheets of massive porphyritic dacite and rhyodacite which are very extensive in the central portion of the province (Blissett et al., 1993). The most precise age for the GRV is 1591 ± 3 Ma, from the central Gawler Craton (Fanning et al., 1988). In the Olympic Dam district, the only published U-Pb

zircon determination for the GRV is 1591 ± 10 Ma from the Wirrda Well prospect (Creaser and Cooper, 1993). The HS comprises granite, granodiorite, quartz monzonite, quartz syenite, and quartz monzodiorite plutons (Drexel et al., 1993). In places, the HS plutons intrude the extensive GRV. It is widespread throughout the central and eastern Gawler Craton, and members of the suite have zircon U-Pb ages ranging from ca. 1575 to ca. 1600 Ma (Fanning et al., 1988; Mortimer et al., 1988; Creaser and Cooper, 1993; Johnson and Cross, 1995; Jagodzinski, 2005). In the Olympic Dam district, members of the HS form a plutonic complex which is here informally termed the Burgoyne Batholith. The Burgoyne Batholith consists of at least two granitoids sub-suites, the White Dam (the eastern part) and Wirrda suites (the western part), which are distinguishable by their mineralogy and composition (Creaser, 1989). The Roxby Downs Granite, a member of the Wirrda suite, hosts the Olympic Dam deposit (Reeve et al., 1990). Where unaltered, the Roxby Down Granite is a pink-red, medium- to coarse-grained, quartz-poor syenogranite (Reeve et al., 1990).

Three districts of iron oxide-rich alteration and Cu-Au ± U ± REE mineralization are recognized in the eastern Gawler Craton: the Mount Woods Inlier, which hosts the Prominent Hill IOCG deposit (Belperio et al., 2007), the Olympic Dam district, including the recently discovered Carrapateena deposit, and the Moonta-Wallaroo historic mining district (Fig. 2.1). These districts form a >500-km-long IOCG metallogenic belt, termed the Olympic Cu-Au-(U) Province (Skirrow et al., 2002). The Olympic Dam deposit is located in the Stuart Shelf region of South Australia. The deposit is on the eastern margin of the Gawler Craton, and unconformably overlain by ~300 m of Adelaidean (Neoproterozoic) to Cambrian age, horizontal sedimentary rocks (Wilpena Group).

Paleoproterozoic basement and early Mesoproterozoic igneous rocks were unconformably overlain by the Mesoproterozoic Pandurra Formation (Fig. 2.1) in much of the eastern Gawler Craton. The Pandurra Formation consists of quartzose and quartzo-feldspathic fluviatile sandstones with minor shale bands (Mason et al., 1978), in the Cariewerloo Basin with a possible depositional age of ca. 1450 Ma to 1424 Ma (Cowley, 1993; Keeling, 2015). The Pandurra Formation is unconformably overlain by the mafic Beda Volcanics (occurring only at the eastern margin of the Gawler Range Craton), which are possibly extrusive equivalents of the Gairdner Dyke Swarm.

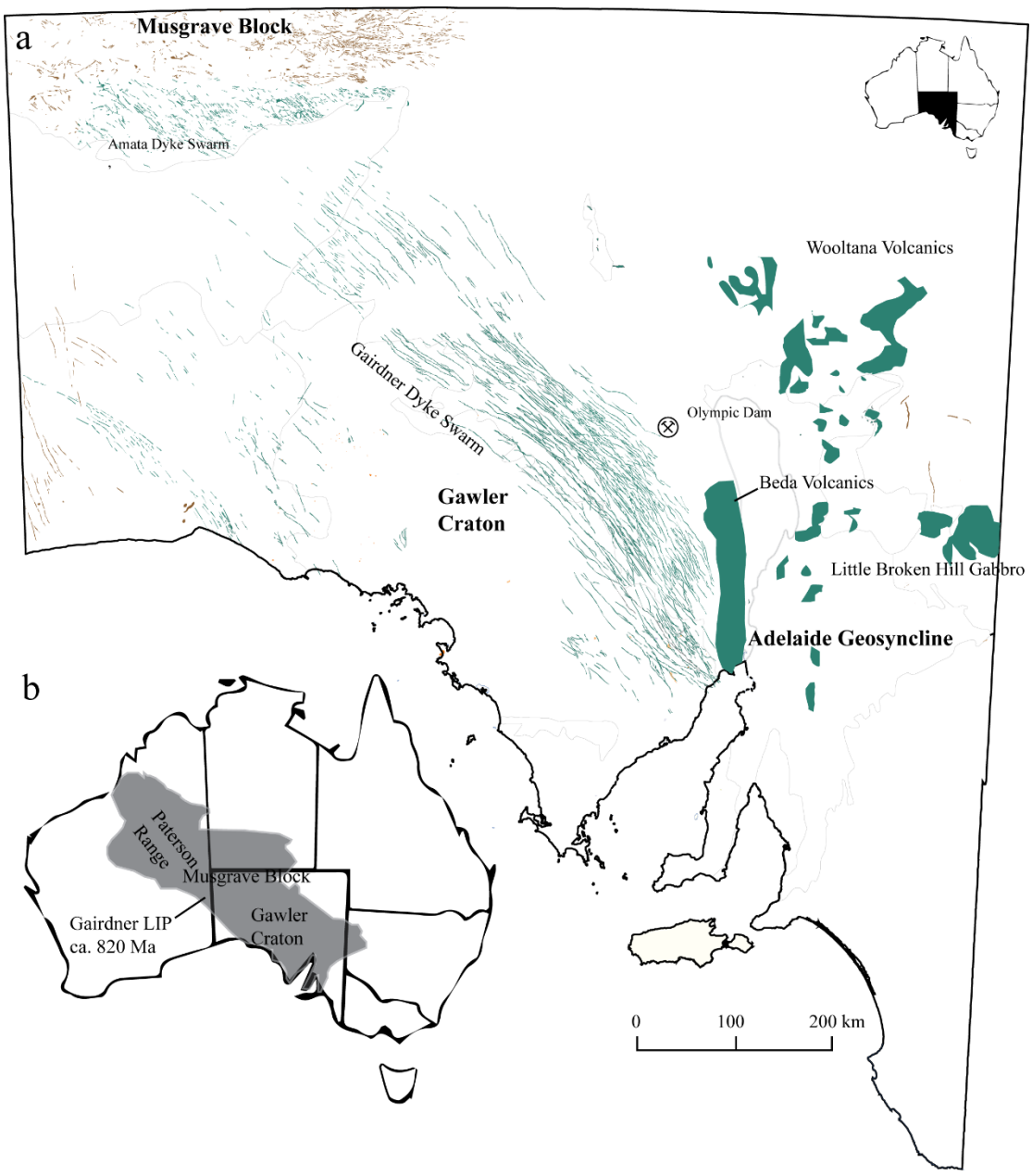

Figure 2.2 (a) Simplified geological map showing the distribution of the ca. 820 Ma Gairdner large igneous province (LIP) in the Gawler Craton. Modified after Crawford and Hilyard (1990). (b) Simplified map showing the distribution of the Gairdner LIP in Australia. Modified after Hoatson et al. (2007).

The Gairdner Dyke Swarm in the Gawler Craton, South Australia was first recognised on aeromagnetic images as a NW-trending array of linear magnetic anomalies (Boyd in Goode, 1970). Goode (1970) correlated this dyke swarm with the similarly striking Amata Dyke Swarm in the Musgrave Block and reported a total length of ~1000 km for the combined Gairdner-Amata Dyke Swarm (Fig. 2.2). Compositional

similarity between the Gairdner Dyke Swarm and other igneous suites such as the Wooltana Volcanics and Beda Volcanics led Crawford and Hilyard (1990) to suggest that these units constitute an igneous province named the "Willouran basic province", which covered an area of at least 210,000 km^2 and had an estimated volume of 105,000 km^3. Zhao and McCulloch (1993) and Zhao et al. (1994) produced Sm-Nd isochron ages for the Gairdner (867 ± 47 Ma and 802 ± 35 Ma) and Amata dyke swarms (790 ± 40 Ma and 797 ± 49 Ma). The emplacement age for the Gairdner Dyke Swarm in the Gawler Craton was subsequently better constrained at 827 ± 6 Ma using U-Pb in baddeleyite by (Wingate et al. (1998)). Zircon U-Pb ages of dolerite dykes and sills from the western Musgrave Block and Paterson Range of Western Australia also yielded results of ca. 820-830 Ma (Hoatson et al., 2008a, b). These suites, together with the Willouran basic province, have been put together to constitute the Gairdner LIP (Claoue-Long and Hoatson, 2009).

2.2 Local geology of the Olympic Dam deposit

Below is a brief introduction to the local geology of the Olympic Dam deposit, mostly adapted from Reeve et al. (1990) and Ehrig et al. (2012) unless specified.

2.2.1 Host rocks—the Olympic Dam Breccia Complex

The host rocks of the Olympic Dam deposit consist of a wide range of breccia types and the principal components of the breccias vary from mainly granitic to hematite-rich end-member lithologies. The breccia complex is named the Olympic Dam Breccia Complex (ODBC). Subdivisions of the ODBC are difficult because there is a complete gradation from sericite-altered Roxby Downs Granite to sericite-altered granite-rich breccias in the periphery, through hematitic-granite breccias, to hematite-

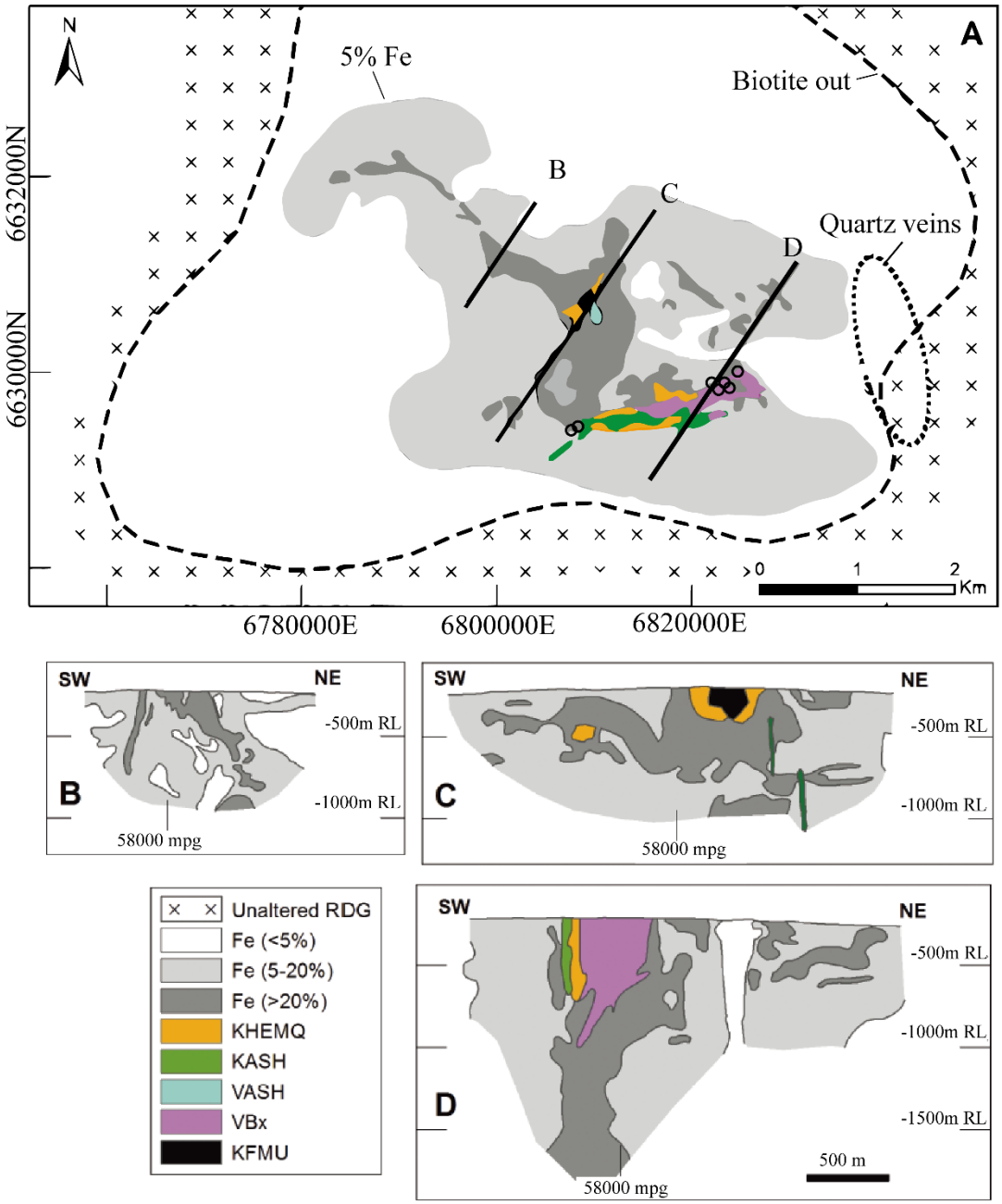

Figure 2.3 Simplified geologic map at –350 mRL (A) and cross sections (B-D) of the Olympic Dam Breccia Complex, showing the distribution of unaltered Roxby Downs Granite (RDG), outer limits of significant brecciation and iron metasomatism (5 wt.% Fe contour), granite-rich breccias (5–20 wt.% Fe), hematite-rich breccias (>20 wt.% Fe), chlorite-bearing, laminated sandstone and mudstone (KASH), well-bedded, hematite-rich sandstone, mudstone, and conglomerate-breccia (KHEMQ), thinly laminated, very hematite-rich mudstones (VASH), polymictic volcanic conglomerate (KFMU), hematite-rich breccias consisting of porphyritic felsic volcanic clasts (VBx). The locations of drill holes with flat-lying olivine-phyric basalt are marked by black circles. The dashed circle indicates the locations of thick quartz veins. Modified after Ehrig et al. (2012).

rich breccias in the deposit centre. This gradation is reflected by the Fe contents of the ODBC (Fig. 2.3). Besides, in some areas of the ODBC, original compositions and textures have been replaced and obliterated because of alteration. The important 'end-member' types are described below, but it must be stressed that there is a complete gradation among these types (Reeve et al., 1990; Ehrig et al., 2012).

a. Granite-rich breccias

Granitic breccias display a wide range of textures, reflecting variable intensities and styles of brecciation, and fragment mobilisation. Most granitic breccias consist of fractured or veined granite, and/or coarse clast supported breccia types. Crackle and jig-saw textures are commonly preserved in matrix poor granite breccias, especially in less altered examples. In general these textures become progressively less recognisable as the proportion of matrix increases. Apart from superimposed alteration, the clasts have the same lithology as the Roxby Downs Granite which hosts the entire breccia complex.

In most cases the majority of clasts are angular to subangular, and so are the fragments which make up the matrix. A minor proportion of granite-rich breccias consists of isolated large clasts of granite supported by a finer-grained, variably altered granite-derived matrix. The matrix of this type may exhibit some sorting and locally developed discontinuous layering. There is only rare evidence of substantial rounding of granite clasts or matrix fragments. Granite-rich breccias envelop, and are complexly intermingled with, the hematite-rich breccias.

b. Hematite-rich breccias

Hematite-rich breccias are widespread and are the most important host rocks for mineralisation. The common textural features of the hematite-rich breccias are as follows:

1. Fabrics vary from matrix-rich to clast-rich types. Matrix supported breccias are generally more abundant than clast supported breccias.

2. Clast size is highly variable, but for most breccias the dimensions of clasts are generally less than 20 cm. Isolated blocks up to meters, or rarely tens of meters in size, have been observed.
3. Most breccias are poorly sorted, but in some localised areas there is a limited degree of sorting.
4. Clasts are generally angular and approximately equidimensional. Irregularly shaped clasts may predominate locally. Where clasts are somewhat elongate, they may be weakly aligned. There is little evidence of substantial rounding of clasts even in areas where the heterolithic nature of the breccias suggests significant mobilisation and mixing.
5. Clasts derived from pre-existing breccias are present in many breccia bodies.

The Hematite-rich Breccias could be subdivided into three groups:

a) Hematite-quartz breccias,
b) Hematite breccias,
c) Heterolithic hematitic breccias.

Hematite breccias occur as relatively small bodies either within or on the margins of larger heterolithic hematitic bodies. They are generally discontinuous and irregular, and may display a gradational relation with heterolithic breccias. They also occur as narrow vein-like bodies within granitic breccias.

a) Hematite-quartz breccias

These rocks are mainly made up of clasts of hematite, quartz, and hematite-quartz within a matrix predominantly composed of hematite and grains of quartz. They are largely confined to the central portion of the breccia complex, with minor occurrences elsewhere in the deposit. The following features are distinctive:

1. High abundance of quartz fragments, particular in the matrix, where they may constitute up to 40% of the volume. The crystal morphology and distinctive undulose extinction indicates that it was derived from the local granitic lithologies.

2. Predominance of fine-grained dusty red-brown to dark purplish hematite in both clasts and matrix. Steely grey to black hematite clasts are also present, but are much less abundant and usually smaller in size than co-existing red-brown and purplish types.

3. Abundance of barite, and scarcity of fluorite, compared to other hematite-rich breccias types. Barite occurs as disseminations, veins and vein fragments. Concentrations of 2 to 5 wt.% of Ba are characteristic.

Hematite-quartz breccias occur predominantly in a central body which has an L-shaped configuration. This body has irregular margins and appears to taper with depth where it breaks up into at least two pipe-like features.

b) Hematite breccias

Both clasts and matrix are composed largely of hematite in these breccias. They show a wide variation in colour, texture and in the composition of the minor non-hematite component. In total volume, hematite breccias are the least important of the three hematitic breccia categories. They may be strongly mineralised, particularly in the north-western parts of the deposit where they preferentially contain the highest grade ore. On the other hand, hematite breccias located well below the bornite-chalcopyrite interface commonly contain abundant pyrite and only minor copper sulfides.

The colour of hematite breccias is generally dark grey to black, resulting from the predominance of hematite grains with well-developed crystal forms. Black hematite breccias vary from dense hard types to very porous or vuggy types. In some instances, the porosity appears to be an original feature of the rocks; however, some hematite breccias contain abundant small vugs which appear to be the result of leaching of sulfides.

Some types are only weakly brecciated, or appear to have been brecciated in situ. In many examples there are only very subtle textural differences between the hematite clasts and hematite matrix, and as a result, the brecciated nature of these rocks is not always obvious macroscopically.

The non-hematite component of these breccias is variable, and may include quartz, chlorite, fluorite, barite, altered granite clasts and granite-derived mineral fragments, siderite, minor relict magnetite, and sulfides ± pitchblende in mineralised zones.

Minor amounts of hematite breccia may contain distinctive components and /or exhibit unusual textures. These features include hematite-rich pisolites, hematite-sulfide pisolites, strongly laminated hematite-rich rock fragments, wispy discontinuous layering, crustiform hematite, and coarse feathery-textured hematite.

c) Heterolithic-hematitic breccias

This broad category accounts for the largest proportion of the hematite-rich breccias within the deposit. The majority of ore reserve/resource tonnage occurs in these breccias. Significant proportions of altered granite clasts may occur, but a variety of hematite-rich clasts predominate. The proportion of the different clast types is highly variable. Hematite-rich clasts vary from fine-grained and dark red-brown in colour to fine and medium-grained crystalline black varieties. The strongly heterolithic nature of these breccias clearly indicates that they have undergone a degree of mixing, and possibly significant transport. However, heterolithic hematitic breccia bodies may contain poorly defined zones where there is a predominance of similar clast types, or in which the granite clasts show a particular alteration type.

A variety of other lithologies also occur as minor clast types. These include highly altered, fine-grained, mafic and felsic igneous intrusive material (derived from the GRV), finely laminated sedimentary rocks consisting predominantly of hematite and quartz and massive to diffusely layered medium to coarse-grained arkose-like rocks composed of altered granite-derived feldspar and quartz fragments (bedded clastic facies, see below). Clasts of massive chalcopyrite, barite, fluorite, or siderite are minor components of some breccias. Siderite clasts are a major component of localised breccia zones near the north-eastern margin of the deposit.

The matrix of heterolithic breccias normally consists of dark red-brown to black, fine to medium-grained hematite, with a variable proportion of quartz and other components largely from granite. Copper sulfides, pyrite, fluorite and barite may also be disseminated in the matrix.

Heterolithic hematite breccias occur as somewhat discrete irregular, elongate, or lenticular bodies located within a broad zone around the central hematite-quartz breccia body. These individual bodies are generally surrounded by granite-rich breccias. The boundaries between heterolithic hematite breccias may be sharp or gradational. Where gradational, the contacts are generally characterised by an abundance of hematite as clastic matrix or as veins in the immediately adjacent granite-rich breccia.

2.2.2 Pre-brecciation lithologies

a. Roxby Downs Granite

The Roxby Downs Granite (Fig. 2.3) is an undeformed, pink, medium- to coarse-grained, equigranular granite. It contains mainly alkali feldspar, quartz, and sodic plagioclase, and minor biotite, amphibole magnetite, titanite, apatite, zircon, allanite, fluorite, ankerite, synchysite, and uranothorite.

b. Felsic volcanic units

This volcanic unit occurs as porphyritic felsic fragments in parts of the ODBC and some beds in the bedded clastic facies.

c. Bedded clastic facies

'Surficial' volcanic and volcaniclastic rocks localized in several distinctive zones within the hematite-quartz breccias have been interpreted by Reeve et al. (1990) as 'diatreme structures'. They found felsic volcanic cobble conglomerates, lapilli tuffs, laminated ash-fall tuffs and blocks of hematite-quartz wall rock in the upper parts of the diatreme, and 'juvenile mafic pyroclasts' and coherent mafic dykes in the lower underlying root zone of the diatreme, based on which they concluded that mafic and felsic magmas invaded the active hydrothermal system, and produced phreatomagmatic explosion and localised diatreme structures.

Ongoing exploration at Olympic Dam has greatly extended the knowledge of the architecture of the host succession and very thick (>350 m) sections of bedded clastic facies of mudstone, sandstone and conglomerate beds extending continuously across a

~1.5 km × 0.9 km area have been found to encompass four of the five 'diatreme structures' of Reeve et al. (1990). The bedded clastic facies occur in the ODBC immediately beneath the unconformity between the ODBC and the Neoproterozoic to Cambrian sedimentary cover (Stuart Shelf). Drill hole intersection intervals are up to 350-m thick (Fig. 2.3).

The source of granite fragments, granite-derived feldspar, quartz, feldspar-phyric felsic and mafic volcanic clasts in these sedimentary faces could have been unroofed HS granites and GRV, respectively. However, components of Cr-spinel and volcanic quartz of the sedimentary faces have no immediate provenance from the Olympic Dam area, which implies that sources outside Olympic Dam contributed to these sediments (McPhie et al. (2011b). Therefore, it has been proposed that the bedded sedimentary facies indicated the former presence of a depocenter at Olympic Dam and that the Olympic Dam depocenter was part of a sedimentary basin that extended beyond the Olympic Dam area and was not limited to local diatremes.

They are distinguished from the hematite-rich breccias by having well-defined planar beds and overall finer grain size (McPhie et al., 2016). Bedded clastic facies comprise four main facies distinguished by composition, grain size, and bed forms (Fig. 2.3): (1) laminated, green sandstone and mudstone (KASH), (2) well-bedded, hematite-rich sandstone, mudstone, and conglomerate-breccia (KHEMQ), (3) thinly laminated, hematite-rich mudstones (VASH), and (4) minor but thick beds of polymict volcanic conglomerate-breccia (KFMU).

d. Flat-lying olivine-phyric basalt

This is an apparent flat-lying unit of Cr-spinel-bearing, olivine-phyric basalt. This unit has been intersected in several drill holes directly beneath the unconformity between the ODBC and the Neoproterozoic to Cambrian sedimentary cover (Fig. 2.3); the drill hole intersections range in thickness from 15 m to 45 m. The basalt is in contact with various hematite-rich breccias; the contacts have been intensely altered and sheared. Even though the basalt has been intensely altered, it retains a well-preserved porphyritic texture comprising skeletal former olivine phenocrysts.

2.2.3 (Pre-) to Syn-brecciation rocks units

At Olympic Dam, mafic and felsic igneous intrusions develop mainly as dykes. Four types of dykes have been recognized on the basis of their compositions and alterations.

a. Aphanitic, sericite-hematite–altered dykes

These dykes comprise micro-crystalline sericite and chlorite. No primary textures are preserved in these dykes, and they tend to show mafic affinity due to elevated concentrations of titanium and magnesium. The dykes vary in thickness from less than 0.5 m to more than 40 m, with inferred strike lengths of up to 1 km.

b. Olivine-phyric basalt dykes

The olivine-phyric basalt dykes (a few centimetres to ~1 m wide) occur in a NW-striking, steeply E-dipping orientation. These dykes locally have very fluidal margins and delicate apophyses and pinch and swell over very short distances (Johnson, 1993). They intrude the Roxby Downs Granite and the ODBC. The contacts with the latter rocks vary from sharp and planar to brecciated and gradational over several metres (Bradbury, 1988). They are generally strongly sericite altered but retain a relic porphyritic texture comprising pseudomorphs of olivine phenocrysts in the very fine groundmass. The petrographical similarity (i.e. porphyritic texture and high former olivine pseudomorph abundance of ~20 vol.%) between these dykes and the flat-lying olivine-phyric basalt unit described above indicates that they were probably derived from the same parental magmas of ultramafic affinity but were emplaced to different depths.

c. Doleritic to porphyritic mafic dykes

The flat-lying olivine-phyric basalt is spatially associated with a series of NW-striking doleritic to porphyritic mafic dykes in which olivine abundance is less than 5 vol.%. These dykes intruded the Roxby Downs Granite and the ODBC. Recognizable (former) primary minerals in these dykes include olivine, pyroxene, plagioclase,

phlogopite, Ti-magnetite and apatite. A variety of textures have been preserved, ranging from porphyritic to doleritic.

d. One quartz-phyric felsic dyke

This dyke has been intersected in the deepest vertical drill hole in the south-eastern part of the ODBC. This dyke has intruded into the Roxby Downs Granite and is composed of melt inclusion-bearing quartz phenocrysts in a groundmass of quartz and sericite with minor zircon and apatite.

2.2.4 Post-brecciation rock units

a. Gairdner Dykes

The basaltic to doleritic Gairdner Dykes intrude the Roxby Downs Granite and the ODBC. Contacts of the dykes with the Roxby Downs Granite or the ODBC are sharp and marked by palagonite-altered formerly glassy margins typically a few millimetres across. The Gairdner Dykes are characterized by generally fresher appearance and better competency, as well as higher magnetic susceptibility, compared to other mafic facies mentioned above. The dykes range from several metres to over 100 m in width, and dykelets of a centimetre width also occur. These dykes are generally subvertical and can be traced along a NW strike for up to 3 km. Euhedral to sub-euhedral clinopyroxene and plagioclase are the dominant mineral phases. Minor Ti-magnetite occurs both as phenocrysts and in the groundmass. Multiple generations of dykes are present in some cases; early doleritic dykes are intruded by later porphyritic dykes.

b. Neoproterozoic to Cambrian sedimentary rocks (Stuart Shelf)

These rocks comprise the cover sequence of the Olympic Dam deposit. They are approximately ~320 m thick, consist of flat-lying, shallow marine shale, quartzite, and dolomite and overlie the eroded upper surface (sub-horizontal unconformity) of the Roxby Downs Granite and the ODBC.

2.2.5 Alteration

The principal alteration phases occurring in Olympic Dam rocks are hematite, magnetite, sericite (i.e. fine-grained muscovite, illite, phengite and paragonite), quartz, chlorite, carbonate (most significantly siderite), fluorite, and barite. Within the ODBC and also common to all alteration assemblages, iron oxide addition and sericite alteration of igneous feldspars (plagioclase and K-feldspar) are the two dominant alteration effects. In many lithologies local alteration effects may be so extreme that the primary rock fabric is unrecognisable. Many subsequently-formed breccias contain clasts or zones of such 'alteration lithologies', and these complicate any regularity which might have been present in early-formed alteration patterns. However, the following deposit-wide generations could be made:

1. Sericite alteration is widespread throughout the ODBC. Sericite replaces igneous sodic plagioclase and K-feldspar, and hydrothermal chlorite.

2. Hematite alteration is more abundant and more intense toward the centre of the deposit. Hematite replaces pre-existing igneous K-feldspar and hydrothermal minerals including magnetite, siderite, chlorite, sericite and rarely sulfides. Hematite is also precipitated in vugs and veins.

3. Chlorite alteration is patchy and widespread and generally of low to intermediate intensity. Chlorite typically replaces amphibole and biotite in the Roxby Downs Granite and olivine and pyroxene in mafic to ultramafic dykes.

4. Hydrothermal quartz occurs as a by-product when sericite replaces the igneous feldspars. Hydrothermal quartz also occurs in 1- to 5-mm-wide veinlets together with apatite, magnetite and/or siderite in the intensely altered Roxby Downs Granite and some mafic to ultramafic dykes. Also, hydrothermal quartz also occurs as 20 to 50-m-thick quartz veins in the altered Roxby Downs Granite, in the south-eastern part of the ODBC (Fig. 2.3).

5. Carbonate alteration is typically weak, and largely restricted to the north-eastern part of the deposit, where siderite veins and vein fragments are abundant.

A number of vein types are present in the ODBC and the surrounding granite. The veins occur as intact continuous types, irregular types, or disrupted types which terminate at clast margins. Discrete fragments of early veins are dispersed within a variety of breccia types.

Essentially monomineralic hematite, sericite, or chlorite veinlets, and more substantial hematite-siderite veins and barite-fluorite (± hematite, siderite, quartz, chalcopyrite, and rare goethite) veins are widespread. Quartz ± chlorite veinlets are abundant in some pervasively silicified breccias, and quartz ± fluorite veinlets occur locally in some granitic breccias. Veinlets containing copper sulfides ± pitchblende with variable amounts of fluorite ± barite are common in some mineralised zones. Banded siderite-chalcopyrite ± quartz veins, quartz-tourmaline ± chlorite ± sericite veins and dolomite veins occur mainly within granite and granite-rich breccias. Relatively late stage barite-quartz ± fluorite are abundant in and near the hematite-quartz breccias in the central portion of the deposit. Late stage chalcopyrite veinlets occupying irregular hairline fractures are ubiquitous and are superimposed on the overall sulfide zonation pattern.

All vein types are generally less than 1 cm in width, except for the major barite-fluorite (± hematite, siderite, quartz, chalcopyrite, and goethite) veins which may be several tens of centimetres in width for individual veins, and to several meters for vein networks. Such veins typically occupy prominent fault zones or fill dilatant fractures and jogs associated with faults.

2.2.6 Mineralization

The Olympic Dam deposit contains anomalous concentrations of iron, copper, uranium, gold, silver, barium, fluorine and the rare earth elements (REE), especially lanthanum and cerium, and the recovery of copper, uranium, gold and silver is considered economic (Ehrig et al., 2012).

Although the ore zones account for only a small proportion of the total volume of breccias within the ODBC, weak mineralization is widespread throughout most breccia types. The central hematite-quartz breccia body is essentially devoid of copper-uranium

mineralisation, although significant gold mineralisation occurs in localised narrow zones at its margins.

Linear distributions of high-grade Cu, Au, and U_3O_8 are evidence for structural control of the mineralization at Olympic Dam. Multiple generations of mafic to ultramafic dykes have also intruded along pre-existing zones of weakness (e.g. faults and fractures). As the deeper and more peripheral parts of the deposit in the north-western extension are drilled, the evidence for a spatial association between the mafic dyke and brecciated zones is becoming increasingly clear (Ehrig et al., 2012). The following paragraphs describing mineralization at Olympic Dam are adapted from Reeve et al., (1990) and Ehrig et al., (2012).

a. Copper

Copper mineralisation most commonly consists of disseminated sulfide grains ranging in size from 0.1 to 2.0 mm. Veinlet sulfides constitute a much less abundant style of mineralisation. Massive sulfide is very rare, occurring either as isolated pods (up to tens of centimetres) or as clasts (millimetres to centimetres). Some granite breccias contain dispersed chalcocite-rich blebs, which are typically intergrown with relatively coarse-grained sericite ± fluorite.

Copper mineralisation is most abundant in hematite-rich lithologies. Economic concentrations are largely restricted to heterolithic hematitic breccia and hematite breccia hosts; although a small proportion occurs within granitic breccias containing an abundance of hematite as matrix. In almost all lithologies, the copper mineralisation at local (centimetre) scale is intimately associated with the hematite component, and hematite-rich matrix material is typically most strongly mineralised. Black hematite clasts are generally more strongly mineralised than finer-grained red-brown or purplish hematite clasts. Granite clasts are generally unmineralised, or poorly mineralised, even where they occur in a strongly mineralised heterolithic hematitic breccia. As a result of these relationships, black hematite breccias and breccias with abundant hematite-rich matrix are the most strongly mineralised lithologies in the deposit.

The principal copper sulfide minerals in the deposits are chalcopyrite, bornite and chalcocite. Other copper bearing minerals present in minor quantities include digenite,

covellite, native copper, carrollite, and roxbyite ($Cu_{1.74-1.82}S$, with a trace of Fe). The distribution of the principal sulfide minerals conforms to a complex, but well developed, deposit-wide zonation pattern. The more sulphur-rich species (chalcopyrite, pyrite) occur most abundantly in the deeper and outer parts of the deposit whereas sulphur-poor species (bornite and chalcocite) typically occur in the upper and more central parts. The boundary between bornite (bn) (± chalcocite) mineralisation and chalcopyrite (cp) mineralisation (hereafter referred to as bn-cp interface) is a sharply defined, readily mapped feature. This boundary forms a highly convoluted three-dimensional surface which is broadly funnel-shaped, dipping inwards under the central hematite-quartz breccia body. There is a gradational increase in the pyrite:chalcopyrite ratio, and a general decrease in the total abundance of sulfide downwards and outwards from this boundary. Underground exposures and closely spaced fan drilling show that the shape of the bn-cp interface is very complex in detail, containing major local inflexions. In many instances, the location of the interface appears to be influenced by the distribution or rock types.

Throughout the deposit, the position of the bn-cp interface typically coincides with the lower margin of the higher grade copper mineralisation. In general, the total sulfide abundance is broadly similar on either side of the interface. However, partly because of the difference in copper tenor between bornite + chalcocite and chalcopyrite, the copper grade on the bornite-chalcocite side of the interface is approximately twice that of the adjacent chalcopyrite mineralisation. Grades of 4 to 6 wt.% of copper are common in the bornite-chalcocite zones. However, chalcopyrite mineralisation rarely exceeds a grade of 3 wt.% of copper.

Typically, the upper margin to the bornite-chalcocite mineralisation is also well defined. Throughout most of the deposit, the bornite-chalcocite mineralisation is restricted to within about 50 m of the bn-cp interface, despite the more widespread distribution of apparently favourable hematite-rich breccias. However, in some localities, large flame-like zones of disseminated chalcocite extend considerably more than 50 m above the bn-cp interface.

Textural relations in copper mineralised breccias typically suggest that copper sulfides either post-date most or all of the closely coexisting or intergrown hematite, or

are essentially coeval with it. The sulfides most commonly occur in interstices between hematite grains, in intergranular positions between polycrystalline aggregates of hematite, as diffuse infiltrational or sharply defined crosscutting veinlets, and less commonly as rims on hematite grains and quartz fragments. However, in some rare instances minor hematite is observed rimming or replacing copper sulfide grains. Copper sulfides also occur in micro-cavities and fractures where they may be accompanied by sericite, hematite, fluorite, chlorite, barite, or hydrothermal quartz.

Chalcopyrite generally coexists with pyrite, although their relative abundance may vary greatly over short distances. Pyrite typically occurs as euhedral or subhedral crystals or crystal fragments, and it is most abundant in black hematite breccias. In most chalcopyrite-mineralised zones, chalcopyrite has at least partially replaced a majority of the pre-existing pyrite grains. Microprobe analyses indicate that Olympic Dam pyrite contains up to several weight per cent of cobalt. This cobalt forms grains of carrollite along some contacts between relict pyrite and replacement chalcopyrite.

In the immediate vicinity of the bn-cp interface, bornite and chalcopyrite may be intimately associated, or coexist as discrete grains and polycrystalline aggregates. In these transitional assemblages bornite commonly rims chalcopyrite, and/or partially replaces it. Also, individual bornite grains may contain exsolution lamellae of chalcopyrite, and some pyrite relicts may be present. Chalcocite usually coexists with bornite, but either sulfide may predominate. Chalcocite and bornite are commonly intergrown and textures range from intricate myrmekitic forms to relatively equiangular aggregates. Locally, chalcocite mineralisation overprints bornite (± chalcocite) and vice versa. More commonly, bornite is seen to overprint chalcopyrite. On a microscopic scale, chalcocite has not been observed in physical contact with chalcopyrite. On a mesoscopic (meter) scale, in the vicinity of chalcopyrite mineralisation, chalcocite appears to be always accompanied by bornite. Chalcopyrite microveinlets occur locally in chalcocite ± bornite mineralised zones.

At several locations trace amounts of native copper occur adjacent to some chalcocite-mineralised zones, in rocks devoid of sulfides. Disseminated native copper appears to be a significant form of mineralisation in a small part of the NW of the deposit.

The textural relations outlined above and the presence of sulfide clasts and/or discrete fragments of sulfide-bearing rock in many breccias, all suggest a complex multi-generational history of brecciation and mineral deposition.

b. Uranium

Above-background concentrations of uranium occur in association with all copper mineralisation. In addition, there is a positive, although inconsistent, correlation between high-grade uranium and high-grade copper.

In a number of areas throughout the deposit, most notably in the NW, higher grade uranium mineralisation occurs within a relatively narrow horizon situated at the upper margin of the bornite-chalcocite zones, and it is more strongly developed and more continuous within the more hematite-rich breccias. On the other hand, some high-grade copper ore zones consisting of bornite-chalcocite mineralisation contain comparatively low grades of U_3O_8 (as low as 0.3 kg/t).

Ore zones composed of chalcopyrite (+ pyrite) mineralisation are generally of medium to low uranium grade, and show comparatively less variability in uranium content. However, some continuous zones of higher grade uranium mineralisation transgress the bn-cp interface on a local scale. A number of discrete zones of significant uranium (± copper) mineralisation also occur in altered granite breccias, some of which are almost devoid of hematite.

Uranium mineralogy appears to be independent of the associated sulfide species. Most of the uranium within the deposit occurs as fine-grained pitchblende in discrete aggregates or in a finely disseminated form. Other significant pitchblende textures include colloform and crustiform types filling fractures and cavities, massive and fractured veinlets (where it often coexists with copper sulfides ± fluorite ± barite), and optically continuous intergranular growths. Pitchblende also occurs as rims, intergrowths or replacement patches in close association with many other breccia components, including copper sulfides. Pitchblende spherules blebs or pisoliths are developed locally.

There are also minor amounts of granular coffinite in close association with pitchblende. Rarely, brannerite may accompany grains of anatase, rutile, or zircon in some granite-rich mineralised zones. Rare uraninite occurs as inclusions in copper sulfides, and the granite contains a trace amount of primary uranothorite.

c. Gold

Gold occurs in two broad associations:

1. It is a low grade but economically significant accessory in all copper-uranium ore zones. The average gold grade of individual copper-uranium ore zones varies from 0.3 g/t to 1.0 g/t, with an overall total average of 0.6 g/t. There is a clear tendency for copper-uranium zones nearer the centre of the deposit to have higher gold grades, whereas those further from the centre have lower gold grades. The gold is very fine-grained, and intimately associated with copper sulfides. Visible gold is rare. The majority of known gold in the deposit is of this type, and it is the large tonnage of the copper-uranium mineralisation which makes the deposit a very significant resource of gold.

2. It also occurs as high-grade gold mineralisation in small complexly shaped zones which are locally separate from, or adjacent to, copper-uranium mineralisation. Designated gold ore zones outlined for mining purposes locally include some of the adjacent copper-uranium mineralisation, and all are located in a restricted area along the eastern side of the main body of unmineralised hematite-quartz breccias. Some higher grade gold zones lie at the steeply dipping margin of this body and may be locally hosted by hematite-quartz breccias or strongly silicified equivalents.

Gold in these higher grade zones occurs as irregularly shaped grains which range from 10 μm to 100 μm in longest-dimension, or as minute, more equant grains. Although the two gold distribution patterns described above differ significantly in their local association, there is clear evidence to suggest that both are part of a broad, deposit scale, total zonation pattern which includes the copper sulfide zonation described above. The gross zonation from the lower and outer part of the ore body, to the upper and inner part is: pyrite → chalcopyrite → bornite → chalcocite → (native copper) → gold → silicification.

In general, uranium is more closely associated with the copper sulfides and rarely exceeds 100 ppm in the gold zones.

d. Silver

Silver occurs with all copper mineralisation. Microprobe analyses confirm that most silver occurs within copper sulfides, and highest silver grades generally occur within bornite-chalcocite mineralisation. In the NW part of the deposit, there is an area of relative silver enrichment within bornite-chalcocite ore zones.

e. Other elements

Most ODBC lithologies are strongly enriched in rare earth elements (REE), particularly the light REE. Abundances of approximately 2,000 ppm lanthanum and 3,000 ppm cerium are common for mineralised hematite-rich breccias. The central body of hematite-quartz breccias, although lacking significant copper-uranium mineralisation, contains generally higher concentrations of lanthanum and cerium than the surrounding hematite-rich breccias, suggesting a broad deposit-wide zonation in REE distribution. High concentrations of lanthanum and cerium are also present in association with some gold mineralisation hosted by hematite poor sericite-altered granitic lithologies.

Bastnaesite is the most abundant REE-bearing mineral, typically occurring as fine-grained intergrowths with hematite, and as disseminations in the sericite-quartz matrix of altered granite-rich breccias. Other significant REE-bearing minerals include florencite, monazite, and xenotime.

Fluorite is the principal fluorine-bearing phase in the ODBC. However, sericite is variably enriched in fluorine, and consequently, many altered granite breccias containing little fluorite are nevertheless noticeably enriched in fluorine relative to the unaltered host granite, which contains up to 0.3 wt.% of fluorine.

Fluorite occurs as dark purple disseminations, clasts, and in veinlets in many breccia types, but is usually most abundant in mineralised heterolithic hematitic breccias. Most breccias containing significant amounts of fluorite are strongly

mineralised with copper sulfides. Some fluorite-rich ore zones contain average values of 1 to 2 wt.% of fluorine. There is a preferential association of disseminated fluorite with heterolithic breccias containing black hematite types rather than red-brown or purple types. However, the central hematite-quartz body contains low abundances of fluorine (generally less than 0.2 wt.% of fluorine).

Most hematite-rich breccias contain abundances of 0.5 to 5.0 wt.% of barium, occurring in barite. There is a generally antipathetic relation between the distribution of barite and fluorite, except for the large late-stage barite-fluorite veins, where these minerals are intimately intergrown. Barite is most abundant in breccias composed of fine-grained red-brown or purple hematite where it occurs both as disseminations and as 'crackle' veins. The central hematitic-quartz breccia is particularly enriched in barite, typically containing 2 to 5 wt.% of barium.

2.2.7 Interpretations of the ore-forming processes at Olympic Dam: previous models

The earliest published article on the Olympic Dam deposit is by Roberts and Hudson (1983). They considered this giant copper-uranium-gold deposit to be a new type of sediment-hosted ore deposit, mainly based on the 'strata-bound' chalcocite-bornite-chalcopyrite-pyrite mineralisation that is typical of stratiform copper occurrences. They interpreted the formation of the host breccias (in what is later called the ODBC) to ore in an arid subaerial environment during rifting or strike-slip faulting and suggested that the introduction of ore metals was related to local volcanism, without much strong evidence but spatial distribution of mineralisation relative to volcanic structures and rocks.

With more exposures in underground mining, Reeve et al. (1990) proposed that the primary ore deposition occurred in a shallow (still argued) level environment controlled by coupled redox reactions involving the oxidation of wall rock components and reduction of elements complexed in the hydrothermal fluids, fluid mixing as a consequence of redox reactions, dilution and/or cooling, and boiling. They owed the formation of the ODBC and the ore contained to the interplay of hydrothermal, volcanogenic, sedimentary and tectonic processes.

The breccias, especially the hematite-quartz breccias, are highly enriched in light and heavy rare earth elements (LREE and HREE) (avg. ~5,000 ppm REE in hematite-rich breccias, with La normally reaching 3,000 times chondrite, and maximum 10,000 times chondrite), and this led to special attention on the REE behaviour during the hydrothermal process. Oreskes and Einaudi (1990) suggested that the hydrothermal fluids responsible for hematite alteration and breccia formation, were REE-rich, based on the high abundance of REE in hydrothermal phases, REE enrichment of altered versus unaltered wall rocks, concentration of REE in the centre of the system, variable slopes of chondrite-normalized patterns, and the lack of unusual intrusions. The occurrence of REE phases in the early quartz-sericite veins and barite-bastnaesite fragments, intergrown with hematite, and as inclusions in sulfide grains, led them to conclude that REE minerals were precipitated during much of the hydrothermal history of Olympic Dam. Moreover, evidence for presence of sedimentary rocks in the breccia complex, which might indicate that mineralisation occurred within 1 to 2 km of the Proterozoic paleosurface or possibly at the surface, in contrast with the coarse-grained, plutonic host rock, together with preliminary radiometric dating results including: ca. 1315 Ma of Rb-Sr analysis of sericite from altered granite wall rock (Gustafson and Compston, 1979), a minimum age of 676 ± 200 Ma indicated by Rb-Sr dating of the Woomera Shale, a correlative of the Tregolana Shale which unconformably overlies the deposits (Webb et al., 1983) and a maximum age of ca. 1400 Ma on pitchblende analysed by ion microprobe (Trueman, 1986), inclined them to believe that mineralisation significantly post-dated emplacement of the host granite and, therefore, did not bear a direct link to it. Data from their work also showed an important role for F complexes—in addition to or instead of CO_3 complexes—in mobilizing REE in low-pressure hydrothermal systems.

Oreskes and Einaudi (1992) investigated fluid inclusion, stable isotope and formation temperatures of various ore types at Olympic Dam, concluding that at least two sources of fluids, of contrasting temperature, composition, and oxygen isotope characteristics, were involved in the formation of Olympic Dam. Early magnetite (dominant iron oxide in early hydrothermal assemblages, replaced by hematite during the subsequent hydrothermal process, with only minor localised relicts of magnetite preserved within the hematite-rich breccias) associated with pyrite and siderite was precipitated from fluids of high $\delta^{18}O$ (approx. 10 ‰) at temperatures near 400℃. In

contrast, hematite within the ODBC formed at lower temperatures (200-400℃) from fluids of lower $\delta^{18}O$ (<9 ‰). Waters of surficial origin—seawater, closed basin water, or ground water—may have been involved in the later stages of hydrothermal activity that formed the hematite-rich breccias, but this was not a necessity required by their isotopic data. They proposed that the early magnetite was coeval with formation of the Roxby Downs Granite (ca. 1590 Ma), forming at relatively high temperatures in a deep seated hydrothermal environment until the hematite and ore-forming stage began 50 to 150 million years later.

Sm-Nd isotope analyses of pyrite, chalcopyrite, and bornite-chalcocite-hematite-rich ores gave the same initial εNd of -2.5, which suggests that these ore types are cogenetic and contain a contribution from a mantle-derived source rock or magma (Johnson and McCulloch, 1995). In contrast to hematite-rich breccias, volumetrically minor magnetite-rich assemblages have the same initial Nd signatures (εNd of -5) as the host granite, suggesting that they could be cogenetic. The initial εNd isotopic values (up to +4) of the altered mafic/ultramafic dykes within the deposit makes these dykes a potential source for the Nd component of the deposit, and thus a likely source of metals (i.e. Cu) (Johnson and McCulloch, 1995).

Haynes et al. (1995) proposed that fluid mixing was the dominant ore-forming process at Olympic Dam. In their model, the mixing of a hotter magmatic or deeply circulated meteoric water (<300℃) and a cooler meteoric water, which may have originated as saline ground water or playa lake water within the volcanic succession, was thought to be responsible for ore genesis. Moreover, their modelling supported the hypothesis that precipitation of magnetite, hematite, sulfides, and uraninite resulted from coupled sulphate reduction and ferrous iron oxidation and that the cooler meteoric waters were oxidized and were derived from a provenance containing mafic volcanic rocks with or without a felsic component. They also concluded that the ODBC contained a major Cu-U-Au-Ag orebody because it formed within a reservoir of saline ground water in contact with mafic and felsic volcanics and subvolcanic intrusions and the ground water was responsible for transport of Cu, U, Au, Ag and most of the S into the breccia complex, where it interacted with the hotter water which introduced most of the Fe, F, Ba, and CO_2 from below. However, they also pointed out that the weak

point of this modelling was that copper and uranium would be supplied to the ore-forming process by hotter waters if their temperature is above 300℃.

The eastern Gawler Craton hosts Australia's premier uranium-bearing iron oxide copper-gold belt, the >500-km-long Olympic Cu-Au-(U) Province, where there are the Olympic Dam Cu-U-Au and Prominent Hill Cu-Au deposits, together with numerous barren and weakly mineralised IOCG prospects. A general investigation of the whole province was conducive to the exploration in this brownfield terrain (Skirrow et al., 2007). Nd isotope compositions for whole rock samples from barren and weakly mineralised Cu-Au prospects and host rocks in the Olympic Dam and Prominent Hill districts (Skirrow et al., 2007) were compared with previous data from Johnson and McCulloch (1995). Both hematite- and magnetite-rich samples from five weakly mineralised prospects yielded generally similar initial εNd_{1590Ma} values that match values from fresh and weakly altered Paleoproterozoic metasedimentary and metagranitic rocks (-6.6 to -3.5, including the Donington Suite, the upper and lower Wallaroo Group), as well as from most felsic HS intrusions and GRV in the eastern Gawler Craton (-6 to -4). These data implied that mainly crustal sources (could not be specified, however) contribute REE, and by implication, Cu to the barren and weakly mineralised prospects (Nd isotope signature is roughly correlated to Cu concentration in whole-rock samples of the altered granitoids and mineralised hematite-rich breccias from the Olympic Cu-Au-(U) Province, indicating that Nd and Cu were co-transported in the same hydrothermal fluids, see Skirrow et al., 2007). However, pyrite, chalcopyrite, and bornite-chalcocite-rich hematitic ore samples at Olympic Dam have higher εNd (-2.5, Johnson and McCulloch, 1995), and there is a roughly positive correlation between Nd isotope signature and Cu concentration but no correlation in the plot of SiO_2 versus initial εNd, which overall indicates that mantle (primitive) sources contributed REE and possibly Cu to the Olympic Dam deposit in the way of hydrothermal process rather than magmatic process (Skirrow et al., 2007).

Bastrakov et al. (2007) proposed a two-stage hydrothermal activity model. In this model, early stage pre-existing hydrothermal magnetite with minor associated copper-gold mineralization was flushed by late-stage oxidized brines that had extensively reacted with sedimentary or metamorphic rocks. The reduction of these brines, driven by conversion of magnetite to hematite, resulted in precipitation of copper and gold,

and the oxidized brines may have contributed additional copper and gold to the system in addition to upgrading pre-existing subeconomic Cu-Au mineralization. At last, they assigned the different abundances of ore between the giant Olympic Dam deposit and those weakly mineralised prospects to the diversity of origins of iron oxide-copper-gold systems, even within the same geologic region. Stable isotope analysis was carried out to place further restrictions on the origin of the hydrothermal fluids of different stages. The Br/Cl ratios of the magnetite-forming fluids lie beyond the range of typical magmatic and/or mantle values, allowing for the possibility that the fluids originated as brines from a sedimentary basin or the crystalline basement.

In the most recent synthesis of the Olympic Dam deposit in Ehrig et al. (2012), a detailed analysis of a large dataset of the compositions of the ODBC gathered over years has shown that some elements (Al, Be, Ca, Hf, K, Li, Mg, Mn, Na, Rb, Si, Th, Ti, and Zr) are negatively correlated with Fe, whereas other elements (Ag, As, Au, Ba, Bi, Cd, Co, CO_2, Cr, Cu, F, Fe, In, Mo, Nb, Ni, P, Pb, S, Sb, Se, Sn, Sr, Te, U, V, W, Y, Zn, and REE) are positively correlated with Fe. The former elements are considered as granite-derived elements that are likely to be contributed from the Roxby Downs Granite, whereas the other elements have been named hydrothermal elements, which have a provenance from other lithologies (e.g. mafic dykes, bedded clastic facies).

2.3 Other IOCG prospects and deposits in the Olympic Cu-Au-(U) Province

2.3.1 Acropolis and Wirrda Well prospects

The Acropolis and Wirrda Well prospects are situated to the south-western margin of the Burgoyne Batholith, ~20 km south-west of Olympic Dam. Subeconomic hydrothermal IOCG-type mineralisation was found in basement rocks at both prospects by Western Mining Company during a program of regional exploration drilling subsequent to the Olympic Dam discovery. The minimum thickness of barren Stuart Shelf sedimentary cover (and Mesoproterozoic Pandurra Formation at Acropolis) unconformably overlying basement rocks at Acropolis and Wirrda Well are ~480 and ~330 m, respectively, and zones of Cu-(U-Au) mineralisation occur tens to hundreds of metres beneath the unconformity.

Most of the mineralisation at Acropolis occurs as magnetite ± hematite-rich vein networks and alteration zones are hosted within pervasively sericite-altered and locally chlorite-altered felsic GRV, comprising ash flow tuffs and felsic to intermediate volcanic rocks, and only a minor amount is known to be hosted by granitic breccia (Paterson, 1986; Parker, 1990; Cross, 1993). The GRV overlie laminated siltstones, most likely of the ca. 1770 to 1740 Ma Wallaroo Group, foliated granite (syn-Kimban Orogeny, the ca. 1850 Ma Donington Suite), and diorite, all of which display strong hematite ± magnetite ± sericite ± chlorite alteration (Cross, 1993). Sulfide mineralisation is associated with the iron oxides, occurring as pyrite with local development of chalcopyrite, and associated barite, fluorite, phlogopite. Sparse drilling has revealed a potential zonation from pyrite to chalcopyrite and locally to bornite. Uranium and to a lesser extent REE mineralisation is mostly found within the main iron-rich lenses.

Brecciation and hematite development are more widespread at Wirrda Well than at Acropolis, and consequently, the Fe-Cu-(U-Au) mineralisation at Wirrda Well more closely resembles that of Olympic Dam. Mineralisation occurs as magnetite-hematite vein networks and alteration zones occur in the brecciated and hematite-altered GRV, and in the underlying metasediments of Hutchison group and granites of the HS Burgoyne Batholith and the Donington Suite.

Iron-rich hydrothermal mineral assemblages at Acropolis were generally deposited at higher maximum temperatures (550 to 440℃ from magnetite-K-feldspar ± quartz ± apatite veins) and under more reduced conditions than those at Wirrda Well which generally record higher temperature and more reduced conditions than those at Olympic Dam (500 to 200℃) (Oreskes and Einaudi, 1992).

2.3.2 Prominent Hill iron oxide Cu-Au deposit

The Prominent Hill iron oxide Cu-Au deposit is located approximately 150 km north-west of Olympic Dam and 650 km NNW of Adelaide in northern South Australia. An applied exploration model focusing specifically at the hematite end member of the IOCG deposit led to the discovery of this deposit in the southern Mount Woods Inlier, which is an aeromagnetically defined region of shallow Paleoproterozoic and Mesoproterozoic basement rocks (Belperio et al., 2007; Schlegel and Heinrich, 2015).

The mineralised breccias and host volcanic-volcaniclastic rocks at Prominent Hill are strongly influenced by major regional NE- and NW-trending conjugate crustal structures, i.e. Bulgunnia (sinistral strike-slip) and Fitzgerald (high-angle reverse) shear zones, respectively.

Four principal domains around Prominent Hill are defined, based on the distribution of host rocks, breccia units, and alteration and mineralisation (Belperio et al., 2007). Domain 1 is located to the north of Prominent Hill, consisting of amphibolite- to granulite-facies Paleoproterozoic metasedimentary rocks. Domain 2 is largely made up of bimodal volcanic rocks ranging from basalt, basaltic andesite to andesite (especially south of Prominent Hill), to interlayered basalt, andesite, dacite and rhyodacite west of Prominent Hill. Domain 3 is characterized by volcaniclastic rocks which are the most intensely altered and modified by hematitic hydrothermal alteration, brecciation, and mineralization. Four types of hematite breccias that hosted the ore deposit are recognized within this domain. Domain 4 is characterized by abundant magnetite and skarn-like metasomatic rocks indicative of higher metamorphic grade.

Four principal styles of mineralization are recognized in accordance with four types of hematite breccias in domain 3: (1) chalcocite + gold ± bornite ± covellite ± digenite (in hematite-sericite matrix breccias), (2) chalcopyrite + gold ± bornite ± uraninite ± fluorite ± pyrite (in hematite-fluorite matrix breccias), (3) gold + hematite + silica + barite (in steely hematite breccias), (4) gold + hematite + carbonate (in earthy hematite matrix breccias). The hematite-sericite matrix breccias carry the highest copper and gold grades (typically 2.5 wt.% copper and 0.6 g/t gold), then come the hematite-fluorite matrix breccias, which typically have copper and gold grade of 1.4 wt.% and 0.6 g/t. Uranium is enriched in the hematite-fluorite matrix breccias, closely associated with chalcopyrite, and this is significantly different from Olympic Dam, where uranium is reported highest in concentration in the upper parts of the chalcocite-bornite zone (Reeve et al., 1990; Cross, 1993). Bornite coexists with chalcocite and chalcopyrite, but chalcocite and chalcopyrite are not observed together (Belperio et al., 2007).

Chapter 3 Neoproterozoic (ca. 820-830 Ma) mafic dykes at Olympic Dam, South Australia: Links with the Gairdner Large Igneous Province*

Qiuyue Huang[1], Vadim S. Kamenetsky[1], Jocelyn McPhie[1], Kathy Ehrig[2], Sebastien Meffre[1], Roland Maas[3], Jay Thompson[1], Maya Kamenetsky[1], Isabelle Chambefort[1,4], Olga Apukhtina[1], Yongbin Hu[5]

[1]School of Physical Sciences, University of Tasmania, Private Bag 79, Hobart, Tasmania, Australia 7001

[2]BHP-Billiton, GPO Box 1777, Adelaide, South Australia 5001, Australia

[3]School of Earth Sciences, University of Melbourne, VIC 3010, Australia

[4]GNS Science, Wairakei Research Centre, Taupo 3377, New Zealand

[5]Guangzhou Institute of Geochemistry, Chinese Academy of Sciences, Guangzhou 510640, China;

*Manuscript published in Precambrian Research (2015), volume 271, pages 160-172. DOI:10.1016/j.precamres.2015.10.001

Abstract

A suite of basaltic to doleritic dykes (named the Olympic Dam dolerite) has been intersected in drill holes at the Olympic Dam iron oxide Cu-U-Au-Ag deposit in the Gawler Craton, South Australia. The dykes intrude the ca. 1600 Ma Roxby Downs Granite as well as the Olympic Dam Breccia Complex, and range from several centimetres to over one hundred metres in width, strike NW and dip subvertically. Clinopyroxene and plagioclase are the major minerals, together with accessory apatite and Ti-magnetite. Magmatic apatite crystals in medium-grained doleritic dykes have been dated by LA-ICPMS (Laser Ablation Inductively Coupled Plasma Mass Spectrometry), and yielded a U-Pb age of 825 ± 18 Ma. The Olympic Dam dolerite has invariably been altered. Secondary apatite and titanite crystals from post-magmatic veinlets cutting the same dykes give similar results of 821 ± 15 Ma and 817 ± 11 Ma, respectively. All these results are, within error, coincident in age with the Gairdner Dyke Swarm, the longest dyke swarm (~1,000 km in length) in Australia. The Olympic Dam dolerite shows similar compositional trends and variations to the Gairdner Dyke Swarm, especially in terms of the relatively immobile High Field Strength Elements (HFSE) and Rare Earth Elements (REE). We conclude that the Olympic Dam dolerite belongs to the Gairdner Dyke Swarm, expanding its known extent and compositional range. The Gairdner Dyke Swarm is a major component of the ca. 820 Ma Gairdner Large Igneous Province (LIP) generated during the break-up of the supercontinent Rodinia. The ca. 1070 Ma Warakurna and the ca. 820 Ma Gairdner LIP in Australia are compositionally distinct, whereas the Gairdner LIP and LIP and mafic suites (Guibei LIP and Kangding LIP in China, and Gunbarrel mafic suite in North America) associated with the break-up of Rodinia in South China and North America are broadly similar. This provides geochemical support for a Gairdner LIP origin for some mafic suites, in particular the Beda Volcanics in South Australia, and for a juxtaposition of South China, South Australia and North America in the tectonic reconstruction of Rodinia at ca. 820 Ma.

Key Words

Olympic Dam, Gairdner Dyke Swarm, Large Igneous Province, Rodinia, dolerite, apatite U-Pb

3.1 Introduction

Large Igneous Provinces (LIP) consist of voluminous lavas (>0.1 Mkm^3), sills and dyke swarms which are emplaced in short duration (>75% of the total volume of igneous rocks in ca. 1-5 Myr); the maximum lifespan duration is ca. 50 Myrs (Coffin and Eldholm, 1994; Bryan and Ernst, 2008). The Gairdner LIP in Australia mainly consists of northwest-striking mafic dykes, including dominantly the Gairdner Dyke Swarm in the Gawler Craton, the Amata Dyke Swarm in the Musgrave Block and scattered dykes in Western Australia; the Wooltana Volcanics and Little Broken Hill Gabbro are additional components (Fig. 3.1a) (Zhao et al., 1994; Claoué-Long and Hoatson, 2009). The age of 827 ± 6 Ma obtained from a drill core sample of the Gairdner Dyke Swarm dolerite (Wingate et al., 1998) has been suggested to represent the age of the Gairdner LIP (Fig. 3.1a, Claoué-Long and Hoatson, 2009). However, more geochronological studies are required to better define the main episode of Gairdner LIP magmatism as well as its duration.

The Gairdner LIP overlaps spatially with the Warakurna LIP (ca. 1070 Ma, Wingate et al., 2004), which extends east-west across western and central Australia (Fig. 3.1) and includes the east-west striking Alcurra Dyke Swarm. These two LIP were contemporaneous with the assembly (Warakurna LIP) and break-up (Gairdner LIP) of the supercontinent Rodinia (Li et al., 2008; Pirajno and Hoatson, 2012). Various suites originally assigned to the Gairdner LIP based on composition and location (Crawford and Hilyard, 1990) have subsequently been shown to match the age of the Warakurna LIP (e.g. Beda Volcanics and RD222 dyke at Olympic Dam, Fig. 3.1, Webb and Coats, 1980; Creaser, 1989); accordingly, the extent and limits of these two LIP remain to be determined.

Igneous units generated during continental break-up may be separated and may exist as separate LIP on different continents (e.g. ca. 180 Ma Karoo LIP in Africa and Ferrar LIP in Antarctica, ca. 130 Ma Parana LIP in South America and Etendeka LIP in Africa, all associated with the break-up of Gondwana, Veevers, 2004). The ca. 820 Ma Gairdner LIP (Australia), the ca. 820 Ma Guibei LIP and the ca. 780 Ma Kangding LIP (South China), and the ca. 780 Ma Gunbarrel mafic suite (North America) are thought to be associated with the break-up of the supercontinent Rodinia (Li et al., 2008,

and references therein). However, there is still a lack of data on the Gairdner LIP, an integral part of Rodinia break-up.

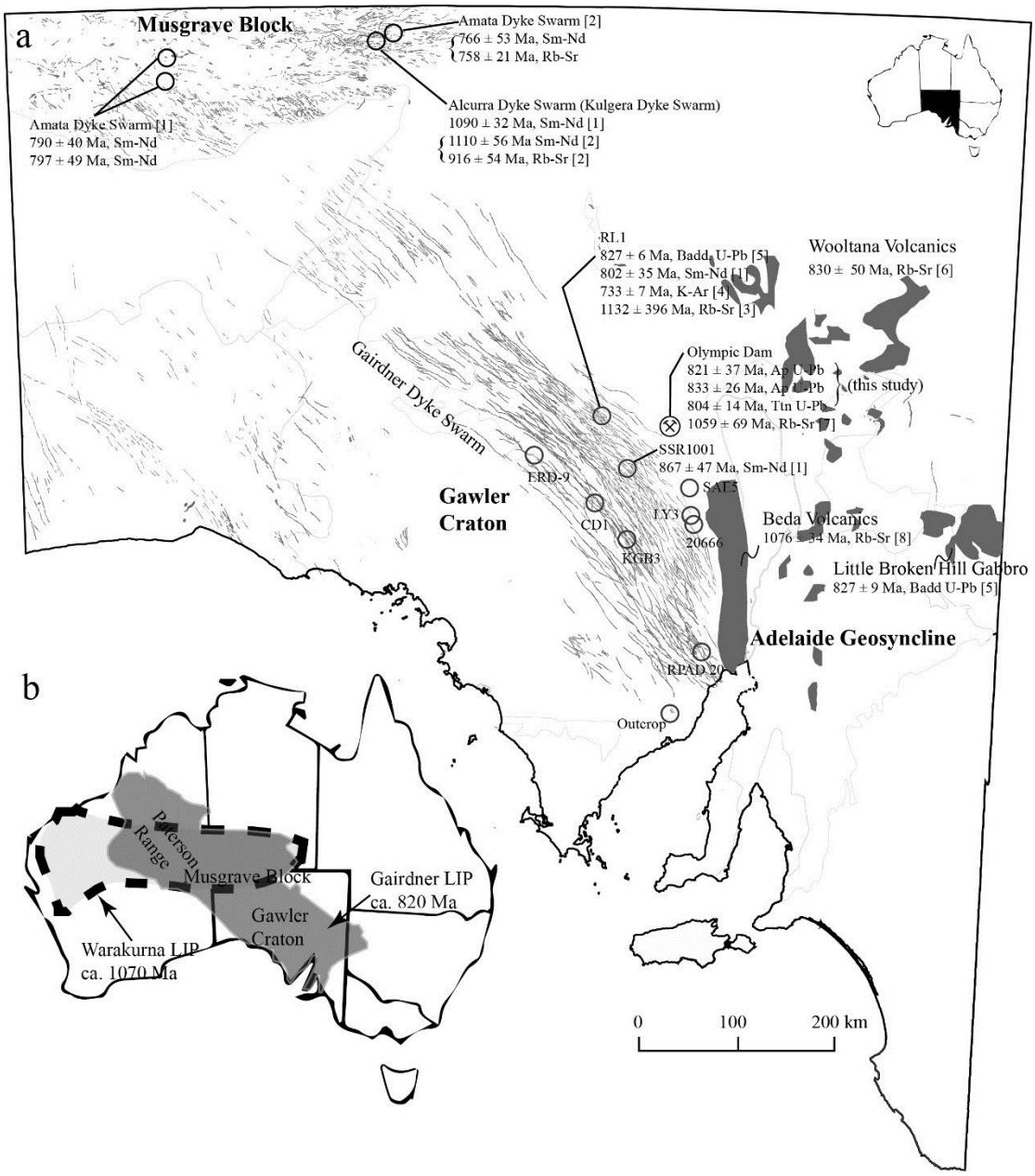

Figure 3.1 (a) Geological map of South Australia, showing major igneous suites within the Gairdner LIP, including the Wooltana Volcanics, the Little Broken Hill Gabbro, the Gairdner Dyke Swarm, and the Amata Dyke Swarm, as well as the Alcurra Dyke Swarm from the Warakurna LIP (modified after Crawford and Hilyard, 1990; Hoatson et al., 2007). Locations of nine drill holes and one outcrop are marked to show the places where the Gairdner Dyke Swarm has been intersected or exposed (drill core locations from the SARIG database, https://sarig.pir.sa.gov.au/Map). The affiliation of the Beda Volcanics remains to be determined, see text for discussion. Dating results are from the following: [1] Zhao and

McCulloch (1993), [2] Werner et al. (2014), [3] Fanning (1984), [4] Cowley and Flint (1993), [5] Wingate et al. (1998), [6] Compston et al. (1966), [7] Creaser (1989), [8] Webb and Coats (1980). (b) The extent of the ca. 1070 Ma Warakurna LIP and ca. 820 Ma Gairdner LIP in Australia (modified after Claoué-Long and Hoatson, 2009).

Dyke swarms are generally better preserved than lavas and may provide the best or the only record of many continental LIP (Ernst and Buchan, 1997). Studies of the Gairdner LIP have been hampered by poor exposure because younger cover sequences are widespread and most of the samples come from drill core (Fig. 3.1a). Here we present the results of a petrological, geochemical, and geochronological study of the basaltic to doleritic dykes intersected by drilling at the Olympic Dam iron oxide Cu-U-Au-Ag deposit in South Australia. We confirm, through U-Pb dating of primary magmatic apatite and secondary apatite and titanite, that these dykes are the same as the ca. 820 Ma Gairdner Dyke Swarm and Gairdner LIP. New geochemical and Nd isotope data for the Olympic Dam dykes are used to re-assess the compositional range of the Gairdner LIP. Finally, we compare the compositions of the Gairdner LIP with those of (i) the ca. 1070 Ma Warakurna LIP in Australia and (ii) other Rodinia break-up related mafic suites in North America and South China, and briefly discuss the implications for petrogenesis and tectonic setting.

3.2 The Gairdner LIP and the Olympic Dam deposit

The Gairdner Dyke Swarm in the Gawler Craton, South Australia was first recognized on aeromagnetic images as a NW-trending array of linear magnetic anomalies (Fig. 3.1, Boyd in Goode, 1970). Goode (1970) correlated this dyke swarm with the similarly striking Amata Dyke Swarm in the Musgrave Block, and reported a total length of ~1,000 km for the combined Gairdner-Amata Dyke Swarm (Fig. 3.1a). Compositional similarity of the Gairdner Dyke Swarm and other igneous suites such as the Wooltana Volcanics and Beda Volcanics led Crawford and Hilyard (1990) to suggest that these units constitute an igneous province named the "Willouran basic province", which covered an area of at least 210,000 km^2 and had an estimated volume of 105,000 km^3. Zhao et al. (1993, 1994) produced Sm-Nd isochron ages for the Gairdner (867 ± 47 Ma and 802 ± 35 Ma) and Amata dyke swarms (790 ± 40 Ma and 797 ± 49 Ma, Fig. 3.1c) and proposed a mantle plume origin for the Willouran basic province and the Amata Dyke Swarm. The emplacement age for the Gairdner Dyke

Swarm in the Gawler Craton was subsequently better constrained at 827 ± 6 Ma using U-Pb in baddeleyite by Wingate et al. (1998). Zircon U-Pb ages of dolerite dykes and sills from the western Musgrave Block and Paterson Range of Western Australia also yielded results of ca. 820-830 Ma (Hoatson et al., 2008a, 2008b) . These suites, together with the Willouran basic province, have been put together to constitute the Gairdner LIP (Fig. 3.1a) by Claoué-Long and Hoatson (2009).

The supergiant Olympic Dam iron oxide Cu-U-Au-Ag ore deposit occurs in the north-eastern Gawler Craton (Fig. 3.1a, Reeve et al., 1990). The ore body is hosted by the Olympic Dam Breccia Complex within the Mesoproterozoic Roxby Downs Granite (1593.1 ± 5.6 Ma, Jagodzinski, 2014). Several mafic facies (mainly dykes) including picrite and dolerite are present at Olympic Dam (Reeve et al., 1990; Ehrig et al., 2012) . Earlier attempts to date the dolerite include a Rb-Sr isochron age of 1059 ± 69 Ma (Creaser, 1989) and a K-Ar age of ca. 610 Ma (Cowley and Flint, 1993). The recent recovery of relatively fresh basaltic to doleritic dykes containing magmatic apatite provide a chance to investigate their age and origin.

3.3 Occurrence and petrography

The basaltic to doleritic dykes (herein named the Olympic Dam dolerite) intrude the Roxby Downs Granite (Fig. 3.2) and the Olympic Dam Breccia Complex. The Olympic Dam dolerite is characterized by its generally fresher appearance and better competency, as well as higher magnetic susceptibility, compared to other mafic facies. The dolerite dykes range from several metres to over 100 m in width, and dykelets of a centimetre width also occur. These dykes are generally subvertical and can be traced along a NW strike for up to 3 km (Ehrig et al., 2012).

Underground subhorizontal drill holes provide many cross sections of the Olympic Dam dolerite dykes. The dykes commonly display chilled margins along contacts with the Roxby Downs Granite, and the texture varies continuously from aphanitic, aphyric, porphyritic, fine-grained doleritic (< 1 mm) to medium-grained (~1 to 3 mm) doleritic (Fig. 3.3c) towards the centre of the dyke. Euhedral to sub-euhedral clinopyroxene and plagioclase are the dominant mineral phases. Minor Ti-magnetite occurs both as phenocrysts and in the groundmass. Phenocrysts of clinopyroxene and plagioclase (less than ~2 mm in size) show a glomerophyric texture (Fig. 3.3a). There is no preferred

alignment of the plagioclase laths. In the porphyritic samples, the groundmass ranges in texture from formerly glassy (now altered), cryptocrystalline, microcrystalline to fine-grained, and such textural variation may be observed within one thin section. Olivine occurs as rare phenocrysts but has been completely altered to a secondary mineral assemblage of chlorite and quartz. In the fine- to medium- grained doleritic texture that occurs in the middle portions of the dykes, accessory Ti-magnetite and apatite fill the interstices between plagioclase and clinopyroxene (Fig. 3.3c).

Figure 3.2 The Olympic Dam dolerite in contact with the Roxby Downs Granite. More than one generation of dyke emplacement occurred, as shown by the early doleritic dyke (pale grey) intruded by fine-grained basaltic dyke (dark grey with black chilled margin).

Many dykes comprise multiple generations (Fig. 3.2), evident from the presence of internal, generally sharp chilled margins (formerly glassy and perlitic, now altered, Fig. 3.3a, b). The internal chilled margins suggest the earlier intrusion had cooled before the injection of a later pulse of magma. In most cases, early porphyritic to doleritic dykes were intruded by later porphyritic dykes (Fig. 3.2, 3.3a, b). The later porphyritic dykes appear darker and are generally less than a few metres in width. The younger dykes commonly occupy the centre of the older dykes rather than follow the intrusive contacts of the early dyke. This relationship could indicate that a plane of weakness formed along the middle of the early dykes due to contraction accompanying cooling inward from both sides (intrusive contacts).

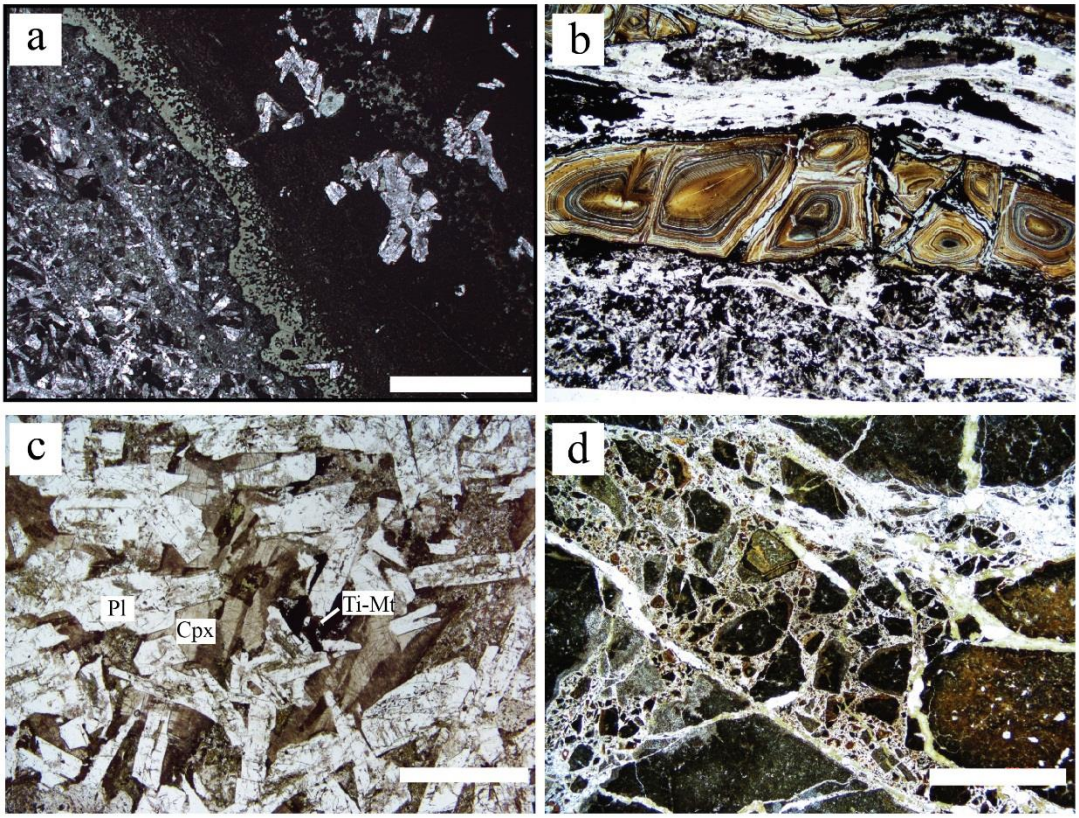

Figure 3.3 Photomicrographs of the Olympic Dam dolerite. (a, b) Porphyritic dyke intrudes a doleritic dykes, and chilled margin is present along the intrusive contact. The former glassy margin in (b) has been altered to palagonite. (c) Medium-grained dolerite, mainly made up of clinopyroxene (Cpx), plagioclase (Pl) and Ti-magnetite (Ti-Mt). (d) Brecciated Olympic Dam dolerite composed of cryptocrystalline to micro-porphyritic clasts cemented by secondary minerals including chlorite, sericite, quartz and carbonate. All the photo micrographs have been taken under plane-polarized light. The scale bars represent 2 mm.

The Olympic Dam dolerite dykes are brecciated along the contacts with the Roxby Downs Granite and the Olympic Dam Breccia Complex (Fig. 3.3d). The brecciated zones generally extend for several metres in both directions away from the intrusive contacts. Brecciated Olympic Dam dolerite is typically clast-supported and commonly shows jigsaw-fit texture; clast-rotated texture is less common. The matrix in the brecciated Olympic Dam dolerite comprises angular to subangular fragments of dolerite, granite and hematite, and crystalline cement of secondary minerals, for example, chlorite, quartz and carbonate (Fig. 3.3d).

The Olympic Dam dolerite is invariably altered. The primary minerals and textures are largely preserved in the interior of the dykes. In the most intensely altered dolerite dykes the primary minerals have been replaced by a secondary mineral assemblage of quartz, chlorite, sericite, albite and locally pumpellyite and carbonates, and also minor titanite, rutile, apatite, magnetite, hematite, pyrite, chalcopyrite, sphalerite and galena. The most intensely altered Olympic Dam dolerite occurs along the intrusive contacts with the Roxby Downs Granite and the Olympic Dam Breccia Complex. Crosscutting veinlets comprising similar secondary minerals are common.

3.4 Analytical methods

3.4.1 Whole-rock major and trace element concentrations

Major and trace elements of whole-rock samples were analysed at the School of Physical Sciences, University of Tasmania, on a Philips PW1480 X-ray Fluorescence Spectrometer and an Agilent 4500 induced coupled plasma-mass spectrometer. Loss on ignition was determined at 1000°C and corresponds to the release of carbon, hydrogen, sulfur (sulfide S but not sulfate S) and a gain due to oxidation in the furnace of Fe^{2+} to Fe^{3+}.

3.4.2 Whole-rock Nd isotope concentrations

Whole-rock Nd isotope data were acquired at the State Key Laboratory of Isotope Geochemistry, Guangzhou Institute of Geochemistry (GIG), Chinese Academy of Sciences (CAS), following the method of Yang et al. (2009). Sample powders were dissolved at low pressure, followed by extraction of Nd using cation exchange and HDEHP chromatography columns. Nd isotope data obtained by MC-ICPMS were normalized to $^{146}Nd/^{144}Nd=0.7219$ and are reported relative to a value of 0.511860 for the La Jolla Nd standard. External precision, estimated from the long-term reproducibility of standards, is approx. ±0.000014 (2sd, Yang, 2009). $^{143}Nd/^{144}Nd$ results for international standards (e.g. La Jolla 0.511849 ± 14; BCR-2 ~0.512638; BHVO-2 ~0.512979) are consistent with TIMS and MC-ICPMS reference results. Sm/Nd ratios for age correction were constrained from trace element data obtained by solution-mode quadrupole ICPMS analyses of separate powder splits (Table 3.1); the resulting $^{147}Sm/^{144}Nd$ ratios have an external precision of ±2%. εNd values are

calculated using the chondrite averages of Bouvier et al. (2008); the Sm decay constant is 6.54×10^{-12}/yr .

3.4.3 U-Pb apatite and titanite dating

U-Th-Pb dating of apatite and titanite was carried out using laser-ablation ICPMS (e.g. Chew et al., 2014 and references therein) on polished rock samples mounted in 25 mm diameter epoxy mounts. Apatite and titanite were recognised using a scanning electron microscope. The crystals were analysed using a Coherent Scientific 193 nm Ar-F excimer gas laser coupled with a Resonetics S155 ablation cell and an Agilent 7500cs quadrupole ICPMS at the University of Tasmania. Both apatite and titanite were ablated in a helium atmosphere (0.35 litres / minute) using a 32 μm laser spot (5 Hz, energy density ~2 J/cm^2). Following a 30 second gas blank samples were ablated for 30 seconds. Ablation in the S155 ablation cell is carried out in He, followed by transfer to the ICP-MS torch in argon via nylon tubing; a mixing manifold (squid) was applied in this work. The isotopes measured were ^{31}P, ^{49}Ti, ^{43}Ca, ^{56}Fe, ^{140}Ce, ^{202}Hg, ^{204}Pb, ^{206}Pb, ^{207}Pb, ^{208}Pb, ^{232}Th and ^{238}U (5 ms dwell time for the major and trace elements, 20 ms for the Pb isotopes, and 10 ms for Th and U). Downhole fractionation, instrument drift and mass bias in apatite analyses were corrected using an in-house apatite standard, OD306, a coarse-grained apatite from an apatite-magnetite vein at the Acropolis Cu-Au prospect in South Australia. Isotope dilution U-Pb data obtained for 6 mg-sized (1.3-4.5 mg) fragments by MC-ICP-MS at the University of Melbourne (e.g. Woodhead and Pickering., 2012) show modest U contents (15-19 ppm), Th/U ~4.8 and variable but generally low common Pb contents (measured ^{206}Pb/^{204}Pb 336-1556, f_{206}=0.011-0.051, n=6, R.Maas, 2012, unpubl. data). After common Pb correction, the data yield concordant to near-concordant (≤2.5% disc.) ^{207}Pb/^{206}Pb ages averaging 1598 ± 4 Ma (2 standard error) and a formal discordia intercept of 1594 ± 7 Ma. At the sampling scale of the laser, the apatite shows a high degree of homogeneity in Pb/U ratios and little evidence of the variable common Pb seen in the bulk analyses. Kovdor and Otter Lake apatite (Amelin and Zaitsev, 2002; Chew et al., 2011; Barfod et al., 2005) were monitored as secondary standards; the ^{207}Pb-corrected ^{206}Pb/^{238}U ages obtained for these crystals are well within error of published reference ages (Table S1). OD306 apatite was preferred as primary standard over the Otter Lake or Kovdor apatites because it provides more homogeneous Pb/U data on the UTAS laser ablation system

(internal precision ±1.1%, n=10 compared to ±1.4% and ±3.9% for Otter Lake and Kovdor, respectively, each based on n=10 analyses), has lower common Pb at the laser sampling scale, and its U-Th contents closely match those in the apatites measured here. Recalculation of the data for apatites from OD850 and 852 with Otter Lake apatite as primary standard yields a concordia intercept age of 810 ± 17 Ma, compared to 821 ± 15 Ma (MSWD=0.60) if OD306 is used. While these ages overlap within errors, it is clear that LA-ICPMS U-Pb dating of apatite has issues similar to those described for zircon (e.g. Black et al., 2004; Klötzli et al., 2009; Allen and Campbell, 2012).

Titanite raw data were corrected with reference to another in-house standard, AUR100606, a magmatic titanite from a mafic intrusion in North Queensland. ID-TIMS U-Pb isotope data for microgram-sized samples obtained at the University of British Columbia are near concordant and define an age of 432.02 ± 0.64 Ma (Best, 2012). Primary standards were analysed at the beginning of each session and between sets of 15 unknowns (i.e. roughly every 30 minutes). Pb isotopic mass bias was monitored using regular analyses of the NIST610 glass (e.g. Baker et al., 2004; Jochum et al., 2011). Data reduction was done using in-house software (e.g. Halpin et al. (2014), with common Pb corrections based on the techniques of Chew et al. (2011, 2014).

3.5 Geochronology

U-Pb geochronology was performed at the University of Tasmania. Magmatic apatite from sample OD850 and OD852, and secondary apatite and titanite from sample OD199, have been analysed in this study using the LA-ICPMS technique (Table 3.1, see Methods for analytical details).

Samples OD850 and OD852 are from drill hole RU65-8230 at 544.1 m and 596.1 m, respectively. These two samples came from the same dyke and are medium-grained (~1 to 2 mm) dolerite composed of clinopyroxene, plagioclase, Ti-magnetite and magmatic apatite. The samples have been slightly hydrothermally altered: clinopyroxene has been partly altered to chlorite, and Ti-magnetite has been partly altered to hematite. Apatite is interstitial between clinopyroxene and plagioclase, typically needle-shaped to tabular, and up to 1.2 mm in length, and has an aspect ratio close to 10 (Fig. 3.4a). Magmatic apatite crystals from both samples have low U contents (2 to 24 ppm) and variable Th/U ratios (3 to 9). During analysis, other silicate

phases such as clinopyroxene and plagioclase were analyzed in addition to apatite to better constrain the common Pb composition for these two samples (Fig. 3.4a, red diamonds). The U-Pb results of apatite and silicate phases for OD850 and OD852 define a single scattered array on the Tera-Wasserburg diagram using Isoplot 3.1 (Ludwig, 2003), consistent with mixing of common Pb (intercept on $^{207}Pb/^{206}Pb$ axis = 0.881) and radiogenic Pb (lower intercept) generated by in situ decay since 823 ± 18 Ma (MSWD=0.90). In Stacey and Kramers' (1975) two-stage model for Pb isotopic evolution, common Pb composition at ca. 820 Ma has a $^{207}Pb/^{206}Pb$ ratio of 0.8941. If we use this common Pb composition as an anchor, an age of 825 ± 18 Ma (MSWD=0.89) is obtained (Fig. 3.4a).

Secondary apatite occurs in the Olympic Dam dolerite in post-magmatic veinlets together with other secondary minerals. Compared to the magmatic apatite, the secondary apatite has variable grain sizes and is overall finer (from less than 0.1 mm to more than 0.5 mm) and mostly present as equant crystals rather than long tabular crystals (Fig. 3.4b). Secondary apatite occurs in sample OD199 (drill hole RD2773, 1329.2 m) which is altered plagioclase-clinopyroxene-phyric dyke. The secondary apatite has low U contents (1 to 8 ppm) and uniformly low common Pb contents but the Th/U ratios are higher (5-14) than in the magmatic apatite in OD850 and OD852. As a result, the U-Pb isotope analyses of apatite crystals cluster near the concordia (Fig. 3.4b). After ^{207}Pb-correction using Stacey and Kramers' (1975) two-stage common Pb composition at 820 Ma, an average lower intercept age of 821 ± 15 Ma (MSWD=0.60) is obtained. This age is taken as the best estimate of the crystallization of the secondary apatite in OD199.

Secondary titanite occurs as rims on primary Ti-magnetite in the Olympic Dam dolerite or as separate grains in post-magmatic veinlets cutting the dolerite. Titanite from a chlorite-quartz-calcite veinlet in sample OD199 displays classic titanite crystal shapes (flat wedge) and grain sizes in the range from ~0.1 to 0.3 mm (Fig. 3.4c). U (10

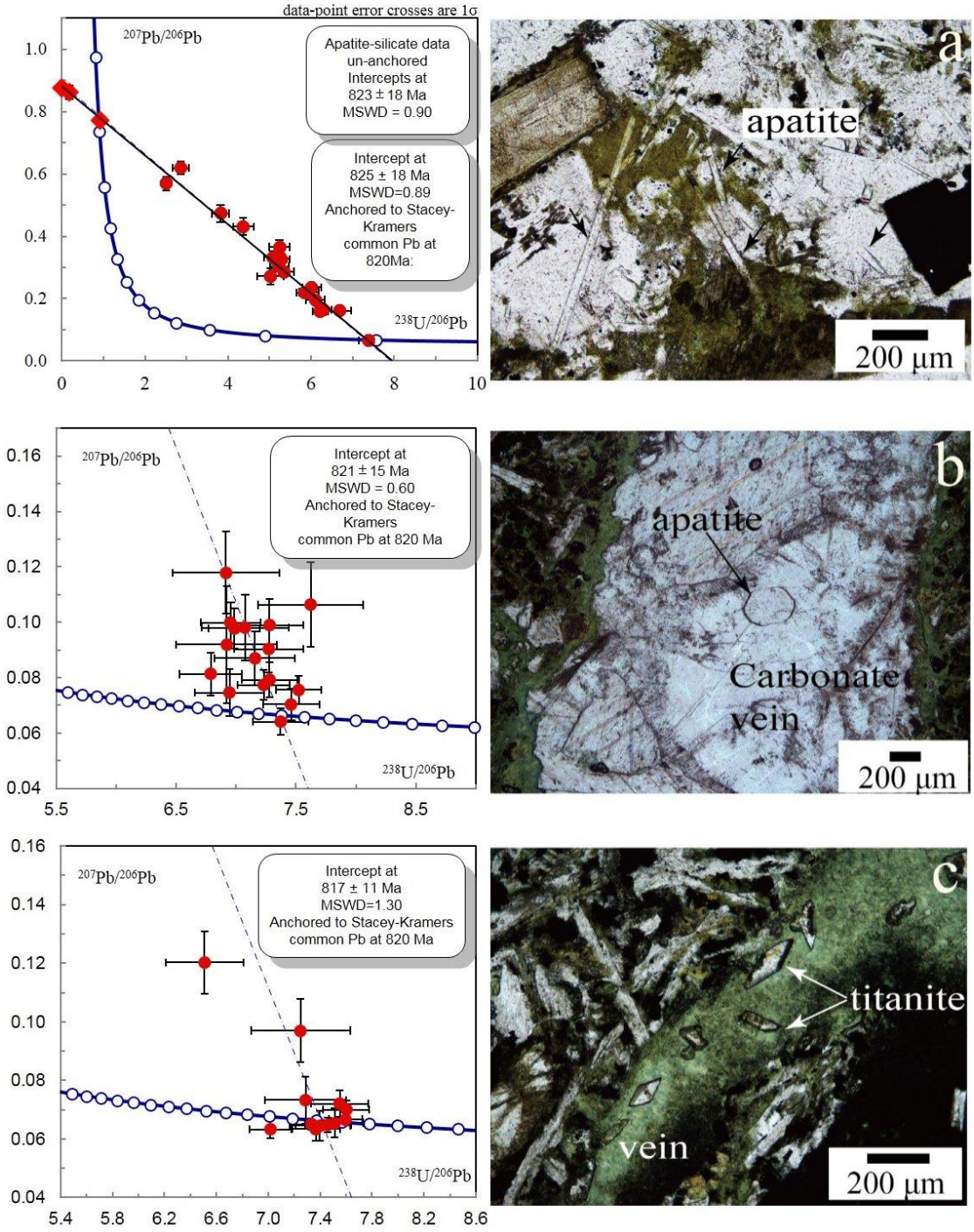

Figure 3.4 Dating results and sample photomicrographs of (a) magmatic apatite, (b) secondary apatite and (c) titanite in the Olympic Dam dolerite. Red diamonds indicate analyses of clinopyroxene and/or plagioclase in samples OD850 and OD852.

to 460 ppm) and Th (17 to 96 ppm, Th/U ratios of 0.1 to 1.6) contents are relatively low (Table 3.1). U-Pb isotope results for titanite grains show a narrow range of compositions and plot close to the concordia (Fig. 3.4c). Using Stacey and Kramers'

(1975) two-stage common Pb composition at 820 Ma, an age of 817 ± 11 Ma (MSWD=1.30) is obtained (Fig. 3.4c).

3.6 Whole-rock geochemistry

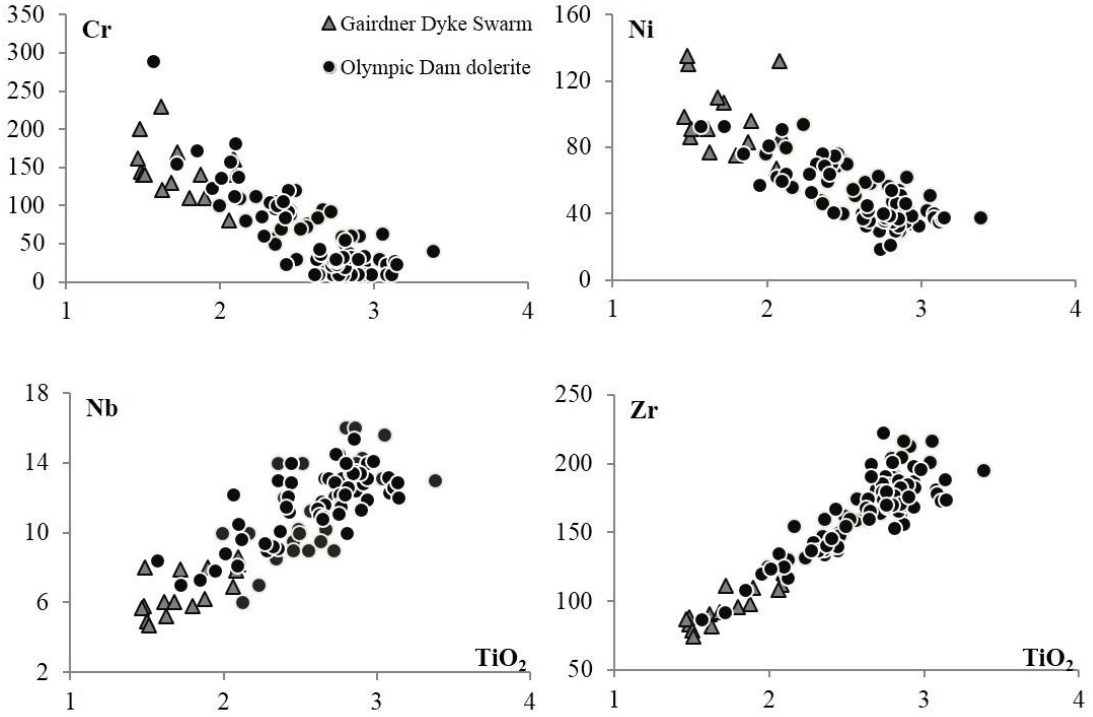

Figure 3.5 Cr, Ni, Nb and Zr (ppm) vs. TiO_2 (wt.%) plots for the Olympic Dam dolerite and the Gairdner Dyke Swarm. The Olympic Dam dolerite data come from this study, Johnson (1993) and the SARIG database (DMITRE, 2014). The Gairdner Dyke Swarm data are from the SARIG database (DMITRE, 2014) and Zhao et al. (1994). Some analyses have values for only a limited number of elements.

The least-altered samples were identified by means of petrographic examination (where applicable, primary minerals partly preserved) and geochemical filters (loss on ignition, LOI, less than 4 wt.%). The major and trace element abundances of least-altered whole-rock samples from the Olympic Dam dolerite are reported in Table 3.2. Previous analyses (the SARIG database, DMITRE, 2014; Johnson, 1993) of similar dolerite at Olympic Dam have also been included, and the same geochemical filters were applied to identify the least–altered samples. The least-altered Olympic Dam dolerite samples have relatively uniform SiO_2 (49.2 to 53.9 wt.%, recalculated volatile-free) and Al_2O_3 (12.7 to 14.1 wt.%) contents, variable MnO (0.2 to 0.5 wt.%), MgO (3.3 to 5.1 wt.%), Na_2O (2.0 to 4.7 wt.%) and TiO_2 (2.0 to 3.4 wt.%) contents, and

highly variable FeO_t (11.4 to 15.4 wt.%, total Fe as FeO) and CaO (5.1 to 10.2 wt.%) contents.

There are no well-constrained linear correlations between TiO_2 and incompatible elements such as Rb, Sr, Ba and U, which implies that even the least-altered Olympic Dam dolerite samples considered in this study have been affected by hydrothermal alteration. A noticeable example of the effects of alteration is the Pb concentration which ranges from 2 to 425 ppm (average ~41 ppm), well above the average of ~13 ppm Pb for the Gairdner Dyke Swarm elsewhere (the SARIG database, DMITRE, 2014; Zhao et al., 1994).

In contrast, correlations exist among the more alteration-resistant ('immobile') elements. Assays of the Olympic Dam dolerite from drill core RU65-7938 (Table S2) have also been included and analyses of the Gairdner Dyke Swarm have been plotted for comparison (Fig. 3.5). Both compatible (e.g. Cr and Ni) and incompatible elements (e.g. Nb, Ta, Zr and Hf) show correlations with TiO_2. With increasing TiO_2, Cr and Ni decrease, whereas Nb, Ta, Zr, P, Hf, and Rare Earth Element (REE) concentrations steadily increase. The correlations between TiO_2 and hydrothermally immobile trace elements probably reflect fractional crystallization trends in the parental magmas from which they were derived. Rare olivine phenocrysts (now pseudomorphed by secondary minerals) are preferentially distributed on the sides of one dyke, and fractional crystallization of olivine could remove Ni and to a lesser extent Cr from the residual magma. Clinopyroxene and plagioclase are the dominant minerals in the Olympic Dam dolerite, and their crystallization would result in the enrichment of incompatible trace elements (e.g Nb, Ta, Zr, Hf) in the residual magmas. On the chondrite-normalized REE diagrams for the Olympic Dam dolerite, all the samples display an enrichment of light REE (LREE) relative to heavy REE (HREE, Fig. 3.6a). The $(La/Yb)_n$ [normalized to chondrite estimates from Sun and McDonough, (1989)] ratios for the Olympic Dam dolerite vary from 2.2 to 6.3; the average ratio is 3.3. Some samples show slight Eu anomalies; the range of Eu/Eu* [$Eu/Eu^*=Eu_n / (0.5*(Sm_n+Gd_n))$] is from 0.6 to 1.8. Samples with negative Eu anomalies are characterized by porphyritic textures, whereas samples showing positive Eu anomalies are commonly fine- to medium-grained dolerite, which implies that the porphyritic dykes may have been affected by

plagioclase fractional crystallization whereas the doleritic counterparts have experienced plagioclase accumulation.

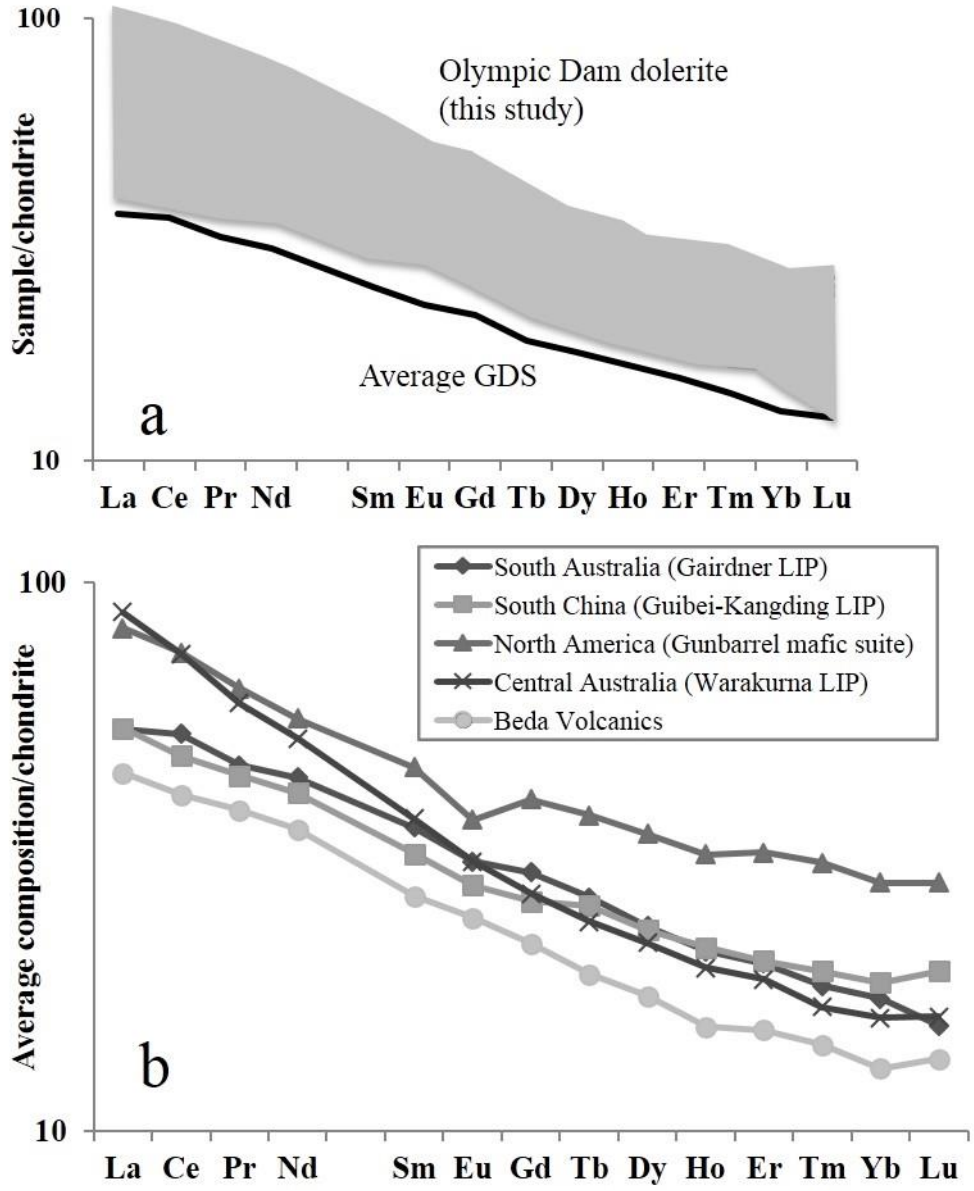

Figure 3.6 Chondrite-normalized REE variation diagrams for (a) the Olympic Dam dolerite (this study) and the average composition of the Gairdner Dyke Swarm, (b) the average compositions of the Gairdner LIP from South Australia (data from this study, SARIG database, Zhao et al., 1994; Wang et al., 2010), the Guibei and Kangding LIP in South China (data from Ling et al., 2003; Wang et al., 2008), Gunbarrel mafic suite in North America (data from Sandeman et al., 2014), the Warakurna LIP from Central Australia (data from Wingate et al., 2004; Geological Survey of Western Australia, GSWA, 2014) and the Beda Volcanics in South Australia (data from Woodget, 1987; Wade et al., 2014). Chondrite estimates are taken from Sun and McDonough (1989).

Eight samples of the Olympic Dam dolerite analyzed in the course of this work have present-day $^{147}Sm/^{144}Nd$ and $^{143}Nd/^{144}Nd$ of 0.149 to 0.174 and 0.512432 to 0.512697, respectively (Table 3.3). Age correction to ca. 825 Ma yields initial ε_{Nd} values in the range from -0.2 to +5.7.

3.7 Discussion

3.7.1 The presence of the Gairdner Dyke Swarm at Olympic Dam

Prior to this study, the age of dolerite at Olympic Dam was poorly constrained. A relatively fresh dolerite (in drill hole RD222) provided a Rb-Sr mineral-whole rock isochron age of 1059 ± 69 Ma (Creaser, 1989). Petrographic examination of this sample did not reveal accessory apatite or other minerals amenable to U-Pb dating. In contrast, accessory magmatic apatite recovered from a medium-grained Olympic Dam dolerite yielded a result of 825 ± 18 Ma, similar to the baddeleyite U-Pb age of 827 ± 6 Ma for the Gairdner Dyke Swarm elsewhere (Wingate et al., 1998). Furthermore, secondary apatite and titanite in hydrothermal veinlets in another Olympic Dam dolerite sample yielded broadly similar U-Pb ages of 821 ± 15 Ma and 817 ± 11 Ma, respectively, in accordance with field and petrographic evidence for localised hydrothermal alteration during and/or after dolerite emplacement. Our new dates confirm that the Olympic Dam dolerite is time-equivalent to the Gairdner Dyke Swarm.

Comparison of the compositions of the Olympic Dam dolerite and the Gairdner Dyke Swarm must consider the effects of alteration, even for the least-altered samples in this study. For example, elevated FeO_t (11.4 to 15.4 wt.%) in the Olympic Dam dolerite compared to Gairdner Dyke Swarm elsewhere (mostly 9 to 13 wt.%) could result from hematite replacement of Ti-magnetite, as suggested by the reddish tint common to the Olympic Dam dolerite samples both in hand specimen and under the microscope. If alteration-sensitive elements are ignored, several similarities are observed. Incompatible element ratios (e.g. Zr/Hf, Nb/Ta, and Nb/La) in the Olympic Dam dolerite are similar to those in the Gairdner Dyke Swarm elsewhere in the Gawler Craton. Correlations of various incompatible elements with TiO_2 (Fig. 3.5) in Olympic Dam dolerite and Gairdner Dyke Swarm are broadly co-collinear. With increasing TiO_2 contents, Cr and Ni concentrations in the Gairdner Dyke Swarm and Olympic Dam

dolerite steadily decrease from 289 to 20 ppm, and from 140 to 30 ppm, respectively, whereas concentrations of incompatible elements such as Nb, Ta, Zr and Hf increase. REE patterns of both groups are also similar (Fig. 3.6a). For example, the $(La/Yb)_n$ ratio of the Olympic Dam dolerite (2.2 to 6.3, average 3.3) is comparable to that of the Gairdner Dyke Swarm elsewhere [average $(La/Yb)_n$ of 2.8]. Finally, εNd_{825} values of the Olympic Dam dolerite (-0.2 to +5.7) overlap with those reported for the Gairdner Dyke Swarm elsewhere (+4.2 to +4.5, Zhao and McCulloch, 1993).

These results indicate that the Olympic Dam dolerite belongs to the Gairdner Dyke Swarm, extending the spatial distribution as well as the compositional spectrum of the Gairdner Dyke Swarm. The success of our U-Pb isotope analyses of magmatic and secondary apatite expands the geochronological tool box for mafic igneous rocks and should be explored in cases where other, more established U-Pb minerals (zircon and/or baddeleyite, e.g. Heaman, 1997; Rainbird et al., 1998; Hanson et al., 1998; Wingate et al., 1998; Li et al., 2002a; Li et al., 2002b; Harlan et al., 2003; Fioretti et al., 2005) are not found (Chew et al., 2014). Additional geochronology research is clearly desirable to better define the ages of various components within the Gairdner LIP. The current definition of the Gairdner LIP includes the Amata Dyke Swarm in the Musgrave Block. Available Sm-Nd and Rb-Sr mineral isochron ages for this dyke swarm are consistent with each other as well as with other components of the Gairdner Dyke Swarm within their large uncertainties. However, the Amata Dyke Swarm ages are nominally 30 to 50 million years younger than the Gairdner Dyke Swarm (Fig. 3.1a, Zhao and McCulloch, 1993; Werner et al., 2014). A re-investigation of the Amata Dyke Swarm (where zircon was not found) using apatite U-Pb dating would help constrain the main episode of this dyke swarm and the Gairdner LIP.

3.7.2 Secular variations in mafic magmas in Australia in the late Mesoproterozoic to early Neoproterozoic: From the Warakurna LIP to the Gairdner LIP

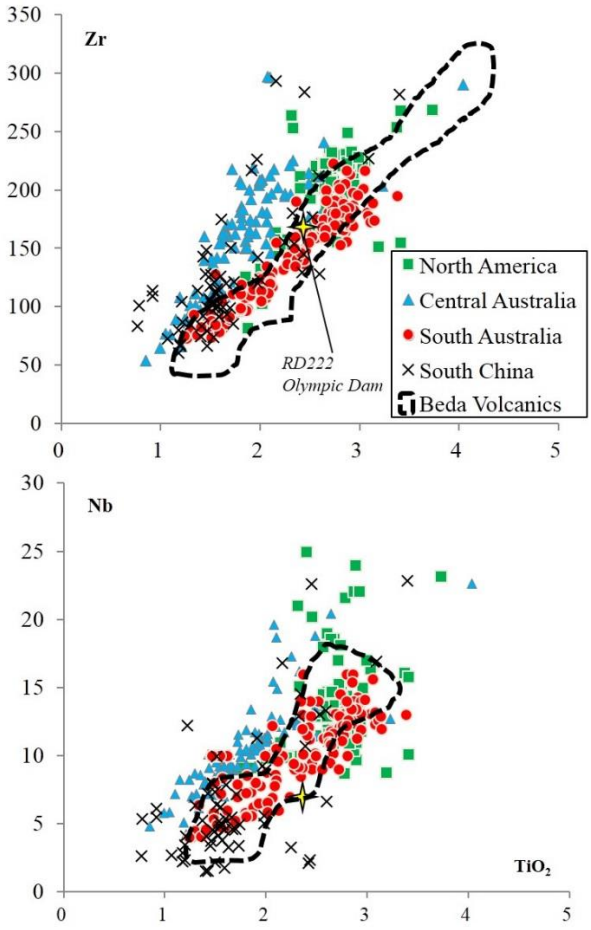

Figure 3.7 Nb and Zr (ppm) vs. TiO_2 (wt.%) plots for the Gairdner LIP in South Australia (same data source as in Figure 6), Gunbarrel mafic suite in North America, Guibei and Kangding LIP in South China, Warakurna LIP in Central Australia. One dyke intersected by drill hole RD222 at Olympic Dam and the Beda Volcanics, dated as 1059 ± 69 Ma and 1076 ± 34 Ma (Fig. 3.1), respectively, show geochemical affinity with the ca. 820 Ma Gairdner LIP.

The ca. 1070 Ma Warakurna LIP and the ca. 820 Ma Gairdner LIP are the two igneous provinces in Australia generated during the existence of Rodinia (Fig. 3.1b). Their extents are still unclear, and the ascription of some units remains to be determined. In particular the Beda Volcanics (Crawford and Hilyard, 1990) and the RD222 dyke from Olympic Dam (Creaser, 1989), show geochemical affinity with the Gairdner LIP but have yielded Rb-Sr isochron ages similar to that of the Warakurna LIP.

A geochemical comparison of the basaltic dykes and sills of the Warakurna LIP with their counterparts in the Gairdner LIP (including the Olympic Dam dolerite in this study) reveals distinct compositional signatures. Mafic units within the Warakurna LIP are characterized by higher concentrations of incompatible elements (e.g. Nb and Zr) at a given TiO_2 content (Fig. 3.7), compared to those of the Gairdner LIP. REE patterns are also different: Warakurna mafic samples have higher $(La/Sm)_n$ and $(La/Yb)_n$ ratios (average of 2.4 and 5.5, respectively) compared to mafic samples of the Gairdner LIP (1.5 and 2.9, respectively, Fig. 3.6b).

Given the consistent compositional differences between the two LIP, the Beda Volcanics and the RD222 mafic dyke at Olympic Dam could be assigned to the Gairdner LIP. Both their Nb-Zr-Ti systematics (Fig. 3.7) and their REE patterns (Beda Volcanics, Fig. 3.6b) support this conclusion, consistent with the observations of Crawford and Hilyard (1990). Further geochronological work on the Beda Volcanics and RD222 dyke is needed to check whether they are part of the Gairdner LIP, or if are the southern extensions of the Warakurna LIP, as suggested by Rb-Sr dates. If the latter is correct, they may be another example of internal compositional heterogeneity with a LIP, as previously observed for the Emeishan LIP (Kamenetsky et al., 2012). Resolution of this issue would provide insights into the late Mesoproterozoic to early Neoproterozoic (ca. 1100 to 1000 Ma) tectonic history of Australia. The Warakurna LIP was proposed to have formed within the Ngaanyantjarra Rift which is part of a wider rift system formed at the triple junction between the North Australian, West Australian and South Australian cratons (Pirajno and Hoatson, 2012). If the Beda Volcanics belong to the Gairdner LIP rather than the Warakurna LIP, the Ngaanyantjarra Rift may not have extended to the South Australian craton (Gawler Craton).

3.7.3 Mafic suites associated with the break-up of Rodinia

There are a number of tectonic reconstructions of the supercontinent Rodinia, based on the identification and correlation of coeval or roughly coeval LIP and mafic igneous suites (Li et al., 2008). The Gairdner LIP in South Australia, the Guibei and Kangding LIP in South China, and the Gunbarrel mafic suite in North America are among the LIP and suites which have been widely studied for their tectonic implications

to the supercontinent Rodinia (e.g. Ling et al., 2003; Wang et al., 2010; Sandeman et al., 2014).

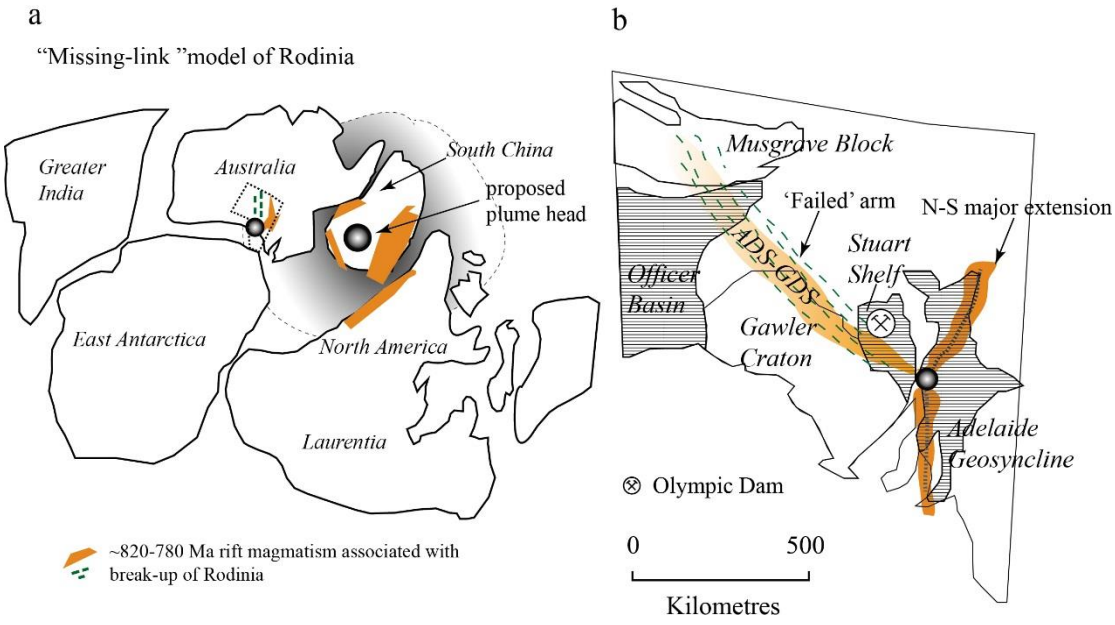

Figure 3.8 (a) The "missing-link" model of the tectonic reconstruction of supercontinent Rodinia at ca. 820-780 Ma. South China was proposed to be situated between Australia-East Antarctica and Laurentia, on top of a plume head (Li et al., 1999), the ascent of which caused rift magmatism in South China. South Australia might be situated at a distance from this plume head or be located on top of another mantle plume head. The area enclosed by the dotted outline is shown in more detail in (b). Modified after Li et al., (1995). (b) An aulacogen-type rift developed in South Australia, which did not result in the break-up of the Australian continent but caused extension accompanied by basin-forming processes. The N-S rift arms accommodated major extension and the Adelaide Rift Complex formed and was preserved as the Adelaide Geosyncline. The third 'failed' arm strikes NW, as indicated by the NW-striking Amata-Gairdner Dyke Swarm (ADS-GDS). Extension along this arm led to the initiation of Officer Basin and Stuart Shelf, but continental break-up did not occur. Olympic Dam, where the giant Olympic Dam iron oxide-Cu-U-Au-Ag deposit was discovered, is located in the Stuart Shelf, and the occurrence of the Gairdner Dyke Swarm at Olympic Dam indicates that this locality was positioned on an active rift at ca. 820 Ma. Modified after Zhao et al., (1994). See text for further discussion.

Mafic LIP in South China and South Australia and the Gunbarrel mafic suite in North America show similar geochemical trends (Figs. 3.6b and 3.7). The mafic LIP in South China and South Australia are compositionally more primitive than the Gunbarrel mafic suite. For example, TiO_2 contents in South China samples (0.8 to 3.4

wt.%, average ~1.7 wt.%) and South Australia samples (1.2 to 3.4 wt.%, average ~2.0 wt.%) are lower than those in the Gunbarrel (1.8 to 3.7 wt.%, average ~2.6 wt.%, Fig. 3.7). The latter has higher concentrations of incompatible elements, such as Nb, Ta, Zr, Hf, and Th (Fig. 3.7). Compared to the Gairdner LIP, the Guibei and Kangding LIP in South China have generally lower TiO_2 and incompatible element contents (Fig. 3.7), possibly representing more primitive magma compositions. Overall, the Neoproterozoic LIP in South China also have greater compositional ranges than the other mafic provinces. REE contents in the Gunbarrel mafic suite are generally higher than LIP from South China and South Australia and REE patterns have persistent negative Eu anomalies, a feature not shared by mafic rocks from South China and South Australia (Fig. 3.6b). These characteristics are consistent with the more evolved character of the Gunbarrel mafic suite, and also implies significant plagioclase fractional crystallization in its evolution. However, REE fractionation is similar everywhere; $(La/Yb)_n$ ratios are in the range of ~2.9 to 3.1. LIP samples from South Australia show slightly stronger HREE fractionation [$(Gd/Yb)_n$ ~1.7] than samples from South China and North America (~1.4, Fig. 3.6b).

The occurrence of compositionally more primitive mafic magmas in South China would fit the "missing-link" model of the tectonic reconstruction of Rodinia (Li et al., 1995, 1999, 2008) which places South China on a mantle plume head between Australia-East Antarctica and Laurentia (Fig. 3.8a). Greater compositional heterogeneity of mafic rocks in South China compared to those in South Australia and North America is consistent with this model, because melting in the vicinity of such a plume head would be expected to produce a wider range of partial melt compositions. South Australia may have been situated away from this mantle plume head and located above another mantle plume (Fig. 3.8a). Whichever is true, South Australia was impacted by rift magmatism, though it did not break up. In fact, it has been suggested that an aulacogen-type rift developed in South Australia and could have been responsible for the formation of the large sedimentary basins, including the Officer Basin, Stuart Shelf and Adelaide Geosyncline, in central-southern Australia (Fig. 3.8b, Zhao et al., 1994; Walter et al., 1995; Barovich and Foden, 2000).

The occurrence of the Gairdner Dyke Swarm at Olympic Dam revealed in this study demonstrates that this locality was situated on an active rift at ca. 820 Ma when

the dykes were emplaced. Considering that there are no recognized flood basalts associated with the Gairdner Dyke Swarm at Olympic Dam, Olympic Dam was more likely to be situated on a secondary rift in the South Australia aulacogen-type rift system (Fig. 3.8b). Further work needs to be done in order to better characterize and evaluate the impact of the emplacement of the Gairdner Dyke Swarm directly on the Olympic Dam deposit, whether positive or negative.

3.8 Conclusions

In this study, basaltic to doleritic dykes named the Olympic Dam dolerite in drill holes at the Olympic Dam iron oxide Cu-U-Au-Ag deposit have been dated and analysed. U-Pb dating of primary and secondary apatite and secondary titanite results reveals that the Olympic Dam dolerite was emplaced at 825 ± 18 Ma, within error of the age of the Gairdner Dyke Swarm, and that hydrothermal activity took place shortly after the dyke intruded. The Olympic Dam dolerite has the same compositional characteristics as the Gairdner Dyke Swarm, an integral part of the ca. 820 Ma Gairdner LIP. Both geochronological and geochemical data allow us to confirm that the Olympic Dam dolerite belongs to the Gairdner Dyke Swarm.

The ca. 1070 Ma Warakurna LIP and the ca. 820 Ma Gairdner LIP in Australia have distinct geochemical signatures. The Beda Volcanics and mafic dykes intersected in drill hole RD222 at Olympic Dam are located within the Gairdner LIP but have Rb-Sr ages that match the Warakurna LIP (Webb and Coats, 1980). We show that the Beda Volcanics and RD222 dykes plot in the same compositional fields as the Gairdner LIP and suggest that a geochronological reinvestigation of their ages using different dating technique is warranted.

The ca. 820 Ma Gairdner LIP in South Australia, the ca. 820 Ma Guibei LIP and the ca. 780 Ma Kangding LIP in South China, and the ca. 780 Ma Gunbarrel mafic suite in North America are considered to be associated with the break-up of Rodinia. Geochemical comparisons among these mafic suites are consistent with the proposition that South China was situated on a plume head whereas South Australia encompassed an aulacogen-type rift system (Li et al., 1995, 1999). The occurrence of the Gairdner Dyke Swarm at Olympic Dam, where the Olympic Dam iron oxide Cu-U-Au-Ag

deposit is situated, indicates that this locality has been impacted by ca. 820 Ma rift magmatism.

Table 3.1 Dating results of magmatic apatite and secondary apatite and titanite in the Olympic Dam dolerite.

	^{207}cor $^{206}Pb/^{238}U$ age[a]	+/-1 ster	$^{238}U/^{206}Pb$ ratio	+/-1 ster	$^{207}Pb/^{206}Pb$ ratio	+/-1 ster	^{204}Pb ppm	^{206}Pb ppm	^{207}Pb ppm	^{208}Pb ppm	^{232}Th ppm	^{238}U ppm
OD850-852 apatite												
1	800	32	6.01	0.22	0.2363	0.0114	0.01	0.4	0.1	0.5	9	3
2	802	34	6.69	0.27	0.1609	0.0119	0.01	0.8	0.1	1.2	30	6
3	826	39	5.23	0.22	0.3028	0.0135	0.01	1.1	0.3	1.8	28	7
4	827	35	5.95	0.24	0.2204	0.0116	0.00	0.4	0.1	0.5	9	3
5	835	32	6.10	0.22	0.1956	0.0096	0.01	0.8	0.1	1.1	25	6
6	843	32	5.85	0.21	0.2189	0.0112	0.01	0.9	0.2	1.5	30	6
7	846	26	6.29	0.19	0.1641	0.0076	0.00	0.8	0.1	1.2	27	6
8	862	27	6.22	0.18	0.1593	0.0094	0.00	0.8	0.1	1.2	29	6
9	705	67	2.86	0.20	0.6189	0.0213	0.22	6.1	3.4	10.3	79	24
10	739	45	5.24	0.24	0.3656	0.0231	0.00	0.3	0.1	0.4	5	2
11	776	60	4.37	0.24	0.4307	0.0271	0.00	0.4	0.1	0.5	5	2
12	785	38	5.28	0.20	0.3269	0.0175	0.00	0.3	0.1	0.4	6	2
13	806	65	3.82	0.20	0.4728	0.0271	0.01	0.5	0.2	0.8	7	2
14	807	44	5.09	0.22	0.3321	0.0200	0.01	0.4	0.1	0.5	7	2
15	820	24	7.38	0.22	0.0664	0.0055	0.01	0.6	0.0	1.5	41	5
16	831	43	5.35	0.25	0.2858	0.0168	0.00	0.4	0.1	0.4	6	2
17	902	66	5.02	0.31	0.2715	0.0261	0.00	0.3	0.1	0.3	5	2
18	941	67	2.51	0.10	0.5690	0.0214	0.03	0.8	0.4	1.2	7	2
19[b] plagioclase			0.92	0.03	0.7715	0.0176						
20[b] plagioclase			0.18	0.02	0.8622	0.0223						
21[b] clinopyroxene			0.00	0.02	0.8765	0.0180						
OD199 apatite												

1	757	44	7.62	0.44	0.1063	0.0153	0.00	0.3	0.0	1.2	33	2
2	795	20	7.52	0.19	0.0755	0.0050	0.00	1.0	0.1	2.7	79	8
3	799	32	7.28	0.29	0.0989	0.0094	0.00	0.3	0.0	0.8	20	3
4	807	25	7.46	0.23	0.0703	0.0056	0.01	0.6	0.0	1.5	40	5
5	808	32	7.27	0.29	0.0903	0.0084	0.00	0.5	0.0	1.3	36	4
6	818	26	7.28	0.23	0.0791	0.0064	0.00	0.5	0.0	1.7	48	4
7	820	53	6.91	0.44	0.1179	0.0148	0.00	0.3	0.0	1.2	32	2
8	822	43	7.08	0.36	0.0980	0.0118	0.01	0.3	0.0	1.2	31	2
9	822	25	7.37	0.23	0.0640	0.0048	0.00	0.6	0.0	1.8	50	5
10	823	38	7.16	0.33	0.0870	0.0097	0.01	0.4	0.0	0.8	23	3
11	825	24	7.23	0.21	0.0773	0.0054	0.01	0.7	0.0	1.1	30	5
12	832	26	6.98	0.22	0.0978	0.0073	0.00	0.6	0.1	1.5	43	5
13	834	30	6.95	0.25	0.0998	0.0075	0.00	0.5	0.0	1.4	36	4
14	846	54	6.92	0.42	0.0919	0.0210	0.00	0.2	0.0	0.9	26	2
15	860	35	6.95	0.29	0.0746	0.0084	0.01	0.4	0.0	1.2	33	3
16	873	34	6.79	0.26	0.0812	0.0078	0.01	0.4	0.0	1.2	34	3
OD199 titanite												
1	793	18	7.60	0.18	0.0700	0.0031	0.01	8.7	0.6	2.0	43	73
2	796	23	7.55	0.22	0.0721	0.0046	0.00	3.9	0.3	1.1	25	33
3	796	13	7.60	0.13	0.0666	0.0013	0.02	53.5	3.5	2.2	52	459
4	804	42	7.25	0.38	0.0970	0.0107	0.00	1.3	0.1	0.9	20	10
5	806	23	7.51	0.22	0.0655	0.0049	0.00	3.9	0.3	1.3	32	30
6	812	19	7.46	0.18	0.0649	0.0025	0.00	10.0	0.6	1.5	36	83
7	819	26	7.40	0.23	0.0645	0.0050	0.01	2.2	0.1	1.0	29	18
8	822	35	7.29	0.31	0.0733	0.0080	0.01	1.2	0.1	0.7	17	10
9	824	20	7.37	0.18	0.0634	0.0039	0.00	5.2	0.3	1.8	45	43
10	826	14	7.33	0.12	0.0650	0.0019	0.02	12.5	0.8	3.6	96	99
11	863	19	7.02	0.16	0.0633	0.0029	0.00	14.7	0.9	3.4	85	116
12	867	40	6.51	0.30	0.1202	0.0106	0.00	1.6	0.2	0.9	20	12

[a]The 207-correction is based on common Pb composition of Stacey and Kramers (1975) at 820 Ma.
[b]Analyses (19–21) of none-apatite primary minerals (i.e. clinopyroxene and plagioclase) in the OD dolerite OD850 and 852. ster, standard error.

Table 3.2 Major and trace element compositions for the least-altered Olympic Dam dolerite.

Sample No.	OD118	OD850	OD849	OD84	OD1	OD82	OD81-2	OD80b	OD80d	OD79	OD952	OD958
SiO_2	52.5	49.2	49.9	51.0	50.9	50.4	50.2	49.4	51.1	50.9	50.6	49.6
TiO_2	2.7	3.0	2.5	2.9	2.5	3.1	2.6	2.8	2.8	2.8	2.9	3.4
Al_2O_3	14.3	14.5	13.1	13.0	13.1	14.5	13.1	12.7	12.8	12.8	15.6	15.4
FeOt	13.5	14.9	14.4	13.7	14.7	14.5	12.2	15.2	14.1	14.3	15.4	13.1
MnO	0.2	0.2	0.3	0.2	0.5	0.1	0.2	0.2	0.4	0.4	0.2	0.2
MgO	5.2	3.8	6.0	5.6	5.4	4.8	5.7	5.7	5.5	5.6	3.3	3.4
CaO	6.7	9.2	9.7	8.1	8.4	5.3	9.6	8.6	8.5	8.5	5.9	10.2
Na_2O	2.5	2.2	2.0	3.1	2.1	4.7	3.8	2.5	2.2	2.1	3.0	2.3
K_2O	0.8	0.8	0.4	0.6	0.5	0.8	1.0	0.9	0.7	0.7	1.0	0.5
P_2O_5	0.2	0.3	0.2	0.3	0.2	0.3	0.2	0.3	0.3	0.3	0.3	0.3
LOI	3.5	1.4	1.9	1.7	3.7	3.0	1.1	1.6	2.6	2.7	2.6	2.6
Li	29.6	10.8	14.8	19.3	41.3	13.3	11.7	23.1	22.1	20.9	17.7	12.4
Be	1.00	1.09	0.90	1.20	2.00	2.06	1.01	1.00	0.80	1.19	1.11	1.70
Sc	46.6	35.2	41.9	43.6	41.1	41.4	33.9	29.9	41.7	39.1	32.8	34.9
Ti	14929	16800	13600	17080	13675	18183	13886	16282	16216	15597	15050	18400
V	403	481	481	435	372	391	368	322	445	378	404	507
Cr	95.2	30.0	120.0	60.9	93.4	63.8	75.9	60.6	59.4	50.3	20.0	40.0
Mn	1596	1550	1630	1813	4513	1058	1612	1122	2370	2548	1340	1550
Ni	58.6	41.9	72.3	62.2	76.0	51.5	50.9	54.2	56.9	47.5	35.0	37.7
Cu	124	335	277	66	272	113	14	203	301	381	160	365
Zn	162	146	145	127	124	132	88	156	171	157	272	456

Ga	23.0	25.5	21.9	24.2	22.0	24.8	20.7	21.8	22.0	22.0	26.7	25.0
As	3.6	0.2	0.6	6.9	5.3	2.2	5.8	9.5	15.4	26.5	8.8	5.4
Rb	21.2	20.0	11.1	20.3	12.6	24.5	33.0	27.7	22.4	26.3	32.0	12.2
Sr	177	237	162	148	197	81	150	147	163	157	331	206
Y	35.7	45.2	35.2	43.2	33.9	44.0	31.9	41.5	38.8	39.7	43.6	41.7
Zr	166	201	162	213	150	217	175	164	204	191	217	195
Nb	10.2	13.1	10.2	14.3	9.5	15.6	11.3	13.4	13.2	12.7	14.0	13.0
Mo	1.00	1.13	0.96	0.80	0.90	1.48	0.70	1.10	1.00	1.03	0.85	0.81
Sb	0.30	0.08	0.09	0.60	0.60	0.25	0.45	0.40	0.30	0.36	0.41	0.27
Cs	0.60	0.45	0.59	0.50	1.40	0.96	0.35	1.00	0.60	0.65	0.30	0.45
Ba	100	123	83	125	755	132	233	187	210	231	148	116
La	17.2	18.5	13.6	22.3	15.5	15.4	13.0	21.8	13.0	20.2	18.3	19.3
Ce	40.2	45.4	33.4	53.3	34.9	35.3	32.8	47.3	43.3	42.4	45.5	45.8
Pr	5.70	6.49	4.68	7.40	5.30	5.07	4.86	6.30	6.50	5.79	6.26	6.04
Nd	27.4	29.9	21.8	34.8	24.8	23.2	22.6	30.0	31.5	26.1	28.4	26.4
Sm	7.00	7.73	5.82	8.70	6.50	6.67	6.24	7.40	8.20	6.97	7.16	6.72
Eu	2.20	2.52	1.94	2.50	2.10	1.93	2.32	2.30	2.70	2.14	2.50	2.48
Gd	7.60	8.63	6.60	9.60	7.60	7.63	7.01	8.40	9.20	7.69	8.00	7.60
Tb	1.30	1.38	1.03	1.50	1.30	1.39	1.18	1.40	1.50	1.31	1.23	1.23
Dy	7.30	8.39	6.46	8.80	7.40	8.46	6.76	7.70	8.30	7.70	7.84	7.53
Ho	1.50	1.68	1.31	1.80	1.40	1.68	1.28	1.60	1.70	1.53	1.59	1.51
Er	3.90	4.68	3.85	4.60	4.00	4.81	3.61	4.10	4.40	4.28	4.36	4.25
Tm	0.60	0.66	0.56	0.70	0.60	0.69	0.51	0.60	0.60	0.61	0.66	0.59
Yb	3.30	4.25	3.55	3.80	3.30	4.27	3.14	3.60	3.80	3.70	4.17	4.01
Lu	0.50	0.66	0.55	0.60	0.50	0.63	0.48	0.50	0.60	0.55	0.63	0.61

Hf	4.40	5.50	4.50	5.50	4.30	5.75	5.02	5.30	5.20	5.11	5.80	5.20
Ta	1.00	1.20	1.00	1.20	0.80	1.16	0.92	1.20	1.30	0.73	1.10	0.90
Tl	0.10	0.07	0.05	0.10	0.00	0.09	0.11	0.10	0.10	0.14	0.16	0.05
Pb	10.2	3.0	3.4	6.3	8.3	10.5	5.8	87.4	161	221	30	425
Th	2.30	2.70	1.90	2.70	1.90	2.89	1.87	2.40	2.40	2.26	2.80	2.60
U	0.50	0.60	0.44	0.90	0.50	0.98	0.64	0.60	0.60	0.53	1.31	0.85

Major element (oxides) compositions are LOI-free, in wt.%, trace element in ppm. LOI: loss on ignition.

Table 3.3 Sm–Nd isotope results, least-altered Olympic Dam dolerite.

	Sm, ppm	Nd, ppm	$^{147}Sm/^{144}Nd$	$^{143}Nd/^{144}Nd$	± 2 Standard Error	εNd(i)
OD80-1bas	7.4	30.0	0.149	0.512667	0.000012	5.7
OD80-2dol	8.2	31.5	0.157	0.512697	0.000018	5.4
OD82	6.7	23.2	0.174	0.512605	0.000012	1.8
OD84	8.7	34.8	0.151	0.512567	0.000008	3.5
OD199	6.4	23.4	0.165	0.512515	0.000010	1.0
OD849	5.8	21.8	0.161	0.512432	0.000014	-0.2
OD850	7.7	29.9	0.156	0.512579	0.000020	3.2
OD422[a]	5.54	20.48	0.163	0.512603	0.000012	2.9

Results from this study are based on unspiked Nd isotope analysis; Sm/Nd ratio based on trace element results, see Table 3.2.
[a]Results for OD422 have been obtained from isotope dilution at Univ. of Melbourne.
$^{143}Nd/^{144N}d$ adjusted to LaJolla = 0.511860.
εNd(i) calculated at 825 Ma, relative to chondrite parameters of Bouvier et al. (2008).

Chapter 4 Mafic magmas in the Mesoproterozoic Gawler silicic large igneous province, South Australia: evidence from olivine-phyric rocks at the Olympic Dam deposit and other localities*

Qiuyue Huang[1], Vadim S. Kamenetsky[1], Kathy Ehrig[2], Jocelyn McPhie[1], Maya Kamenetsky[1], Ken Cross[3], Sebastien Meffre[1], Andrea Agangi[4], Isabelle Chambefort[1, 5], Nicholas G. Direen[1], Roland Maas[6], Olga Apukhtina[1]

[1]School of Physical Sciences, University of Tasmania, Private Bag 79, Hobart, Tasmania, Australia 7001

[2]BHP Billiton Olympic Dam, Adelaide, SA 5000, Australia

[3]Terramin Australia Ltd, Level 3, 70 Hindmarsh Square, Adelaide, South Australia, 5000

[4]Curtin University of Technology, Department of Applied Geology, Bentley 6102 WA, Australia

[5]GNS Science, Wairakei Research Centre, Taupo 3377, New Zealand

[6]School of Earth Sciences, University of Melbourne, VIC 3010, Australia

*Manuscript published in Precambrian Research (2016), volume 281, pages 185-199. DOI: 10.1016/j.precamres.2016.05.019

Abstract

The felsic-dominant Gawler Range Volcanics and cogenetic Hiltaba Suite granitoids constitute the ca. 1590 Ma Gawler silicic large igneous province in the Gawler Craton, South Australia. The province includes minor occurrences of olivine-phyric basalt at Kokatha and Mount Gunson. In this study, we describe additional olivine-phyric basalts intersected by drill holes at the Olympic Dam Cu-U-Au-Ag deposit and the Wirrda Well Cu-Au prospect. Laser Ablation Inductively Coupled Plasma Mass Spectrometry U-Pb dating results (un-anchored) of apatite in the mafic rocks at Mount Gunson (1576 ± 33 Ma), Wirrda Well (1596 ± 17 Ma), and Olympic Dam (1621 ± 20 Ma) confirm their correlation with the ca. 1590 Ma Gawler silicic large igneous province.

Compositions of Cr-spinel inclusions enclosed in former olivine phenocrysts (forsterite number >80) in basalts at Mount Gunson, Wirrda Well and Olympic Dam imply derivation from a heterogeneous mantle source that may have been modified by subduction. Least-altered olivine-phyric basalts at Mount Gunson and Kokatha are characterized by negative Nb and Ta anomalies, which are typical of arc basalts but are also common in back-arc basin basalts, in accordance with the result suggested by the Cr-spinel source indicator. The mafic Gawler Range Volcanics generally have higher Zr contents and Zr/TiO_2 ratios than those of high-Mg basalts and picrites produced in variable tectonic settings worldwide, possibly reflecting continental crustal components involved in their mantle source.

High abundances (typically ~20 vol.%) of former olivine phenocrysts in the basalt at Olympic Dam imply high-Mg whole-rock compositions and a high temperature of the primary magma. This result is in accordance with previous models in which the heat flux from mantle magmas caused large-scale partial melting of crustal rocks that subsequently gave rise to silicic magmas erupted and intruded to form the Gawler silicic large igneous province.

Key words

Gawler silicic large igneous province; Olivine-phyric basalt; Apatite-U-Pb dating; Cr-spinel; Petrogenesis; Olympic Dam;

4.1 Introduction

Large igneous provinces (LIP) involve emplacement of voluminous magma into and/or onto the Earth's crust in events of relatively short duration (Coffin and Eldholm, 1994; Ernst et al., 2005; Bryan and Ernst, 2008). Most LIP are mafic-dominated, consisting of flood basalt lavas, dyke swarms and layered intrusions (Bryan and Ferrari, 2013), composed of mantle-derived magmas. However, a wider range of magma compositions from basaltic to rhyolitic may be present in LIP, and silicic large igneous provinces (SLIP) have been defined, where silicic igneous rocks (>65 wt.% SiO_2) predominate (Bryan et al., 2002). The paucity of outcropping mafic and ultramafic igneous rocks in SLIP may result either from 1) poor exposure of these units due to concealment beneath felsic units, or from 2) stalling of mafic magmas at lower crustal levels or at the mantle-crust boundary. That is, SLIP may be associated with 'hidden mafic large igneous provinces' (Ernst, 2014). Whichever is true, the thermal (± mass) input from underplating mafic and ultramafic magmas (Bryan et al., 2002) required to drive large-scale crustal partial melting and to generate large volumes of silicic magmas makes the investigation of the mafic igneous units in any SLIP of special interest.

The formation of the ca. 1590 Ma Gawler SLIP (Allen et al., 2008), consisting of the Gawler Range Volcanics (GRV) and the Hiltaba Suite (HS), in South Australia (Fig. 4.1) was probably associated with the assembly of the Laurentian supercontinent (Blissett et al., 1993; Creaser, 1995; Allen and McPhie, 2002; Payne et al., 2009). However, rare exposures of mafic units in the Gawler SLIP and the generally evolved character (clinopyroxene-plagioclase-phyric) of these units have hampered follow-up research into the petrogenesis (importantly, characteristics of mantle source) and any implications for the tectonic setting of the overlying crust at ca. 1590 Ma.

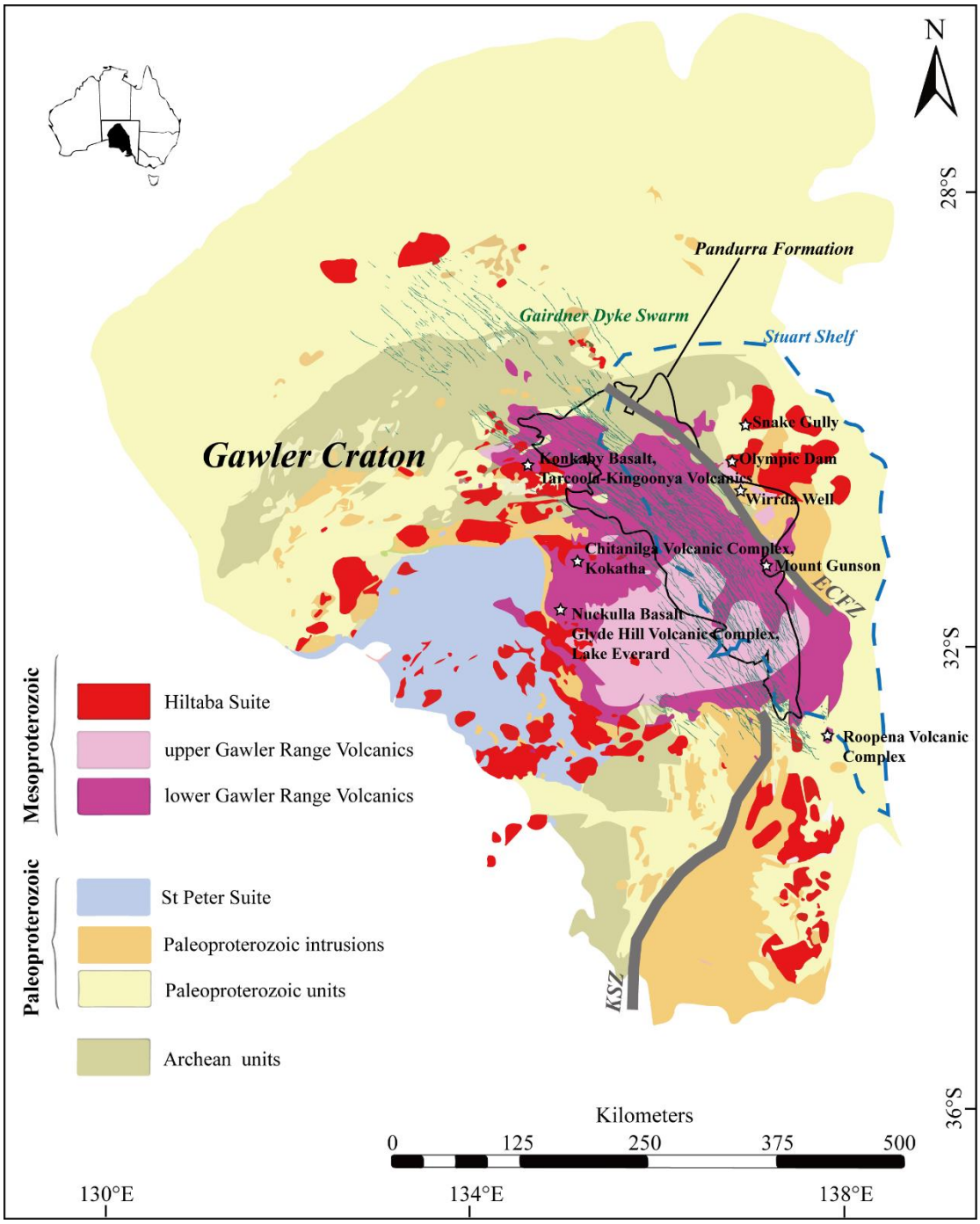

Figure 4.1 Simplified geological map of the Gawler Craton, South Australia. This map highlights the distribution of the Gawler SLIP, which includes the Hiltaba Suite and Gawler Range Volcanics. Modified after Fairclough et al., (2003) and Betts et al. (2009). ECFZ: Elizabeth Creek Fault Zone; KSZ: Kalinjala Shear Zone.

In this study, we focus on the occurrence of olivine-bearing mafic igneous rocks at four locations in the Gawler SLIP: Kokatha (Giles, 1988; Blissett et al., 1993), the Mount Gunson copper deposit (Knutson et al., 1992), the Wirrda Well Cu-Au prospect

and the Olympic Dam Cu-U-Au-Ag deposit. These rocks have comparable petrographic features. U-Pb apatite dating results support correlation with the GRV and the Gawler SLIP. Compositions of Cr-spinel inclusions in the olivine pseudomorphs and whole-rock samples provide constraints on the parental melt compositions and magma sources. We consider the significance of the magma sources in relation to interpretations of the tectonic setting of the Gawler SLIP.

4.2 Regional geology

The Gawler Craton records several cycles of magmatism, sedimentation, and orogenesis in its protracted evolution from the Meso-Archean to Mesoproterozoic. A brief introduction is presented here and further details can be found in Hand et al. (2007) and Reid and Hand (2012).

Meso-Archean to early Paleoproterozoic rocks occur centrally in the Gawler Craton, and comprise highly deformed metasedimentary sequences including aluminous metasedimentary units interlayered with banded iron formations, carbonates, and siliceous rocks, and broadly coeval felsic and mafic to ultramafic volcanic rocks, which were deposited or erupted in the interval ca. 2560 Ma to 2500 Ma (Fig. 4.1, Daly et al., 1998; Hand et al., 2007). During the Paleoproterozoic, sedimentation associated with rift basins to the east of the Archean core commenced, and the basin sequences were subsequently intruded by voluminous granitoids at ca. 1850 Ma (i.e. Donington Suite) (Reid et al., 2008). The Elizabeth Creek Fault Zone and Kalinjala Shear Zone (Fig. 4.1) are understood to be the boundaries between the Archean nucleus to the west and Proterozoic sequences to the east (Direen and Lyons, 2007; Hayward and Skirrow, 2010) .

On the eastern margin of the Gawler Craton, post-intrusion rift-related volcanism and sedimentation continued until ca. 1740 Ma. These rocks were deformed during the ca. 1740 Ma to 1700 Ma Kimban Orogeny (Daly et al., 1998; Dutch et al., 2008). The northern and western Gawler Craton contains poorly exposed Paleoproterozoic metasedimentary units including pelite, iron formations, and carbonates (Direen et al., 2005; Payne et al., 2006, 2008; Thomas et al., 2008). Granitoids of the St Peter Suite in the southwestern Gawler Craton were emplaced at ca. 1620 Ma, and this suite has been

interpreted to have formed in a magmatic arc setting (Fig. 4.1, Swain et al., 2008; Symington et al., 2014).

The GRV-HS magmatic event occurred between ca. 1595 and 1575 Ma (Blissett et al., 1993; Jagodzinski, 2005; Reid and Fabris, 2015). This event was associated with a major thermal and metallogenic episode that affected much of the Gawler Craton (Daly et al., 1998; Hand et al., 2007; Skirrow et al., 2002, 2007) (51). The Hiltaba Suite comprises granite, granodiorite, quartz syenite and quartz monzodiorite plutons (Drexel et al., 1993). According to Blissett et al. (1993) and Allen et al. (2003), the GRV have a maximum preserved thickness of ~1.5 km and are exposed over more than 25,000 km^2 across the central Gawler Craton. The upper GRV consist of widespread, thick (250-300 m), rhyolitic and dacitic units considered to be lavas (Garner and McPhie, 1999; Morrow and McPhie, 2000; Allen and McPhie, 2002; Allen et al., 2003). The lower GRV range in composition from basalt to rhyolite and comprise lavas, ignimbrites and minor volcaniclastic facies (Blissett et al., 1993; Allen et al., 2008; Agangi et al., 2012). Mafic units are subordinate to dacite and rhyolite (~90 vol.%). Mafic GRV outcrop at Lake Everard (Nuckulla Basalt in the Glyde Hill Volcanic Complex), Kokatha, and Tarcoola-Kingoonya (Konkaby Basalt) (Fig. 4.1, Blissett et al., 1993), and are also intersected by drill holes at the Mount Gunson copper deposit (Knutson et al., 1992), Roopena (Blissett et al., 1993), the Olympic Dam Cu-U-Au-Ag deposit (Reeve et al., 1990; Johnson, 1993), Snake Gully (Jagodzinski, 2005), and the Wirrda Well Cu-Au prospect (Ehrig, 2013). Among all these occurrences, only one age of 1596.5 ± 3.8 Ma by zircon SHRIMP U-Pb dating has been obtained on a micro-gabbro dyke at Snake Gully (Jagodzinski, 2005), whereas ages of mafic GRV at the other locations have yet to be constrained by radiometric dates. The mafic GRV units are commonly altered. Intensely altered alkaline mafic to ultramafic GRV at Olympic Dam were proposed to have been a major source of the copper (~50 % of the contained Cu) found in the deposit (Johnson, 1993; Johnson and McCulloch, 1995).

Continental sedimentation recorded by the Pandurra Formation (Fig. 4.1) in the Cariewerloo Basin has a possible depositional age of ca. 1450 to 1424 Ma (Cowley, 1993; Keeling, 2015). The Gairdner Dyke Swarm intruded the Gawler Craton at ca. 820 Ma (Wingate et al., 1998).

4.3 Mafic GRV at Kokatha, Mount Gunson, Wirrda Well, and Olympic Dam

Former-olivine-bearing mafic GRV units have been reported at Kokatha (Giles, 1988; Blissett et al., 1993), Mount Gunson (Knutson et al., 1992), Wirrda Well (Ehrig, 2013) and Olympic Dam (Johnson, 1993). Outcrop (Kokatha) and drill core (Mount Gunson, Wirrda Well and Olympic Dam) samples collected for this study are described below.

4.3.1 Chitanilga Volcanic Complex, Kokatha

A section of basalt, basaltic andesite and andesite up to 1,000 m thick occurs at the base of the Chitanilga Volcanic Complex at Kokatha (Branch, 1978; Stewart, 1994; Giles, 1988; Blissett et al., 1993; Agangi, 2011). These lithologies are greenish-grey to black. Porphyritic (Fig. 4.2a and b) and amygdaloidal textures are common in the basalt. Olivine (pseudomorphs) and clinopyroxene are the dominant phenocryst phases; plagioclase rarely occurs as phenocrysts. Former olivine phenocrysts have prismatic and/or skeletal shapes, and are entirely replaced by secondary minerals including tremolite, chlorite, quartz, hematite and carbonate (Fig. 4.2b). Cr-spinel crystals are present as inclusions in the olivine pseudomorphs. Olivine pseudomorphs vary in size from less than 0.5 mm to more than 2.5 mm, and the bulk of the olivine pseudomorphs are ~1 mm in size. Fresh clinopyroxene phenocrysts have been preserved in some samples, and they range from ~1 mm to 2 mm in size. The groundmass of the olivine-clinopyroxene-phyric basalt is fine-grained (Fig. 4.2b) to cryptocrystalline. The fine-grained groundmass mainly consists of tabular plagioclase (Fig. 4.2b) and lesser amounts of clinopyroxene and magnetite. Quartz crystals with embayed rims also occur in some olivine (pseudomorphs)-clinopyroxene-phyric basalt units and are interpreted to be xenocrysts derived from granitoids. The amygdaloidal basalt in the upper part of the section generally contains less than ~3 vol.% of olivine pseudomorphs. Amygdales are filled with tremolite, and to a lesser amount, chlorite, quartz, hematite and carbonate. The same minerals have partly replaced clinopyroxene and plagioclase in the basalt.

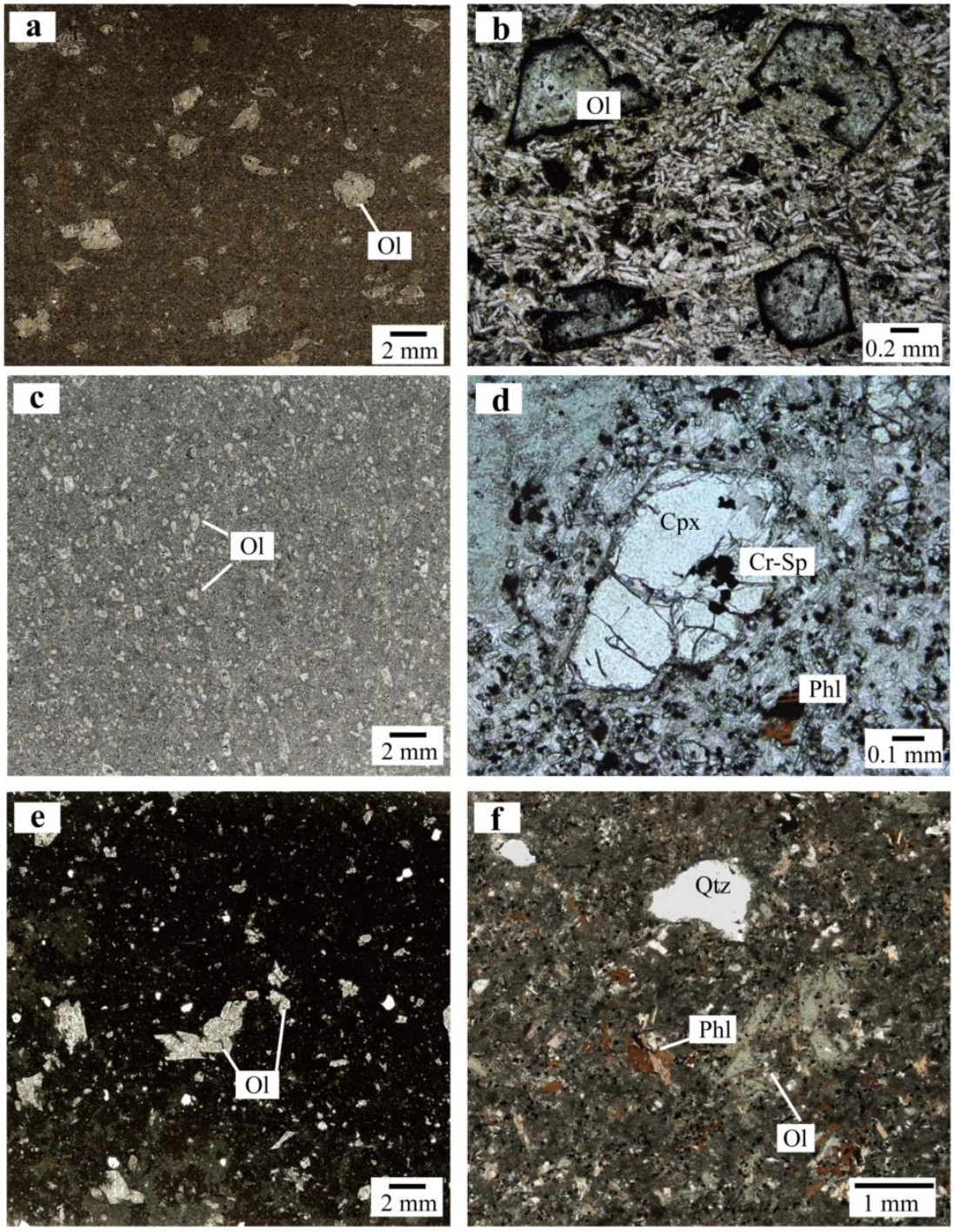

Figure 4.2 Representative photomicrographs of olivine-phyric basalts from (a, b) Kokatha (Sample EGC-13-06K), (c, d) Mount Gunson (Sample RX3456, Drill Hole PY-1, 946 m) and (e, f) Wirrda Well (Sample OD394, Drill Hole WRD33, 1119.9 m). (a, c, e) These rocks generally contain less than 12 vol.% of olivine (Ol) pseudomorphs. (b) Olivine pseudomorphs in a fine-grained groundmass of dominantly tabular plagioclase show different shapes at Kokatha. (d) Clinopyroxene (Cpx) and phologopite (Phl) phenocrysts occur in the olivine-phyric basalt at Mount Gunson, and clinopyroxene contains Cr-spinel (Cr-Sp) inclusions. The groundmass is mainly made up of clinopyroxene and plagioclase. (f) The olivine-phyric

basalt dyke at Wirrda Well contains phlogopite phenocrysts as well as quartz xenocrysts. All photos are taken under plane-polarized light.

4.3.2 Mount Gunson

A lower unit (200 to 400 m thick) of mafic to intermediate volcanic rocks has been intersected by drilling at Mount Gunson. This unit overlies a 200-m-thick metamorphosed carbonate sequence and is overlain by felsic volcanic units interbedded with tuff, siltstone, and minor mafic igneous rocks (Knutson et al., 1992).

Basalt at Mount Gunson has been partly altered; chlorite, quartz, carbonate, sericite and clays are the dominant secondary phases. Amygdales in the basalt are filled with the same secondary minerals. The basalt has a porphyritic texture (Fig. 4.2c and d). Similar to the basalt at Kokatha, olivine (pseudomorphed) and clinopyroxene are the dominant phenocryst phases. Former olivine phenocrysts have been replaced by secondary minerals, mainly sericite and chlorite. Cr-spinel occurs as inclusions in the olivine pseudomorphs. Olivine pseudomorph sizes range from less than 1 mm to more than 4.5 mm; the majority of the olivine pseudomorphs are ~1 mm in size. Fresh clinopyroxene phenocrysts are up to 0.5 mm in size and altered counterparts are composed of fine-grained chlorite and quartz. They commonly contain melt inclusions and rarely contain Cr-spinel inclusions (Fig. 4.2d). In some samples, (former) clinopyroxene phenocrysts form a glomerophyric texture. In contrast to basalt at Kokatha, phlogopite occurs as micro-phenocrysts in the basalt at Mount Gunson (Fig. 4.2d). Fresh phlogopite crystals (~5 vol.%) are up to 0.5 mm in size and may contain apatite inclusions. The groundmass is mostly cryptocrystalline to microcrystalline, and in the latter case, fresh clinopyroxene and phlogopite are observed to be the most abundant minerals. Amygdaloidal basalt also occurs at Mount Gunson but lacks olivine pseudomorphs. Quartz crystals with embayed rims in the basalt at Mount Gunson are considered to be xenocrysts derived from granitoids.

4.3.3 Wirrda Well

The Wirrda Well prospect is situated ~25 km to the southeast of the Olympic Dam deposit (Fig. 4.1). The rock unit hosting the Cu-Au prospect at Wirrda Well is the ca. 1850 Ma Donington Suite granite (Hand et al., 2007). The mafic rocks at Wirrda Well

can be subdivided into two groups based on their field relationship to Cu sulfides: pre-Cu sulfides mafic dykes (intersected in most drill holes at Wirrda Well) and a syn- to post-Cu sulfides olivine-phyric dyke (one drill hole only, WRD33). The former dykes contain Cu sulfides and are altered and variably deformed. These dykes significantly pre-date the GRV (Ehrig, 2013), and will not be discussed further. The syn- to post-Cu sulfides olivine-phyric dyke (up to ~20 m wide) crosscuts the mineralised zones and is undeformed; U-Pb apatite dates (reported below) are consistent with this dyke belonging to the GRV. It has been invariably altered. Chlorite dominates the secondary minerals; sericite, quartz and carbonate are subordinate. The olivine-phyric dyke has a porphyritic texture (Fig. 4.2e and f). Olivine and clinopyroxene were the major phenocryst phases, and phlogopite is present as micro-phenocrysts and in the groundmass. Former olivine phenocrysts are mostly replaced by chlorite, quartz and sericite, and range in size from less than 1 mm to more than 2 mm (Fig. 4.2e). Cr-spinel occurs as inclusions in the olivine pseudomorphs. Clinopyroxene is recognized based on the occurrence of equant pseudomorphs that consist of chlorite, in contrast to the olivine pseudomorphs which are characterized by skeletal shapes. Phlogopite is still fresh in the olivine-phyric dyke at Wirrda Well (Fig. 4.2f); crystals are generally less than 1 mm in size, and some contain accessory apatite inclusions.

The abundance of olivine pseudomorphs and phlogopite micro-phenocrysts varies inversely. Samples with the highest abundance of olivine pseudomorphs (~6 vol.%) generally contain less than 3 vol.% of phlogopite micro-phenocrysts and have a cryptocrystalline groundmass, whereas samples with few olivine pseudomorphs (less than 2 vol.%) have more phlogopite micro-phenocrysts (~10 vol.%) and have holocrystalline, fine-grained groundmasses. Compared to the olivine-phyric basalts at Kokatha and Mount Gunson, the olivine-phyric dyke at Wirrda Well appears to contain higher volumes of granitoid-derived quartz xenocrysts (~3 vol.%) (Fig. 4.2f). Quartz xenocrysts have embayed margins and display a large size range, from less than 0.5 mm to more than 1.5 cm (Fig. 4.2f).

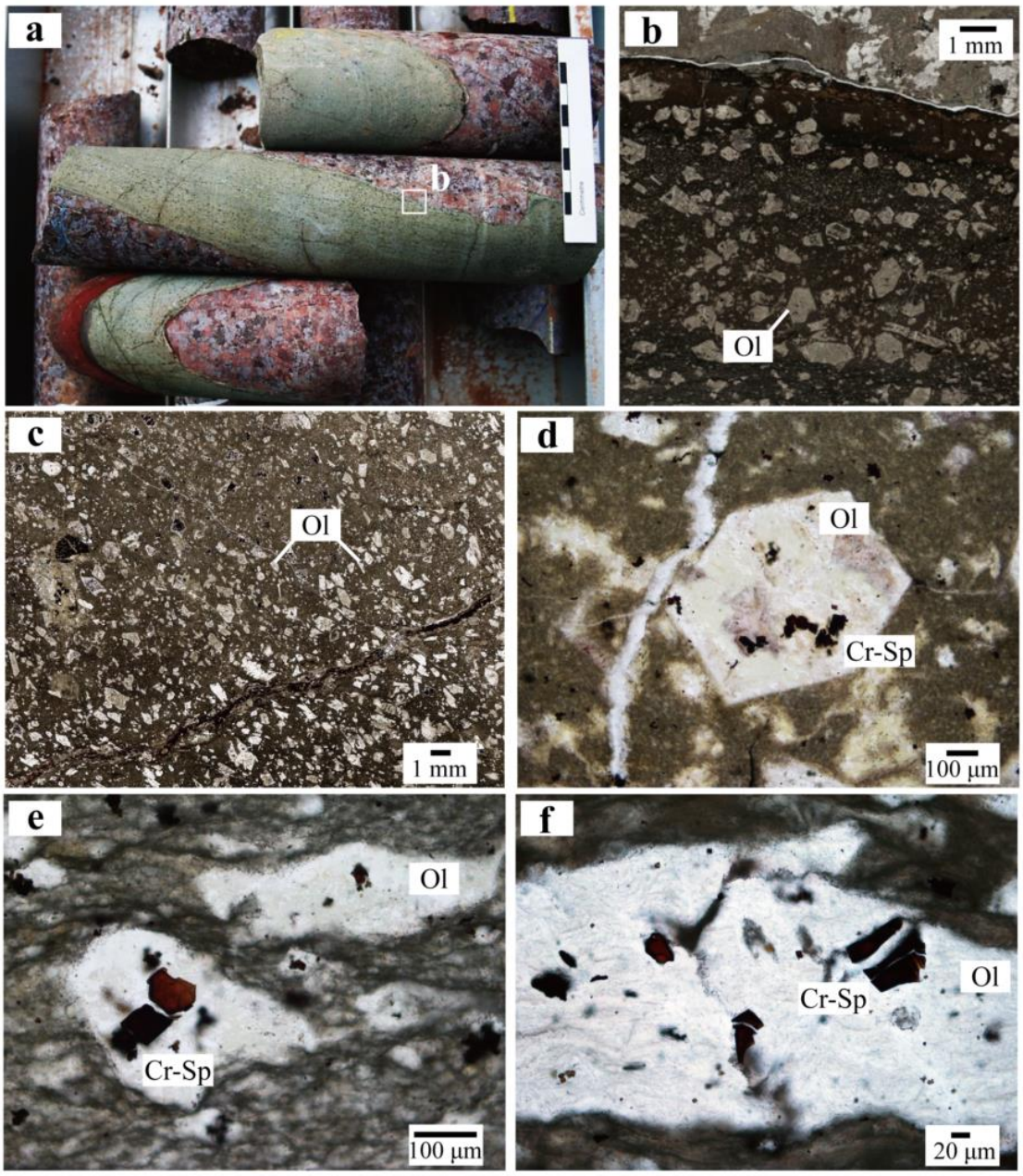

Figure 4.3 Olivine (Ol)-phyric basalt at Olympic Dam. (a-b) The olivine-phyric dyke intrudes the Roxby Downs Granite (Sample OD7, Drill Hole RD2570, 764.4 m). (c) The olivine-phyric basalt (Sample OD862, Drill Hole RD1687, 449.5 m) typically contains a high abundance (~20 vol.%) of olivine pseudomorphs. (d-f) Olivine-phyric basalt is characterized by porphyritic texture; euhedral to deformed olivine pseudomorphs contain euhedral and/or fragmented Cr-spinel (Cr-Sp) inclusions. (b-f) photomicrographs are taken under plane-polarized light.

4.3.4 Olympic Dam

The Olympic Dam Cu-U-Au-Ag deposit is situated in the north-eastern part of the Gawler Craton beneath undeformed Neoproterozoic to Cambrian sedimentary rocks (Fig. 4.1, Hand et al., 2007). Beneath this sedimentary cover, the deposit is restricted to the Olympic Dam Breccia Complex, which occurs entirely within the Roxby Downs Granite, a member of the Hiltaba Suite (Reeve et al., 1990; Ehrig et al., 2012) . There are two groups of mafic rocks present at the Olympic Dam deposit. The first group consists of intensely altered olivine-phyric basalt which has been interpreted to belong to the GRV (Reeve et al., 1990; Johnson, 1993; Johnson and McCulloch, 1995). This group also includes variably altered aphanitic, doleritic and porphyritic mafic dykes, which may belong to the GRV, as indicated by apatite U-Pb dating of one suite of doleritic dykes. The second group comprises commonly less altered dolerite and pyroxene-plagioclase-phyric basaltic dykes, and is correlated with the ca. 820 Ma Gairdner Dyke Swarm (Gairdner dykes) (Huang et al., 2015, Chapter 3).

The intensely altered olivine-phyric basalt of the first group occurs in two situations. (1) An apparent flat-lying unit of this basalt has been intersected in six drill holes directly beneath the unconformity between the Olympic Dam Breccia Complex and the Neoproterozoic to Cambrian sedimentary cover; the drill hole intersections range in thickness from 15 m to 45 m. (2) Olivine-phyric basalt dykes (a few centimetres to ~1 m wide) occur in a NW-striking, steeply E-dipping orientation. These dykes locally have very fluidal margins and delicate apophyses, and pinch and swell over very short distances (Johnson, 1993). They intrude the Roxby Downs Granite (Fig. 4.3a and b) and the Olympic Dam Breccia Complex. The contacts with the latter rocks vary from sharp and planar (Fig. 4.3a and b) to brecciated and gradational over several metres (Bradbury, 1988).

The intensely altered olivine-phyric basalt contains ~5 to 20 vol.% of former olivine phenocrysts (Fig. 4.3b and c). The olivine pseudomorphs have a variety of both euhedral (Fig. 4.3d) and anhedral shapes (Fig. 4.3e), and range in size from less than 0.1 mm to more than 3 mm. Cr-spinel occurs as inclusions in the olivine pseudomorphs (Fig. 4.3d, e and f), and may contain melt inclusions. Former phlogopite micro-phenocrysts may have been present but are now represented by tabular to platy

pseudomorphs composed of fluorite + chlorite in the groundmass. No other phenocryst phases have been identified in the intensely altered olivine-phyric basalt at Olympic Dam. The groundmass is cryptocrystalline, may contain former plagioclase, or may have been originally glassy. Some of the originally olivine-phyric basalt intervals at Olympic Dam are amygdaloidal. The intensely altered olivine-phyric basalt has been replaced by fine-grained chlorite, quartz, carbonate, sericite and hematite.

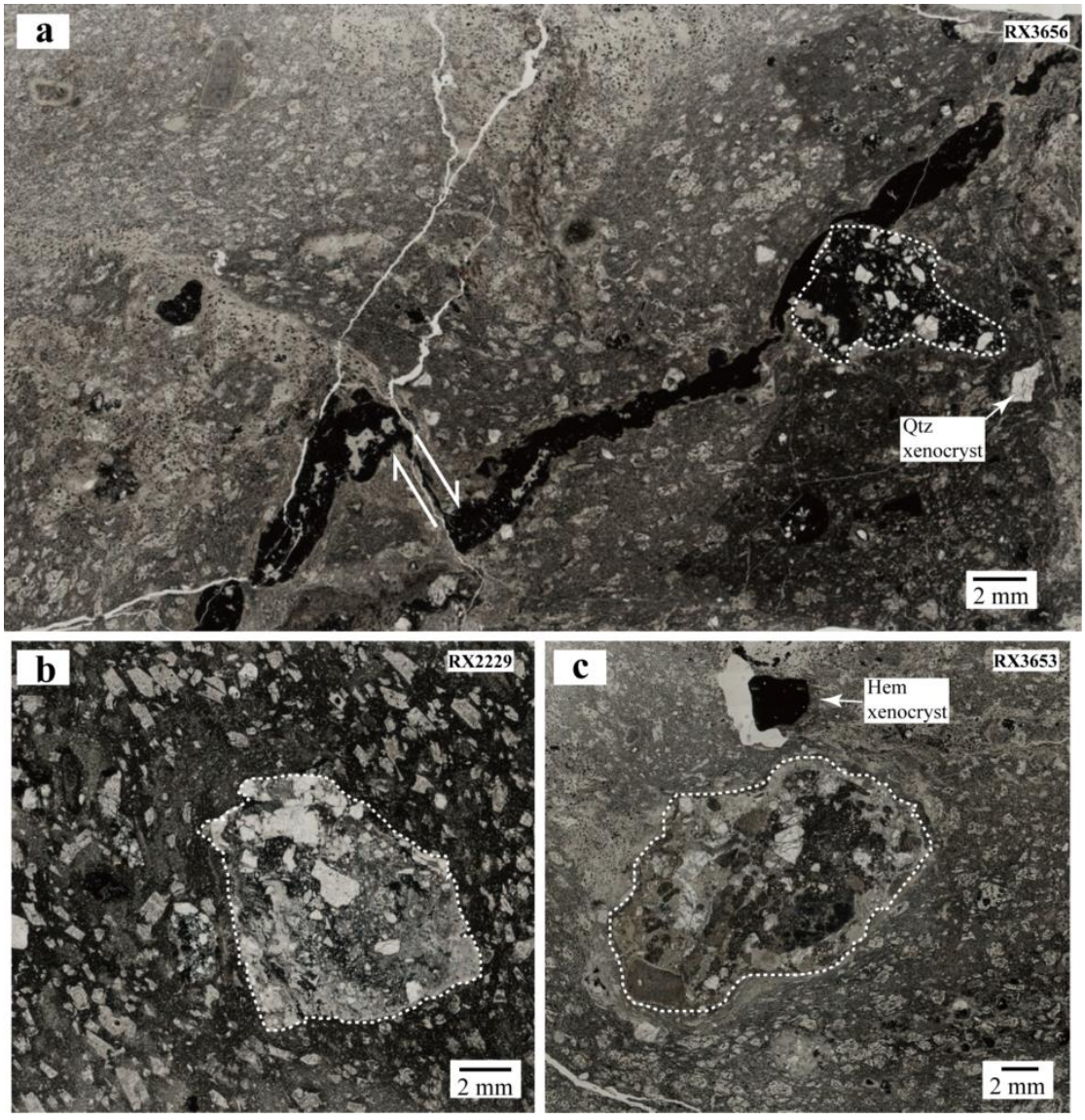

Figure 4.4 Olivine-phyric basalt at Olympic Dam, containing quartz (Qtz) and hematite (Hem) xenocrysts and xenoliths (circled by dashed lines). Plane-polarized light.

Xenocrysts and xenoliths are common in the flat-lying unit of olivine-phyric basalt. Quartz and hematite xenocrysts range up to 2 mm in size (Fig. 4.4a and c). Milky quartz xenocrysts have reaction rims and are partially embayed (Fig. 4.4a). Xenoliths

generally range from 5 mm to 1 cm in size. The contacts between xenoliths and host basalt vary from sharp and planar (Fig. 4.4b) to gradational (Fig. 4.4c). In the latter case, the basalt around the xenolith is pale green and may have been glassy (altered to chlorite). Xenoliths are mainly made up of fine-grained quartz, chlorite, sericite and hematite; intense alteration has obscured the nature of the protoliths (e.g. hematite-altered xenolith in sample RX3656, Fig. 4.4a; chlorite- and sericite-altered xenolith in samples RX2229 and RX3653, Fig. 4.4b and c).

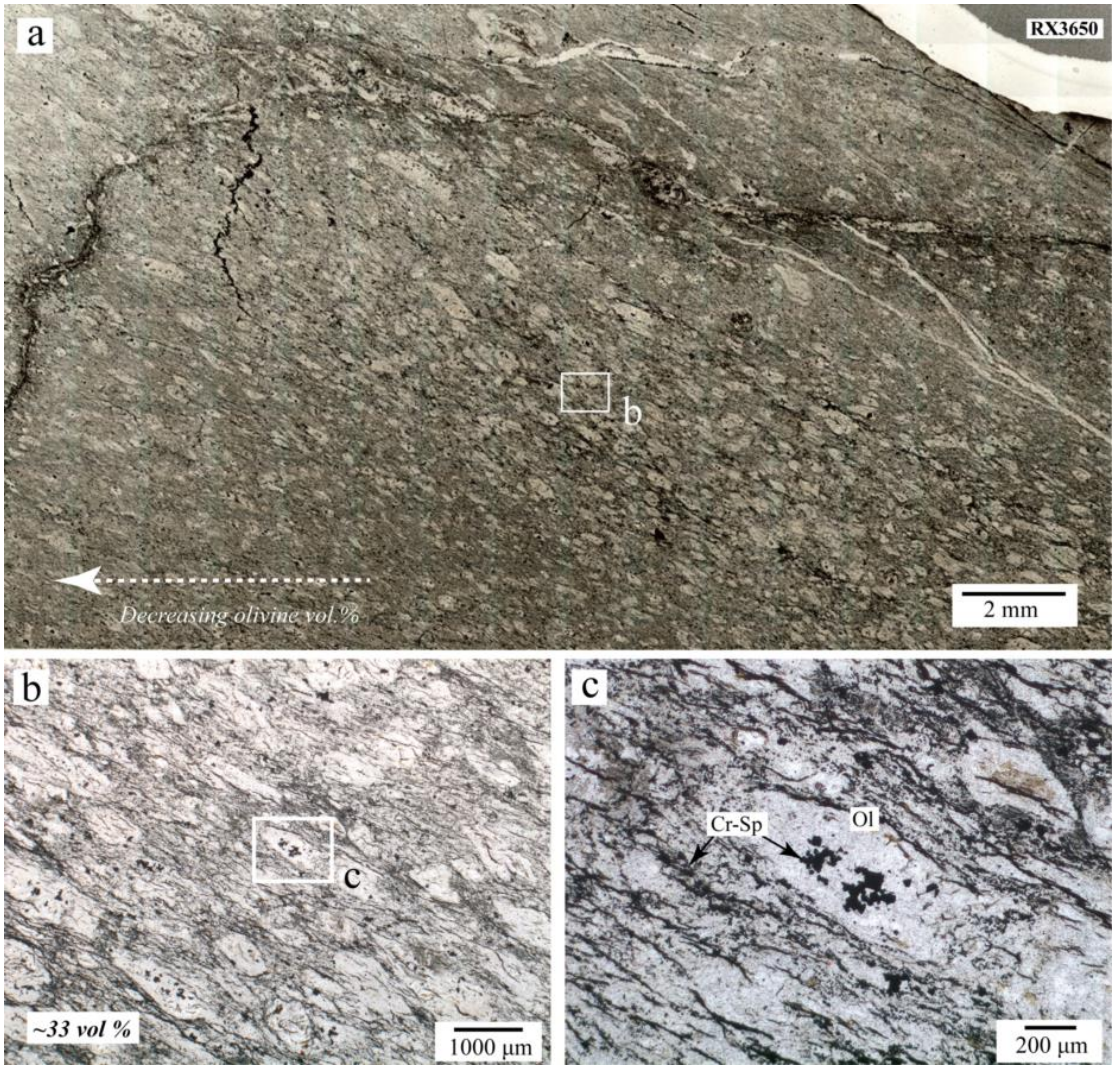

Figure 4.5 Deformed olivine-phyric basalt at Olympic Dam. (a) The abundance of olivine pseudomorphs varies on a thin-section scale. (b) Locally, more than 33 vol.% of olivine (Ol) pseudomorphs can be observed. (c) Cr-spinel (Cr-Sp) inclusions in the groundmass were probably originally within olivine phenocrysts that have been strongly altered and sheared. Plane-polarized light.

Olivine pseudomorphs are commonly deformed and/or fragmented (Fig. 4.3e and f, and Fig. 4.5c), and Cr-spinel inclusions have also been fragmented (Fig. 4.3f). Some olivine-phyric basalt samples show a strong alignment of elongate (flattened and stretched) olivine pseudomorphs, and a large number of former Cr-spinel inclusions in olivine pseudomorphs can be found outside their original hosts (Fig. 4.5c). Gradual changes in the abundance of olivine pseudomorphs (from ~10 to 30 vol.%, Fig. 4.5a and b) across the foliation have been observed. All these petrographic features probably resulted from a combination of post-magmatic alteration, especially hydrothermal dissolution, and shearing. An example of brittle deformation is evident from the dextral offset of a hematite veinlet in sample RX3656 (Fig. 4.4a).

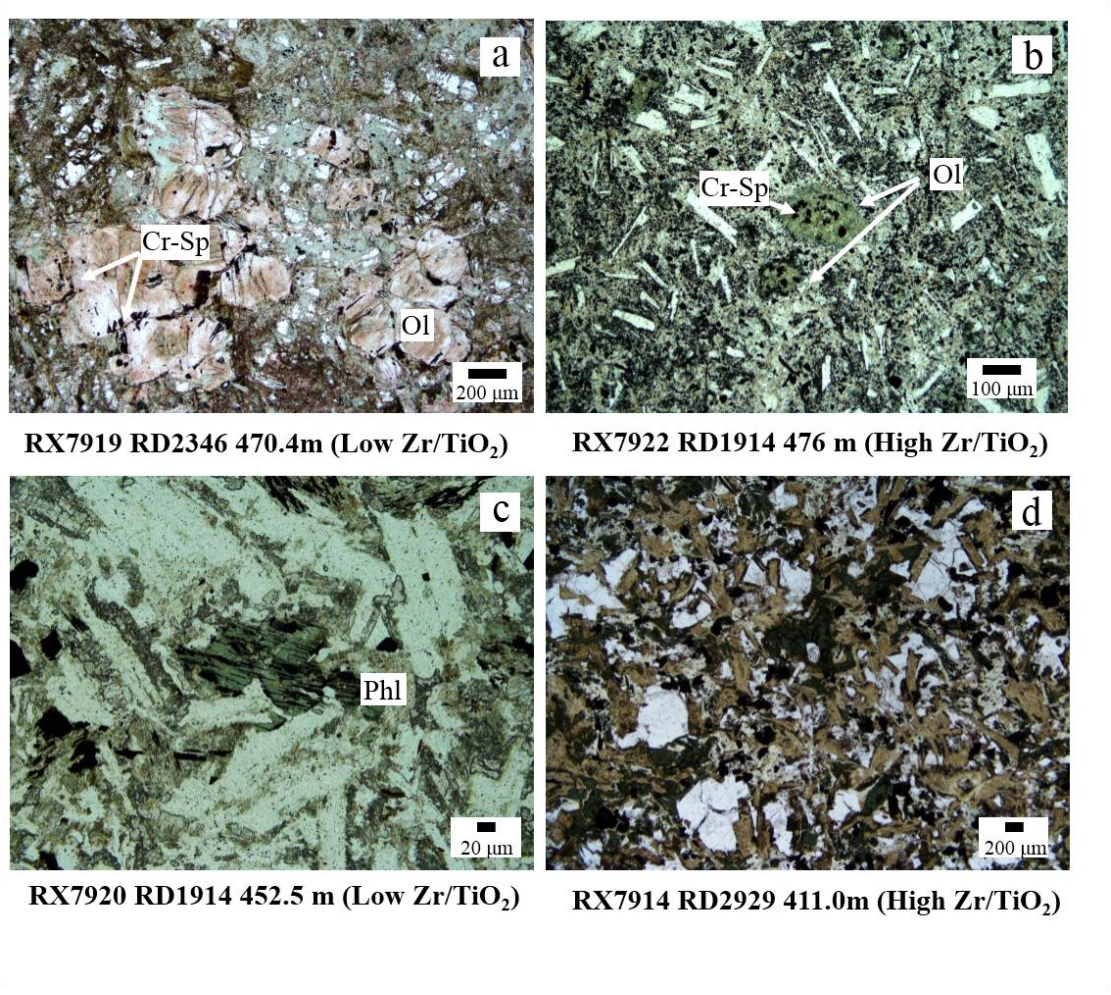

Figure 4.6 Low and High Zr/TiO_2 mafic dykes at Olympic Dam. Both groups of dykes display (a, b) porphyritic to (c, d) doleritic textures. (a, b) Olivine (Ol) pseudomorphs contain Cr-spinel inclusions in both groups of dykes. Phlogopite (Phl) pseudomorphs (altered to chlorite) occur only in the Low Zr/TiO_2 dykes (c). Plane-polarized light.

The olivine-phyric basalt is spatially associated with a series of NW-striking doleritic to porphyritic mafic dykes in which olivine abundance is less than 5 vol.%. These dykes intruded the Roxby Downs Granite and Olympic Dam Breccia Complex. They range in thickness from several meters to tens of meters, and consist of at least two generations that are petrographically similar but can be subdivided into two groups on the basis of composition.

Recognizable (former) primary minerals in these dykes include olivine, pyroxene, plagioclase, phlogopite, Ti-magnetite and apatite. A variety of textures have been preserved, ranging from porphyritic (Fig. 4.6a and b) to doleritic (grain size <0.1 mm to 1 mm, Fig. 4.6c and d). Former olivine phenocrysts commonly occur in the porphyritic dykes, together with other minerals (e.g. pyroxene and plagioclase). Cr-spinel inclusions occur in the pseudomorphed olivine phenocrysts (up to ~1.5 mm in size, Fig. 4.6a and b). Chlorite pseudomorphs possibly after phlogopite have been recognized in some samples (e.g. RX7920, Fig. 4.6c). Other primary minerals, except for Cr-spinel, Ti-magnetite and apatite, have been completely replaced by secondary minerals including chlorite, sericite, carbonate and quartz.

4.4 Analytical methods

4.4.1 Mineral composition of Cr-spinel

Major elements in Cr-spinel were analysed using a Cameca SX100 electron microprobe at the Central Science Laboratory, University of Tasmania. Operating conditions were 40 degrees take-off angle, with beam energy of 15 kV. The beam current was 30 nA, and the beam diameter was 2 microns. Elements were acquired using analysing crystals LIF (large lithium fluoride) for Fe, Mn, Ti, Cr, Zn, LPET (large pentaerythritol) for P, K, Ca, and TAP (thallium acid pthalate) for Al, Si, Na, Mg. The standards were Bustamite (Astimex block) for Mn, Hematite (Astimex block) for Fe, Rutile (Astimex block) for Ti, Clinopyroxene, Delegate (UTAS1 block) for Ca, Si, Olivine, San Carlos, USNM111312/444 (UTAS1 block) for Mg, Plagioclase, Labradorite, USNM115900 (UTAS1 block) for Al, Chromite Tiebaghi USNM117075 (UTAS2 block) for Cr, Gahnite Brazil USNM145883 (UTAS2 block) for Zn, (K-) Anorthoclase, USNM133868 (UTAS3 block) for Na, Microcline (UTAS3 block) for K,

and Apatite Durango (Apatites block) for P. The counting time was 10 seconds for Na, Mn, Ti, K, Ca, P, 20 seconds for Zn, 30 seconds for Si, and 40 seconds for Al, Fe, Cr, Mg. The off peak counting time was 10 seconds for Na, Mn, Ti, K, Ca, P, and 20 seconds for Fe, Mg, Al, Si, Cr, Zn. Off-peak correction method was Linear for Na, Mg, Fe, Ti, K, Ca, Al, Si, Cr, Zn, and Slope (Hi) for Mn and P. Unknown and standard intensities were corrected for deadtime. Standard intensities were corrected for standard drift over time. Interference corrections were applied to Mn for interference by Cr. Oxygen was calculated by cation stoichiometry and included in the matrix correction. Further details can be seen in Armstrong (1988).

4.4.2 Whole rock major and trace element concentrations

Selected samples were crushed in an agate mill for X-ray fluorescence (XRF) and inductively coupled plasma mass spectrometry (ICP-MS) whole-rock analysis at the University of Tasmania. Samples were digested in HF/H_2SO_4 with the PicoTrace high pressure digestion equipment and analysed with a Philips PW1480 X-ray Fluorescence Spectrometer for major elements and an Agilent 4500 ICP-MS for trace elements. Detection limits for trace elements in ICP-MS are $\leq$0.01 ppm (REE) and $\leq$0.5 ppm for other elements, except As (5 ppm). A comparison of XRF and ICP-MS trace element data indicates a good correlation between the two methods, the difference being <20%.

4.4.3 Sample assays

Samples (from Mount Gunson) have been assayed for major and trace elements using a combination of four-acid digestion and inductively coupled plasma-optical emission spectroscopy (ICP-OES) for Cu, Ag, As, Co, Ni, Pb, and Zn; lithium metaborate fusion and ICP-OES for Ba, Al, Ca, Ce, Fe, K, La, Mg, Mn, Na, P, Si, Sr, Ti, Y, and Zr; lithium metaborate fusion and inductively coupled plasma-mass spectroscopy (ICP-MS) for U_3O_8, Bi, Sb, and Mo; induction furnace-infrared spectrometry (IF-IS) for CO_2 and S; and fire assay-flame atomic absorption spectrometry (FA-AAS) for Au. Please refer to Ehrig et al. (2012) for further details.

4.4.4 U-Pb apatite geochronology

U-Th-Pb dating of apatite was carried out using laser-ablation ICPMS (e.g. Chew et al., 2014 and references therein) on polished rock samples mounted in 25 mm diameter epoxy mounts. Apatite crystals were recognised using a scanning electron microscope. The crystals were analysed using a Coherent Scientific 193 nm Ar-F excimer gas laser coupled with a Resonetics S155 ablation cell and an Agilent 7500cs quadrupole ICPMS at the University of Tasmania. Apatite was ablated in a helium atmosphere (0.35 litres / minute) using a 32 μm laser spot (5 Hz, energy density ~2 J/cm^2). Following a 30 second gas blank, samples were ablated for 30 seconds. Ablation in the S155 ablation cell is carried out in He, followed by transfer to the ICP-MS torch in argon via nylon tubing; a mixing manifold (squid) was applied in this work. The isotopes measured were ^{31}P, ^{49}Ti, ^{43}Ca, ^{56}Fe, ^{140}Ce, ^{202}Hg, ^{204}Pb, ^{206}Pb, ^{207}Pb, ^{208}Pb, ^{232}Th and ^{238}U (5 ms dwell time for the major and trace elements, 20 ms for the Pb isotopes, and 10 ms for Th and U). Downhole fractionation, instrument drift and mass bias in apatite analyses were corrected using an in-house apatite standard, OD306, a coarse-grained apatite from an apatite-magnetite vein at the Acropolis Cu-Au prospect in South Australia. Isotope dilution U-Pb data obtained for 6 mg-sized (1.3-4.5 mg) fragments by MC-ICP-MS at the University of Melbourne (e.g. Woodhead and Pickering, 2012) show modest U contents (15-19 ppm), Th/U ~4.8 and variable but generally low common Pb contents (measured ^{206}Pb/^{204}Pb 336-1556, f_{206}=0.011-0.051, n=6, R.Maas, 2012, unpublished data). After common Pb correction, the data yield concordant to near-concordant (≤2.5% disc.) ^{207}Pb/^{206}Pb ages averaging 1598 ± 4 Ma (2 standard error) and a formal discordia intercept of 1594 ± 7 Ma. At the sampling scale of the laser, the apatite shows a high degree of homogeneity in Pb/U ratios and little evidence of the variable common Pb seen in the bulk analyses. Kovdor and Otter Lake apatite (Amelin and Zaitsev, 2002; Barfod et al., 2005; Chew et al., 2011) were monitored as secondary standards; the ^{207}Pb-corrected ^{206}Pb/^{238}U ages obtained for these crystals are well within error of published reference ages. OD306 apatite was preferred as primary standard over the Otter Lake or Kovdor apatites because it provides more homogeneous Pb/U data on the UTAS laser ablation system (internal precision ±1.1%, n=10 compared to ±1.4% and ±3.9% for Otter Lake and Kovdor, respectively, each based on n=10 analyses), has lower common Pb at the laser sampling

scale, and its U and Th contents closely match those in the apatite measured here. Further details on the method can be seen in Chapter 3 (Huang et al., 2015).

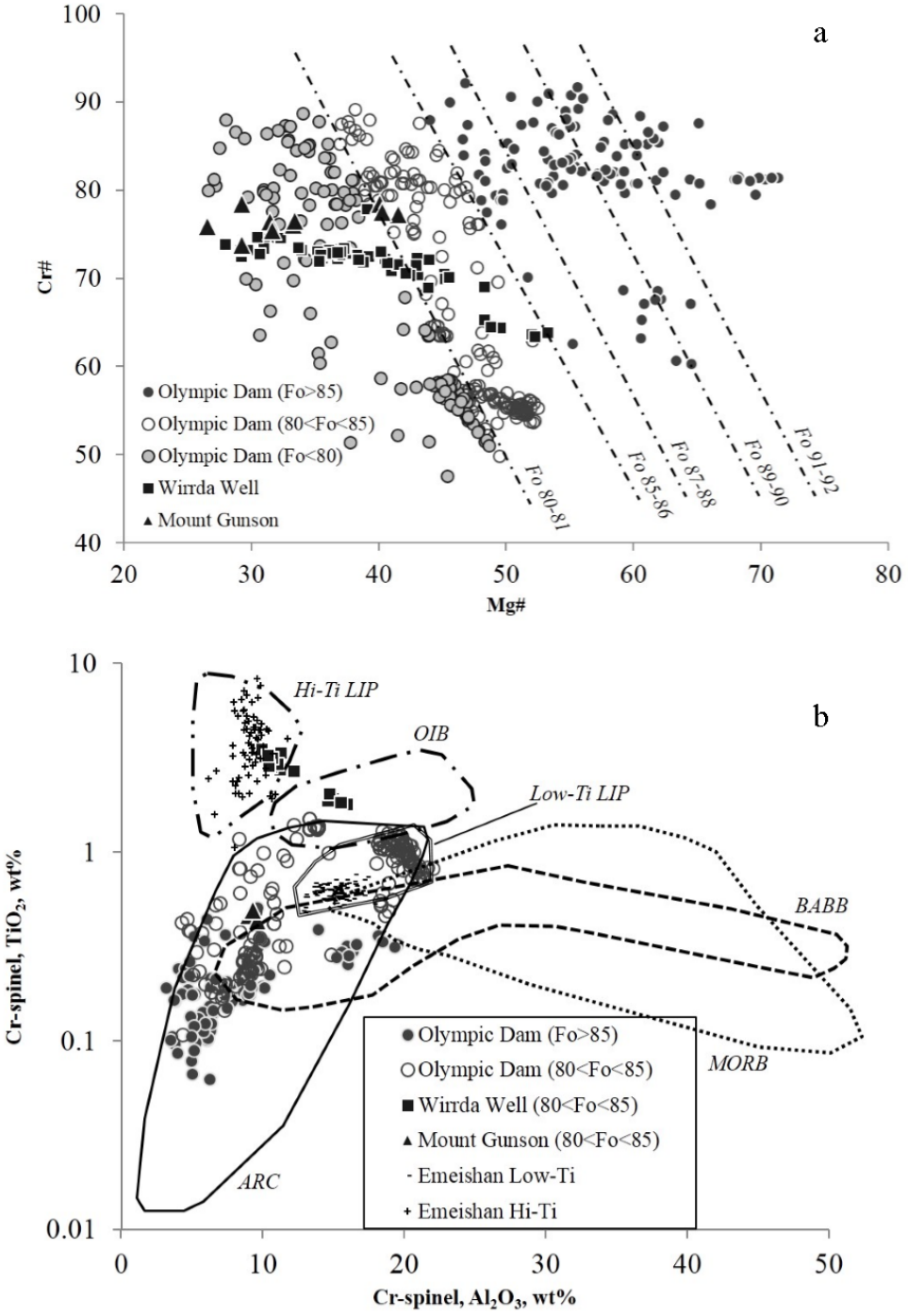

Figure 4.7 (a) Cr# vs. Mg# plot and (b) TiO_2 vs. Al_2O_3 plot for Cr-spinel inclusions in mafic GRV from Mount Gunson, Wirrda Well and Olympic Dam. Diagrams are after Kamenetsky et al. (2001) and have been modified to include recent Cr-spinel analyses from the Emeishan Low-Ti and Hi-Ti LIP basalts in Kamenetsky et al. (2012). Abbreviations: Fo,

Forsterite; ARC, island arc basalt; Hi-Ti LIP, high-titanium large igneous province; OIB, ocean island basalt; Low-Ti LIP, low-titanium large igneous province; BABB, back-arc basin basalt; MORB, mid-ocean ridge basalt.

4.5 Cr-spinel compositions

Cr-spinel mainly occurs as inclusions in the olivine pseudomorphs in all studied olivine-phyric rocks described above. Less commonly, it is enclosed in the clinopyroxene phenocrysts and present in the groundmass. Compositions of Cr-spinel inclusions within olivine pseudomorphs have been analyzed.

Considering that all the olivine-phyric rocks in this study are altered and that primary olivine has been invariably replaced by a variety of secondary minerals, it is likely that the compositions of Cr-spinel inclusions have also been modified by hydrothermal processes. A geochemical filter of MgO >5.0 wt.%, ZnO <0.3 wt.% and MnO <0.6 wt.% has been adopted to avoid altered Cr-spinel inclusions (Kamenetsky et al., 2001). Using this geochemical filter, we obtained 481 analyses (Table S3).

Olympic Dam Cr-spinel inclusions have a wider Al_2O_3 compositional range (3.1 to 22.4 wt.%), compared to those from Mount Gunson (7.1 to 10.3 wt.%) and Wirrda Well (8.0 to 15.9 wt.%). Cr-spinel inclusions at Wirrda Well are distinguished from those at Mount Gunson and Olympic Dam by their higher TiO_2 contents (1.8 to 4.0 wt.%), for a given Al_2O_3 content. Almost all the Cr-spinel analyses for samples from the latter two locations have TiO_2 contents below 1.8 wt.%. Mount Gunson Cr-spinel has an Mg# [Mg/(Mg + Fe^{2+}), mol.%] from 27 to 42 and a Cr# [Cr/(Cr + Al), mol.%] from 73 to 78. The Mg# of Wirrda Well Cr-spinel ranges from 28 to 53 and the Cr# varies from 63 to 78. Olympic Dam Cr-spinel inclusions have higher values of Mg# (up to 71) at given Cr# (from 43 to 92) (Fig. 4.7a).

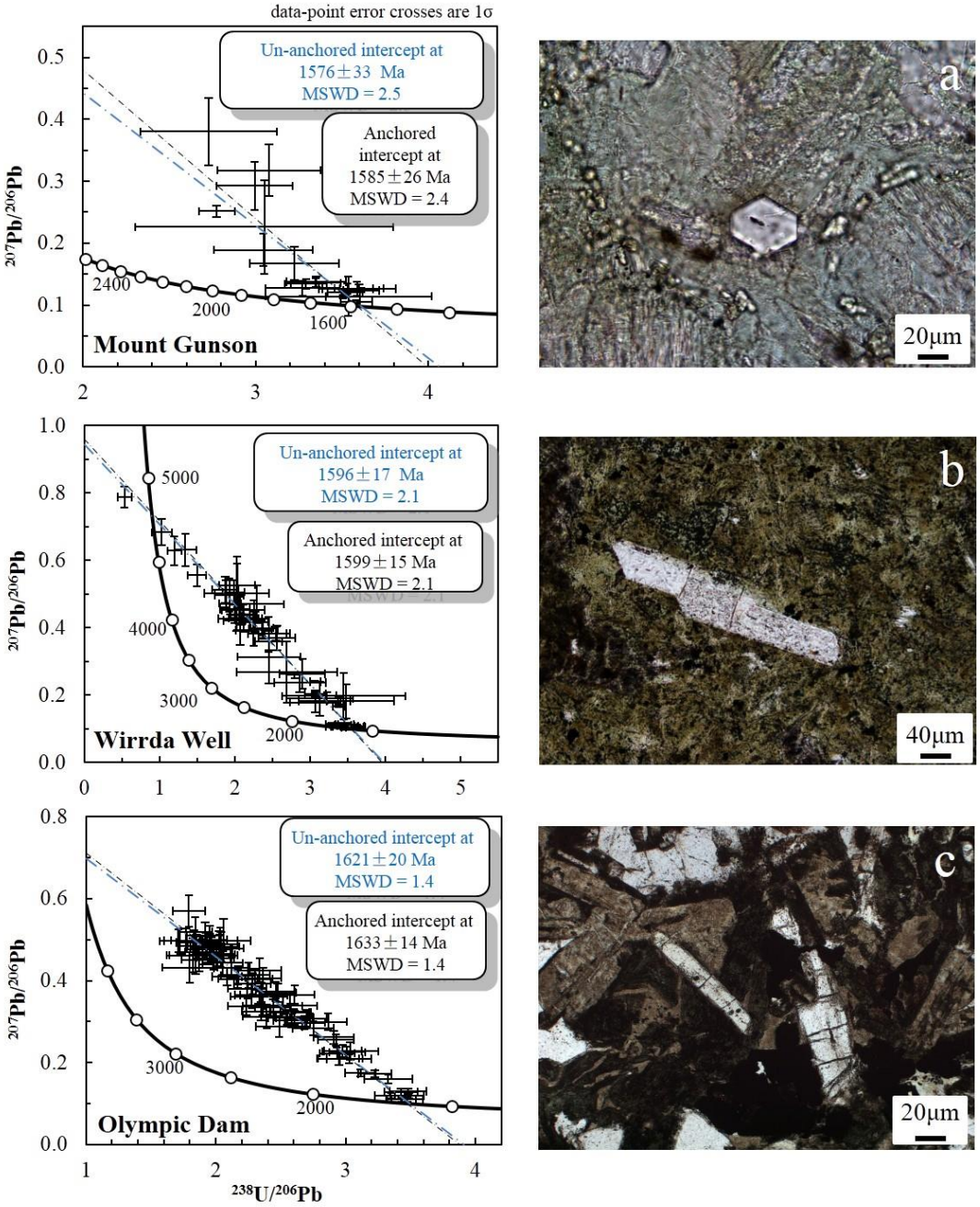

Figure 4.8 Apatite U-Pb dating results for olivine-phyric basalts at (a) Mount Gunson (sample RX3453 from PY-1 at 939.0 m), (b) Wirrda Well (three samples of OD394, 1119.9 m; OD891, 1121.7 m; OD893, 1202.9 m, from drill hole WRD33), and (c) High Zr/TiO2 doleritic dykes at Olympic Dam (sample RX7913, RD2929, 401.3m). Photomicrographs of representative apatite from each location were taken under plane-polarized light. See text for further details.

4.6 Apatite U-Pb dating of the olivine-phyric rocks and mafic dykes

Apatite occurs as a primary accessory phase in the olivine-phyric basalt at Mount Gunson and Wirrda Well, and in the NW-striking doleritic to porphyritic dykes at Olympic Dam. Spongy apatite in the basalt at Olympic Dam occurs in the groundmass and occasionally in the olivine pseudomorphs. The Laser Ablation Inductively Coupled Plasma Mass Spectrometry (LA-ICPMS) U-Pb dating of apatite (Chew et al., 2011, 2014) in these rocks for the first time provides an opportunity to constrain their emplacement ages (Fig. 4.8, Table S4).

Nineteen analyses of single apatite grains recovered from one Mount Gunson basalt sample (RX3453), collected from PY-1 at 939.0 m, plot on a discordia on the Tera-Wasserburg diagram intersecting the concordia curve at 1576 ± 33 Ma (MSWD=2.5), and the $^{207}Pb/^{206}Pb$ axis at 0.87 (Fig. 4.8a). A slightly older age of 1585 ± 26 Ma (MSWD=2.4) is obtained if the discordia is anchored to the common $^{207}Pb/^{206}Pb$ ratio of 0.96 estimated by the model of Stacey and Kramers (1975) for the common Pb composition at 1590 Ma using the average crustal growth curve (μ=9.74).

A comparable result was obtained from accessory apatite crystals in the olivine-phyric dyke at Wirrda Well (Fig. 4.8b). Fifty-seven analyses of single apatite grains in three samples from drill hole WRD33 at Wirrda Well were carried out. The analyses display a wide range of $^{238}U/^{206}Pb$ and $^{207}Pb/^{206}Pb$ ratios. All these analyses plot on a discordia on the Tera-Wasserburg diagram, indicating mixing of common Pb (intersecting the $^{207}Pb/^{206}Pb$ axis at 0.94) and radiogenic Pb (lower intercept) generated by the in situ decay of U since 1596 ± 17 Ma (MSWD=2.1). This age is slightly younger than the result of 1599 ± 15 Ma (MSWD=2.1) obtained if the discordia is anchored to the common $^{207}Pb/^{206}Pb$ ratio of 0.96 (Fig. 4.8b).

Eighty-one apatite crystals from a doleritic dyke sample (RX7913, RD2929, 401.3 m) at Olympic Dam were analysed. A discordia line intersects the concordia curve at 1621 ± 20 Ma (MSWD=1.4) and the $^{207}Pb/^{206}Pb$ axis at 0.9378. This age is also in agreement with the age of 1633 ± 14 Ma (MSWD=1.4) obtained by anchoring the discordia to the common $^{207}Pb/^{206}Pb$ ratio of 0.96 (Fig. 4.8c).

Twenty seven analyses of spongy apatite in the olivine-phyric basalt (Chapter 5, Table S6) at Olympic Dam yielded an unanchored age of 1615 ± 68 Ma (MSWD=12). The high MSWD and the poor precision on the regression, combined with petrographical observation, imply that the apatite is secondary in origin and that the U-Pb systematics of the apatite have been disturbed.

The LA-ICPMS U-Pb isotope analyses of apatite from the Mesoproterozoic mafic igneous rocks in this study provide geochronological data for mafic lithologies that lack zircon and/or baddeleyite (Chew et al., 2014; Huang et al., 2015, Chapter 3).

4.7 Geochemistry of the mafic GRV

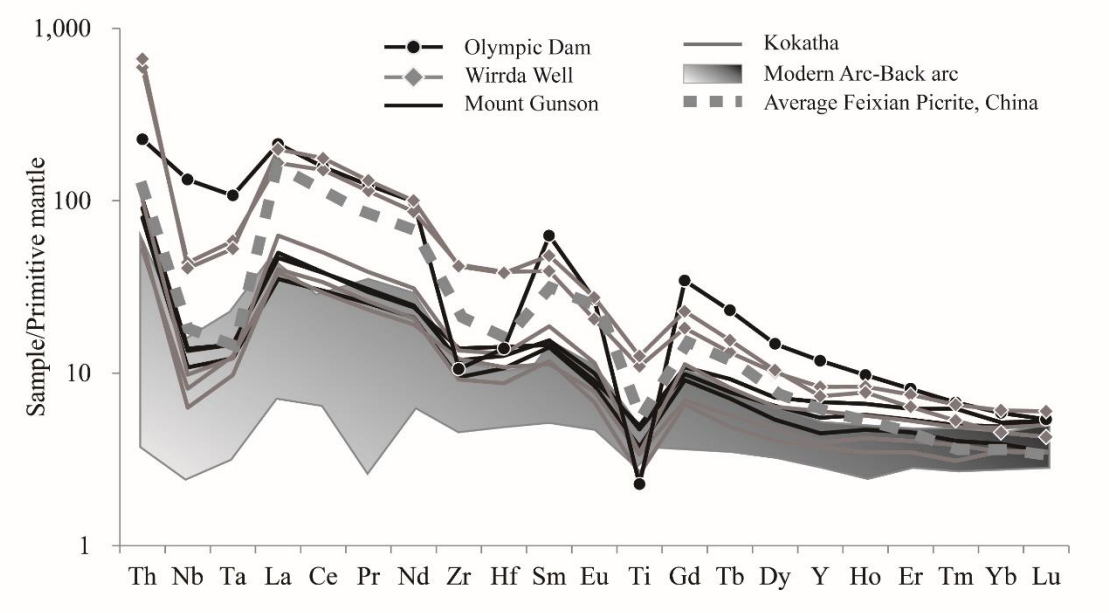

Figure 4.9 Primitive mantle-normalized lithophile element (HFSE-REE) concentration variation diagram for the olivine-phyric mafic GRV from Kokatha (GH81 and GH88 analysed in this study, together with one analysis of GH50 in Agangi, 2011), Mount Gunson (3 analyses, this study), Wirrda Well (OD395 and OD398, this study) and Olympic Dam (one olivine-phyric basalt sample OD24, this study). Compositions of primitive mantle are sourced from Sun and McDonough (1989). Modern arc-Back arc field is after Kelemen et al., (2014) and Taylor and Martinez (2003), respectively, and includes arc basalt analyses from Kermadec, Lesser Antilles, Marianas, New Hebrides, Scotia, Tonga, Aleutian, Andean, Cascades, Central America, Greater Antilles, Honshu, Kamchatka, Luzon arcs and back-arc basin basalt analyses from Lau Basin, Manus Basin, Mariana Tough, and East Scotia Basin. Average composition of Feixian Picrite is from Gao et al. (2008).

The compositions of the olivine-phyric basalts at all locations have been modified by secondary processes to variable degrees, as indicated by their petrographic features (Figs. 2-5). In the case of the most intensely altered olivine-phyric basalt at Olympic Dam, the major element compositions largely reflect different proportions of hydrothermal chlorite, quartz, carbonate, sericite and hematite, rather than primary magmatic features. Drill core assays (Chapter 5, Table S5) of the Olympic Dam olivine-phyric basalts show that they all contain less than 11.1 wt.% MgO and have estimated loss on ignition (LOI) above 5.0 wt.%. Carbonate-altered samples are characterized by high CO_2 contents (up to 26 wt.%), whereas hematite-altered samples contain up to 31.1 wt.% Fe_2O_3. One representative sample (OD24) of the olivine-phyric basalt analysed in this study (Table 4.1) has relatively low MgO contents (11.5 wt.%, LOI-free, same below) and extremely high LOI (up to 17.5 wt.%). Olivine-phyric basalt dyke at Wirrda Well has low MgO contents (~5 wt.%) and relatively high LOI (4.7 to 5.1 wt.%) (Table 4.1). In contrast, olivine-phyric basalt at Kokatha has lower LOI (<1.5 wt.%), and one Mount Gunson basalt sample (RX3456) contains the highest amount of MgO (14.6 wt.%) among all the samples analysed in this study (Table 4.1).

A primitive mantle-normalized lithophile element diagram (Fig. 4.9) shows that the least-altered olivine-phyric basalt samples, from Kokatha and Mount Gunson, have indistinguishable geochemical patterns, and are characterized by negative Nb, Ta, Zr, Hf and Ti anomalies. The olivine-phyric dyke at Wirrda Well has a similar geochemical pattern to the Mount Gunson and Wirrda Well samples and contains higher amounts of high field strength elements (HFSE) and rare earth elements (REE). Olivine-phyric basalt (OD24) at Olympic Dam generally has a comparable compositional pattern but less significant negative Nb and Ta anomalies and more distinct negative Zr and Hf anomalies, and higher concentrations of HFSE and REE.

The multiple generations of mafic rocks at OD (Ehrig et al., 2012; Huang et al., 2015, Chapter 3) have comparable petrographic features, making field classification difficult. Accordingly, the Zr vs. TiO_2 diagram has been introduced as a reliable method for distinguishing the ca. 1590 Ma mafic rocks (olivine-phyric basalt and NW-striking doleritic to porphyritic dykes) from the ca. 820 Ma Gairdner dykes (Fig. 4.10). Both Zr and Ti are HFSE, which presumably have similarly low mobility during hydrothermal alteration. As Zr is more incompatible in magmas than Ti, we used the Zr/TiO_2 ratio to

characterise the geochemical signature (i.e. enrichment/depletion) of parental magmas. The NW-striking doleritic to porphyritic mafic dykes at Olympic Dam can be subdivided into two groups (Low vs. High Zr/TiO_2, of ~250 and 150, ppm to wt.%) based on their Zr and TiO_2 compositions (Fig. 4.10). Both groups of dykes show comparable igneous textures, and primary and secondary mineral assemblages. In general, there are no definite petrographic features that could be used to distinguish the High versus Low Zr/TiO_2 dykes. The olivine-phyric basalt at Olympic Dam has similar Zr/TiO_2 ratios to the High Zr/TiO_2 dykes, whereas the ca. 820 Ma Gairdner dykes have lower Zr/TiO_2 ratios of ~50.

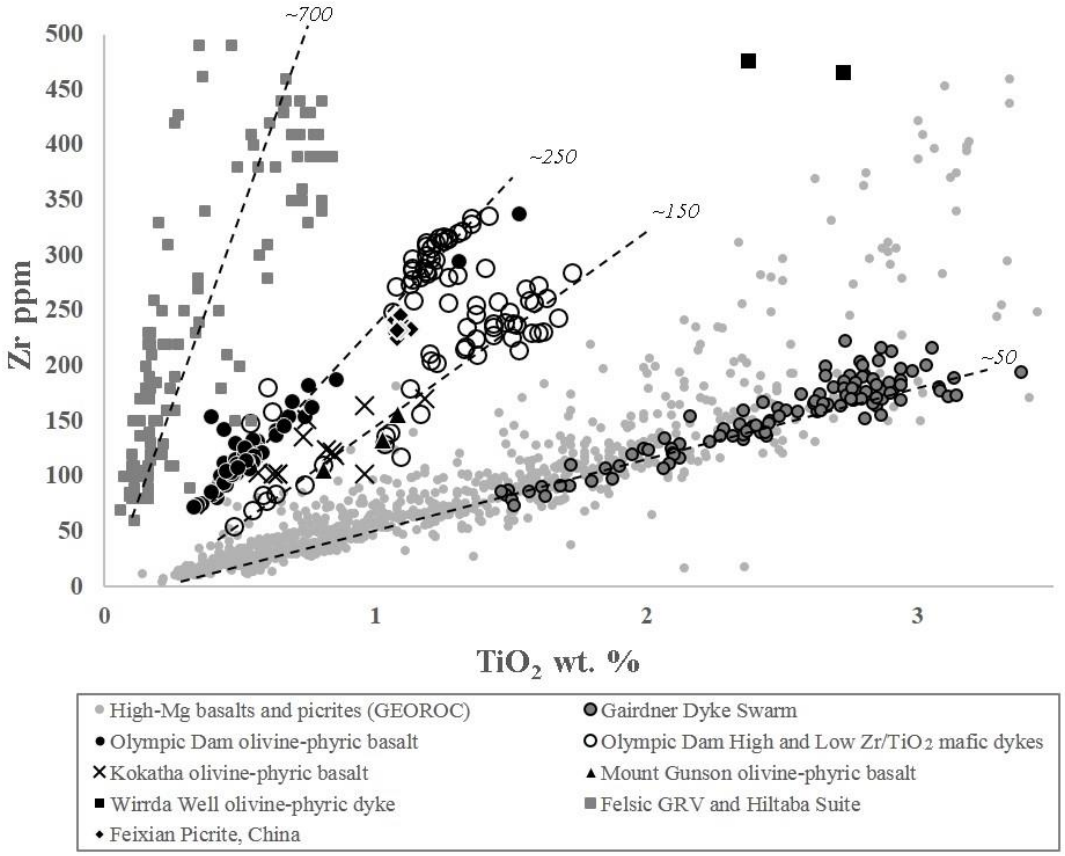

Figure 4.10 Zr vs. TiO_2 diagram for mafic GRV at Kokatha (2 analyses from this study, other data from Giles, 1980, 1988; Stewart, 1994, PIRSA, 2006), Mount Gunson (3 analyses, this study), Wirrda Well (2 analyses, this study), Olympic Dam (drill core assays of the olivine-phyric basalt, Table S5, and NW-striking doleritic to porphyritic dykes, BHP Billiton Olympic Dam, unpublished data). Felsic GRV and Hiltaba Suite data are from PIRSA (2006) and McPhie et al. (2011a). High-Mg (MgO >12 wt.%) basalts and picrites are sourced from the GEOROC database (http://georoc.mpch-mainz.gwdg.de/georoc/Start.asp). Feixian picrite data are from Gao et al., (2008). The NW-striking doleritic to porphyritic dykes at

Olympic Dam can be subdivided into two groups (High and Low Zr/TiO_2) based on this diagram. Olivine-phyric basalt at Olympic Dam shows similar Zr/TiO_2 ratios to the High Zr/TiO_2 dykes. Zr/TiO_2 ratios (ppm to wt.%) of four trends (dashed lines) have been given in the diagram, ranging from ~50 to 700. Data for the Gairdner Dyke Swarm are from Chapter 3 (Huang et al., 2015).

4.8 Discussion

4.8.1 Recognition of high-Mg rocks in the Gawler SLIP

Weakly deformed to undeformed olivine-phyric basalt at Olympic Dam has similar petrographic textures (e.g. porphyritic and amygdaloidal) and comparable mineralogy (e.g. olivine, Cr-spinel, and possible phlogopite) to other olivine-phyric mafic rocks at Kokatha, Mount Gunson and Wirrda Well, but generally contains a higher abundance of olivine pseudomorphs (commonly ~20 vol.%).

Compositional relationships between Cr-spinel inclusions and host olivine phenocrysts in mafic volcanic rocks in different geodynamic settings (Kamenetsky et al., 2001) allow reconstruction of the composition (forsterite number, Fo, mol.%) of former olivine phenocrysts in this study. The Mg#-Cr# systematics of the studied Cr-spinel correspond to former host olivine Fo numbers from less than 80 to above 90 (Fig. 4.7a). This range implies that some of the former olivine phenocrysts, especially those in the Olympic Dam olivine-phyric basalt, were derived from primitive magmas and that the compositions of the olivine phenocrysts evolved with magma fractionation. Assuming an average Fo number of 85 for the olivine phenocrysts (density ~3300 kg/m^3) and a basaltic composition (~8 wt.% MgO, density ~2500 kg/m^3) for the groundmass, the presence of 20 vol.% of such olivine phenocrysts would hypothetically yield an initial whole-rock MgO content of ~16.5 wt.% for the olivine-phyric basalt at Olympic Dam.

Mafic lithologies are known to be part of the GRV, based on their field relationships with dated felsic GRV at the same location (e.g. interlayered mafic and felsic units; Blissett et al., 1993). Accessory apatite in the olivine-phyric basalt and mafic dykes from Mount Gunson, Wirrda Well, and Olympic Dam yields ages (Fig. 4.8) that can be correlated with the U-Pb zircon ages (from ca. 1570 to 1595 Ma, with apparent peaks at ca. 1580 Ma and 1590 Ma, Hand et al., 2007; and references therein)

of the felsic GRV and Hiltaba Suite. The apatite dates constrain the ages of these mafic rocks and lend further support for their correlation with the GRV and the Gawler SLIP. Although far subordinate to the felsic GRV, the mafic GRV units (in particular the olivine-phyric basalt at Olympic Dam) indicate the presence of primitive high-Mg compositions at widely separated locations in the Gawler SLIP.

4.8.2 Tectonic setting and mantle source of the Gawler SLIP

4.8.2.1 Tectonic setting of the Gawler SLIP: a review

The Gawler SLIP was initially considered to have formed in an intraplate setting, where magmatism was initiated above a mantle diapir (Giles, 1988). However, there are now a number of new tectonic interpretations that place the Gawler SLIP in a continental margin or back-arc setting, with or without a mantle plume influence, though no consensus has been reached on the position and polarity of subduction (Wade et al., 2006; Hand et al., 2008; Betts et al., 2009; Skirrow, 2010; and references therein). "Arc-like" ca. 1590 to 1550 Ma igneous rocks in the Musgrave Block ~300 km to the north of the Gawler Craton have been interpreted by Wade et al. (2006) as products of southward subduction of the North Australian Craton towards the South Australian Craton (Gawler Craton). In this interpretation, the "arc-like" igneous rocks in the Musgrave Block are considered to represent island-arc volcanic formations, whereas the GRV are thought to represent continental arc or back-arc counterparts. Compression and accretion of volcanic arcs at the convergent margin have led to metamorphism within strongly deformed zones at the margins of the Gawler Craton (Hand et al., 2008). Betts et al. (2009) placed the Gawler Craton in an overriding plate on top of a northward-subducting plate, and proposed that a mantle plume was involved in the petrogenesis of the Gawler SLIP. Skirrow (2010) suggested that the Gawler SLIP formed in an intracontinental or "far-field" (at a remote distance from the subduction zone) continental back-arc setting, and that mafic to ultramafic magmatism as a result of removal and detachment of mantle lithosphere led to the formation of the Gawler SLIP. It is worthy to note that none of the interpretations that involve a convergent margin place the margin within the extent of the Gawler SLIP.

4.8.2.2 Implications of Cr-spinel and whole-rock compositions

The compositions of Cr-spinel inclusions and the least-altered olivine-phyric mafic GRV units (from Kokatha and Mount Gunson) allow us to evaluate these models. High-Fo olivine is the earliest mineral to crystallize during magma evolution. Hence, Cr-spinel inclusions enclosed within such olivine record some characteristics of the primary melts, and the mantle source. Positive correlations exist between Al_2O_3 and TiO_2 contents in Cr-spinel and coexisting melt over significant compositional intervals sampled from a variety of magma types and tectonic environments, indicating that magmatic Al_2O_3 and TiO_2 exert control on the Al_2O_3 and TiO_2 contents of corresponding Cr-spinel (Kamenetsky et al., 2001). Cr-spinel enclosed within former olivine phenocrysts of Fo >90 (i.e. having the highest Mg# at a given Cr#; Fig. 4.7a, all from Olympic Dam) contain 0.10 to 0.23 wt.% TiO_2 (average 0.18 wt.%), and 4.9 to 10.5 wt.% Al_2O_3 (average 8 wt.%). These ranges correspond to former primary magmatic TiO_2 and Al_2O_3 contents of ~0.3 to 0.6 wt.% and ~6 to 10 wt.%, respectively, based on the correlations demonstrated in Kamenetsky et al. (2001).

The dependence of Cr-spinel Al_2O_3 and TiO_2 concentrations on the parental melt composition allows Cr-spinel to be used as a tectonic indicator, at least for Phanerozoic magmas (Arai, 1992; Barnes and Roeder, 2001; Kamenetsky et al., 2001). This relationship is particularly valuable where the host olivine phenocrysts and rocks have been altered. In this study, only Cr-spinel within relatively primitive (Fo >80) olivine phenocrysts has been considered for its tectonic significance (Fig. 4.7b). Such Cr-spinel inclusions are more likely to record characteristics of primary melts and includes Cr-spinel inclusions in basalt at Mount Gunson, Wirrda Well and Olympic Dam. Cr-spinel inclusions from Mount Gunson and Olympic Dam are mostly within the island arc basalt (ARC), low-titanium large igneous province (Low-Ti LIP) and back-arc basin basalt (BABB) fields (note that there are overlaps among these three fields). The bulk of Cr-spinel analyses from Wirrda Well are within the high-titanium large igneous province (Hi-Ti LIP) and ocean island basalt (OIB) fields, mostly due to their high TiO_2 contents, implying an alkaline affinity (cf. Kamenetsky et al., 2001). It is also significant that Cr-spinel enclosed in former olivine phenocrysts of inferred Fo number above 85 (solid circle, all from Olympic Dam) plot uniformly within the ARC and BABB fields (Fig. 4.7b). Though the tectonic indicator (Kamenetsky, 2001) should be

used with caution when applied to Precambrian rocks, it is likely that the mafic GRV in the Gawler SLIP were characterized by a heterogeneous mantle source, and further, that the mantle source had been largely modified by subduction processes prior to its partial melting.

Whole-rock compositions of the olivine-phyric rocks in the GRV are consistent with this inference. Basalts at Mount Gunson (and presumably Kokatha) have Cr-spinel compositions comparable to those in the olivine-phyric basalt at Olympic Dam, and are much less altered compared to the latter. They have indistinguishable trace element compositions characterised by negative Nb and Ta anomalies (Fig. 4.9) which are typical of arc basalts (Perfit et al., 1980; McCulloch and Gamble, 1991), and are also common in back-arc basin basalts (Saunders and Tarney, 1984; Taylor and Martinez, 2003). Olivine-phyric basalt samples at Wirrda Well and Olympic Dam display negative Nb and Ta anomalies and have relatively high abundances of HFSE and REE, in accordance with their alkaline characteristics (i.e. Wirrda Well, this study; Olympic Dam, Johnson, 1993; Johnson and McCulloch, 1995), indicating a heterogeneous mantle source. The trend shown by these samples on the Zr vs. TiO_2 diagram (Fig. 4.10) also implies that their mantle source was heterogeneous. Accordingly, Cr-spinel and whole-rock compositions together suggest that the formation of the Gawler SLIP was associated with either a "fossil", or active (at that time) supra-subduction zone setting. Magmatism triggered by active subduction as suggested by either Wade et al. (2006) or Betts et al. (2009), or "far-field" back-arc continental lithospheric mantle delamination and asthenosphere upwelling (Skirrow, 2010) under the Gawler Craton finally led to the formation of the mafic GRV and the Gawler SLIP.

4.8.2.3 A Cretaceous analogy

A further comparison between the mafic GRV, and high-Mg basalts (MgO >12 wt.%) and picrites from various tectonic settings (from the GEOROC database) has revealed that mafic GRV tend to contain higher Zr than high-Mg basalts and picrites worldwide but lower than that of felsic GRV and Hiltaba Suite Granite, at analogous TiO_2 contents (Fig. 4.10). After an extensive search of the GEOROC database, only one mafic volcanic suite, namely the Feixian Picrite (Gao et al., 2008), was found to

match the studied rocks in terms of Zr and TiO_2 contents, Zr/TiO_2 ratios and immobile trace element patterns (Figs. 4.9 and 4.10).

The Cretaceous Feixian Picrite lava is located in the North China Craton and spatially associated with high-Mg andesite and dacite (Pei et al., 2004; Gao et al., 2008). It is considered to be genetically associated with subduction of the South China Craton beneath the North China Craton (Pei et al., 2004, Gao et al., 2008; Yang et al., 2012). The high Zr/TiO_2 ratios (~250, Fig. 4.10) of the Feixian Picrite have been interpreted as a crustal signature, introduced into the mantle source by either delaminated North China Craton continental crust (Gao et al., 2008), or subducted South China Craton continental crust (Yang et al., 2012). By analogy, the subduction-related "continental crust" input can also be tentatively applied to the studied high Zr/TiO_2 mafic GRV. In this case, melts/fluids derived from completed or ongoing subduction had modified the subcontinental lithospheric mantle beneath the Gawler Craton, with possible involvement of delaminated or subducted continental crust, resulting in a heterogeneous mantle source.

4.8.3 Crustal melting induced by mantle magmatism in the Gawler SLIP

High thermal (± mass) input from underlying hot mantle, via intrusion of mantle-derived mafic to ultramafic magmas, is likely to be a critical factor in driving SLIP magmatism (Huppert and Sparks, 1988; Bryan et al., 2002). Previous studies have demonstrated the substantial contribution from crustal partial melting to the formation of SLIP magmatism (Bryan and Ferrari, 2013; and references therein).

Regarding the formation of the Gawler SLIP, three models have been proposed (Giles, 1988): 1) production of silicic magmas via fractionation of mantle-derived parental mafic magmas; 2) coeval melting of separate mantle and crustal sources to produce mafic and silicic magmas, and large-scale mixing or contamination of compositionally distinct mafic and silicic magmas; and 3) coeval melting of separate mantle and crustal sources to produce mafic and silicic magmas, with limited contamination and/or mixing. The first two models have been considered less likely because the mafic to silicic magma volume ratio is very low, and rocks with

intermediate composition (i.e. andesite) are exceedingly rare in the Gawler SLIP (Giles, 1988). The last model appears to be the most promising explanation, and involves partial melting of both mantle and crust, which was supported by compositions of both mafic and felsic GRV (Giles, 1988; Stewart, 1994; Agangi, 2011).

The recognition of high-Mg primitive (high Fo number)-olivine-phyric basalt at Olympic Dam agrees with the proposal that magma from a mantle source contributed to the Gawler SLIP. Such high-Mg magma is believed to have the potential to provide high heat flux into the crust and to induce large-scale partial melting of the crust. The presence of quartz xenocrysts and felsic xenoliths in the mafic GRV is also in accordance with the heating and partial melting of continental crust by mafic to ultramafic magmas (Garner and McPhie, 1999).

4.9 Conclusions

U-Pb dating of primary accessory apatite in mafic rocks at Mount Gunson, Wirrda Well and Olympic Dam, and the occurrence of olivine-phyric basalt (high abundance of former olivine phenocrysts) at Olympic Dam, demonstrate that primitive high-Mg magmas were produced as an integral component of the Gawler SLIP. The compositions of Cr-spinel inclusions in the olivine-phyric basalts and whole-rock samples allow us to evaluate the tectonic setting of the mafic GRV from the perspective of geochemistry, and imply their derivation from a heterogeneous mantle source that may have had a connection with either a “fossil” or active supra-subduction zone. Models proposing the heat flux from mafic to ultramafic magmas into the continental crust as a cause of large-scale crustal partial melting (e.g. Huppert and Sparks, 1988; Bryan et al., 2002) explain the voluminous silicic magmas of the Gawler SLIP.

Table 4.1 Major and trace element concentrations of representative olivine-phyric basalts from Olympic Dam, Kokatha, Mount Gunson and Wirrda Well analysed in this study.

Location	Olympic Dam	Kokatha	Kokatha	Wirrda Well	Wirrda Well	Mount Gunson[1]	Mount Gunson[1]	Mount Gunson[1]
Sample No.	OD024	GH80	GH81	OD395	OD398	RX3453	RX3454	RX3456
Drill hole	RD3008	Outcrop	Outcrop	WRD33	WRD33	PY-1	PY-1	PY-1
depth (m)	406.2			1121.4	1206.4	939.0	939.5	946.0
SiO_2	41.8	54.9	54.7	46.6	47.4	47.9	50.9	49.6
TiO_2	0.6	2.3	0.7	2.5	2.9	1.1	1.0	0.8
Al_2O_3	11.4	14.6	12.3	13.7	13.5	13.5	12.1	10.1
Fe_2O_3	18.8	11.2	10.8	26.3	17.1	12.8	11.9	11.2
MnO	1.3	0.2	0.3	0.2	0.4	0.4	0.2	0.3
MgO	11.5	3.1	8.2	5.6	5.4	4.3	5.3	14.6
CaO	11.9	6.2	10.4	1.9	5.2	9.2	9.7	8.3
Na_2O	0.9	3.5	0.8	0.1	0.1	0.8	2.6	1.5
K_2O	1.5	2.7	1.5	1.6	6.1	2.5	2.5	2.4
P_2O_5	0.4	1.3	0.2	1.4	1.8	0.3	0.3	0.3
CO_2	n.m.	n.m.	n.m.	n.m.	n.m.	7.2	3.3	0.9
LOI	17.5	0.8	1.3	4.7	5.1	n.m.	n.m.	n.m.
Li	57.4	13.7	22.7	115.1	71.5	83.4	29.9	94.7
V	175	106	184	288	343	256	258	221
Cr	2671	1550	850	460	446	1071	1018	1600
Ni	729	400	266	261	228	254	188	455
Cu	83	85	145	246	115	<1	16	13
Zn	454	113	86	1273	1450	537	259	427
As	16.6	1.3	0.4	3.4	3.0	2.9	6.7	4.3
Rb	52	79	34	110	207	138	106	86
Sr	82	681	636	121	297	103	408	291
Y	54	27	17	38	33	31	25	20
Zr	118	152	103	477	467	156	133	106
Nb	94.60	7.00	4.50	31.23	28.95	9.90	9.60	7.70
Mo	2.30	0.42	0.40	0.71	0.77	0.60	0.40	0.30
Cs	1.50	2.14	2.85	5.18	3.22	2.69	15.25	6.37
Ba	222	505	578	652	1171	587	805	944
La	146.7	43.2	27.6	113.9	136.5	34.3	32.0	24.2
Ce	279.2	89.0	59.8	267.4	312.8	68.1	67.7	53.4
Pr	34.00	10.6	7.21	31.44	36.16	8.15	8.48	7.02
Nd	133.8	42.1	28.3	117.0	135.7	32.6	33.4	28.5
Sm	27.90	8.31	5.23	17.36	21.32	6.47	6.89	6.28
Eu	4.50	1.93	1.14	3.45	4.62	1.52	1.68	1.42
Gd	20.50	6.72	3.91	10.87	13.61	6.46	5.89	5.43
Tb	2.50	0.89	0.53	1.43	1.68	1.00	0.84	0.77
Dy	10.90	4.71	2.99	7.42	7.67	5.33	4.77	3.96
Ho	1.60	0.93	0.57	1.37	1.27	1.09	0.94	0.77
Er	3.90	2.54	1.67	3.60	3.06	2.99	2.58	2.18

Tm	0.50	0.36	0.23	0.49	0.39	0.46	0.37	0.30
Yb	2.90	2.39	1.74	3.01	2.23	2.56	2.42	1.92
Lu	0.40	0.37	0.26	0.44	0.32	0.39	0.38	0.26
Hf	4.30	4.00	2.70	11.98	11.77	4.40	3.90	3.30
Ta	4.40	0.50	0.40	2.39	2.16	0.60	0.60	0.50
W	n.m.	3.0	1.0	4.6	2.8	132	339	179
Tl	0.40	0.36	0.15	0.43	3.50	1.06	0.82	0.45
Pb	24	15	32	101	538	28	52	9
Bi	0.40	0.26	0.13	0.06	0.05	1.80	0.03	0.14
Th	19.30	8.60	4.90	50.38	56.51	8.71	7.70	6.79
U	22.50	1.12	0.73	9.39	8.40	3.04	1.69	1.52

n.m. = not measured. LOI, loss on ignition. Major elements (oxides) are in wt. % (LOI-free), trace elements are in ppm. [1]Mount Gunson samples were assayed by BHP Billiton Olympic Dam.

Chapter 5 Alterations of mafic lithologies at the Olympic Dam iron oxide Cu-U-Au-Ag deposit*

Qiuyue Huang[1*], Vadim S. Kamenetsky[1], Kathy Ehrig[2], Jocelyn McPhie[1], Roland Maas[3], Maya Kamenetsky[1], Olga Apukhtina[1], Isabelle Chambefort[1,4]

[1]*School of Physical Sciences, University of Tasmania, Private Bag 79, Hobart, Tasmania, Australia 7001*

[2]*BHP-Billiton, GPO Box 1777, Adelaide, South Australia 5001, Australia*

[3]*School of Earth Sciences, University of Melbourne, VIC 3010, Australia*

[4]*GNS Science, Wairakei Research Centre, Taupo 3377, New Zealand*

**unpublished manuscript*

Abstract

Mafic magmas and/or rocks can be important sources (e.g. sulfur and metals) to hydrothermal deposits. In the early exploration model leading to the discovery of the Olympic Dam iron oxide Cu-U-Au-Ag deposit, South Australia, the sedimentary sequence on top of altered mafic to ultramafic rocks was considered desirable targets. Previous studies have revealed the occurrence of two generations of mafic to ultramafic lithologies at the Olympic Dam deposit. The first group consists of the olivine-phyric basalt and various mafic dykes belonging to the ca. 1590 Ma Gawler Range Volcanics; the second group is the Olympic Dam dolerite affiliated with the ca. 820 Ma Gairdner Dyke Swarm.

Both generations of mafic rocks are spatially adjacent to the Olympic Dam Breccia Complex, the immediate host to the deposit, and have been altered. They contain similar major secondary minerals, including chlorite, sericite, and carbonate, and are both characterized by a mineral assemblage of magnetite-apatite ± chlorite ± quartz, which is comparable to the inferred early reduced Fe oxide alteration present in the periphery and at depth of the Olympic Dam Breccia Complex. U-Pb dating of secondary apatite in the ca. 1590 Ma olivine-phyric basalt yielded an age that is broadly coeval with the emplacement of the basalt. Intensely sericite-altered olivine-phyric basalt samples yielded a post-primary Rb-Sr isochron age of ca. 1180 Ma, probably recording the last widespread sericite alteration event in these rocks. Drill core assays (e.g. up to 26 wt. % CO_2 and 50 wt.% of Fe_2O_3) of the basalt reflect the variable abundance of various secondary minerals. A wide range of compositional variation (six-fold) of Cr with extreme concentrations up to ~6,000 ppm and positive correlation between Cr and other incompatible elements (e.g. Ti and Zr) in the olivine-phyric basalt suggest significant whole-rock mass and/or volume loss due to hydrothermal alteration, in accordance with its previously proposed role as an important source of copper. Geochemical comparisons between the more altered ca. 820 Ma Olympic Dam dolerite reported in this study and the least altered equivalents reveal that some elements (e.g. Cu, U, Pb, Zn) have been added or removed as a consequence of alteration. Elevated Zn and Pb but depleted Cu concentrations in a number of Olympic Dam dolerite samples suggest that the dolerite can potentially be an additional source of Cu to the Olympic Dam deposit. This inference is also supported by evidence from petrography, Pb isotope

compositions of whole-rock and chalcopyrite, and drill core assays. Cu depletion in the dolerite tends to be accompanied by sodic alteration.

Magmatic-hydrothermal activities (ca. 1590 Ma, 1180 Ma, 820 Ma) recorded in both generations of mafic rocks can be correlated with ages (spanning from ca. 1590 Ma to 570 Ma) obtained on the Olympic Dam Breccia Complex. This implies a multi-stage hydrothermal system at the Olympic Dam deposit.

Key words

Olivine-phyric basalt, Dolerite, Geochronology, Whole-rock compositions, Alteration and mineralization.

5.1 Introduction

The Olympic Dam iron oxide Cu-U-Au-Ag deposit, South Australia, contains the world's largest published uranium, fifth largest copper and third largest gold resource (10,100 Mt at 0.78% Cu, 0.25 kg/t U3O8, 0.30 g/t Au, 1 g/t Ag, BHP Billiton 2015 Annual Report). It was discovered by Western Mining Corporation in 1975 based on a sediment-hosted copper deposit model developed in Haynes (1972). This is a source-oriented model, in which altered mafic lithologies were considered a potential source of copper and sedimentary sequences on top of altered mafic lithologies were regarded as exploration targets. In the early exploration of Olympic Dam, the copper depletion signature of one suite of Proterozoic basalt (i.e. Roopena Volcanics) in South Australia drew immediate attention to the Stuart Shelf which contains flat-lying upper Proterozoic sediments (Haynes, 2006). Geophysical investigation of the Stuart Shelf defined five geophysical (gravity and aeromagnetic) anomalies of interest, including the anomaly at Olympic Dam which had the shallowest interpreted depth to the source (Haynes, 2006). Therefore, the anomaly at Olympic Dam was targeted, and the Stuart Shelf therein was drilled, but no mineralization was found. However, in the Gawler Craton basement beneath the Stuart Shelf, copper sulfides were discovered, in what is later referred to as the Olympic Dam Breccia Complex (ODBC) (Reeve et al., 1990). The ODBC occurs at the intersections of a number of fault sets and is the immediate host to the Olympic Dam deposit (Reeve et al., 1990; Ehrig et al., 2012). This complex

is hosted within the Roxby Downs Granite, part of the ca. 1590 Ma Hiltaba Suite (Creaser, 1989).

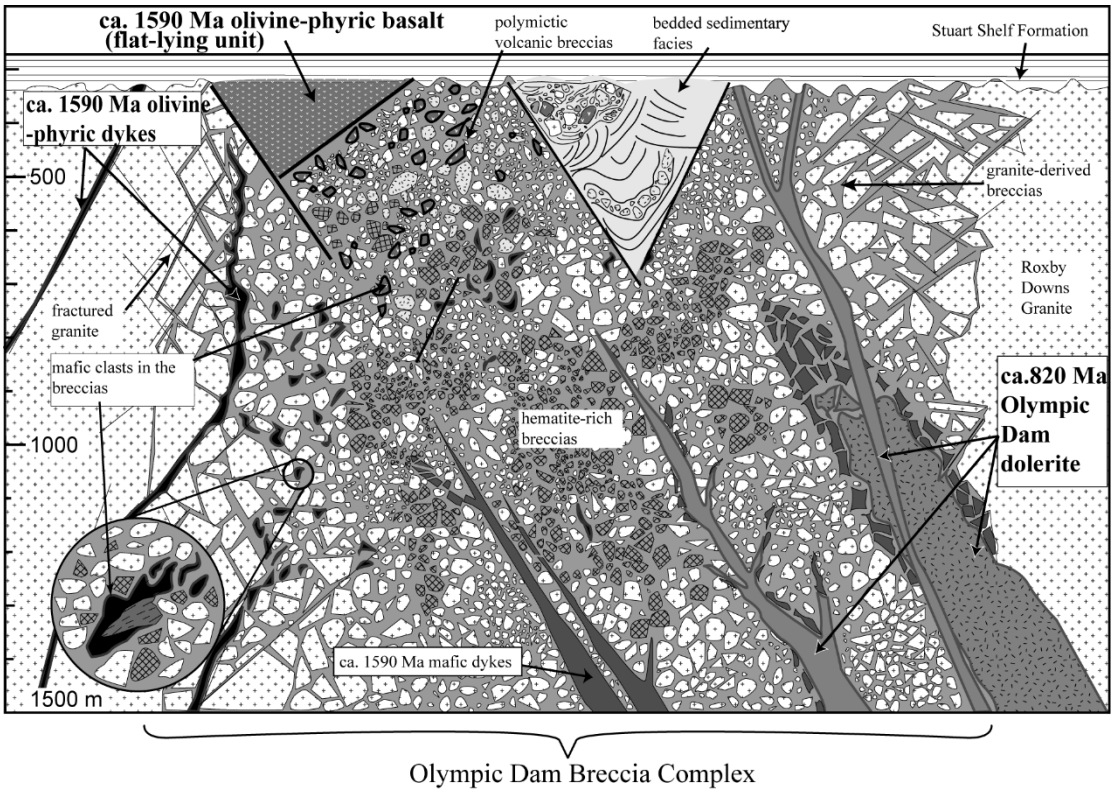

Figure 5.1 Illustration of the Olympic Dam Breccia Complex at the Olympic Dam iron oxide Cu-U-Au-Ag deposit. There are two generations of mafic rocks present: olivine-phyric basalt, as well as other mafic dykes, belonging to the ca. 1590 Ma Gawler Range Volcanics, and basaltic to doleritic dykes (Olympic Dam dolerite) affiliated with the ca. 820 Ma Gairdner Dyke Swarm. Further details about the geology of the deposit can be seen in McPhie et al. (2011b) and Ehrig et al. (2012).

Despite the success of the exploration model, no mafic lithologies were recognized during the discovery stage, even though mafic rocks occurred in RD6 (5th drill hole at Olympic Dam). More mafic lithologies have been intersected by subsequent drilling, and are considered to be closely related to the brecciation, hydrothermal circulation (by providing heat), and mineralization (Reeve et al., 1990; Johnson and Cross, 1995; Johnson and McCulloch, 1995; Ehrig et al., 2012). There are two generations of mafic lithologies present at Olympic Dam. The first group is correlated with the ca. 1590 Ma Gawler Range Volcanics (Chapter 4), consisting of intensely altered olivine-phyric basalt, and other mafic dykes of various textures (aphanitic, porphyritic, and doleritic)

(Ehrig et al., 2012). The second group comprises basaltic to mainly doleritic dykes, belonging to the ca. 820 Ma Gairdner Dyke Swarm in the Gawler Craton (Huang et al., 2015, Chapter 3). The ca. 1590 Ma olivine-phyric basalt (flat-lying basalt unit) occurs within the ODBC immediately below the unconformity with the Neoproterozoic Stuart Shelf sedimentary formations, and coeval dykes intrude the ODBC and the Roxby Downs Granite (Fig. 5.1). The ca. 820 Ma Olympic Dam dolerite also intrudes the ODBC and the Roxby Downs Granite (Fig. 5.1).

Geochronological results obtained on uraninite, iron oxides, and sulfides in the ODBC by previous studies (Trueman et al., 1986; Johnson, 1993; McInnes et al., 2008; Meffre et al., 2010; Maas et al., 2011; Ciobanu et al., 2013) suggest that the Roxby Downs Granite, the ODBC and the mafic lithologies have interacted with hydrothermal systems repeatedly over hundreds of million years. The effects of alteration on the Roxby Downs Granite and ODBC have been characterized in Ehrig et al. (2012), and the elements that have been added to the deposit from the granite have been determined.

In this study, drill core assays of the ca. 1590 Ma intensely altered olivine-phyric basalt (flat-lying basalt unit) and whole-rock analyses of the invariably altered ca. 820 Ma Olympic Dam dolerite, combined with petrography and whole-rock, chalcopyrite and galena Pb isotope compositions, allow us to assess whether the alteration of these rocks had a potential to contribute to the Olympic Dam ore endowment. Geochronological investigations (apatite U-Pb and whole-rock Rb-Sr isochron dating) of the ca. 1590 Ma olivine-phyric basalt provides another piece of evidence in support of the multi-stage hydrothermal evolution at the Olympic Dam deposit.

5.2 Geological background

The Olympic Dam iron oxide Cu-U-Au-Ag deposit is located in the northeast of the Gawler Craton. The deposit occurs in Mesoproterozoic rocks below undeformed Neoproterozoic and Cambrian sedimentary rocks of the Stuart Shelf. A synthesis of the geology of the Gawler Craton can be found in Hand et al. (2007) and Reid and Hand (2012). In terms of the magmatic events particularly mafic magmatism that concerns this study, the Olympic Dam deposit is situated at the place where two large igneous provinces (LIP), i.e. the ca. 1590 Ma Gawler silicic LIP (SLIP) and the ca. 820 Ma Gairdner LIP, overlap with each other.

The consanguineous Gawler Range Volcanics (GRV) and Hiltaba Suite granitoids, occurring between ca. 1595 and 1575 Ma (Blissett et al., 1993; Hand et al., 2007; Jagodzinski, 2014), constitute the Gawler SLIP. The GRV have a maximum preserved thickness of ~1.5 km and extend more than 25,000 km^2 across the central Gawler Craton (Blissett et al., 1993; Allen et al., 2003). Subordinate (~10 vol.%) mafic units only occur in the lower GRV which range in composition from basalt to rhyolite and comprise lavas, ignimbrites and minor volcaniclastic facies (Blissett, 1993); the upper GRV consist of widespread, thick (250-300 m), rhyolitic and dacitic lavas (Garner and McPhie, 1999; Morrow and McPhie, 2000; Allen and McPhie, 2002; Allen et al., 2003). At Olympic Dam, the immediate ore host, i.e., the ODBC, is situated within the Roxby Downs Granite, a member of the Hiltaba Suite (Fig. 5.1). Mafic GRV at Olympic Dam consist of intensely altered olivine-phyric basalt, and aphanitic, doleritic and porphyritic mafic dykes (Fig. 5.1, Ehrig et al., 2012; Chapter 4). The intensely altered olivine-phyric basalt occurs in two situations (Fig. 5.1): 1) an apparent flat-lying unit which has been intersected in six drill holes (intersections ranging in thickness from 15 to 45m) directly beneath the unconformity between the ODBC and the Neoproterozoic to Cambrian sedimentary cover; 2) olivine-phyric basalt dykes (a few centimetres to ~1 m wide) occur in a NW-striking, steeply E-dipping orientation.

The Gairdner Dyke Swarm in the Gawler Craton, South Australia was first recognized on aeromagnetic images as a NW-trending array of linear magnetic anomalies (Fig. 5.1, Boyd in Goode, 1970). It intruded the Gawler Craton at ca. 820 Ma (Wingate et al., 1998) and constitutes the Gairdner LIP together with other igneous suites such as the Wooltana Volcanics and Beda Volcanics (Crawford and Hilyard, 1990; Claoué-Long and Hoatson, 2009; Huang et al., 2015, Chapter 3). At Olympic Dam, the Gairdner Dyke Swarm has been recognized as basaltic to mainly doleritic dykes (named as Olympic Dam dolerite) intruding the Roxby Downs Granite and the ODBC (Fig. 5.1). These subvertical dykes are commonly several metres to more than 100 m in width and can be traced for up to 3 km along a NW-strike. Compared to the ca. 1590 Ma mafic GRV, the Olympic Dam dolerite is characterized by its generally fresher appearance, higher magnetic susceptibility and better competency. The presence of sharp chilled margins within dykes justifies multiple generations of the dykes.

5.3 Analytical techniques

5.3.1 Mineral compositions

Preliminary compositional analyses of minerals (i.e. Cr-Spinel, uranite, and magnetite) were conducted using an FEI MLA650 environmental scanning electron microscope (ESEM) and a Hitachi SU-70 field emission scanning electron microscope (FESEM), at the Central Science Laboratory, University of Tasmania. High magnification images, including SEM images and back-scattered electron (BSE) images, were also acquired using the same instruments.

Trace element compositions of chalcopyrite were analyzed by laser-ablation inductively coupled plasma mass spectrometry (LA-ICPMS) at CODES, University of Tasmania, using an Agilent 7700 ICP-MS coupled to a RESOlution SE 193 nm ArF excimer ATL Atlex ILR laser ablation system. The following analytical parameters and conditions were used: laser beam diameter of 20 μm, laser beam fluence of ~3 J/cm^2 at the sample; laser pulse rate of 5 Hz; ablation occurred in the atmosphere of pure He flowing at a rate of 0.42 litres/minute; immediately past the ablation point within the cell, He carrier gas was mixed with Ar (1.05 litres/minute) for improved efficiency of aerosol transport. The following isotopes were measured: ^{27}Al, ^{47}Ti, ^{55}Mn, ^{57}Fe, ^{59}Co, ^{60}Ni, ^{65}Cu, ^{66}Zn, ^{75}As, ^{77}Se, ^{89}Y, ^{90}Zr, ^{93}Nb, ^{95}Mo, ^{109}Ag, ^{111}Cd, ^{118}Sn, ^{121}Sb, ^{125}Te, ^{140}Ce, ^{157}Gd, ^{172}Yb, ^{178}Hf, ^{181}Ta, ^{182}W, ^{185}Re, ^{197}Au, ^{204}Pb, ^{205}Tl, ^{206}Pb, ^{207}Pb, ^{208}Pb, ^{209}Bi, ^{232}Th, ^{235}U, ^{238}U. The total acquisition time for each analysis was 60 seconds, comprising a 20-second measurement of the background (laser off) and a 40-second analysis with the laser on.

Data reduction was undertaken according to standard methods (Longerich et al., 1996), using Fe as the internal standard. Two primary calibration standards were used: GSD-1G (Guillong et al., 2005) was used for the quantification of ^{27}Al, ^{47}Ti, ^{55}Mn, ^{89}Y, ^{90}Zr, ^{93}Nb, ^{95}Mo, ^{140}Ce, ^{157}Gd, , ^{172}Yb, ^{178}Hf, ^{181}Ta, ^{182}W, ^{185}Re, ^{232}Th, ^{235}U, ^{238}U and STDGL2b2 (Danyushevsky et al., 2003, 2011) was used for the quantification of all other elements. Both standards were analyzed twice every 1–1.5 hour to monitor drift in sensitivities. Linear drift corrections were applied between each set of standard analyses.

Pb isotope compositions of galena were analyzed by laser-ablation inductively coupled plasma mass spectrometry (LA-ICPMS) at CODES, University of Tasmania, using an Agilent 7700 ICP-MS coupled to a New Wave UP213 laser ablation system operating at the 213 nm wavelength (5th harmonic). The following analytical parameters and conditions were used: laser beam diameter of 10 μm, laser beam fluence of 5 J/cm^2 at the sample; laser pulse rate of 10 Hz; ablation occurred in the atmosphere of pure He flowing at a rate of 0.8 litres/minute; immediately past the ablation point within the cell He carrier gas was mixed with Ar (1.05 litres/minute) and sent into the ICP-MS. The following isotopes were measured: ^{57}Fe, ^{63}Cu, ^{66}Zn, ^{202}Hg, ^{204}Pb, ^{206}Pb, ^{207}Pb, ^{208}Pb, ^{232}Th, ^{238}U. The total acquisition time for each analysis was 60 seconds, comprising a 10-second measurement of the background (laser off) and a 50-second analysis with the laser on.

Isotopic data was reduced using an in-house macro based Excel workbook using galena from Broken Hill (Townsend et al., 1998) as the primary standard for Pb isotope ratios measured. Analyses of the standard (n=2) over the measurement period provided average ^{208}Pb/^{204}Pb, ^{207}Pb/^{204}Pb, ^{206}Pb/^{204}Pb ratios of 35.6937±0.1501, 15.3895±0.0255, and 15.9966±0.0292, respectively.

5.3.2 Whole-rock compositions

Whole-rock samples were crushed in a WC (Tungsten Carbide) mill for X-ray fluorescence (XRF) and inductively coupled plasma mass spectrometry (ICP-MS) analyses at the University of Tasmania. Major and some trace elements (V, Cr, Ni, Cu, Zn, Rb, Sr, Y, Zr, Nb, Ba, and La) were measured by XRF; trace elements were analysed by ICP-MS. Samples were digested in HF/H_2SO_4 with the PicoTrace high-pressure digestion equipment and analysed with an Agilent 4500 ICPMS. XRF analyses were made on a Philips PW1480 X-ray Fluorescence Spectrometer. Detection limits for trace elements in ICP-MS are ≤0.01 ppm (rare earth element) and ≤0.5 ppm for other elements, except As (5 ppm). Comparison of XRF and ICP-MS trace element data indicates a good correlation between the two methods.

Drill cores of the olivine-phyric basalt (flat-lying basalt unit) at Olympic Dam was assayed at 1-m intervals by BHP Billiton Olympic Dam. All drill core samples have been assayed for the same suite of elements using a combination of four-acid digestion

and inductively coupled plasma-optical emission spectroscopy (ICP-OES) for Cu, Ag, As, Co, Ni, Pb, and Zn; ICP-OES for Ba, Al, Ca, Ce, Fe, K, La, Mg, Mn, Na, P, Si, Sr, Ti, Y, and Zr; lithium metaborate/tetraborate fusion and inductively coupled plasma-mass spectroscopy (ICP-MS) for U_3O_8, Bi, Sb, and Mo; induction furnace-infrared spectrometry (IF-IS) for CO_2 and S; and fire assay-flame atomic absorption spectrometry (FA-AAS) for Au. Further details are in Ehrig et al., (2012).

5.3.3 Whole-rock radiogenic isotope (Sr-Nd-Pb) compositions

Sliced and cleaned (distilled water) surfaces of drill core sections OD906, OD914, and OD968 were spot-sampled with a hand-held Dremel-type drill to obtain ~20-30 mg of powder away from visible macroscopic veining. Additional single samples of carbonate vein material were also collected. Isotopic and trace element analyses were conducted at the University of Melbourne (Maas et al., 2005). Powders were weighed into Savillex beakers and dissolved in HF/HNO_3 and 5M HNO_3 on a hotplate; vein samples were dissolved in HNO_3 only. The clear solutions were equilibrated with ^{85}Rb-^{84}Sr and ^{149}Sm-^{150}Nd tracers for Rb-Sr/SmNd isotope dilution work; small splits of the solutions for OD914 and 968 were used for trace element analysis on an Agilent 7700s quadrupole Laser Ablation Inductively Coupled Plasma Mass Spectrometry (ICPMS). Rb and Sr were extracted using a combination of EICHROM SR resin and AG50-X8 (200-400) cation exchange resin. Sm and Nd were extracted using EICHROM TRU and LN resin. Total analytical blanks were <100 pg, resulting in sample/blank ratios >104 in most cases; blank corrections to Rb/Sr in low-Rb carbonate vein samples amounted to <0.5%.

Isotopic analyses were carried out on a NU Plasma multi-collector ICP-MS with sample uptake via a CETAC Aridus desolvator and PFA nebuliser operated at an uptake rate ~0.07 ml/min, with sensitivities of 100 V/ppm Sr and 150 V/ppm Nd. Analyses were carried out in static multi-collection mode with signals near 8V Sr and 15V. Each run consists of 30-40 cycles (10 sec/cycle). Instrumental mass bias was corrected by normalizing to $^{88}Sr/^{86}Sr=8.37521$ and $^{146}Nd/^{145}Nd=2.0719425$ (equivalent to $^{146}Nd/^{144}Nd = 0.7219$), using the exponential law as part of an on-line iterative spike-stripping/internal normalization procedure. Data are reported relative to SRM987 = 0.710230 and La Jolla Nd = 0.511860. Typical in-run precisions (2se) are ±0.005-0.008%

(Sr) and ±0.002% (Nd); external precision (reproducibility, 2sd) is ±0.01% (Sr) and ±0.004% (Nd). Rb isotope dilution analyses were performed using the Zr-doping method (Waight et al., 2002). External precisions for $^{87}Rb/^{86}Sr$ and $^{147}Sm/^{144}Nd$ obtained by isotope dilution are ±0.5% and ±0.2%, respectively. Results for international standards agree with TIMS reference values. For example, long-term (2011-2014) averages for BCR-2 are 0.704997±42 (2sd, n=44) and 0.512641±24 (2sd, n=74), and $^{147}Sm/^{144}Nd$ is 0.1382±0.0002. Rb-Sr data for biotite and hornblende from Mt Dromedary monzonite (NSW, Australia) define an isochron age of 99.7±0.3 Ma (n=11, Sri 0.70445±4, MSWD 1.3), consistent with ^{40}Ar-^{39}Ar dates for biotite (GA1550 biotite standard e.g. 98.5±1.6 Ma, Spell and McDougall, 2003; 98.8±1 Ma, Renne et al., 1998) and U-Pb zircon dates (99.12±0.14 Ma, Schoene et al., 2006) from the same locality. The Rb decay constant is ^{87}Rb 1.395 10-11/yr. Rb-Sr ages were calculated using ISOPLOT 3.0 (Ludwig, 2003). Modern CHUR has $^{147}Sm/^{144}Nd$ = 0.1960, $^{143}Nd/^{144}Nd$ = 0.512632 (Bouvier et al., 2008).

The whole-rock Pb isotope analysis of Olympic Dam dolerite was carried out at the State Key Laboratory of Isotope Geochemistry, Guangzhou Institute of Geochemistry (GIG), Chinese Academy of Sciences (CAS). The isotope measurements were performed on a Neptune Plus multi-collection inductively coupled plasma mass spectrometry (MC-ICPMS). Samples were doped with Tl, and mass discrimination was corrected relative to a certified $^{205}Tl/^{203}Tl$ ratio. Details of Pb isotopic analytical methods can be seen in Chernyshev et al. (2007). Analyses of standard NIST SRM 981 (n=6), over the measurement period provided average $^{208}Pb/^{204}Pb$, $^{207}Pb/^{204}Pb$, $^{206}Pb/^{204}Pb$ ratios of 36.6787±0.0008 (2σ), 15.4874±0.0002 (2σ) and 16.9366±0.0003 (2σ), respectively.

5.3.4 Apatite U-Pb dating

U-Th-Pb dating of apatite was carried out using LA-ICPMS (e.g. Chew et al., 2014 and references therein) on polished rock samples mounted in 25 mm diameter epoxy mounts, at CODES, University of Tasmania. Apatite crystals were recognised using a scanning electron microscope. The crystals were analysed using a Coherent Scientific 193 nm Ar-F excimer gas laser coupled with a Resonetics S155 ablation cell and an Agilent 7500cs quadrupole ICPMS at the University of Tasmania. Apatite was ablated

in a helium atmosphere (0.35 litres/minute) using a 32 μm laser spot (5 Hz, energy density ~2 J/cm^2). Downhole fractionation, instrument drift and mass bias in apatite analyses were corrected using an in-house apatite standard, OD306, a coarse-grained apatite from an apatite-magnetite vein at the Acropolis Cu-Au prospect in South Australia. Further details of the method are in Chapter 3 (Huang et al., 2015).

5.4 Petrography and mineralogy

Detailed petrographical descriptions of primary igneous mineralogy and texture of the ca. 1590 Ma olivine-phyric basalt and the ca. 820 Ma Olympic Dam dolerite are in Chapter 4 and Chapter 3 (Huang et al., 2015), respectively. This section focuses on the petrographical features caused by secondary processes (i.e. hydrothermal alteration and deformation).

5.4.1 ca. 1590 Ma olivine-phyric basalt

Hydrothermal alteration and deformation are particularly intense within the ca. 1590 Ma olivine-phyric basalt, largely obliterating primary igneous mineralogy and texture. As a consequence, undeformed ca. 1590 Ma olivine-phyric basalt at Olympic Dam is rare and typically contains ~5 to 20 vol.% of pseudomorphed olivine phenocrysts in a cryptocrystalline or formerly glassy groundmass (Fig. 5.2a). Cr-spinel mostly occurs as inclusions within olivine pseudomorphs and is rarely present in the groundmass of undeformed olivine-phyric basalt.

The deformed samples show a strong alignment of elongate (flattened and stretched) olivine pseudomorphs (Fig. 5.2b and c) and typically contains higher volume percentage (up to ~30 vol. %) of olivine pseudomorphs (Fig. 5.2b and c). In this case, Cr-spinel is also widespread in the groundmass (Fig. 5.2b and d).

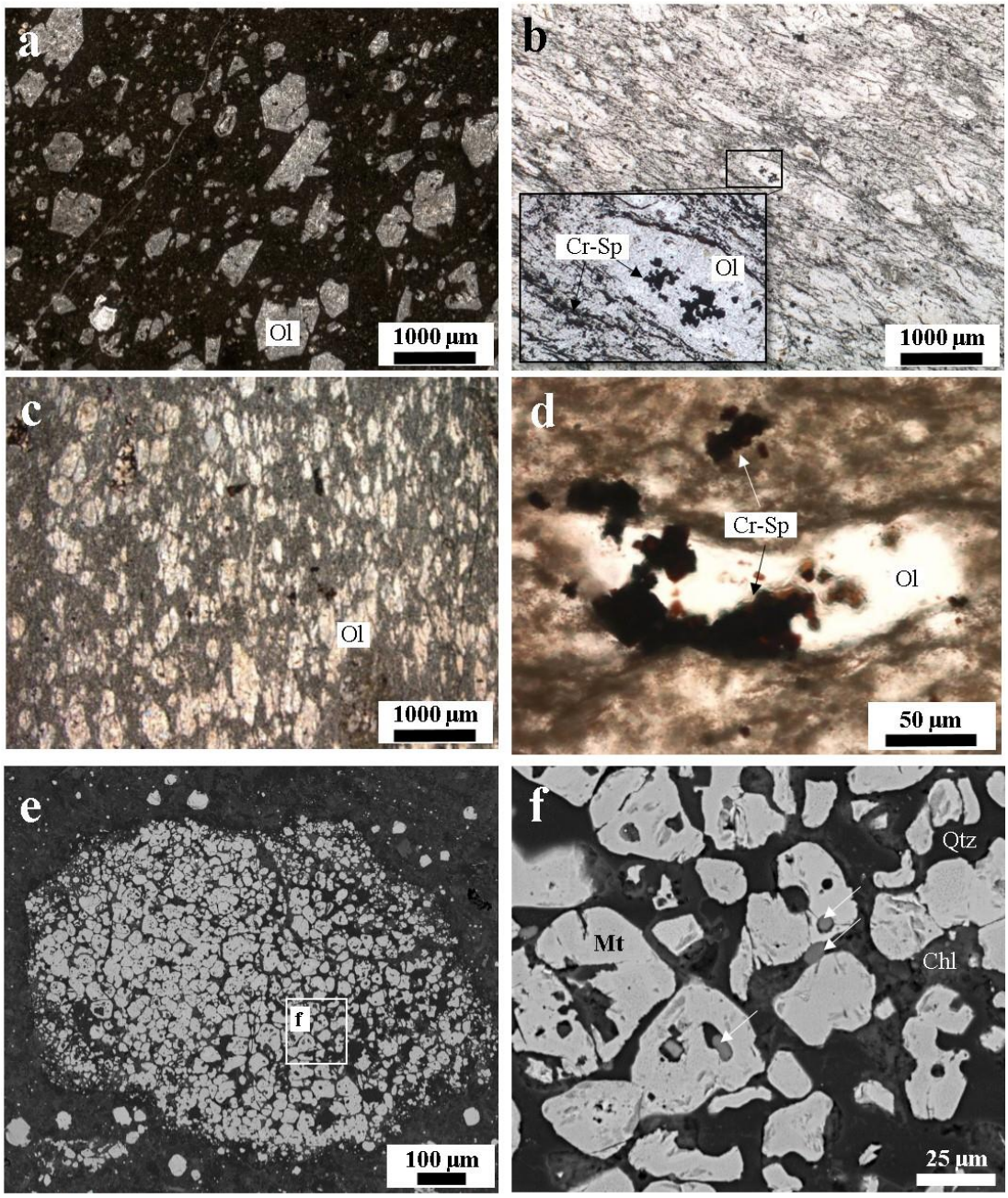

Figure 5.2 The ca. 1590 Ma olivine-phyric basalt. (a) The undeformed basalt contains ~5 to 20 vol.% of olivine (Ol) pseudomorphs, in a cryptocrystalline or formerly glassy groundmass. (b-d) Deformed basalt contains higher volume percentage of squashed olivine pseudomorphs, and Cr-spinel (Cr-sp) is also widespread in the groundmass. (e, f) Secondary magnetite (Mt)-apatite (white arrow)-chlorite (Chl)-quartz (Qtz) assemblage is common in the olivine-phyric basalt. (a-d) plane polarized light photomicrographs; (e-f) BSE images.

Apart from some Cr-spinel, all other igneous minerals have been completely replaced in the olivine-phyric basalt. The majority of Cr-spinel crystals have been partly or completely replaced by chlorite + magnetite, or carbonate. Chlorite, sericite,

carbonates (mostly ankerite, with minor siderite, dolomite and calcite), and iron oxides (i.e. magnetite and hematite) are among the dominant secondary phases. Minor quartz, fluorite, rare earth element (REE)-bearing minerals (e.g. bastnasite, monazite, florencite, synchysite and xenotime), apatite, barite and sulfides (bornite, chalcopyrite and pyrite) are also present. Disseminated Cr-bearing magnetite in the groundmass shows rounded to sub-rounded shapes and is compositionally zoned. The core contains higher concentrations of Cr, whereas the rim consists of magnetite (low or no Cr) and chlorite. Magnetite aggregations also occur (Fig. 5.2e), and typically involve an assemblage of magnetite-apatite ± chlorite ± quartz. In this assemblage, magnetite contains low or no Cr. Apatite occurs both within magnetite crystals and in the interstices between magnetite (Fig. 5.2f). This assemblage can be partly or completely replaced by hematite ± fluorite. Hydrothermal veinlets of chlorite, quartz, carbonates and iron oxides cut across the olivine-phyric basalt.

5.4.2 ca. 820 Ma Olympic Dam dolerite

The ca. 820 Ma Olympic Dam dolerite is invariably altered. The previously reported dolerite is the least altered, and primary minerals and textures are mostly preserved (Huang et al., 2015, Chapter 3). Euhedral to sub-euhedral clinopyroxene and plagioclase are the dominant mineral phases in the least altered dolerite (Fig. 5.3a). Minor Ti-magnetite and accessory apatite also occur.

The petrographically more altered and/or brecciated Olympic Dam dolerite is located along the immediate intrusive contacts with the Roxby Downs Granite and the ODBC, where the dyke has been replaced by mainly chlorite, quartz, sericite, albite, and carbonate and minor pumpellyite, apatite, titanite, iron oxides (i.e. magnetite and hematite) and sulfides (e.g. pyrite, chalcopyrite, minor galena and sphalerite).

A common case of a dyke intruding the Roxby Downs Granite is accompanied by the brecciation of the host granite and quenching of the mafic magma at the contact (i.e. formation of chilled margins; Fig. 5.4). The brecciated host rock is represented by fragmented granite-derived quartz cemented by chlorite + sericite + magnetite ± apatite. The dyke shows a spherulitic texture within the chilled margin (Fig. 5.4b). The spherulites commonly contain chalcopyrite (Fig. 5.4b). Thin veinlets cut across the dyke (Fig. 5.4a and c) and consist of chlorite, sericite, magnetite and minor carbonate

and apatite. Magnetite is characterized by oscillatory zonation (Fig. 5.4d) and contains chalcopyrite and Au-Ag-bearing tellurides and/or sulfides (Fig. 5.4e). The hydrothermal veinlets are also surrounded by disseminated chalcopyrite.

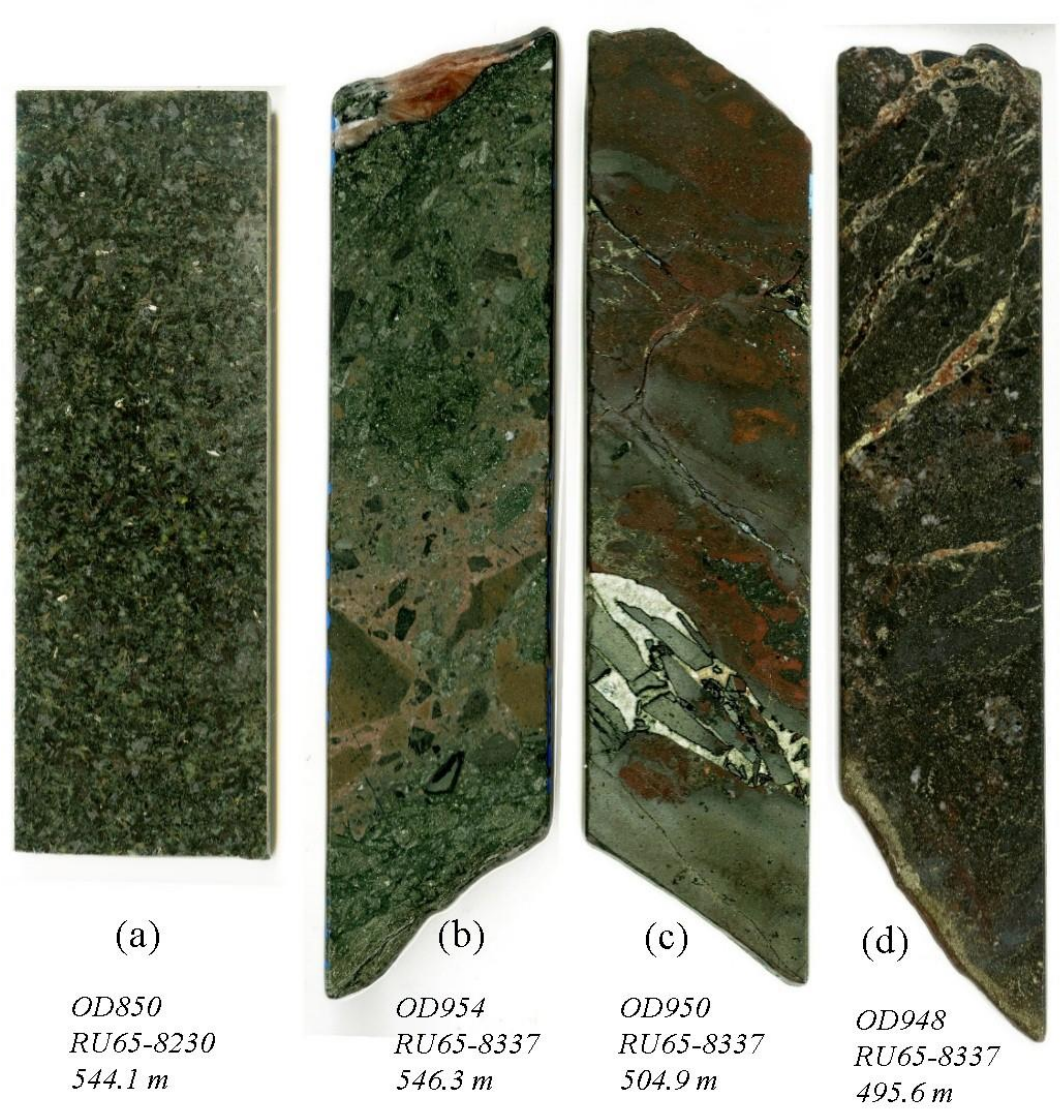

Figure 5.3 Polished drill cores of the ca. 820 Ma Olympic Dam dolerite. Drill cores are ~5 cm in width. Sample number, drill hole number, and depth have been indicated.

A single dyke may show a variety of alteration and/or brecciation styles (Fig. 5.3b-d). Large clasts of chlorite-altered porphyritic to doleritic dykes are situated in a groundmass of fine-grained mafic fragments (Fig. 5.3b). Chlorite-altered fragmented mafic clasts have been cemented by carbonate (ankerite and calcite) and minor fluorite (Fig. 5.3c). Brecciated dolerite next to the intrusive contact with the ODBC can be

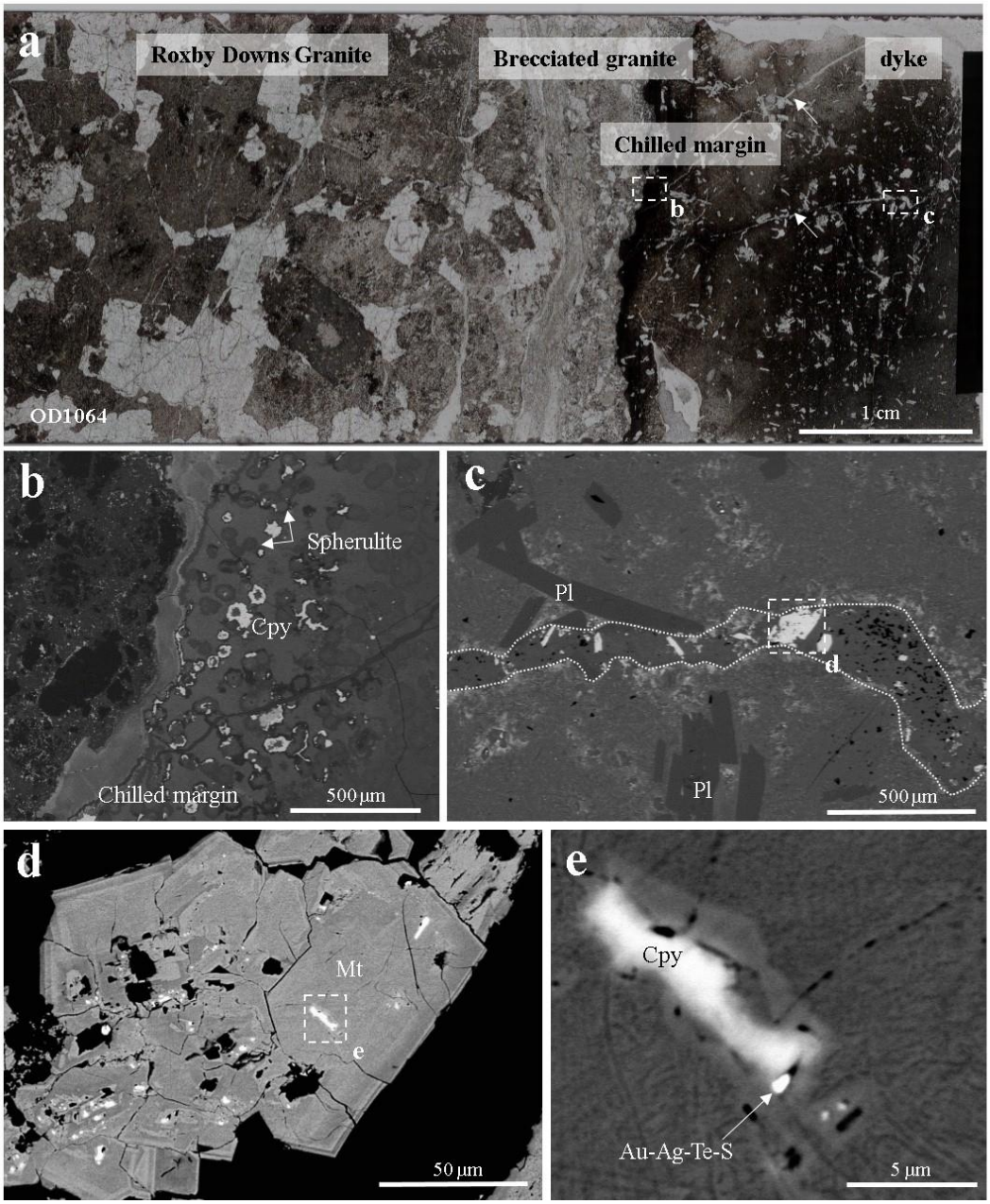

Figure 5.4 The ca. 820 Ma Olympic Dam dolerite dyke sample OD1064. (a) A full thin section scan of this sample. Two white arrows mark hydrothermal veinlets cutting across the dyke. (b) The intrusive contact consists of brecciated granite and a chilled margin. The dyke shows a spherulitic texture in the chilled margin. Some spherulites contain chalcopyrite (Cpy). (c) Hydrothermal veinlets comprise chlorite, sericite, magnetite (Mt) and minor carbonate and apatite. Plagioclase (Pl) is a dominant primary component of the dyke. (d, e) Magnetite (Mt) in veinlets shows oscillatory zonation and contains chalcopyrite and Au-Ag-bearing telluride and/or sulfide (Au-Ag-Te-S).

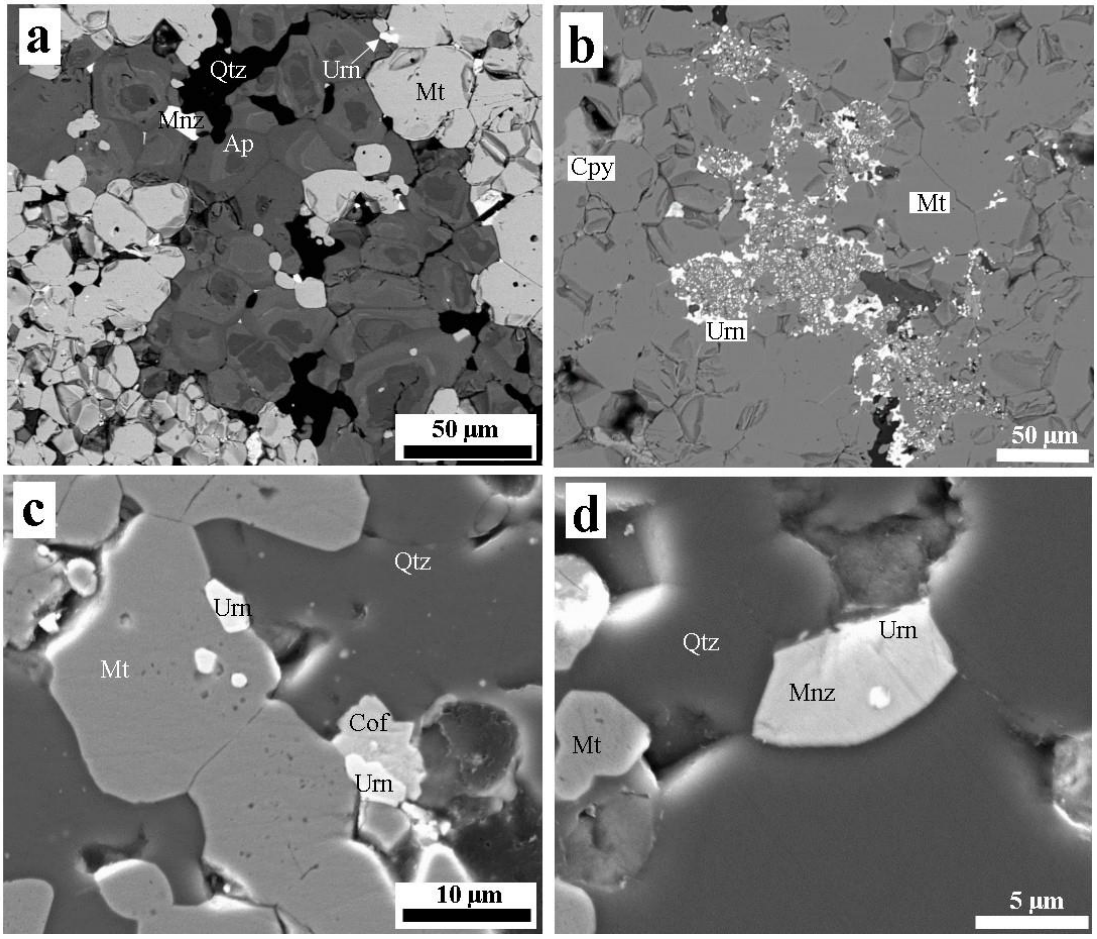

Figure 5.5 Magnetite-altered Olympic Dam dolerite (OD948, Fig. 5.3d). Abbreviations: Qtz-quartz; Mt-magnetite; Urn-uraninite; Cof-coffinite; Mnz-monazite; Cpy-chalcopyrite; Ap-apatite. (a,b) BSE images; (c,d) SEM images.

replaced by an assemblage of magnetite, apatite, chlorite, and quartz with minor monazite, uraninite, coffinite and chalcopyrite (Figs. 5.3d and 5.5). Magnetite and apatite crystals are granular in shape; apatite crystals commonly show compositional zonation (Fig. 5.5a). Uraninite, coffinite and/or chalcopyrite occur in the interstices between magnetite and quartz crystals (Fig. 5.5a, b, and c), within magnetite crystals (Fig. 5.5c), or rarely within monazite crystals (Fig. 5.5d). Semi-quantitative SEM-EDAX analyses of uraninite (Fig. 5.5b) yielded U/Pb ratios ranging from 7.85 to 10.4, with an average of 8.54, corresponding to apparent uraninite chemical ages from 704 to 538 Ma, based on the expression $\mathrm{t} = \lambda_{238}^{-1}\ln(1.104Pb/U + 1)$ given in Bowles (1990).

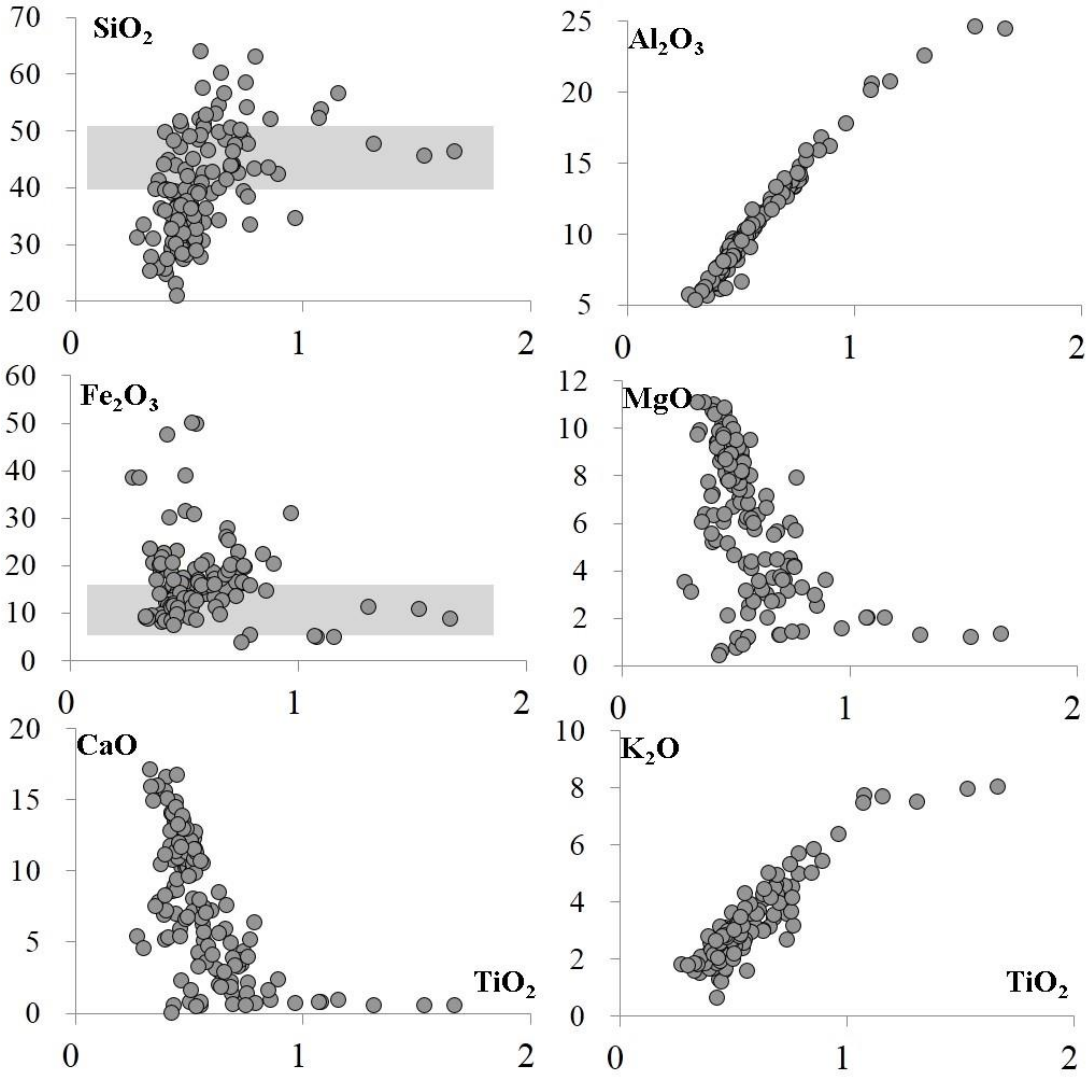

Figure 5.6 Major element compositions (wt.%) of the ca. 1590 Ma olivine-phyric basalt. Compositional fields (grey) for SiO_2 and Fe_2O_3 represent those of primary high-Mg basalts (MgO>12 wt.%) collected from the GEOROC database (http://georoc.mpch-mainz.gwdg.de/georoc/).

5.5 Results

5.5.1 Geochemistry of the ca. 1590 Ma olivine-phyric basalt

Olivine-phyric basalt (flat-lying unit) contains less than 11.1 wt.% of MgO (Fig. 5.6, Table S5), and shows a wide range of compositional variations of other major components, for example, Al_2O_3 (5.4 to 25 wt.%), Fe_2O_3 (3.8 to 50.2 wt.%, total Fe as Fe_2O_3) and K_2O (0.6 to 8.1 wt.%). MgO (0.6 to 11.1 wt.%), CaO (0.6 to 17.1 wt.%) and

MnO (0 to 2.5 wt.%) are positively correlated with CO_2 (0 to 26 wt.%), whereas SiO_2 (21 to 64 wt.%) is negatively correlated with CO_2 (Fig. 5.7).

Near linear positive correlations exist among a number of components including Al_2O_3, K_2O, Cr and high field strength elements (HFSE) such as Ti, Nb, Ta, Zr, Hf and Th (Figs. 5.6 and 5.8). Light rare earth elements (LREE, i.e. La, Ce, Nd, and Sm) and heavy rare earth elements (HREE, i.e. Dy, Ho, Er, Tm, Yb and Lu) also show positive linear correlations, respectively. But neither shows such correlations with each other or HFSE. All these components show around five to six-fold of compositional variations. Some analyses have extremely high concentrations of certain elements, most strikingly ~6,000 ppm of Cr. As for other trace elements (e.g. large-ion lithophile elements, LILE)

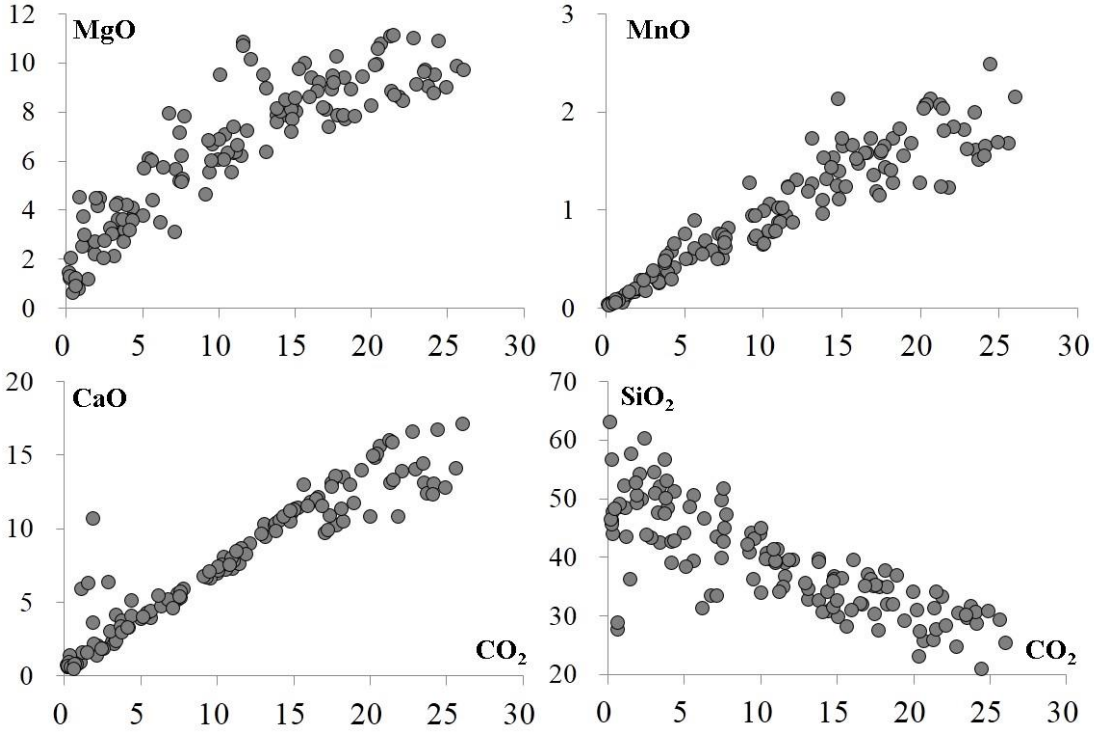

Figure 5.7 MgO, MnO, CaO, SiO_2 vs. CO_2 (wt.%) of the ca.1590 Ma olivine-phyric basalt. Same dataset as Fig. 5.6.

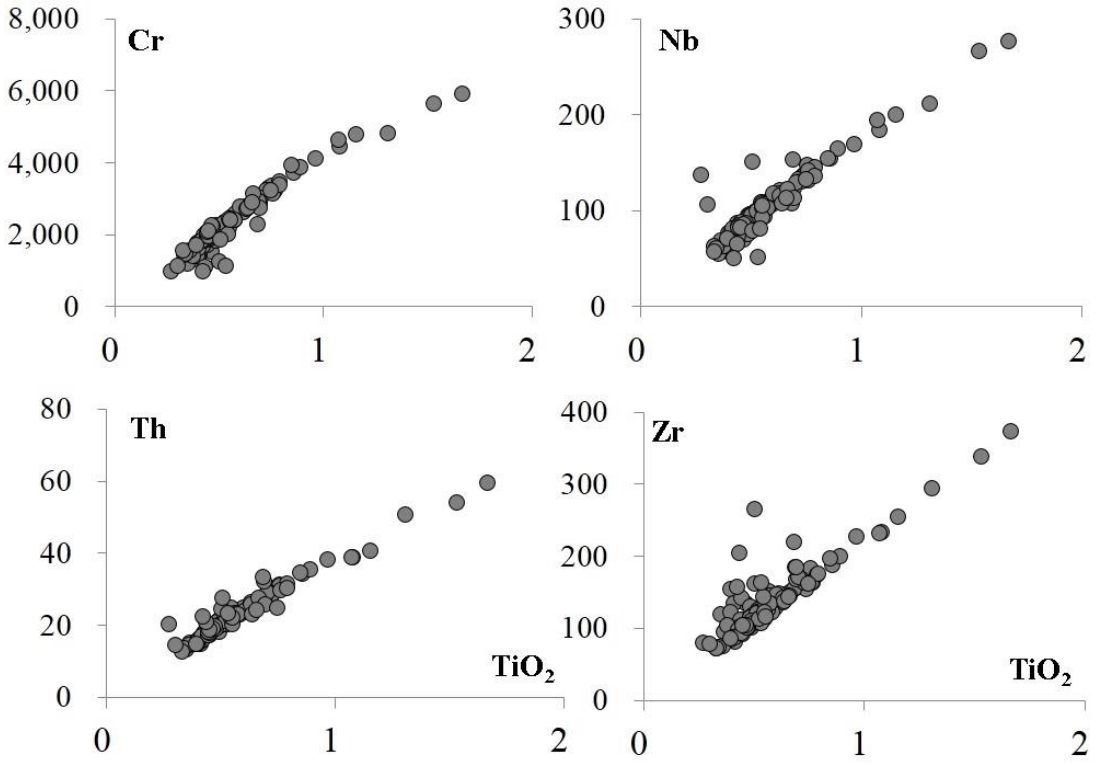

Figure 5.8 Selected trace element compositions (ppm) vs. TiO_2 (wt.%) of the ca. 1590 Ma olivine-phyric basalt. Same dataset as Fig. 5.6.

which are commonly more hydrothermally mobile compared to Cr and HFSE, there are no well-constrained linear co-variations, except for Sr and Ba. Components which are commonly positively correlated in mafic to ultramafic igneous suites such as MgO, Ni and Cr do not show linear correlations.

5.5.2 Geochronology of the ca. 1590 Ma olivine-phyric basalt

Apatite crystals in two olivine-phyric basalt samples (OD24, flat-lying basalt unit and OD7, dyke) have been analysed (Fig. 5.9a, Table S6). Both samples display the same petrographic features, i.e., porphyritic texture, the same type of alteration, in particular, spongy secondary apatite (Fig. 5.9b). Apatite from two samples (OD24 and OD7) yielded results of 1457 ± 500 Ma (MSWD=14, intersecting the $^{207}Pb/^{206}Pb$ axis at 0.71) and 1616 ± 72 Ma (MSWD=13, intersecting the $^{207}Pb/^{206}Pb$ axis at 0.74), respectively. All analyses combined produced an age of an age of 1615 ± 68 Ma (MSWD=12), intersecting the $^{207}Pb/^{206}Pb$ axis at 0.74 (Fig. 5.9a).

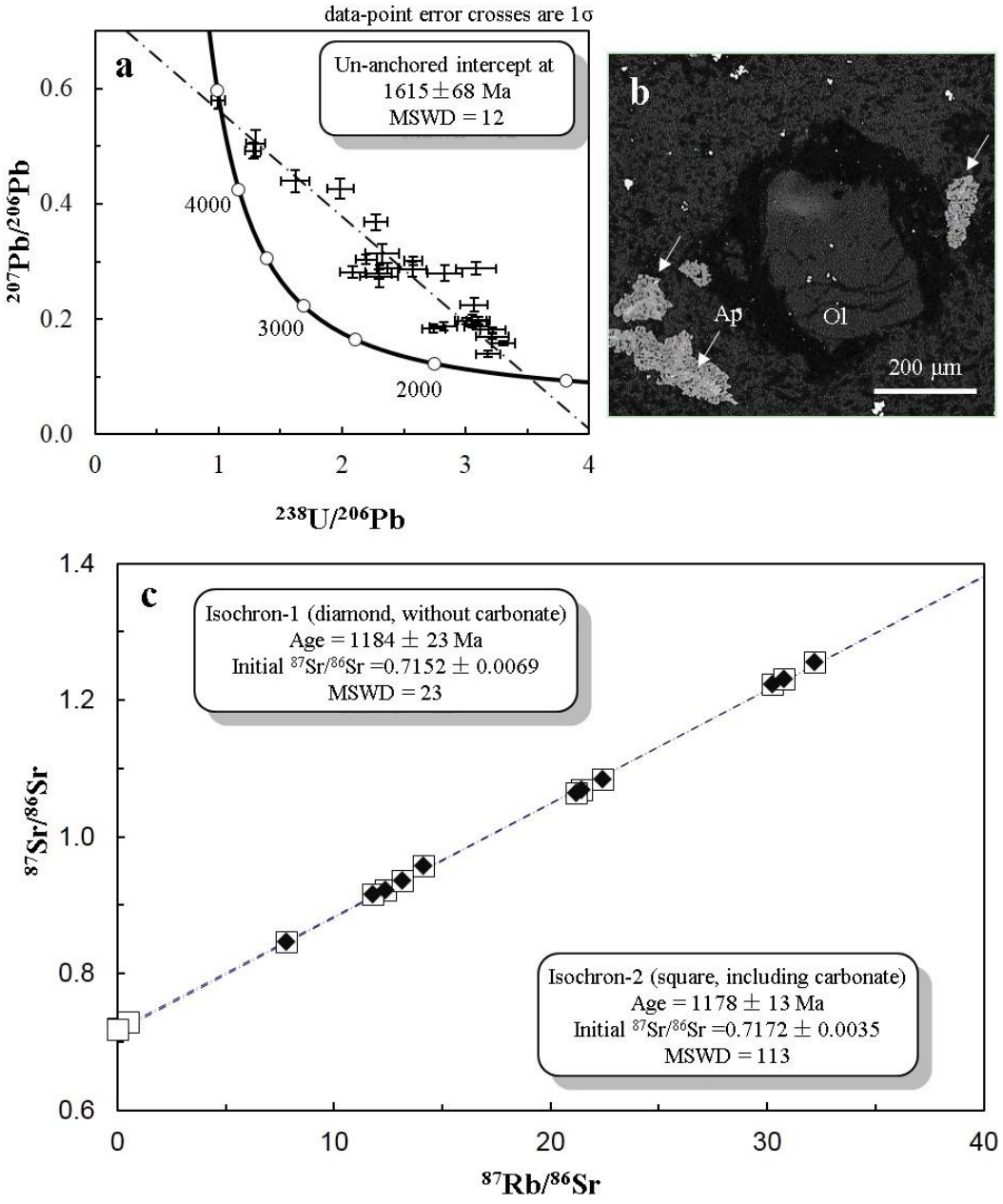

Figure 5.9 Geochronology of the ca. 1590 Ma olivine-phyric basalt. (a) LA-ICPMS U-Pb dating of secondary apatite in two samples (flat-lying basalt sample, OD24, drill hole RD3008 and dyke sample, OD7, drill hole RD2570). (b) Secondary apatite (Ap, white arrow) shows a spongy shape in the groundmass surrounding a former olivine (Ol) phenocryst. BSE image. (c) Rb-Sr isochrons of three sericite-altered basalt samples (one flat-lying basalt sample OD968, drill hole RD635, and two dyke sample OD906 and OD914, drill hole RD2715). Two isochrons have been drawn, with and without carbonate vein materials (squares versus solid black diamonds, respectively), yielding comparable ages and initial $^{87}Sr/^{86}Sr$ ratios. See text for further discussion.

Intensely sericite-altered olivine-phyric basalt (including one flat-lying basalt sample OD968 from drill hole RD635, and two dyke samples OD906 and OD914 from drill hole RD2715) were sampled for Rb-Sr dating, using powders abraded from several<1 cm^2 areas on sliced drill core material. Rb contents in these powders are relatively high (156-258 ppm), Sr is low (23.9-58.4 ppm), and Rb/Sr (2.66-10.57; $^{87}Rb/^{86}Sr$ 7.81-32.20) and measured $^{87}Sr/^{86}Sr$ ratios are high (0.845-1.254, Table 5.1). Hydrothermal veinlets cut across the samples. Carbonate vein material in each sample has very low Rb concentrations (1.4-2.4 ppm) and much lower $^{87}Rb/^{86}Sr$ (0.009-0.514) and $^{87}Sr/^{86}Sr$ (0.7178-0.7277) than the sericite-altered olivine-phyric basalt.

Limited Sm-Nd isotope results for the basalt samples indicate relatively high LREE concentrations (57-184 ppm Nd), low Sm/Nd ratios and strongly negative present-day εNd (-8.8 to -20.2, Table 5.1). Carbonates in two hydrothermal veinlets (OD914 and OD968), have variable LREE contents (8 to 33 ppm of Nd), Sm/Nd ($^{147}Sm/^{144}Nd$ 0.1963 to 0.3646) and present-day εNd (-0.6 to 4.5).

The two olivine-phyric dykes, OD906 and OD914, have the most mica-like Rb-Sr systems and define well-fitted isochrons (excluding carbonate vein analyses), with ages of 1158 ± 3 (MSWD=0.047) and 1181 ± 3 Ma (MSWD=0.23), respectively. The flat-lying basalt sample OD968 has lower Rb/Sr ratios, and the data are more scattered, producing an age of 1188 ± 39 Ma (MSWD=24, excluding carbonate vein analyses). If the carbonate vein fractions are included in the age calculations, they greatly extend the dispersion in each case and thus have a strong control on the derived ages and their uncertainties. Inclusion of the carbonate vein data points into age calculation may not be warranted because εNd calculated at ca. 1180 Ma for two of the veins differs strongly from the basalt values (Table 5.1, OD914: basalt -5.6, vein -0.7; OD968: basalt -0.4 and -0.6, vein -21.2). However, pooling of all the data for OD906, OD914 and OD968, with and without carbonate veins, yields similar results of 1178 ± 13 (MSWD=113, intercepting $^{87}Sr/^{86}Sr$ axis at 0.7172) and 1184 ± 23 Ma (MSWD=23, intercepting $^{87}Sr/^{86}Sr$ axis at 0.7152), respectively (Fig. 5. 9c).

5.5.3 Geochemistry of the ca. 820 Ma Olympic Dam dolerite

Data of the least altered Olympic Dam dolerite (igneous mineralogy mostly preserved) and Gairdner Dyke Swarm show primary compositional trends (Huang et al., 2015, Chapter 3) and have been plotted for comparison (Fig. 5.10). Petrographically more altered Olympic Dam dolerite samples (e.g. primary igneous minerals replaced, elevated loss on ignition) from this study tend to follow the same primary magmatic trend defined by the least altered Olympic Dam dolerite and Gairdner Dyke Swarm. But more altered sampels show wider dispersions of major element compositions, in particular SiO_2, FeO_t (total Fe as FeO), MgO, CaO, Na_2O, and K_2O as opposed to Al_2O_3 and P_2O_5. Compared to the least altered dolerite, the more altered dolerite samples display elevated FeO_t (up to 29 wt.%, loss on ignition free, same below), MgO (up to 12 wt.%), and K_2O (up to 4.4 wt.%), but generally lower Na_2O (as low as 0.1 wt.%) and CaO (down to 0.4 wt.%) contents at similar TiO_2 contents (Fig. 5.10, Table 5.2).

With increasing TiO_2 contents, compatible elements (e.g. Cr and Ni) in the Olympic Dam dolerite and Gairdner Dyke Swarm decrease, whereas incompatible elements (e.g. HFSE) increase (Fig. 5.11), as expected for magmatic fractionation. Among all the trace elements, Cr, Ni, and HFSE including Y, Zr, Nb, Hf, Ta and Th exhibit near linear correlations with TiO_2, though it is not uncommon to see slight dispersion in binary plots. However, for other trace elements, for example, LILE (Cs, Ba, Rb, and Sr) and REE, the more altered Olympic Dam dolerite samples tend to deviate from the primary magmatic trend defined by the least altered counterparts (Fig. 5.11).

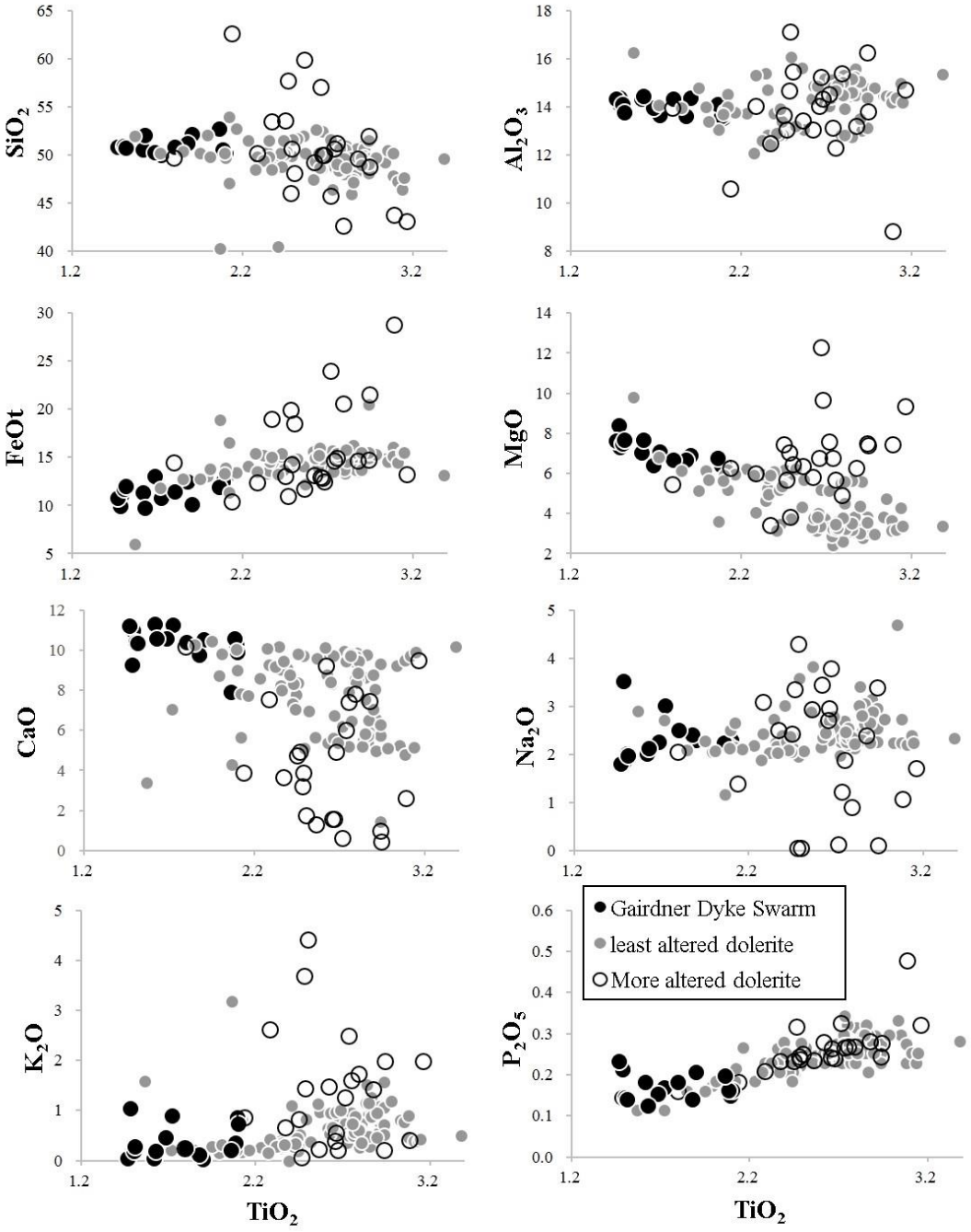

Figure 5.10 Major element compositions (wt.%) of the ca. 820 Ma Olympic Dam dolerite. Gairdner Dyke Swarm has also been plotted for comparison. Data of the least altered Olympic Dam dolerite and Gairdner Dyke Swarm have been combined in Chapter 3 (Huang et al., 2015). Data of more altered Olympic Dam dolerite are from this study.

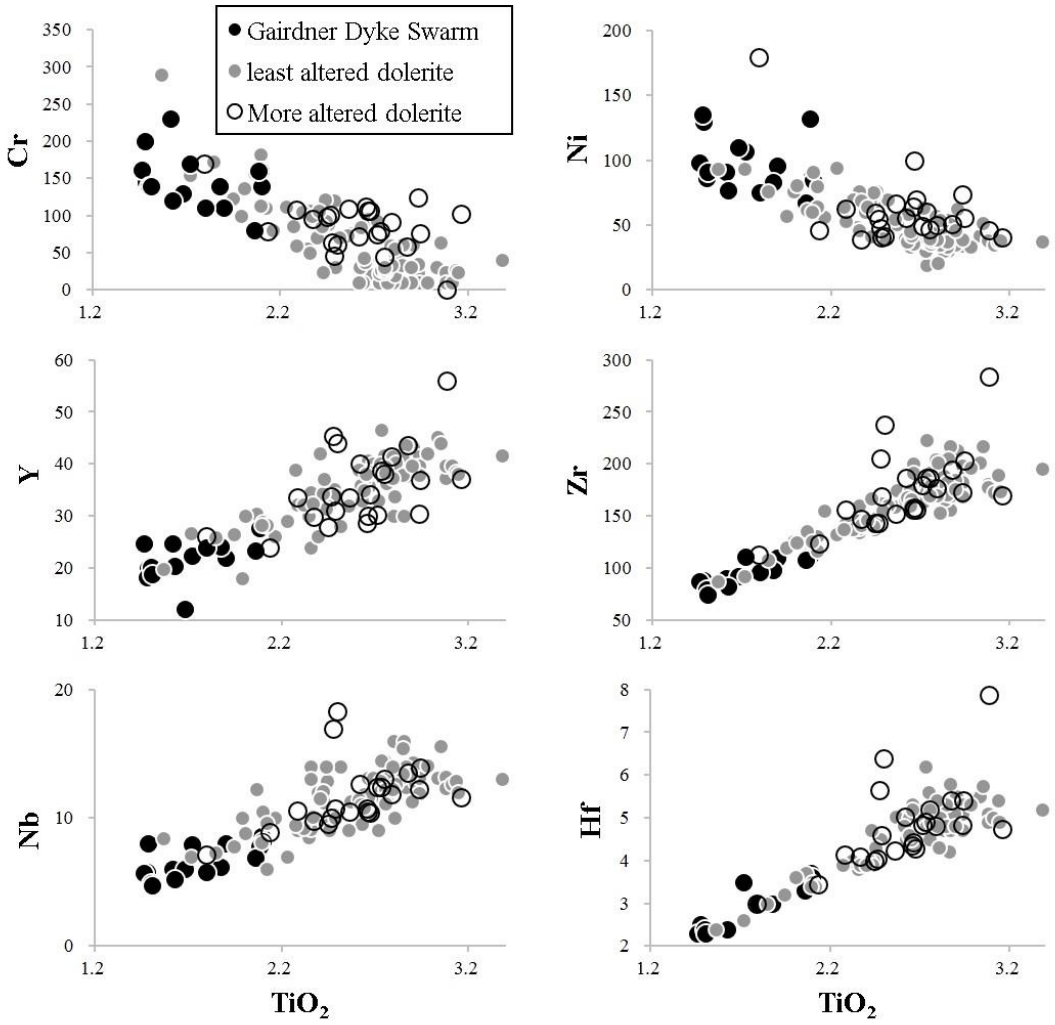

Figure 5.11 Selected trace elements compositions (ppm) and ratios vs. TiO_2 (wt.%) of the ca. 820 Ma Olympic Dam dolerite. Same dataset as Fig. 5.10.

Pb isotope compositions of the Olympic Dam dolerite, and chalcopyrite and galena within have been analysed (Tables S7-9). The dolerite (both least and more altered samples) show indistinguishable Pb isotope variations ($^{204}Pb/^{206}Pb$ from 0.0290 to 0.0306; $^{207}Pb/^{206}Pb$ from 0.500 to 0.558). The chalcopyrite in the sample OD1064 (Fig. 5.4), including both chalcopyrite grains in the spherulites and in the dyke near the hydrothermal veinlets, also display indistinguishable Pb isotope signatures, have $^{204}Pb/^{206}Pb$ and $^{207}Pb/^{206}Pb$ ratios from 0.0170 to 0.0292 and 0.327 to 0.469, and plot in between the Olympic Dam dolerite and the ODBC (Fig. 5.12). Disseminated galena crystals from one dolerite sample (OD852b) show comparable Pb isotope compositions to the chalcopyrite (Fig. 5.12).

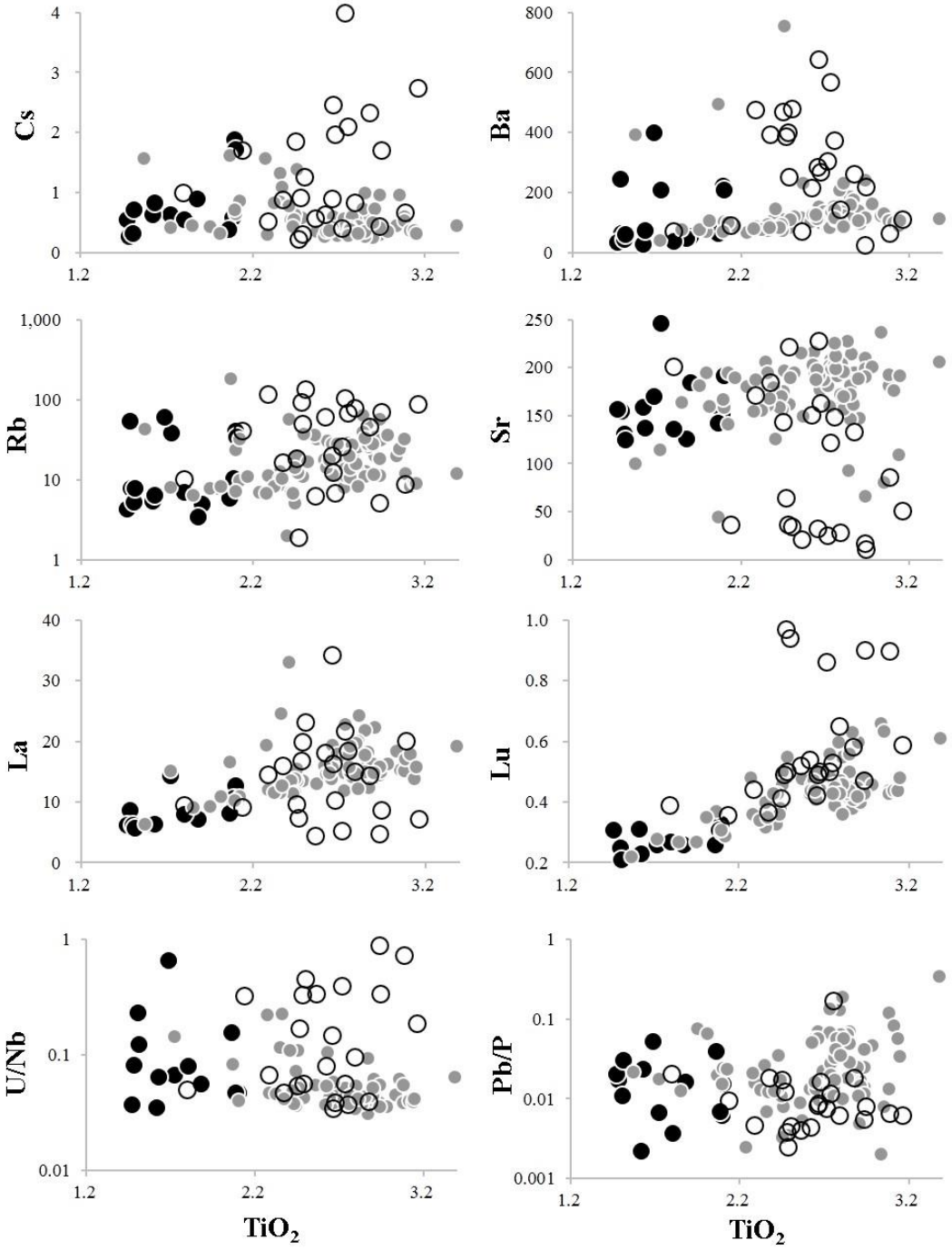

Fig. 5.11 continued.

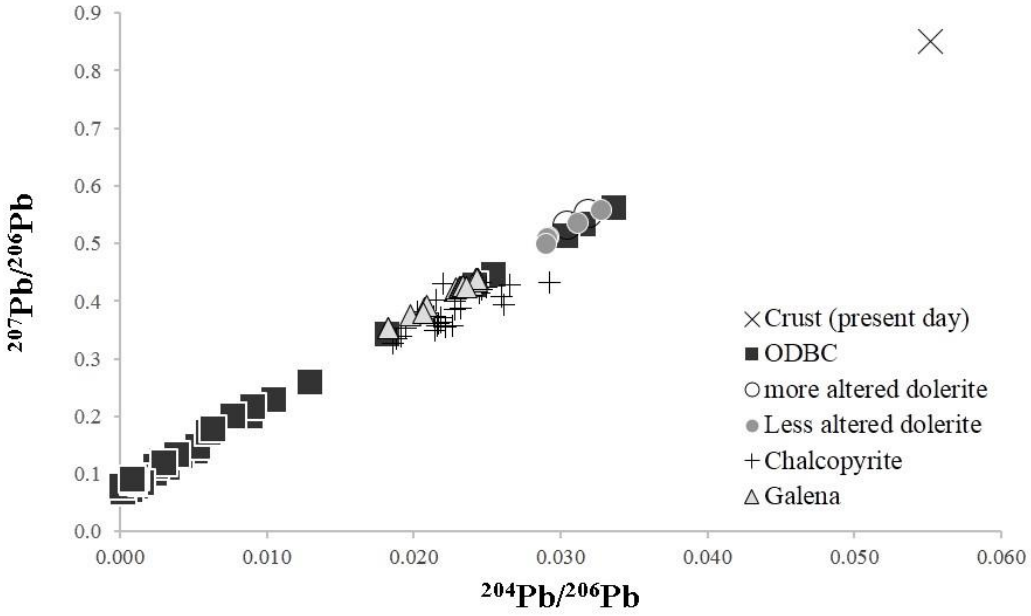

Figure 5.12 Present-day $^{204}Pb/^{206}Pb$ vs. $^{207}Pb/^{206}Pb$ diagram for the Olympic Dam dolerite, chalcopyrite in the dolerite sample OD1064 (Fig. 5.4), galena in one dolerite sample OD852b. Pb isotope compositions of the ODBC (unpublished data in Kirchenbaur et al., 2016) have also been plotted for comparison. Crustal Pb isotope composition (present day, μ=9) is from Stacey and Kramers (1975). See text for details.

5.6 Discussion

5.6.1 Alteration of the ca. 1590 Ma olivine-phyric basalt at Olympic Dam

U-Pb dating of secondary spongy apatite in the olivine-phyric basalt yielded a result (Fig. 5.9a) that is broadly coeval with the age of the basalt, probably recording a hydrothermal activity shortly after the emplacement at ca. 1590 Ma, even though the age is poorly constrained, and the great MSWD and poor regression imply that the U-Pb systematics of the apatite have been disrupted.

Rb-Sr isochron dating of sericite-altered olivine-phyric basalt yielded similar ages of ca. 1180 Ma and comparable initial $^{87}Sr/^{86}Sr$ ratios, with or without carbonate vein analyses (Fig. 5.9c), though distinct Nd isotope signatures existed between olivine-phyric basalt and carbonate vein analyses, implying that carbonate veins may not be cogenetic with sericite alteration of the olivine-phyric basalt in all cases. The scatter within both arrays may be due to the pronounced isotopic heterogeneity of the ODBC

after ca. 1590 Ma (Johnson, 1993; Johnson and McCulloch, 1995). The isotopic compositions of Sr and Nd in circulating hydrothermal fluids would have changed continuously through exchange with locally accessible breccia components; variable $^{87}Sr/^{86}Sr$ in intensely altered olivine-phyric basalt in different parts of the deposit can be expected. It is, therefore, remarkable that the Rb-Sr systems of the three altered samples define such a consistent isotopic trend. Furthermore, local resetting of an original ca. 1590 Ma signature, a commonly proposed explanation for post-primary Rb-Sr ages within such a large U deposit, would not be expected to produce such a consistent trend in widely dispersed samples. The apparent age of ca. 1180 Ma is therefore interpreted as evidence for a widespread sericite alteration in the olivine-phyric basalt long after the emplacement of mafic to ultramafic magmas and the inferred formation of the ODBC at ca. 1590 Ma (Reeve et al., 1990).

The basalt contains ~6.2 wt.% MgO on average (Fig. 5.6) which is below 16 wt.% estimated based on the volume (~20 vol.% for undeformed samples) and compositions (inferred from compositions of a large number of Cr-spinel inclusions) of former olivine phenocrysts (Chapter 4). The positive correlations among MgO, CaO, MnO and CO_2 indicate that these components reside in secondary carbonates (mostly ankerite, minor siderite, dolomite and calcite) in the basalt. Strongly sericite-altered equivalents are enriched in K_2O, Al_2O_3 (Fig. 5.6) and Rb. Drill core intervals strongly overprinted by iron oxides display high Fe_2O_3 contents (up to 50 wt.%).

Clearly the extreme trace element compositions (e.g. up to ~6,000 ppm Cr, ~280 ppm Nb, ~370 ppm Zr, Fig. 5.8) of some assays are unlikely to be primary igneous values for volcanic/subvolcanic olivine-bearing rocks. They must, therefore, result either from the hydrothermal introduction of Cr, Nb and Zr, and/or from the residual concentration of these elements as other elements were removed. In this regard, we note the near linear co-variations between Cr and HFSE (Fig. 5.8). In the evolution of mafic magmatism (i.e. partial melting, cooling and crystallization), Cr is a compatible element, and its concentration decreases with increasing concentrations of incompatible elements such as HFSE (cf. Rollinson, 1993). Therefore, the most likely explanation for the positive correlations between Cr and HFSE is that variable degrees of mass and/or volume loss were accompanied with at least the most recent hydrothermal alteration, during which these components were almost all retained in iron oxides in the

basalt rather than carried away by hydrothermal fluids. We also note that the sericite-altered olivine-phyric basalt contains the highest amounts of retained trace elements such as Cr and HFSE (Figs. 5.6 and 5.8). This implies that the sericite alteration was more intense in terms of hydrothermal modification of primary whole-rock compositions of the ca. 1590 Ma olivine-phyric basalt than other alteration types and that the sericite alteration was likely to be accompanied by higher degree of whole-rock mass and/or volume waste (thus concentrations of retained elements built up). These implications are in agreement with the field observation that the most intensely sericite-altered drill core intersections of the basalt are the most strongly degraded.

However, the retained characteristic of such elements as Cr and HFSE does not mean that they were 'immobile' during hydrothermal alteration. For example, deformation led to the break-up of pseudomorphed olivine and the release of Cr-spinel (the major Cr-bearing phase) inclusions into the groundmass. Alteration of Cr-spinel (replaced by chlorite + magnetite, or carbonate) and precipitation of secondary Cr-bearing magnetite supports Cr mobility on a local scale.

Therefore, we conclude that the compositions of the ca. 1590 Ma olivine-phyric basalt have been so intensely modified by multiple hydrothermal activities (at ca. 1590 Ma and 1180 Ma) that they largely reflect the signatures of various secondary minerals (dominantly chlorite, sericite, carbonates, and iron oxides) and secondary processes (e.g. deformation and mass/volume loss) rather than primary geochemical features.

5.6.2 Alteration of the ca. 820 Ma Olympic Dam dolerite

There were hydrothermal activities accompanying the emplacement of the ca. 820 Ma Olympic Dam dolerite, verified by the U-Pb dating of secondary apatite and titanite (Huang et al., 2015, Chapter 3; Apukhtina et al., 2016). In contrast with the intensely altered ca. 1590 Ma olivine-phyric basalt, the presence of least altered dolerite samples assist in the recognition of the primary magmatic compositional range and fractionation trend (Huang et al., 2015, Chapter 3). Accordingly, hydrothermal modifications of the dolerite can be readily seen by comparing petrographically more altered samples analysed in this study against the least altered equivalents.

Major components including Al_2O_3 and P_2O_5, and a number of trace elements such as Cr, Ni, Y and HFSE (i.e. Zr, Nb, Hf, Ti and Ta) are among the least altered constituents in the dolerite, as the more altered samples comply with the primary compositional range (Figs. 5.10 and 5.11). The negative correlation between Cr and TiO_2 in the dolerite (Fig. 5.11) is most likely to represent a primary magmatic trend, suggesting insignificant whole-rock mass and/or volume waste in the course of alteration, in contrast with that of the older olivine-phyric basalt (Fig. 5.8) present at the same deposit.

Elevated FeO_t, MgO and K_2O and depleted CaO and Na_2O contents shown by a few more altered samples indicate that the former components have probably been added in whereas the latter removed from the corresponding samples (Fig. 5.10). Concentrations of hydrothermally mobile trace elements (e.g. LILE) have been modified to variable degrees, and such modifications are straightforward on element vs. TiO_2 binary diagrams: Cs, Rb, and Ba were enriched in the dolerite whereas Sr was depleted (Fig. 5.11). We note that LREE (e.g. La) behaved differently from HREE (e.g. Lu) as a result of alteration (Fig. 5.11). The former are mostly depleted in the more altered dolerite, whereas the latter are largely enriched in the same rocks, suggesting the hydrothermal introduction of LREE but depletion of HREE. U and Pb have similar compatibility to Nb and P, respectively, during mafic magmatism (i.e. partial melting, cooling and crystallization) (Sun and McDonough, 1989). Nb and P are among the least modified components in the dolerite, as aforementioned. Therefore, U/Nb and/or Pb/P ratios would remain consistent in the dolerite unless U and/or Pb were affected by hydrothermal activities. The least altered dolerite shows more constrained and lower U/Nb ratios compared to the more altered counterparts, implying that U was introduced to the more altered dolerite as a result of hydrothermal alteration (Fig. 5.11). Whereas the wide range of Pb/P ratios (Fig. 5.11) and the elevated Pb concentrations (see below, Fig. 5.13) indicate that Pb contents in both the least and more altered samples have been modified by alteration.

In brief, though not as intensely altered as the ca. 1590 Ma basalt, the ca. 820 Ma dolerite was involved in the hydrothermal system at Olympic Dam. Considering that the older mafic rocks have been proposed as an important Cu source (Johnson and

McCulloch, 1995), this raises a further question whether the younger dolerite (also mafic) could be a metal source to the ore hosted in the ODBC.

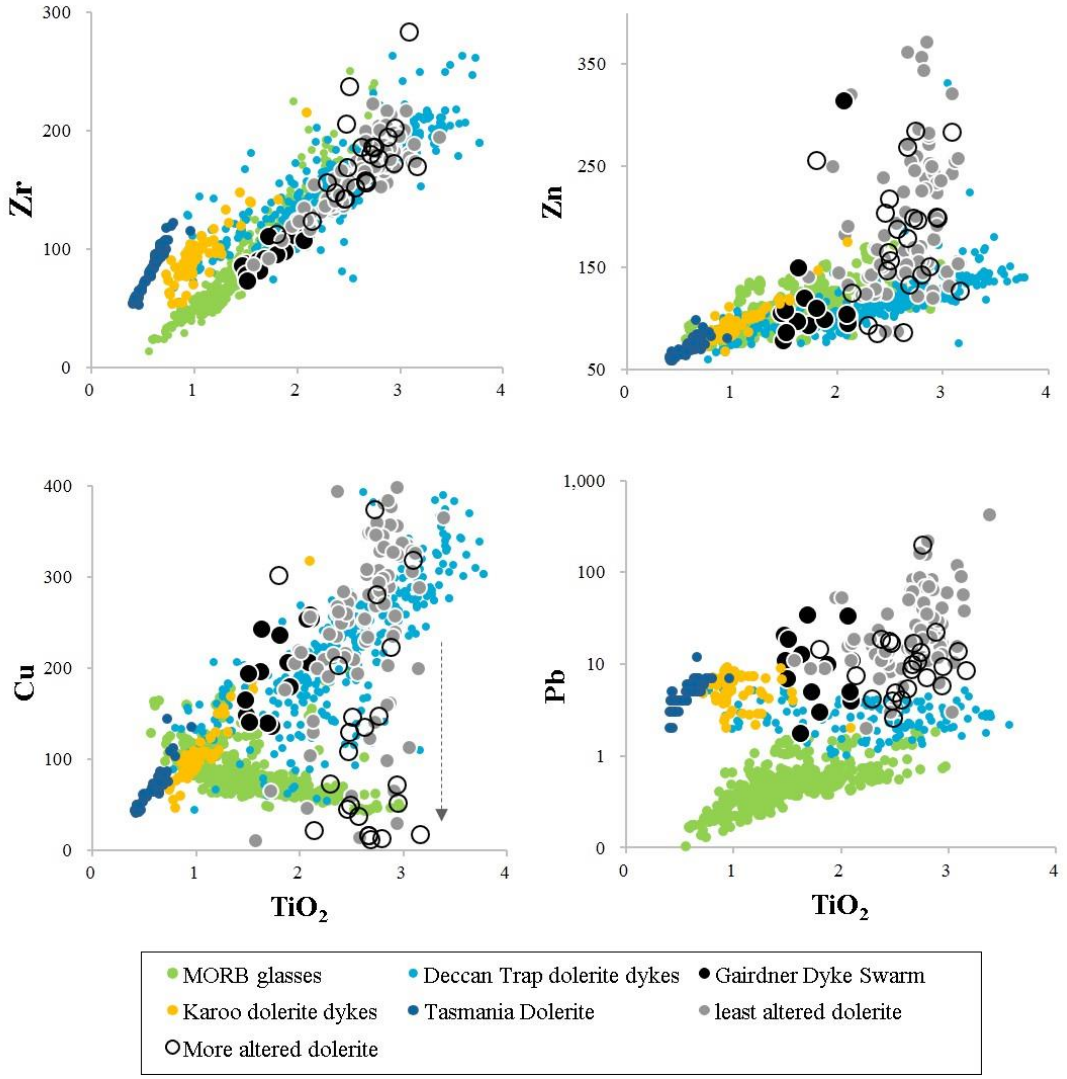

Figure 5.13 Zr, Zn, Cu and Pb (ppm) vs. TiO_2 (wt.%) of the ca. 820 Ma Olympic Dam dolerite compared to a number of volcanic to subvolcanic mafic suites including MORB glasses (Jenner and O'Neill, 2012), Karoo (Galerne et al., 2008; Neumann et al., 2011) and Deccan dolerite dykes (Peng et al., 1998; Vanderkluysen et al., 2011), and Tasmania dolerite (Hergt, 1987) . See text for further discussion. Data of the Gairdner Dyke Swarm and the Olympic Dam dolerite are the same as Fig. 5.10. The dashed arrow on the Cu vs. TiO_2 plot indicates copper depletion in a number of Olympic Dam dolerite samples.

An investigation of some trace elements concentrations (i.e. Zr, Zn, Cu and Pb, Fig. 5.13) of the Olympic Dam dolerite and a comparison of the dolerite with well-studied unmineralised mafic suites, especially dolerite, may provide a hint to this question. Zr is an incompatible element during magmatic evolution and presumably

immobile during hydrothermal alteration. Its concentration increases with increasing TiO_2 contents, representing a primary magmatic signature, evident from volcanic to subvolcanic suites including the Gairdner Dyke Swarm, the Olympic Dam dolerite, mid-ocean ridge basalts (MORB), Tasmania Dolerite, Karoo and Deccan dolerite dykes. Zn may have a similar geochemical property to Zr during magmatic evolution but more sensitive to hydrothermal alteration. Hence, the invariably altered Olympic Dam dolerite shows irregular and generally elevated Zn concentrations in contrast with other unmineralised mafic suites displaying near linear Zn-TiO_2 correlations (Fig. 5.13). Cu tends to have different geochemical characteristics from Zr and Zn. Cu may be compatible in certain volcanic suites (e.g. MORB) and this is shown by the negative near linear Cu-TiO_2 correlation (Fig. 5.13). It may also be incompatible in some subvolcanic suites as inferred from the positive near linear Cu-TiO_2 correlation by the Gairdner Dyke Swarm, most of the least altered Olympic Dam dolerite, Tasmania Dolerite, Karoo and Deccan dolerite dykes. It is also apparent from the same diagram that some Olympic Dam dolerite samples (most more altered dolerite samples and even a number of the least altered equivalents) are depleted in Cu, indicating that the Olympic Dam dolerite can potentially be a subordinate Cu source (rather than Zn source) to the Olympic Dam deposit. The Olympic Dam dolerite shows a wider range of Pb concentrations than other igneous suites; the elevated Pb concentrations in the majority of the dolerite indicate derivation of Pb from hydrothermal fluids.

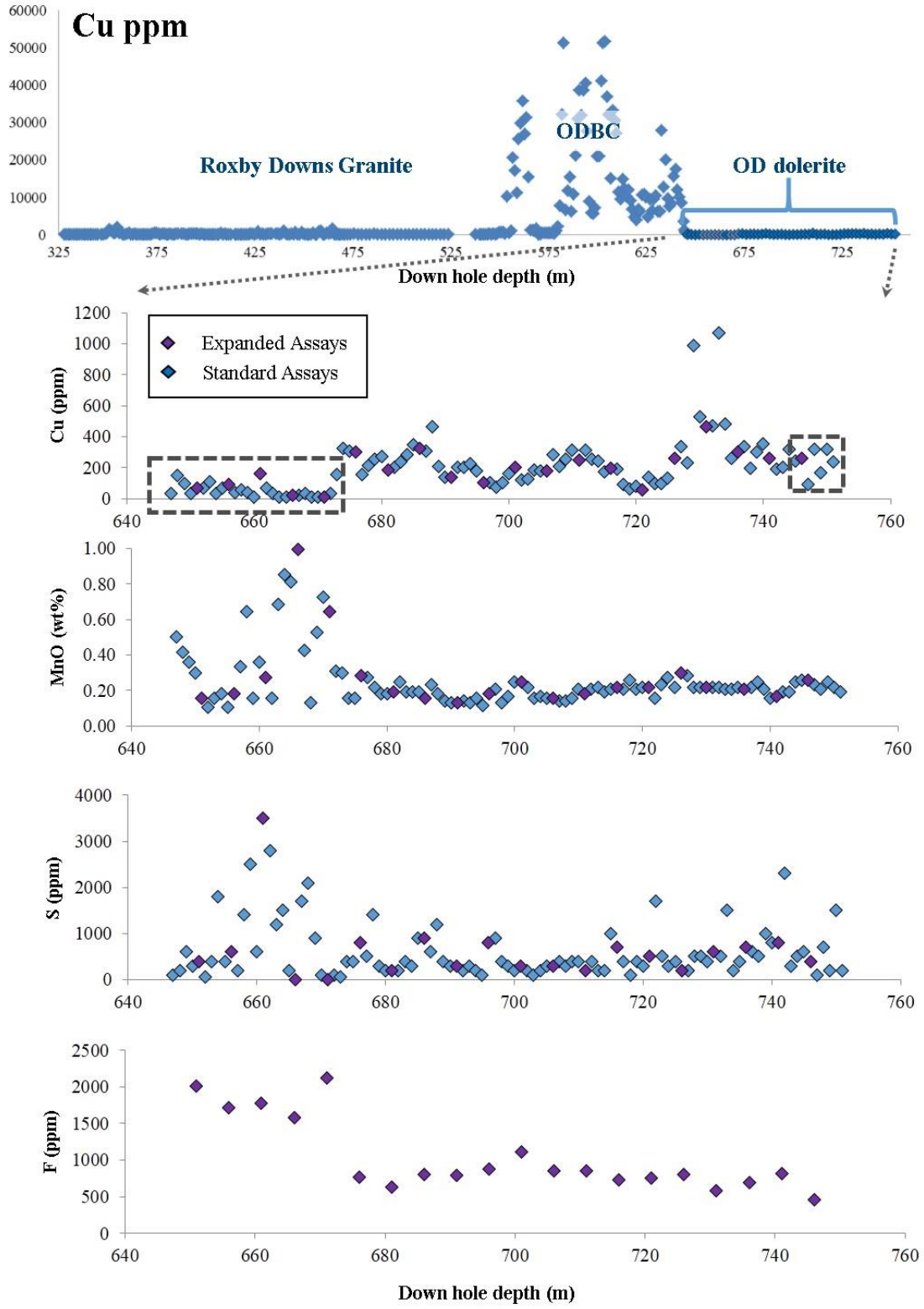

Figure 5.14 Drill core assays of RD271, with a particular focus on the Olympic Dam dolerite interval (646 to 752 m). RD271 intersects the Roxby Downs Granite, the ODBC and the Olympic Dam dolerite downhole. The ODBC is characterized by its higher copper concentration (up to 50,000 ppm) in contrast to the other two units. The Olympic Dam

dolerite in immediate contact with the ODBC shows apparent compositional variations of selected mobile elements. There are two groups of assays plotted in the diagram. Standard assays (33 elements analyzed, blue) took every one-meter interval and expanded assays (71 elements analyzed, purple) took every five-meter interval. Two dashed black squares in the Cu concentration diagram represent the two intervals (altered vs. relatively fresh, respectively) adopted in the Isocon analysis.

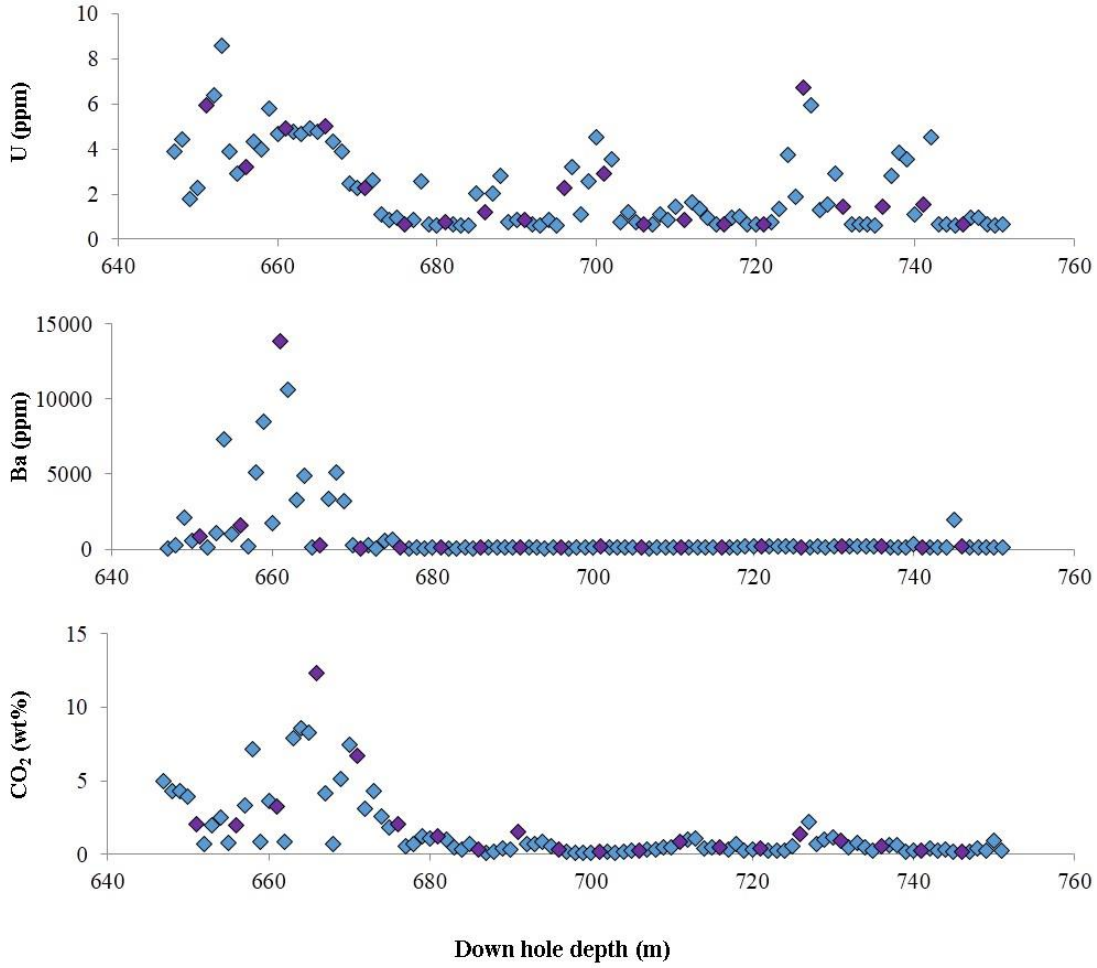

Fig. 5.14 continued

Further evidence for Cu depletion in the ca. 820 Ma Olympic Dam dolerite can be seen in drill core assays of RD271. RD271 is a sub-vertical, surface drill hole. It intersected the Roxby Downs Granite, the ODBC and Olympic Dam dolerite downhole from 325 to 752 m (end of the hole) (Fig. 5.14). In this hole, the Olympic Dam dolerite intruded the ODBC (intrusive contact at 646 m). The Olympic Dam dolerite in immediate contact (646 to 676 m) with the ODBC has been more altered than the rest of the dolerite, as indicated by the common occurrence of secondary minerals such as chlorite, sericite and carbonate, and apparent compositional variations of a number of

mobile elements such as Mn, S, F, U, Ba and CO_2 (Fig. 5.14, Table S10). The Olympic Dam dolerite away from the contact is petrographically fresher (dominant primary minerals such as plagioclase and clinopyroxene have been preserved), and have more consistent concentrations of selected mobile elements (Fig. 5.14).

It is worthy to note that the 30-meter interval (646 to 676 m) of Olympic Dam dolerite in immediate contact with the ODBC appears to be uniformly depleted in copper. This 'depletion' could be a result of the copper loss from the dolerite or due to the mass gain of the dolerite during alteration while copper was retained (i.e. copper concentrations were diluted). This 'depletion' is also accompanied by apparent 'enrichment' of Mn, S, F, U, Ba and CO_2 in the same interval (Fig. 5.14). Isocon analysis (Zr, Ta, Nb, Hf and Ti selected as inertia elements, Grant, 1986; 2005) using the GEOISO program (Coelho, 2006) shows that this 30-meter interval of dolerite lost 60 to 70 wt. % of its original copper (200 to 350 ppm), compared to the last 10-meter interval of fresher dolerite (Fig. 5.14), assuming that the whole Olympic Dam dolerite interval (646 to 752 m) contained consistent copper concentration before hydrothermal alteration.

A likely destination for the missing copper of the dolerite was the ODBC. In this case, the Olympic Dam dolerite may have contributed to the deposit's copper resource, though the total amount may be insignificant. Isocon analysis also indicates that this hydrothermal activity has also been responsible for adding other elements including Mn, S, F, U, Ba and CO_2 to the dolerite in immediate contact with the ODBC.

The more and least altered Olympic Dam dolerite show indistinguishable, radiogenic Pb isotope compositions, in between those of the ODBC and the crust (Fig. 5.12), indicating derivation of radiogenic Pb in the dolerite from hydrothermal fluids circulating the ODBC. Chalcopyrite (Fig. 5.4) and galena crystals within the dolerite show slightly more radiogenic Pb isotope compositions than the dolerite; this suggests that Pb in the chalcopyrite and galena were supplied by fluids flowing through both the ODBC and the dolerite. Chances are that Cu in the chalcopyrite share a similar origin to Pb, in agreement with the proposal of the dolerite being a potential Cu source.

In summary, hydrothermally altered petrographic features and modified whole-rock compositions (most importantly, depletion of Cu and enrichment of radiogenic Pb)

of the Olympic Dam dolerite suggest that the dolerite was an indispensable part of the Olympic Dam hydrothermal system that was active at ca. 820 Ma.

5.6.3 Ore-forming processes at Olympic Dam: multiple sources and a multi-stage hydrothermal system?

Geochronological investigations of the ODBC using different methods have yielded a wide range of results. These results include hematite U-Pb ages of ca. 1590 Ma by Ciobanu et al. (2013); an uraninite U-Pb age of ca. 1400 Ma by Trueman et al. (1986); four distinct ages of pitchblende growth at ca. 1350 to 1400 Ma, ca. 1220 Ma, ca. 830 Ma and ca. 570 Ma, respectively, by Johnson (1993); chalcopyrite Re-Os age of ca. 1258 Ma by McInnes et al. (2008); uranium introduction no earlier than ca. 1300-1100 Ma constrained by Pb isotopes in galena and pyrite by Meffre et al. (2010); copper sulfides Sm-Nd and Rb-Sr apparent ages of ca. 1300 Ma by Maas et al. (2011).

It has been suggested by Reeve et al. (1990) that extensive hydrothermal brecciation of the Roxby Downs Granite was initiated by the emplacement of one or more mafic-felsic plutons at ca. 1590 Ma. The U-Pb dating of secondary apatite (Fg. 9a) in the olivine-phyric basalt indicates alteration of the basalt at ca. 1590 Ma and is well in agreement with this proposal. The Rb-Sr dating result (Fig. 5.9c) obtained on the sericite-altered olivine-phyric basalt suggests that the last hydrothermal activity that brought widespread sericite alteration to the basalt occurred probably at ca. 1180 Ma; this activity is broadly coeval with the formation of some copper sulfides and introduction and/or mobilization of uranium in the ODBC. There is no recognized ca. 1180 Ma magmatism in the Gawler Craton where the Olympic Dam deposit is situated, but magmatic events of similar ages have been well-documented in the Musgrave Province (~500 km to the north of the Gawler Craton) (e.g. White et al., 1999). A tentative suggestion of a Grenville-age magmatic event in the Gawler Craton has been made by Belousova et al. (2009), in which detrital zircons collected across the Gawler Craton display a prominent 1169 ± 48 Ma age population without the 1300 to 1400 Ma event that is also known to be pronounced in the Musgrave Province (e.g. Birksgate Complex, Wade et al., 2005). Accordingly, the ca. 1180 Ma post-primary Rb-Sr age of the olivine-phyric rocks at Olympic Dam, as well as other previously published broadly coeval ages obtained on the ODBC mentioned above, may either reflect an

unrecognized, coeval magmatic event in the Gawler Craton or represent a hydrothermal activity corresponding to the Grenville-age magmatism in the Musgrave Block.

The basalt is intensely altered and commonly contains a magnetite-apatite ± chlorite ± quartz assemblage (Fig. 5.2e and f) which resembles the inferred early reduced Fe oxide alteration assemblage in the ODBC (Reeve et al., 1990; Haynes et al., 1995; Ehrig et al., 2012). Hence, chances are that there were compositional exchanges facilitated by hydrothermal fluids between the ODBC and the olivine-phyric basalt at ca. 1590 Ma and 1180 Ma. Also, positive near linear correlation between Cr and TiO_2 of the basalt also indicates large degree of mass and/or volume loss of the basalt as a result of hydrothermal alteration. All these observations and results are consistent with the proposal that the ca. 1590 Ma mafic GRV were an important source of the Cu (~50% of the contained Cu) found in the deposit (Johnson et al., 1993; Johnson and McCulloch, 1995).

Further, there were proved hydrothermal activities accompanied with the emplacement of the ca. 820 Ma Olympic Dam dolerite (Huang et al., 2015, Chapter 3; Apukhtina et al., 2016). Altered and/or brecciated dolerite adjacent to the intrusive contacts with the Roxby Downs Granite and the ODBC contains a similar magnetite-apatite ± chlorite ± quartz (± sulfide ± uraninite ± monazite) assemblage (Fig. 5.5), to that of the ca. 1590 Ma olivine-phyric basalt (Fig. 5.2) and to the inferred early reduced Fe oxide alteration assemblage in the ODBC (Reeve et al., 1990; Haynes et al., 1995; Ehrig et al., 2012). This observation, combined with hydrothermally modified whole-rock compositions, indicates that the hydrothermal system at Olympic Dam was active at ca. 820 Ma and that copper and uranium were both mobile during this period of hydrothermal activity. In addition, the compositional comparison between the more and least altered dolerite suggests the younger Olympic Dam dolerite can potentially be a subordinate copper source to the deposit, even though the total amount of copper contributed may be insignificant. Besides, copper depletion of the dolerite seems to be accompanied with sodic alteration, as revealed by petrographic observation and in the Cu vs. Na_2O/CaO diagram (Fig. 5.15): invariably altered dolerite with lower copper concentrations tend to have higher Na_2O/CaO ratios. This is in agreement with the conclusion drawn in Haynes (1972) that sodic alteration of basalts was responsible for mobilizing and leaching copper out from these rocks. More importantly, we may

envisage similar processes (i.e. copper depletion and sodic alteration) in the ca. 1590 Ma olivine-phyric basalt, even though the intense alteration (chlorite, sericite, carbonates and iron oxides) probably overprinted the sodic alteration and was also responsible for copper depletion in these older rocks, hampering detailed investigations of such processes.

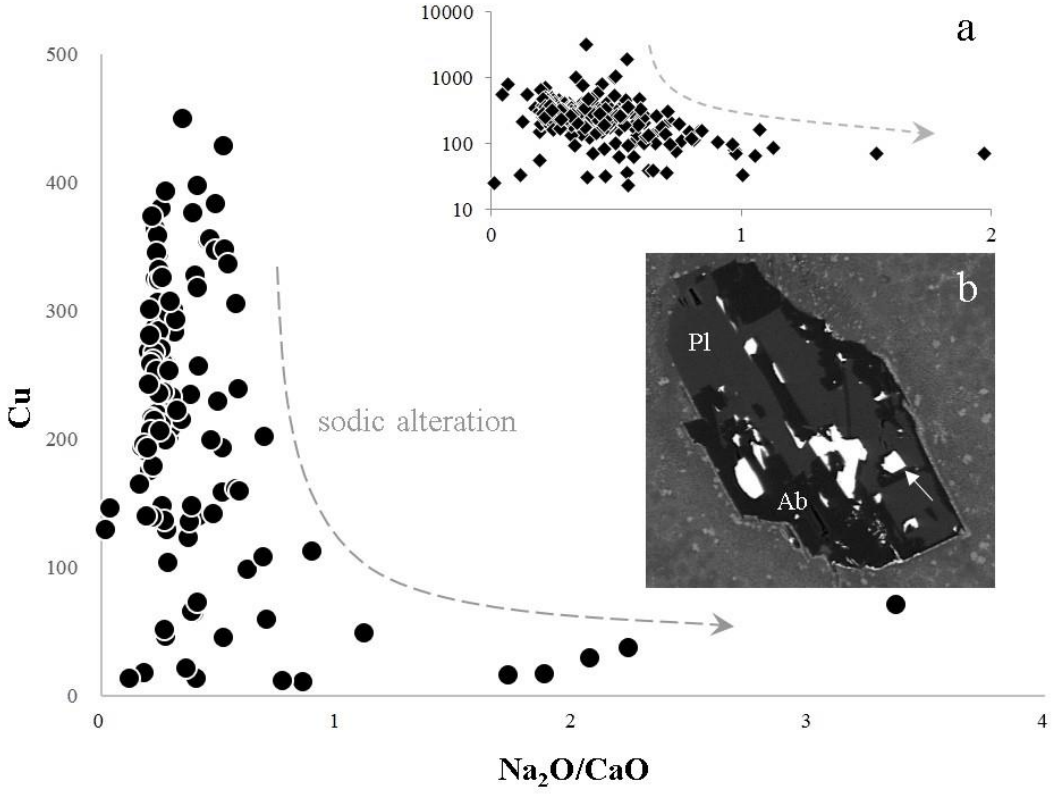

Figure 5.15 Cu (ppm) vs. Na_2O/CaO diagram of the Olympic Dam dolerite. Same data as in Fig. 5.10. Inset (a) displays the same plot for drill core assays of the Olympic Dam dolerite (BHP Billiton Olympic Dam, unpublished data). Both diagrams show that the invariably altered Olympic Dam dolerite with lower copper concentrations tend to have higher Na_2O/CaO ratios (dashed arrows), which is likely to correspond to sodic alteration. Inset (b) shows a plagioclase (Pl) phenocryst in the dyke (OD1064, Fig. 5.4) partly replaced by albite (Ab) and chalcopyrite (white arrow), indicating sodic alteration accompanied by copper mobilization.

All magmatic-hydrothermal activities (ca. 1590 Ma, 1180 Ma, 820 Ma) recorded in the two generations of mafic rocks can be correlated with aforementioned ages obtained on the ODBC. Compositional variations of both generations of mafic rocks support their roles as potent or potential copper sources. With all taken into account, an ensuing implication is that the ore-forming process at Olympic Dam might have

accommodated multiple sources (i.e. two generations of mafic rocks) and a multi-stage hydrothermal system (e.g., 1590 Ma, 1180 Ma, and 820 Ma).

5.7 Conclusions

Mafic rocks have long been proposed as important material sources, especially copper, to the Olympic Dam iron oxide Cu-U-Au-Ag deposit. Near linear variations between Cr and HFSE in the ca. 1590 Ma olivine-phyric basalt at Olympic Dam reflect not only the retained characteristics of these elements but also indicate whole-rock mass and/or volume loss of the basalt in the course of hydrothermal alteration, in accordance with its previously proposed role as an important copper source. Besides, commonly depleted copper contents in the ca. 820 Ma Olympic Dam dolerite suggest that it could be another metal contributor to the Olympic Dam deposit's copper endowment though the total amount was likely to be insignificant. More importantly, we can anticipate similar copper depletion processes of the ca. 1590 Ma olivine-phyric basalt to those of the younger Olympic Dam dolerite. Both generations of mafic rocks record multiple magmatic-hydrothermal activities (ca. 1590 Ma, 1180 Ma and 820 Ma), and indicate a multi-stage hydrothermal evolution at the Olympic Dam deposit.

The Olympic Dam deposit is an archetype of the iron-oxide copper gold (IOCG)-type deposit. Unlike other magmatic-hydrothermal and hydrothermal deposits (e.g. porphyry copper deposits, low and high sulfidation epithermal deposits, and volcanic massive sulfide deposits) which have comparable number of young (or modern) and old deposits (or more young deposits than old equivalents), the sensu stricto IOCG deposit comprises dominantly Precambrian deposits (Groves et al., 2010). This implies either that the formation of sensu stricto IOCG type deposit did not follow the commonly applied uniformitarianism or that it took a long time (ca. 500 million years) for the typical sensu stricto IOCG type mineralization to become economic. If the latter is true, multiple activities (e.g. multi-stage hydrothermal system) and/or sources accommodated in one sensu stricto IOCG type deposit are not unexpected, as recorded in the mafic lithologies at the Olympic Dam deposit

Table 5.1 Rb-Sr isotope results for the ca. 1590 Ma sericite-altered olivine-phyric basalt at Olympic Dam

Sample No.	Materials analyzed	CaO (wt.%)	Rb (ppm)	Sr (ppm)	$^{87}Rb/^{86}Sr$	$^{87}Sr/^{86}Sr$	Sm (ppm)	Nd ppm	$^{147}Sm/^{144}Nd$	$^{143}Nd/^{144}Nd$	$\varepsilon Nd_{present}$	Rb-Sr isochron age (Ma)	εNd_{1180} (Ma)
OD906.1	basalt	1.66	200.0	26.77	22.40	1.08286							
OD906.2	basalt	0.85	197.9	27.62	21.45	1.06762	11.39	60.28	0.1141	0.511660	-19.0	1158	-6.8
OD906.3	basalt	1.18	201.3	28.41	21.21	1.06334	12.81	70.05	0.1104	0.511599	-20.2	1158	-7.5
OD906.4	carbonate vein	1.11	1.4	431	0.0092	0.71839							
OD914.1	basalt	5.19	245.0	24.61	30.249	1.22202							
OD914.2	basalt	4.48	252.2	23.87	32.199	1.25427							
OD914.3	basalt	4.80	258.2	25.47	30.814	1.23027	11.71	56.51	0.1251	0.511797	-16.3	1181	-5.6
OD914.4	carbonate vein	30.42	2.4	13.20	0.514	0.72769	10.65	32.77	0.1963	0.512599	-0.6	1181	-0.7
OD968.1	basalt	7.96	192.5	45.9	12.374	0.92088							
OD968.2	basalt	6.84	207.6	51.8	11.832	0.91478							
OD968.3	basalt	7.69	217.7	45.6	14.149	0.95624	40.03	183.86	0.1315	0.512108	-10.2	1188	-0.4
OD968.4	basalt	9.32	155.6	58.4	7.812	0.84526	29.76	126.81	0.1417	0.512179	-8.8	1188	-0.6
OD968.5	basalt	6.10	193.0	43.3	13.166	0.93506							
OD968.6	carbonate vein	28.87	1.4	147	0.027	0.71779	4.89	8.11	0.3646	0.512865	4.5	1188	-21.2

Compositions of carbonate veins were analysed by ICP-MS using a split of the sample (vein) solution. Blank cells represent not measured.

Table 5.2 Major and trace element compositions for the altered Olympic Dam dolerite

Sample No.	SiO_2	TiO_2	Al_2O_3	FeOt	MnO	MgO	CaO	Na_2O	K_2O	P_2O_5	NiO	LOI	Li	Be
OD117	43.1	3.2	14.7	13.3	1.4	9.4	9.5	1.7	2.0	0.3	0.01	15.0	45.2	2.4
OD73	42.7	2.8	15.4	20.6	0.7	4.9	7.8	0.9	1.7	0.3	0.01	9.4	28.9	2.3
OD110	62.6	2.1	10.6	10.4	0.6	6.3	3.9	1.4	0.9	0.2	0.01	8.4	60.6	2.6
OD113	57.7	2.5	13.0	11.0	0.3	5.7	4.9	3.4	0.1	0.3	0.01	7.3	50.6	1.4
OD194	46.1	2.5	14.7	20.0	0.4	7.0	3.2	0.1	3.7	0.2	0.01	6.7	34.8	1.8
OD4	50.0	2.7	14.3	12.5	0.3	9.7	4.9	3.8	0.2	0.2	0.04	6.6	52.7	0.8
OD74	45.7	2.7	14.5	24.0	0.4	7.6	0.6	0.1	1.3	0.3	0.02	6.4	36.3	2.6
OD6	53.5	2.4	13.6	13.0	0.2	7.5	4.7	2.4	0.8	0.2	0.01	6.1	60.3	1.1
OD78	50.6	2.7	13.1	14.6	0.4	6.8	6.0	1.2	2.5	0.3	0.00	5.9	30.5	1.3
OD3-2	50.0	2.7	15.2	12.9	0.2	12.3	1.6	3.0	0.6	0.3	0.02	5.8	76.7	1.0
OD112	57.0	2.7	14.0	13.0	0.2	6.8	1.6	2.7	0.4	0.2	0.01	5.6	67.6	2.1
OD76	48.1	2.5	15.5	18.6	0.3	6.4	1.8	0.1	4.4	0.3	0.02	5.6	30.9	1.8
OD116	52.0	2.9	16.2	14.8	0.1	7.5	1.0	3.4	0.2	0.2	0.01	5.4	72.7	2.0
OD75	48.8	2.9	13.8	21.6	0.3	7.4	0.4	0.1	2.0	0.3	0.00	5.4	40.5	2.9
OD114	59.9	2.6	13.4	11.7	0.1	6.3	1.3	2.9	0.2	0.2	0.02	5.1	75.8	2.0
OD942	49.7	1.8	14.0	14.5	0.3	5.5	10.2	2.1	0.2	0.2	0.04	4.5	39.0	1.9
OD119	43.8	3.1	8.8	28.8	0.3	7.4	2.6	1.1	0.4	0.5	0.01	4.5	34.2	1.2
OD198-2	51.2	2.8	12.3	14.9	0.4	5.7	7.4	1.9	1.6	0.3	0.01	4.1	25.1	1.1
OD120	50.7	2.5	17.1	14.2	0.2	3.8	3.9	4.3	1.4	0.2	0.00	3.2	18.9	1.0
OD198-1	49.6	2.9	13.2	14.7	0.2	6.3	7.5	2.4	1.4	0.3	0.01	3.1	31.3	1.5
OD3-1	53.5	2.4	12.5	19.0	0.1	3.4	3.7	2.5	0.7	0.2	0.01	2.5	25.0	0.9
OD81-1	50.2	2.3	14.0	12.4	0.3	6.0	7.6	3.1	2.6	0.2	0.02	1.6	12.4	0.7
OD83	49.2	2.6	13.0	13.1	0.2	5.8	9.2	3.5	1.5	0.3	0.01	1.3	10.8	1.1

Table 5.2 continued

Sample No.	Sc	Ti	V	Cr	Mn	Ni	Cu	Zn	Ga	As	Rb	Sr	Y
OD117	78.4	15793	382	103	9084	40.3	18	128	18.7	4.5	89.7	51	37.1
OD73	41.2	14964	378	91	4568	50.1	14	143	23.3	5.8	79.1	29	41.4
OD110	34.7	11512	307	79	3969	45.9	22	125	14.8	6.5	41.0	36	24.0
OD113	37.0	13444	285	101	2056	54.3	109	147	16.9	3.5	1.9	64	33.7
OD194	23.0	13797	254	64	2978	47.4	130	165	23.9	2.3	94.7	37	45.4
OD4	43.2	14987	377	106	2067	69.5	12	133	19.7	12.7	6.8	164	34.1
OD74	31.3	15121	340	75	2818	48.9	374	199	23.0	2.9	25.9	25	30.2
OD6	39.8	13454	370	99	1671	59.5	46	204	19.7	11.1	18.3	144	27.8
OD78	41.2	15098	430	78	3109	60.0	281	284	21.9	7.3	105.8	122	38.7
OD3-2	38.9	15040	369	106	1144	99.5	17	269	25.4	6.5	12.5	228	30.0
OD112	28.9	14768	343	112	1381	64.0	16	179	19.3	3.1	20.1	32	28.6
OD76	23.8	13996	259	61	2281	41.3	147	157	24.3	3.4	134.6	34	44.1
OD116	31.1	16390	419	124	634	73.4	72	200	24.2	4.2	5.2	17	30.5
OD75	42.9	16240	450	77	1958	55.3	52	199	23.0	7.9	71.1	11	36.9
OD114	29.9	14260	292	109	727	66.3	38	188	19.7	2.2	6.3	21	33.6
OD942	39.2	8780	372	170	1920	179.5	302	256	20.0	2.7	10.3	201	26.0
OD119	34.7	17064	320	<5	2332	46.2	319	284	20.7	10.4	9.0	86	55.9
OD198-2	38.4	15863	392	45	2709	46.9	148	197	21.2	16.5	68.0	149	38.0
OD120	32.8	13394	334	46	1673	40.3	50	218	24.8	5.5	49.9	222	30.9
OD198-1	41.0	16563	407	59	1232	50.9	223	151	22.2	20.2	45.7	133	43.6
OD3-1	42.3	13758	429	95	564	39.3	203	86	17.7	12.5	16.5	185	29.8
OD81-1	38.5	13746	375	108	1927	62.7	73	94	20.7	2.4	117.1	172	33.6
OD83	38.6	15712	390	72	1661	55.4	136	86	21.7	3.3	62.2	151	40.0

Table 5.2 continued

Sample No.	Zr	Nb	Mo	Sb	Cs	Ba	La	Ce	Pr	Nd	Sm	Eu	Gd
OD117	170	11.6	1.1	0.36	2.75	111	7.3	18.3	2.78	13.5	4.22	1.16	5.43
OD73	177	11.8	0.4	1.41	0.83	145	15.1	33.0	4.32	18.4	5.15	1.20	6.25
OD110	124	8.9	10.3	0.71	1.71	91	9.3	18.4	2.33	9.8	2.73	0.93	3.49
OD113	143	10.0	47.4	0.74	0.22	386	7.4	17.7	2.70	13.1	4.34	1.47	5.52
OD194	206	17.0	0.8	0.53	0.92	400	16.8	34.3	4.20	16.6	4.40	0.98	5.51
OD4	156	10.4	0.6	0.49	1.96	270	10.3	26.1	3.84	18.6	5.28	1.62	6.24
OD74	180	12.4	0.4	1.00	0.40	305	5.4	13.2	1.76	7.9	2.48	0.65	3.46
OD6	143	9.5	0.9	1.31	1.85	469	9.7	22.8	3.30	16.0	4.74	1.72	5.76
OD78	186	12.4	0.9	0.70	4.00	567	21.7	49.5	6.80	31.5	7.70	2.30	8.70
OD3-2	158	10.5	0.4	0.49	2.46	643	16.3	44.8	6.56	30.9	6.86	1.88	6.44
OD112	156	10.8	2.3	0.59	0.91	287	34.3	64.3	8.47	37.2	8.71	2.54	8.13
OD76	237	18.3	0.8	0.70	1.27	478	23.1	46.1	5.40	20.9	5.11	1.14	5.82
OD116	173	12.2	1.4	0.57	0.44	24	4.8	12.9	1.96	9.4	3.13	1.03	4.27
OD75	203	13.9	0.8	1.10	1.70	220	8.7	24.5	3.20	14.2	3.90	0.80	5.00
OD114	152	10.5	1.5	0.46	0.57	71	4.5	11.9	1.82	8.9	3.08	0.99	4.21
OD942	113	7.1	1.1	0.35	1.00	72	9.5	23.2	3.37	15.2	4.14	1.53	4.80
OD119	284	20.2	147.8	0.87	0.68	65	20.1	49.6	7.13	33.0	8.77	2.13	10.10
OD198-2	187	13.0	0.6	0.35	2.10	374	18.5	37.3	5.04	23.3	6.26	1.68	7.09
OD120	169	10.7	2.2	0.10	0.30	253	20.0	45.5	6.00	27.7	6.70	2.20	7.30
OD198-1	195	13.5	1.0	0.55	2.34	263	14.4	37.7	5.64	26.5	7.33	2.60	8.30
OD3-1	147	9.7	1.2	0.86	0.89	395	16.1	37.2	5.26	24.3	6.52	2.40	7.36
OD81-1	156	10.5	0.5	0.27	0.52	478	14.5	34.1	4.74	21.4	5.74	1.78	6.37
OD83	186	12.6	0.7	0.52	0.64	217	18.1	42.4	6.03	26.9	7.11	2.03	7.77

Table 5.2 continued

Sample No.	Tb	Dy	Ho	Er	Tm	Yb	Lu	Hf	Ta	Tl	Pb	Th	U
OD117	1.05	6.72	1.42	4.19	0.62	3.93	0.59	4.74	0.36	0.23	8.6	2.16	2.18
OD73	1.28	8.04	1.67	4.90	0.71	4.42	0.65	4.80	0.75	0.17	7.2	2.04	1.14
OD110	0.73	4.86	1.04	3.00	0.42	2.51	0.36	3.45	0.40	0.13	7.6	2.34	2.89
OD113	1.00	6.05	1.24	3.52	0.52	3.26	0.49	4.03	0.43	0.22	17.0	2.03	1.69
OD194	1.11	7.27	1.64	5.34	0.88	6.11	0.97	5.64	0.42	0.29	4.1	8.78	5.61
OD4	1.09	6.59	1.33	3.80	0.54	3.41	0.50	4.28	0.56	0.03	17.2	1.88	0.40
OD74	0.75	5.08	1.19	4.14	0.72	5.23	0.86	4.82	0.73	0.11	10.9	2.27	4.86
OD6	0.98	5.74	1.12	3.18	0.45	2.77	0.41	3.99	0.46	0.09	17.8	1.74	0.52
OD78	1.50	8.00	1.60	4.10	0.60	3.60	0.50	4.90	1.20	0.60	13.5	2.40	0.70
OD3-2	0.95	5.62	1.15	3.43	0.50	3.17	0.49	4.42	0.64	0.05	10.0	1.79	0.36
OD112	1.06	5.49	1.07	3.08	0.46	2.86	0.42	4.35	0.61	0.05	8.7	2.02	1.60
OD76	1.13	7.30	1.59	5.23	0.88	5.97	0.94	6.38	1.27	0.37	4.9	17.30	8.25
OD116	0.84	5.35	1.16	3.40	0.51	3.19	0.47	4.83	0.80	0.03	5.8	2.25	10.84
OD75	1.10	6.80	1.60	4.90	0.90	5.80	0.90	5.40	1.10	0.30	9.6	3.20	4.70
OD114	0.86	5.73	1.25	3.75	0.56	3.46	0.52	4.23	0.58	0.04	4.2	1.81	3.52
OD942	0.74	4.63	0.97	2.67	0.38	2.58	0.39	3.00	0.60	0.04	14.6	1.40	0.36
OD119	1.79	10.81	2.19	6.32	0.93	5.91	0.90	7.88	1.15	0.07	13.8	4.80	14.79
OD198-2	1.22	7.22	1.44	4.04	0.58	3.56	0.53	5.20	0.67	0.31	200.9	2.25	0.49
OD120	1.10	6.60	1.30	3.50	0.50	3.20	0.50	4.60	1.20	0.20	2.6	2.60	0.60
OD198-1	1.43	8.23	1.63	4.55	0.65	3.95	0.58	5.41	0.80	0.18	22.5	2.33	0.54
OD3-1	1.25	7.22	1.33	3.49	0.45	2.62	0.37	4.09	0.51	0.07	18.8	1.82	0.46
OD81-1	1.09	6.40	1.25	3.53	0.50	3.02	0.44	4.13	0.75	0.32	4.3	1.91	0.71
OD83	1.32	7.65	1.51	4.23	0.60	3.66	0.54	5.02	0.96	0.21	5.4	2.25	1.02

Major element (oxides) compositions are LOI-free, in wt.%, trace element in ppm. LOI-Loss On Ignition.

Chapter 6 Summary and conclusions

6.1 Olivine-phyric basalt at Olympic Dam: implications for the petrogenesis and tectonic circumstance of the ca. 1590 Ma Gawler SLIP

6.1.1 Olivine-phyric basalts and dykes in the Gawler SLIP

Mafic lithologies are only a minor (less than 10 vol.%) component to the Gawler Range Volcanics (GRV) and the Gawler silicic large igneous province (SLIP). Mafic GRV are known/inferred to occur at Lake Everard (Nuckulla Basalt in the Glyde Hill Volcanic Complex), Kokatha, Tarcoola-Kingoonya (Konkaby Basalt) (Blissett et al., 1993), Roopena (Blissett et al., 1993), the Mount Gunson copper deposit (Knutson et al., 1992), the Olympic Dam Cu-U-Au-Ag deposit (Reeve et al., 1990; Johnson, 1993), and the Wirrda Well Cu-Au prospect (Ehrig, 2013).

Among all these places, potential olivine-bearing mafic GRV have been discovered in the latter four localities. The Laser Ablation Inductively Coupled Plasma Mass Spectrometry (LA-ICPMS) U-Pb dating of apatite (Chew et al., 2011, 2014) in these rocks yields ages that can be correlated with the U-Pb zircon ages of felsic GRV (from ca. 1570 to 1595 Ma, with apparent peaks at ca. 1580 Ma and 1590 Ma, Hand et al., 2007; and references therein) and therefore confirm the correlations of these olivine-bearing rocks with the GRV and the Gawler SLIP.

The olivine-phyric mafic GRV share comparable petrographic features. They all display porphyritic textures; pseudomorphed former olivine was the dominant phenocryst phase. The volume percentage of former olivine phenocrysts varies from less than 5 vol.% to more than 20 vol.%. Clinopyroxene and phlogopite typically occur as micro-phenocrysts in the groundmass. Apatite and magnetite are present as accessory phases in the olivine-phyric basalts and dykes. Quartz crystals with embayed rims are common in these rocks and are interpreted to be xenocrysts derived from granitoids.

Compared to the olivine-phyric basalts and dykes at Kokatha, Mount Gunson and Wirrda Well, the olivine-phyric rocks at Olympic Dam can be distinguished in the

following aspects: 1) Both flat-lying basalt unit and dykes at Olympic Dam commonly contain higher abundance (~20 vol.%) of former olivine phenocrysts. This implies that these rocks were likely to be derived from magmas of more primitive compositions and higher temperatures; 2) These olivine-phyric rocks also contain a noticeable amount of xenoliths. Xenoliths are mainly made up of fine-grained quartz, chlorite, sericite and hematite, and intense alteration has obscured the nature of the protoliths; 3) the olivine-phyric rocks at Olympic Dam have been commonly deformed and intensely altered. This is shown by the common occurrence of elongate (flattened and stretched) former olivine phenocrysts and fragmented Cr-spinel inclusions. The high abundance of olivine pseudomorphs (up to 30 vol.%) in some samples may be a result of the combined effect of hydrothermal alteration and deformation. The preliminary estimate of the original composition of the undeformed flat-lying olivine-phyric basalt at Olympic Dam yields a whole-rock MgO content of ~16.5 wt.%, and thus this unit has been considered to have the highest affinity for primitive ultramafic magmas.

6.1.2 Tectonic implications from Cr-spinel and whole-rock compositions

There are a number of tectonic interpretations for the ca. 1590 Ma Gawler SLIP, ranging from intraplate (Giles, 1988), to continental margin (Wade et al., 2006; Hand et al., 2008; Betts et al., 2009), and back-arc setting (Skirrow, 2010). Cr-spinel contained within primitive olivine phenocrysts (high Forsterite number, Fo) tends to record some characteristics of the primary melts. Moreover, previous studies have demonstrated that magmatic Al_2O_3 and TiO_2 exert control on the Al_2O_3 and TiO_2 contents of corresponding Cr-spinel, allowing Cr-spinel to be used as a tectonic indicator, in particular for Phanerozoic magmas (Arai, 1992; Barnes and Roeder, 2001; Kamenetsky et al., 2001).

Cr-spinel enclosed in the inferred most primitive former olivine phenocrysts (Fo number above 85, all from Olympic Dam) plot uniformly within the arc-basalt (ARC) and back-arc basin basalt (BABB) fields in the Cr-spinel tectonic indicator diagram (Fig. 4.7). Therefore, it is highly likely that the mantle source for the GRV and the Gawler SLIP had been largely modified by subduction processes prior to its partial melting. This inference is also supported by the whole-rock compositions of the olivine-

phyric basalts at Kokatha and Mount Gunson that have a lower grade of hydrothermal alteration. They have indistinguishable trace element compositions characterised by negative Nb and Ta anomalies (Fig. 4.9) which are typical of arc basalts (Perfit et al., 1980; McCulloch and Gamble, 1991), and are also common in back-arc basin basalts (Saunders and Tarney, 1984; Taylor and Martinez, 2003). Therefore, we conclude that the Gawler SLIP was likely to be situated close to a continental margin or in a back-arc setting.

A number of tectonic reconstructions have pointed to Australia-East Antarctica as the conjugate landmass of western Laurentian supercontinent (Dalziel, 1991; Ross et al., 1992; Borg and DePaolo, 1994). The tectonic setting of the Gawler SLIP inferred from this study is compatible with these tectonic reconstructions and in agreement with the proposal that the formation of the Gawler SLIP was associated with the assembly of the Laurentian supercontinent (Blissett et al., 1993; Creaser, 1995; Allen and McPhie, 2002; Payne et al., 2009).

6.1.3 Petrogenesis of the Gawler SLIP

Regarding the formation of the Gawler SLIP, coeval melting of the separate mantle and crustal sources to produce mafic and silicic magmas, with limited contamination and/or mixing, is thus far the most acceptable interpretation (Giles, 1988; Stewart, 1994; Agangi, 2011).

The recognition of high-Mg primitive (high Fo number)-olivine-phyric basalt at Olympic Dam agrees with the proposal that magma from a mantle source contributed to the Gawler SLIP. The basalt at Olympic Dam was likely to be derived from ultramafic magmas of primitive composition and high temperature. Such primitive magmas are believed to have the potential to provide high heat flux into the crust and to induce large-scale partial melting of the crust. The occurrence of quartz xenocrysts and xenoliths (in particular in the flat-lying olivine-phyric basalt) lends further support for heating and partial melting of continental crust by mafic to ultramafic magmas.

Besides, as previously pointed out in Bryan et al. (2010), the main controlling factor in the generation of large igneous province volumes of rhyolite, rather than basalt, is crustal setting. All Phanerozoic examples of SLIP have formed along long-lived

plaeo- and active continental margins characterised by a relatively young fertile, hydrous lower crust. For example, basement to the Whitsunday Volcanic and Chon Aike provinces, and in large part the Sierra Madre Occidental, comprises Paleozoic-Mesozoic igneous and sedimentary rocks accreted and/or deposited along the continental margin. These crustal materials have been generated by subduction up to one hundred million years prior to the emplacement of the Silicic LIP (Bryan, 2007).

As mentioned above, compositions of Cr-spinel and whole-rock indicate that the Mesoproterozoic Gawler SLIP was also situated proximally to a continental margin, suggesting that SLIP (no matter in the Proterozoic or the Phanerozoic) may share similar tectonic settings sited along paleo- and active continental margins, where past and/or ongoing subduction have prepared appropriate hydrous lower crust for anatexis facilitated by heat transferred from underplating mantle-derived mafic to ultramafic magmas.

6.2 Neoproterozoic Gairdner Dykes at Olympic Dam: links with the ca. 820 Ma Gairdner LIP

6.2.1 Occurrence of the Gairdner Dykes at Olympic Dam

The basaltic to doleritic dykes (named the Olympic Dam dolerite) are characterised by its fresher appearance and better competency, as well as higher magnetic susceptibility, compared to other mafic facies (i.e. ca. 1590 Ma mafic GRV) at Olympic Dam. These dykes show a wide range of width, from one centimetre to more than one hundred metres, and can be traced along a NW strike for up to 3 km. Many dykes comprise multiple generations. The common scenario is that early porphyritic to doleritic dykes were intruded by later porphyritic dykes. Though the Olympic Dam dolerite is invariably altered, primary textures and minerals have been preserved in a number of drill core intersections. In the porphyritic dykes, the groundmass has a wide range of textures from former glassy, cryptocrystalline, microcrystalline to fine-grained. Olivine rarely occurs as phenocrysts and has been replaced by secondary minerals (i.e. chlorite and quartz). Clinopyroxene and plagioclase are the dominant phenocryst phases, and minor Ti-magnetite is present as microphenocrysts. Clinopyroxene, plagioclase, minor Ti-magnetite and accessory apatite comprise the doleritic dykes. The

Olympic Dam dolerite shows similar petrographic features to the Gairdner Dykes in the Gawler Craton, except that some accessory phases such as zircon and baddeleyite that are present in the Gairdner Dykes (Cowley and Flint, 1993) have not been observed in the Olympic Dam dolerite.

In this study, LA-ICPMS U-Pb dating of accessory apatite recovered from a medium-grained Olympic Dam dolerite yielded a result of 825 ± 18 Ma, within the error of the baddeleyite U-Pb age of 827 ± 6 Ma for the Gairdner Dyke Swarm in the Gawler Craton (Wingate et al., 1998).

The Olympic Dam dolerite is invariably altered. However, if the alteration-sensitive elements are ignored, the Olympic Dam dolerite shows comparable compositional features to the Gairdner Dykes. There are significant overlaps among the major element compositions between the Olympic Dam dolerite and the Gairdner Dykes. Regarding trace element geochemistry, the Olympic Dam dolerite shows the same collinear trends among a significant number of elements including rare earth elements (REE) and high field strength elements (HFSE) to those of the Gairdner Dykes. Besides, εNd_{825Ma} values of the Olympic Dam dolerite (-0.2 to +5.7) also overlap with those reported for the Gairdner Dykes (+4.2 to +4.5) elsewhere (Zhao and McCulloch, 1993).

Therefore, petrographical, geochronological and geochemical similarities between the Olympic Dam dolerite and the Gairdner Dykes allow us to confirm that the Olympic Dam dolerite belongs to the Gairdner Dyke Swarm, extending the spatial distribution and the compositional spectrum of the latter.

6.2.2 Compositions of mafic magmas in large igneous provinces associated with the supercontinent Rodinia

The Gairdner Dyke Swarm was first recognised on aeromagnetic images as a NW-trending array of linear magnetic anomalies in South Australia (Boyd in Goode, 1970). Field observations, and geochronological and geochemical investigations of a number of other volcanic units including the Amata Dyke Swarm in the Musgrave Block, Wooltana Volcanics and Beda Volcanics in the Adelaide Geosyncline, dykes and sills in the Paterson Range of Western Australia led to the proposal that all these units

constitute the Gairdner LIP (Crawford and Hilyard, 1990; Claoué-Long and Hoatson 2009).

The ca. 820 Ma Gairdner LIP spatially overlaps with the ca. 1070 Ma Warakurna LIP in Australia. These two LIP were contemporaneous with the assembly (Warakurna LIP) and break-up (Gairdner LIP) of the supercontinent Rodinia (Li et al., 2008; Pirajno and Hoatson,2012). Moreover, the Gairdner LIP in South Australia, the Guibei and Kangding LIP in South China, and the Gunbarrel mafic suite in North America are among the LIP and suites which have been widely studied for their tectonic implications for the break-up of the supercontinent Rodinia (e.g. Ling et al.,2003; Wang et al., 2010; Sandeman et al., 2014).

A geochemical comparison between the Warakurna LIP and the Gairdner LIP has revealed that the former is characterised by more fertile compositions (i.e. higher HSFE concentrations at a given TiO_2 content) and also a higher degree of light REE to heavy REE fractionation. This provides a geochemical background for future classification of igneous units (age undetermined) present in the localities where the two LIP overlap. On the contrary, mafic LIP in South China and South Australia and the Gunbarrel mafic suite in North America show comparable geochemical trends. It is important to note that the mafic LIP in South China, as indicated by their generally low incompatible element concentrations, are compositionally more primitive than the Gairdner LIP in South Australia and the Gunbarrel mafic suite in North America. This observation agrees with the tectonic reconstruction of Rodinia in the "missing-link" model (Li et al., 1995, 1999, 2008) which places South China on a mantle plume head between Australia-East Antarctica and Laurentia (Fig. 3.8a). South Australia may have been situated away from this mantle plume head and/or located above another mantle plume of smaller scale at ca. 820 Ma. Whichever is true, the important implication is that South Australia (including Olympic Dam) was impacted by rift magmatism and subsequent extension was likely to be responsible for the formation of the large sedimentary basins, including the Officer Basin, Stuart Shelf and Adelaide Geosyncline, in central-southern Australia (Zhao et al., 1994; Walter et al., 1995; Barovich and Foden, 2000).

6.3 Occurrence and hydrothermal alteration of the two generations of mafic rocks at Olympic Dam: implications for the tectonic evolution and ore-forming processes

6.3.1 Tectonic evolution of the Olympic Dam deposit: links with supercontinent cycles

This study has confirmed the occurrence of two generations of time-punctuated mafic lithologies at the Olympic Dam iron oxide Cu-U-Au-Ag deposit. The first generation comprises olivine-phyric basalt and other mafic dykes of various textures, and has been correlated with the ca. 1590 Ma GRV and the Gawler SLIP. The second generation is mainly composed of porphyritic to doleritic mafic dykes that belong to the ca. 820 Ma Gairdner Dyke Swarm and the Gairdner LIP. There have been previously established tectonic interpretations on the Gawler SLIP and the Gairdner LIP. Correlating the two generations of mafic lithologies present at Olympic Dam to the two LIP allows us to apply the tectonic circumstances of the latter to the Olympic Dam deposit in the corresponding geological period (i.e. ca. 1590 Ma and 820 Ma), to better evaluate the pre-exiting tectonic interpretations with new analyses produced in this study, and to constrain the tectonic evolution of the deposit.

Compositions of Cr-spinel and whole-rock samples of the olivine-phyric GRV imply that the Gawler SLIP formed in a setting proximally to a continental margin or in a back-arc, likely to be associated with the assembly of the Laurentian supercontinent. Considering that components of the Gawler SLIP (i.e. the Hiltaba Suite Granite and GRV) are also the dominant lithologies present at Olympic Dam and the most significant contributors to the ODBC, it is likely that the Olympic Dam deposit was also situated proximally to a continental margin or in a back-arc setting at ca.1590 Ma.

The ca. 820 Ma Gairdner Dyke Swarm and the Gairdner LIP were likely to be products of rift magmatism associated with the break-up of the supercontinent Rodinia (Li et al., 2008). The occurrence of the Gairdner Dykes at Olympic Dam revealed in this study demonstrates that this locality was situated on an active rift at ca. 820 Ma when the dykes were emplaced.

Therefore, from the perspective of mafic magmatism, the evolution of the Olympic Dam deposit can be linked to two supercontinent cycles: the assembly of Laurentian at ca. 1590 Ma and the break-up of Rodinia at ca. 820 Ma.

6.3.2 Multiple sources of copper?

The ca. 1590 Ma mafic GRV were proposed to have been a major source of the copper (~50% of the contained Cu) found in the Olympic Dam deposit (Johnson et al., 1993; Johnson and McCulloch, 1995). Petrographically, they are more intensely altered than the younger ca. 820 Ma Gairdner Dykes present at the same deposit. Major element compositions of the flat-lying olivine-phyric basalt reported in this study have been so intensely modified by hydrothermal fluids that now they reflect the abundance of various secondary minerals rather than primary geochemical features. Collinear variations between TiO_2 and Al_2O_3, K_2O, Cr, Nb, Ta, Zr, Hf, and Th, along with the extreme concentrations of some trace elements (e.g. up to ~6,000 ppm Cr, ~280 ppm Nb, ~370 ppm Zr), indicate that these trace elements remained in the rocks in the course of the most recent hydrothermal alteration during which significant mass and/or volume loss occurred. This agrees with their previously proposed role as a major copper contributor to the deposit.

The younger ca. 820 Ma Gairdner Dykes at Olympic Dam are invariably altered, though not as intensely as the mafic GRV. Geochemical comparisons between the (petrographically) more altered ca. 820 Ma Gairdner Dykes and the least-altered equivalents reveal that a number of elements have been added or removed as a consequence of alteration. Generally elevated Zn and Pb but depleted Cu concentrations in a number of Gairdner Dykes suggest that these dykes can be a potential subordinate Cu source to the Olympic Dam deposit.

This inference is also supported by evidence from petrographical observation and drill core assays. Tiny veinlets cutting cross the Gairdner Dykes at Olympic Dam contain magnetite with chalcopyrite inclusions. A previous study (Apukhtina et al., 2016) on the same kind of veinlets has shown than Fe along with other components such as Ca, P and Si of the veinlets was locally sourced from the dykes. This implies that Cu may be derived from the same local source. Pb isotope analyses on the chalcopyrite and galena within the dolerite also agree with this inference. Intersections

of drill hole RD271 show an example of one Gairdner Dyke intruding the ODBC, and the isocon analysis of the dyke shows that Cu was leached out from the dyke interval in immediate contact with the ODBC.

The total amount of copper derived from the ca. 820 Ma Gairdner Dykes was likely to be insignificant. However, we can probably envisage similar copper depletion processes in the ca. 1590 Ma mafic GRV to those in the Gairdner Dykes, though the intensely altered characteristic of the older rocks has hampered detailed investigations of such processes.

6.3.3 A multi-stage hydrothermal system at Olympic Dam？

Geochronological investigations of the ODBC on different minerals using different methods have yielded a wide range of results, with a number of apparent peaks: ca. 1590 Ma, ca. 1400 Ma, ca. 1200 Ma, ca. 820 Ma, and ca. 570 Ma (Trueman et al., 1986; Johnson, 1993; McInnes et al., 2008; Meffre et al., 2010; Maas et al., 2011; Ciobanu et al., 2013).

Spongy secondary apatite in the ca. 1590 Ma olivine-phyric basalt yielded ages coeval with the emplacement of the basalt. The Rb-Sr dating result obtained on the sericite-altered olivine-phyric basalt in this study suggests that the last hydrothermal activity that brought widespread sericite alteration to the ca. 1590 Ma olivine-phyric basalt probably occurred at ca. 1180 Ma. U-Pb dating of secondary apatite and titanite in hydrothermal veinlets in the Gairdner Dyke samples yielded broadly similar results to the age of the Gairdner Dykes. This confirms that there were hydrothermal activities accompanied with and/or shortly after the emplacement of these dykes at ca. 820 Ma.

With all ages taken into account, an ensuing implication is that the ore-forming process at OD might have accommodated multiple sources (at least two generations of mafic rocks as potent/potential copper sources) and a multi-stage hydrothermal system (e.g., 1590 Ma, 1180 Ma, and 820 Ma). The Olympic Dam deposit is a ‘flagship’ of the iron-oxide copper gold (IOCG) type deposit. Unlike other magmatic-hydrothermal and hydrothermal deposits (e.g. porphyry copper deposits, low and high sulfidation epithermal deposits, and volcanic massive sulfide deposits) which have comparable number of young (or modern) and old counterparts (or more young deposits than old

equivalents), the sensu stricto IOCG deposit comprises dominantly Precambrian deposits (Groves et al., 2010). This implies that either that the formation of sensu stricto IOCG type deposit did not follow the commonly applied uniformitarianism or that it took a long time (at least ca. 500 million years) for typical sensu stricto IOCG type mineralisation to become economic. If the latter is true, multiple activities and/or sources accommodated in one sensu stricto IOCG type deposit are not unexpected, as recorded in the mafic rocks as well as other lithologies at the Olympic Dam IOCG deposit.

References

Agangi, A., 2011. Magmatic and volcanic evolution of a silicic large igneous province (SLIP): the Gawler Range Volcanics and Hiltaba Suite, South Australia. University of Tasmania, unpublished PhD theis.

Agangi, A., Kamenetsky, V.S., McPhie, J., 2012. Evolution and emplacement of high fluorine rhyolites in the Mesoproterozoic Gawler silicic large igneous province, South Australia. Precambrian Research 208–211, 124-144.

Allen, C.M., Campbell, I.H., 2012. Identification and elimination of a matrix-induced systematic error in LA–ICP–MS $^{206}Pb/^{238}U$ dating of zircon. Chemical Geology 332–333, 157-165.

Allen, S.R., McPhie, J., 2002. The Eucarro Rhyolite, Gawler Range Volcanics, South Australia: A >675 km^3, compositionally zoned lava of Mesoproterozoic age. Geological Society of America Bulletin 114, 1592-1609.

Allen, S.R., McPhie, J., Ferris, G., Simpson, C., 2008. Evolution and architecture of a large felsic Igneous Province in western Laurentia: The 1.6 Ga Gawler Range Volcanics, South Australia. Journal of Volcanology and Geothermal Research 172, 132-147.

Allen, S.R., Simpson, C.J., McPhie, J., Daly, S.J., 2003. Stratigraphy, distribution and geochemistry of widespread felsic volcanic units in the Mesoproterozoic Gawler Range Volcanics, South Australia. Australian Journal of Earth Sciences 50, 97-112.

Amelin, Y., Zaitsev, A.N., 2002. Precise geochronology of phoscorites and carbonatites:: The critical role of U-series disequilibrium in age interpretations. Geochimica Et Cosmochimica Acta 66, 2399-2419.

Apukhtina, O.B., Kamenetsky, V.S., Ehrig, K., Kamenetsky, M.B., McPhie, J., Maas, R., Meffre, S., Goemann, K., Rodemann, T., Cook, N.J., Ciobanu, C.L., 2016. Postmagmatic magnetite–apatite assemblage in mafic intrusions: a case study of dolerite at Olympic Dam, South Australia. Contributions to Mineralogy and Petrology 171, 1-15.

Arai, S., 1992. Chemistry of chromian spinel in volcanic rocks as a potential guide to magma chemistry. Mineralogical Magazine 56, 173-184.

Armstrong, J., 1988. Quantitative analysis of silicate and oxide minerals: comparison of Monte Carlo, ZAF and phi-rho-z procedures. Microbeam analysis 23, 239-246.

Baker, J., Peate, D., Waight, T., Meyzen, C., 2004. Pb isotopic analysis of standards and samples using a ^{207}Pb–^{204}Pb double spike and thallium to correct for mass bias with a double-focusing MC-ICP-MS. Chemical Geology 211, 275-303.

Barfod, G.H., Krogstad, E.J., Frei, R., Albarède, F., 2005. Lu-Hf and PbSL geochronology of apatites from Proterozoic terranes: A first look at Lu-Hf isotopic closure in metamorphic apatite. Geochimica Et Cosmochimica Acta 69, 1847-1859.

Barnes, S.J., Roeder, P.L., 2001. The range of spinel compositions in terrestrial mafic and ultramafic rocks. Journal of Petrology 42, 2279-2302.

Barovich, K., Foden, J., 2000. A Neoproterozoic flood basalt province in southern-central Australia: geochemical and Nd isotope evidence from basin fill. Precambrian Research 100, 213-234.

Bastrakov, E.N., Skirrow, R.G., Didson, G.J., 2007. Fluid evolution and origins of iron oxide Cu-Au prospects in the Olympic Dam district, Gawler Craton, south Australia. Economic Geology 102, 1415-1440.

Belousova, E.A., Reid, A.J., Griffin, W.L., O'Reilly, S.Y., 2009. Rejuvenation vs. recycling of Archean crust in the Gawler Craton, South Australia: Evidence from U-Pb and Hf isotopes in detrital zircon. Lithos 113, 570-582.
Belperio, A., Flint, R., Freeman, H., 2007. Prominent Hill: A hematite-dominated, iron oxide copper-gold system. Economic Geology 102, 1499-1510.
Best, F.C., 2012. The Petrogenesis and Ni-Cu-PGE Potential of the Dido Batholith, North Queensland, Australia. University of Tasmania. Unpublished Ph.D thesis. 291 pp.
Betts, P.G., Giles, D., Foden, J., Schaefer, B.F., Mark, G., Pankhurst, M.J., Forbes, C.J., Williams, H.A., Chalmers, N.C., Hills, Q., 2009. Mesoproterozoic plume-modified orogenesis in eastern Precambrian Australia. Tectonics 28.
Black, L.P., Kamo, S.L., Allen, C.M., Davis, D.W., Aleinikoff, J.N., Valley, J.W., Mundil, R., Campbell, I.H., Korsch, R.J., Williams, I.S., Foudoulis, C., 2004. Improved $^{206}Pb/^{238}U$ microprobe geochronology by the monitoring of a trace-element-related matrix effect; SHRIMP, ID–TIMS, ELA–ICP–MS and oxygen isotope documentation for a series of zircon standards. Chemical Geology 205, 115-140.
Blissett, A.H., Creaser, R.A., Daly, S.J., Flint, R.B., Parker, A.J., 1993. Gawler Range Volcanics, in: Drexel, J.F., Preiss, W.V., Parker A.J. (Eds.), The Geology of South Australia. Vol. 1, The Precambrian, Geological Survey of South Australia, pp. 107-131.
Borg, S.G., DePaolo, D.J., 1994. Laurentia, Australia, and Antarctica as a Late Proterozoic supercontinent: Constraints from isotopic mapping. Geology 22, 307-310.
Bouvier, A., Vervoort, J.D., Patchett, P.J., 2008. The Lu–Hf and Sm–Nd isotopic composition of CHUR: Constraints from unequilibrated chondrites and implications for the bulk composition of terrestrial planets. Earth and Planetary Science Letters 273, 48-57.
Bradbury, J., 1988. The volcanic and shallow sub-volcanic component of the breccia hosted Olympic Dam U-Cu-Au deposit: Implications for breccia pipe development, Department of Earth Sciences. Monash University, B. Sc. (hons), unpublished.
Branch, C.D., 1978. Evolution of the middle Proterozoic Chandabooka Caldera, Gawler range acid volcano - plutonic province, South Australia. Journal of the Geological Society of Australia 25, 199-218.
Bryan, S.E., Ernst, R.E., 2008. Revised definition of Large Igneous Provinces (LIPs). Earth-Science Reviews 86, 175-202.
Bryan, S.E., Ferrari, L., 2013. Large igneous provinces and silicic large igneous provinces: Progress in our understanding over the last 25 years. Geological Society of America Bulletin.
Bryan, S.E., Riley, T.R., Jerram, D.A., Stephens, C.J., Leat, P.T., 2002. Silicic volcanism: an undervalued component of large igneous provinces and volcanic rifted margins. SPECIAL PAPERS-GEOLOGICAL SOCIETY OF AMERICA, 97-118.
Chernyshev, I.V., Chugaev, A.V., Shatagin, K.N., 2007. High-precision Pb isotope analysis by multicollector-ICP-mass-spectrometry using $^{205}Tl/^{203}Tl$ normalization: Optimization and calibration of the method for the studies of Pb isotope variations. Geochemistry International 45, 1065-1076.
Chew, D.M., Petrus, J.A., Kamber, B.S., 2014. U–Pb LA–ICPMS dating using accessory mineral standards with variable common Pb. Chemical Geology 363, 185-199.
Chew, D.M., Sylvester, P.J., Tubrett, M.N., 2011. U–Pb and Th–Pb dating of apatite by LA-ICPMS. Chemical Geology 280, 200-216.

Ciobanu, C.L., Wade, B.P., Cook, N.J., Schmidt Mumm, A., Giles, D., 2013. Uranium-bearing hematite from the Olympic Dam Cu–U–Au deposit, South Australia: A geochemical tracer and reconnaissance Pb–Pb geochronometer. Precambrian Research 238, 129-147.
Claoué-Long, J.C., Hoatson, D.M., 2009. Proterozoic Large Igneous Provinces: Map Sheets 1 and 2, Geoscience Australia, Canberra.
Claoue-Long, J.C., Hoatson, D.M., 2009. Guide to using the Map of Australian Proterozoic Large Igneous Provinces. Record 2009/044, Geoscience Australia, Canberra.
Coelho, J., 2006. GEOISO—a Windows™ program to calculate and plot mass balances and volume changes occurring in a wide variety of geologic processes. Computers & geosciences 32, 1523-1528.
Coffin, M.F., Eldholm, O., 1994. Large igneous provinces: Crustal structure, dimensions, and external consequences. Reviews of Geophysics 32, 1-36.
Compston, W., Crawford, A.R., Bofinger, V.M., 1966. A radiometric estimate of the duration of sedimentation in the Adelaide geosyncline, South Australia. Journal of the Geological Society of Australia 13, 229-276.
Cowley, W., Conor, C., Zang, W., 2003. New and revised Proterozoic stratigraphic units on northern Yorke Peninsula. MESA Journal 29, 46-58.
Cowley, W.M., 1993. Pandurra Formation, in: Drexel, J.F., Preiss, W.V., Parker, J.K. (Eds.), The Geology of South Australia. Vol. 1, The Precambrian, Geological Survey of South Australia.
Cowley, W.M., Flint, R.B., 1993. Epicratonic igneous rocks and sediments, in: Drexel, J.F., Preiss, W.V., Parker, J.K. (Eds.), The Geology of South Australia. Vol. 1, The Precambrian, Geological Survey of South Australia.
Crawford, A.J., Hilyard, D., 1990. Geochemistry of late Proterozoic tholeiitic flood basalts, Adelaide Geosyncline, South Australia. In: Jago, J.B., Moore, P.S. (Eds.), The evolution of a Late Precambrian-Early Palaeozoic rift complex: The Adelaide Geosyncline. Geological Society of Australia Special Publication 16, 49-67.
Creaser, R.A., 1989. The geology and petrology of Middle Proterozoic felsic magmatism of the Stuart Shelf, South Australia. La Trobe University. Unpublished Ph.D thesis. 434 pp.
Creaser, R.A., 1995. Neodymium isotopic constraints for the origin of Mesoproterozoic felsic magmatism, Gawler Craton, South Australia. Canadian Journal of Earth Sciences 32, 460-471.
Creaser, R.A., Cooper, J.A., 1993. U-Pb Geochronology of Middle Proterozoic Felsic Magmatism Surrounding the Olympic Dam Cu-U-Au-Ag and Moonta Cu-Au-Ag Deposits, South Australia. Economic Geology and the Bulletin of the Society of Economic Geologists 88, 186-197.
Cross, K., 1993. Acropolis and Wirrda Well prospects. The Geology of South Australia 1, 138.
Daly, S.J., Fanning, C.M., Fairclough, M.C., 1998. Tectonic evolution and exploration potential of the Gawler Craton, South Australia. AGSO Journal of Australia Geology and Geophysics 17, 145-168.
Dalziel, I.W.D., 1991. Pacific margins of Laurentia and East Antarctica-Australia as a conjugate rift pair: Evidence and implications for an Eocambrian supercontinent. Geology 19, 598-601.
Danyushevsky, L., Robinson, P., Gilbert, S., Norman, M., Large, R., McGoldrick, P., Shelley, M., 2011. Routine quantitative multi-element analysis of sulphide minerals by

laser ablation ICP-MS: Standard development and consideration of matrix effects. Geochemistry: Exploration, Environment, Analysis 11, 51-60.
Danyushevsky, L., Robinson, P., McGoldrick, P., Large, R., Gilbert, S., 2003. LA-ICPMS of sulphides: evaluation of an XRF glass disc standard for analysis of different sulphide matrixes. Geochimica et Cosmochimica Acta Supplement 67, 73.
Direen, N.G., Cadd, A.G., Lyons, P., Teasdale, J.P., 2005. Architecture of Proterozoic shear zones in the Christie Domain, western Gawler Craton, Australia: Geophysical appraisal of a poorly exposed orogenic terrane. Precambrian Research 142, 28-44.
Direen, N.G., Lyons, P., 2007. Regional crustal setting of iron oxide Cu-Au mineral systems of the Olympic Dam region, south Australia: Insights from potential-field modeling. Economic Geology 102, 1397-1414.
DMITRE Resources and Energy Group, G.o.S.A., 2014. South Australian Resources Information Geoserver, https://sarig.pir.sa.gov.au/Map.
Drexel, J.F., Preiss, W.V., Parker, A.J., 1993. The geology of South Australia,Volumue 1, The Precambrian, Bulletin 54.
Dutch, R., Hand, M., Kinny, P.D., 2008. High-grade Paleoproterozoic reworking in the southeastern Gawler Craton, South Australia. Australian Journal of Earth Sciences 55, 1063-1081.
Ehrig, K., 2013. Geology of the Wirrda Well IOCG Deposit, 10th Annual SA Exploration and Mining Conference.
Ehrig, K., McPhie, J., Kamenetsky, V., 2012. Geology and mineralogical zonation of the Olympic Dam iron oxide Cu-U-Au-Ag Deposit, South Australia, in: Hedenquist, J.W., Harris, M., Camus, F. (Eds.), Economic Geology Special Publication 16, pp. 237-267.
Ernst, R.E., 2014. Large Igneous Provinces (LIPs). Cambridge University Press, Cambridge, UK.
Ernst, R.E., Buchan, K.L., 1997. Giant Radiating Dyke Swarms: Their Use in Identifying Pre-Mesozoic Large Igneous Provinces and Mantle Plumes, Large Igneous Provinces: Continental, Oceanic, and Planetary Flood Volcanism. American Geophysical Union, pp. 297-333.
Ernst, R.E., Buchan, K.L., Campbell, I.H., 2005. Frontiers in large igneous province research. Lithos 79, 271-297.
Fairclough, M.C., Schwarz, M.P., Ferris, G.M., Daly, S.J., Cowley, W.M., Zang, W., Davies, M.B., Direen, N.G., Lyons, P., Skirrow, R.G., Hoatson, D.M., Raymond, O.R., Fraser, G., Neumann, N., Whitaker, A.J., Lane, R.J.L., Betts, P., McPhie, J., Allen, S., 2003. Interpreted crystalline basement geology of the Gawler Craton, South Australia. Geological Survey Special Map. 1: 1 000 000 Department of Primary Industries and Resources SA, Adelaide, Department of Primary Industries and Resources SA, Adelaide.
Fanning, C.M., 1984. Evaluation of suitability for Rb-Sr dating of drillcore from Aquitaine SSR-1001 and Rb-Sr dating of pyroxene from Reedy Lagoon I, Amdel report.
Fanning, C.M., Flint, R.B., Parker, A.J., Ludwig, K.R., Blissett, A.H., 1988. Refined Proterozoic evolution of the Gawler Craton, South Australia, through U-Pb zircon geochronology. Precambrian Research 40, 363-386.
Fanning, M., Reid, A.J., Teale, G.S., Teale, G.S., SA, P.I.a.R., 2007. A geochronological framework for the Gawler Craton, South Australia, Adelaide: Primary Industries and Resources SA, 2007.

Fioretti, A.M., Black, L.P., Foden, J., Visonà, D., 2005. Grenville-age magmatism at the South Tasman Rise (Australia): A new piercing point for the reconstruction of Rodinia. Geology 33, 769-772.
Fraser, G., McAvaney, S., Neumann, N., Szpunar, M., Reid, A., 2010. Discovery of early Mesoarchean crust in the eastern Gawler Craton, South Australia. Precambrian Research 179, 1-21.
Galerne, C.Y., Neumann, E.-R., Planke, S., 2008. Emplacement mechanisms of sill complexes: Information from the geochemical architecture of the Golden Valley Sill Complex, South Africa. Journal of Volcanology and Geothermal Research 177, 425-440.
Gao, S., Rudnick, R.L., Xu, W.-L., Yuan, H.-L., Liu, Y.-S., Walker, R.J., Puchtel, I.S., Liu, X., Huang, H., Wang, X.-R., Yang, J., 2008. Recycling deep cratonic lithosphere and generation of intraplate magmatism in the North China Craton. Earth and Planetary Science Letters 270, 41-53.
Garner, A., McPhie, J., 1999. Partially melted lithic megablocks in the Yardea Dacite, Gawler Range Volcanics, Australia: implications for eruption and emplacement mechanisms. Bulletin of Volcanology 61, 396-410.
GEOROC, 2014. The database GEOROC (Geochemistry of Rocks of the Oceans and Continents), http://georoc.mpch-mainz.gwdg.de/georoc/Start.asp.
Giles, C.W., 1980. A comparative study of Archaean and Proterozoic felsic volcanic associations in Southern Australia. University of Adelaide, unpublished.
Giles, C.W., 1988. Petrogenesis of the Proterozoic Gawler Range Volcanics, South Australia. Precambrian Research 40–41, 407-427.
Goode, A.D.T., 1970. The petrology and structure of the Kalka and Ewarara layered basic intrusions, Giles Complex, Central Australia. University of Adelaide. Unpublished Ph.D thesis, unpublished.
Grant, J.A., 1986. The isocon diagram; a simple solution to Gresens' equation for metasomatic alteration. Economic Geology 81, 1976-1982.
Grant, J.A., 2005. Isocon analysis: A brief review of the method and applications. Physics and Chemistry of the Earth, Parts A/B/C 30, 997-1004.
Groves, D.I., Bierlein, F.P., Meinert, L.D., Hitzman, M.W., 2010. Iron Oxide Copper-Gold (IOCG) Deposits through Earth History: Implications for Origin, Lithospheric Setting, and Distinction from Other Epigenetic Iron Oxide Deposits. Economic Geology 105, 641-654.
GSWA, 2014. Geological Survey of Western Australia database, http://www.dmp.wa.gov.au/371.aspx.
Guillong, M., Hametner, K., Reusser, E., Wilson, S.A., Günther, D., 2005. Preliminary Characterisation of New Glass Reference Materials (GSA-1G, GSC-1G, GSD-1G and GSE-1G) by Laser Ablation-Inductively Coupled Plasma-Mass Spectrometry Using 193 nm, 213 nm and 266 nm Wavelengths. Geostandards and Geoanalytical Research 29, 315-331.
Gustafson, L., Compston, W., 1979. Rb-Sr dating of Olympic Dam core samples. Report to Western Mining Corporation, Research School of Earth Sciences, Australian National University 18.
Halpin, J.A., Jensen, T., McGoldrick, P., Meffre, S., Berry, R.F., Everard, J.L., Calver, C.R., Thompson, J., Goemann, K., Whittaker, J.M., 2014. Authigenic monazite and detrital zircon dating from the Proterozoic Rocky Cape Group, Tasmania: Links to the Belt-Purcell Supergroup, North America. Precambrian Research 250, 50-67.

Hand, M., Reid, A., Jagodzinski, L., 2007. Tectonic framework and evolution of the Gawler Craton, Southern Australia. Economic Geology 102, 1377-1395.
Hand, M.P., Reid, A.J., Szpunar, M.A., Direen, N., Wade, B., Payne, J., Barovich, K.M., 2008. Crustal architecture during the early Mesoproterozoic Hiltaba-related mineralisation event: are the Gawler Range Volcanics a foreland basin fill? MESA Journal 51, 19-24.
Hanson, R.E., Martin, M.W., Bowring, S.A., Munyanyiwa, H., 1998. U-Pb zircon age for the Umkondo dolerites, eastern Zimbabwe: 1.1 Ga large igneous province in southern Africa–East Antarctica and possible Rodinia correlations. Geology 26, 1143-1146.
Harlan, S.S., Geissman, J.W., Premo, W.R., 2003. Paleomagnetism and geochronology of an Early Proterozoic quartz diorite in the southern Rind River Range, Wyoming, USA. Tectonophysics 362, 105-122.
Haynes, D.W., 1972. Geochemistry of altered basalts (continental tholeiites) and associated copper deposits. The Australian National University, unpublished.
Haynes, D.W., 2006. The Olympic Dam ore deposit discovery–A personal view. SEG Newsletter 66, 1-15.
Haynes, D.W., Cross, K.C., Bills, R.T., Reed, M.H., 1995. Olympic Dam Ore Genesis - a Fluid-Mixing Model. Economic Geology & the Bulletin of the Society of Economic Geologists 90, 281-307.
Hayward, N., Skirrow, R., 2010. Geodynamic setting and controls on iron oxide Cu-Au (±U) ore in the Gawler Craton, South Australia. Hydrothermal iron oxide copper-gold and related deposits: A global perspective 3, 105-131.
Heaman, L.M., 1997. Global mafic magmatism at 2.45 Ga: Remnants of an ancient large igneous province? Geology 25, 299-302.
Hergt, J.M., 1987. The origin and evolution of the Tasmanian dolerites. Australian National University.
Hitzman, M.W., Oreskes, N., Einaudi, M.T., 1992. Geological characteristics and tectonic setting of Proterozoic Iron-Oxide (Cu-U-Au-Ree) Deposits. Precambrian Research 58, 241-287.
Hoatson, D.M., Claoué-Long, J.C., Jaireth, S., 2008a. Australian Proterozoic Mafic-Ultramafic Magmatic Events: Sheets 1 and 2 (1:5000000 and 1:10000000 scale maps). Geoscience Australia, Australia.
Hoatson, D.M., Claoué-Long, J.C., Jaireth, S., 2008b. Gude to using the 1:5000000 map of the Australian Proterozoic mafic-ultramafic magmatic events, p. 140.
Hoatson, D.M., Jaireth, S., Jaques, A.L., Huleatt, M.B., 2007. A synthesis of Australian Proterozoic mafic-ultramafic magmatic events. Part 2, Northern Territory and South Australia. . Geoscience Australia.
Huang, Q., Kamenetsky, V.S., McPhie, J., Ehrig, K., Meffre, S., Maas, R., Thompson, J., Kamenetsky, M., Chambefort, I., Apukhtina, O., Hu, Y., 2015. Neoproterozoic (ca. 820–830 Ma) mafic dykes at Olympic Dam, South Australia: Links with the Gairdner Large Igneous Province. Precambrian Research 271, 160-172.
Huppert, H.E., Sparks, R.S.J., 1988. The generation of granitic magmas by intrusion of basalt into continental crust. Journal of Petrology 29, 599-624.
Jagodzinski, E., 2014. The age of magmatic and hydrothermal zircon at Olympic Dam, Australian Earth Sciences Convention, Newcastle.
Jagodzinski, E.A., 2005. Compilation of SHRIMP U-Pb geochronological data Olympic Domain, Gawler Craton, South Australia, 2001-2003: Geoscience Australia Record 2005/20, 211p.

Jenner, F.E., O'Neill, H.S.C., 2012. Analysis of 60 elements in 616 ocean floor basaltic glasses. Geochemistry, Geophysics, Geosystems 13.
Jochum, K.P., Weis, U., Stoll, B., Kuzmin, D., Yang, Q., Raczek, I., Jacob, D.E., Stracke, A., Birbaum, K., Frick, D.A., 2011. Determination of reference values for NIST SRM 610–617 glasses following ISO guidelines. Geostandards and Geoanalytical Research 35, 397-429.
Johnson, J.P., 1993. The geochronology and radiogenic isotope syetematics of the Olympic Dam copper-uranium-gold-silver deposit, South Australia. The Australian National University. Unpublished Ph.D thesis. 251 pp., unpublished.
Johnson, J.P., Cross, K.C., 1995. U-Pb geochronological constraints on the genesis of the Olympic Dam Cu-U-Au-Ag Deposit, South Australia. Economic Geology & the Bulletin of the Society of Economic Geologists 90, 1046-1063.
Johnson, J.P., McCulloch, M.T., 1995. Sources of mineralising fluids for the Olympic Dam Deposit (South Australia) - Sm-Nd isotopic constraints. Chemical Geology 121, 177-199.
Kamenetsky, V.S., Chung, S.-L., Kamenetsky, M.B., Kuzmin, D.V., 2012. Picrites from the Emeishan Large Igneous Province, SW China: a compositional continuum in primitive magmas and their respective mantle sources. Journal of Petrology 53, 2095-2113.
Kamenetsky, V.S., Crawford, A.J., Meffre, S., 2001. Factors controlling chemistry of magmatic spinel: an empirical study of associated olivine, Cr-spinel and melt inclusions from primitive rocks. Journal of Petrology 42, 655-671.
Keeling, J., 2015. Gawler Craton: potential for unconformity-related uranium-spectral insights, South Australian Resources & Energy Investment Conference, Adelaide.
Kelemen, P.B., Hanghøj, K., Greene, A.R., 2014. 4.21 - One view of the geochemistry of subduction-related magmatic arcs, with an emphasis on primitive andesite and lower crust, in: Holland, H., Turekian, K. (Eds.), Treatise on Geochemistry (Second Edition). Elsevier, Oxford, pp. 749-806.
Kirchenbaur, M., Maas, R., Ehrig, K., Kamenetsky, V.S., Strub, E., Ballhaus, C., Münker, C., Uranium and Sm isotope studies of the supergiant Olympic Dam Cu-Au-U-Ag deposit, South Australia. Geochimica Et Cosmochimica Acta.
Klötzli, U., Klötzli, E., Günes, Z., Kosler, J., 2009. Accuracy of Laser Ablation U-Pb Zircon Dating: Results from a Test Using Five Different Reference Zircons. Geostandards and Geoanalytical Research 33, 5-15.
Knutson, J., Donnelly, T.H., Eadington, P.J., Tonkin, D.G., 1992. Hydrothermal alteration of middle Proterozoic basalts, Stuart Shelf, South-Australia - a possible source for Cu mineralization. Economic Geology 87, 1054-1077.
Li, X., Li, Z., Zhou, H., Liu, Y., Kinny, P.D., 2002a. U–Pb zircon geochronology, geochemistry and Nd isotopic study of Neoproterozoic bimodal volcanic rocks in the Kangdian Rift of South China: implications for the initial rifting of Rodinia. Precambrian Research 113, 135-154.
Li, Z., Li, X., Zhou, H., Kinny, P.D., 2002b. Grenvillian continental collision in south China: New SHRIMP U-Pb zircon results and implications for the configuration of Rodinia. Geology 30, 163-166.
Li, Z., Zhang, L., Powell, C.M., 1995. South China in Rodinia: Part of the missing link between Australia–East Antarctica and Laurentia? Geology 23, 407.
Li, Z.X., Bogdanova, S.V., Collins, A.S., Davidson, A., De Waele, B., Ernst, R.E., Fitzsimons, I.C.W., Fuck, R.A., Gladkochub, D.P., Jacobs, J., Karlstrom, K.E., Lu, S., Natapov, L.M., Pease, V., Pisarevsky, S.A., Thrane, K., Vernikovsky, V., 2008.

Assembly, configuration, and break-up history of Rodinia: A synthesis. Precambrian Research 160, 179-210.
Li, Z.X., Li, X.H., Kinny, P.D., Wang, J., 1999. The breakup of Rodinia: Did it start with a mantle plume beneath South China? Earth and Planetary Science Letters 173, 171-181.
Ling, W., Gao, S., Zhang, B., Li, H., Liu, Y., Cheng, J., 2003. Neoproterozoic tectonic evolution of the northwestern Yangtze craton, South China: Implications for amalgamation and break-up of the Rodinia Supercontinent. Precambrian Research 122, 111-140.
Longerich, H.P., Jackson, S.E., Günther, D., 1996. Inter-laboratory note. Laser ablation inductively coupled plasma mass spectrometric transient signal data acquisition and analyte concentration calculation. Journal of Analytical Atomic Spectrometry 11, 899-904.
Ludwig, K.R., 2003. User's manual for Isoplot 3.00: a geochronological toolkit for Microsoft Excel. Kenneth R. Ludwig.
Maas, R., Kamenetsky, M.B., Sobolev, A.V., Kamenetsky, V.S., Sobolev, N.V., 2005. Sr, Nd, and Pb isotope evidence for a mantle origin of alkali chlorides and carbonates in the Udachnaya kimberlite, Siberia. Geology 33, 549-552.
Maas, R., Kamenetsky, V., Ehrig, K., Meffre, S., McPhie, J., Diemar, G., 2011. Olympic Dam U-Cu-Au deposit, Australia: New age constraints Goldschmidt Conference Abstracts, Mineralogical Magazine 75, 1.
Mason, M., Thomson, B., Tonkin, D., 1978. Regional stratigraphy of the Beda Volcanics, Backy Point Beds and Pandurra Formation on the southern Stuart Shelf, South Australia. South Australian Geological Survey Quarterly Geological Notes 66, 2-9.
McCulloch, M.T., Gamble, J.A., 1991. Geochemical and geodynamical constraints on subduction zone magmatism. Earth and Planetary Science Letters 102, 358-374.
McInnes, B.I.A., Keays, R.R., Lambert, D.D., Hellstrom, J., Allwood, J.S., 2008. Re-Os geochronology and isotope systematics of the Tanami, Tennant Creek and Olympic Dam Cu-Au deposits. Australian Journal of Earth Sciences 55, 967-981.
McPhie, J., Kamenetsky, V., Allen, S., Ehrig, K., Agangi, A., Bath, A., 2011a. The fluorine link between a supergiant ore deposit and a silicic large igneous province Geology.
McPhie, J., Kamenetsky, V.S., Chambefort, I., Ehrig, K., Green, N., 2011b. Origin of the supergiant Olympic Dam Cu-U-Au-Ag deposit, South Australia: Was a sedimentary basin involved? Geology 39, 795-798.
McPhie, J., Orth, K., Kamenetsky, V., Kamenetsky, M., Ehrig, K., 2016. Characteristics, origin and significance of Mesoproterozoic bedded clastic facies at the Olympic Dam Cu–U–Au–Ag deposit, South Australia. Precambrian Research 276, 85-100.
Meffre, S., Ehrig, K., Kamenetsky, V., Chambefort, I., Maas, R., McPhie, J., 2010. Pb isotopes at Olympic Dam: Constraining sulphide growth, Proceedings, 13th Quadrennial IAGOD Symposium, Giant Ore Deposits Down Under, Adelaide, South Australia, pp. 6-9.
Morrow, N., McPhie, J., 2000. Mingled silicic lavas in the Mesoproterozoic Gawler Range Volcanics, South Australia. Journal of Volcanology and Geothermal Research 96, 1-13.

Mortimer, G.E., Cooper, J.A., Paterson, H.L., Cross, K., Hudson, G.R.T., Uppill, R.K., 1988. Zircon U-Pb Dating in the Vicinity of the Olympic Dam Cu-U-Au Deposit, Roxby Downs, South-Australia. Economic Geology 83, 694-709.
Neumann, E.-R., Svensen, H., Galerne, C.Y., Planke, S., 2011. Multistage Evolution of Dolerites in the Karoo Large Igneous Province, Central South Africa. Journal of Petrology 52, 959-984.
Oreskes, N., Einaudi, M.T., 1990. Origin of rare-earth element-enriched hematite breccias at the Olympic-Dam Cu-U-Au-Ag Deposit, Roxby Downs, south Australia. Economic Geology 85, 1-28.
Oreskes, N., Einaudi, M.T., 1992. Origin of Hydrothermal Fluids at Olympic Dam: Preliminary Results from Fluid Inclusions and Stable Isotopes. Economic Geology and the Bulletin of the Society of Economic Geologists 87, 64-90.
Parker, A., 1990. Gawler Craton and Stuart Shelf—regional geology and mineralisation. Geology of the Mineral Deposits of Australia and Papua New Guinea (editor Hughes FE). The Australasian Institute of Mining & Metallurgy, Melbourne, 999-1008.
Parker, A., Lemon, N., 1982. Reconstruction of the early Proterozoic stratigraphy of the Gawler Craton, South Australia. Journal of the Geological Society of Australia 29, 221-238.
Paterson, H., 1986. The Acropolis Prospect, Paterson, HL,(Compiler), Basement geology of the Stuart Shelf region, 8th Australian Geological Convention, pp. 17-23.
Payne, J.L., Barovich, K.M., Hand, M., 2006. Provenance of metasedimentary rocks in the northern Gawler Craton, Australia: Implications for Palaeoproterozoic reconstructions. Precambrian Research 148, 275-291.
Payne, J.L., Hand, M., Barovich, K.M., Reid, A., Evans, D.A.D., 2009. Correlations and reconstruction models for the 2500-1500 Ma evolution of the Mawson Continent. Geological Society, London, Special Publications 323, 319-355.
Payne, J.L., Hand, M., Barovich, K.M., Wade, B.P., 2008. Temporal constraints on the timing of high-grade metamorphism in the northern Gawler Craton: implications for assembly of the Australian Proterozoic. Australian Journal of Earth Sciences 55, 623-640.
Pearce, J., 1996. A user's guide to basalt discrimination diagrams. Trace element geochemistry of volcanic rocks: applications for massive sulphide exploration. Edited by DA Wyman. Geological Association of Canada, Short Course Notes 12, 79-113.
Pei, F., Xu, W., Wang, Q., Wang, D., Lin, J., 2004. Mesozoic basalt and mineral chemistry of the mantle-derived xenocrysts in Feixian, western Shandong, China: constraints on nature of Mesozoic lithospheric mantle. Geological Journal of China Universities 10, 88-97.
Peng, Z.X., Mahoney, J.J., Hooper, P.R., Macdougall, J.D., Krishnamurthy, P., 1998. Basalts of the northeastern Deccan Traps, India: Isotopic and elemental geochemistry and relation to southwestern Deccan stratigraphy. Journal of Geophysical Research: Solid Earth 103, 29843-29865.
Perfit, M.R., Gust, D.A., Bence, A.E., Arculus, R.J., Taylor, S.R., 1980. Chemical characteristics of island-arc basalts: Implications for mantle sources. Chemical Geology 30, 227-256.
Pirajno, F., Hoatson, D.M., 2012. A review of Australia's Large Igneous Provinces and associated mineral systems: Implications for mantle dynamics through geological time. Ore Geology Reviews 48, 2-54.
PIRSA, 2006. Primary industries and resources of South Australia Geoscientific GIS Dataset, unpublished.

Rainbird, R.H., Stern, R.A., Khudoley, A.K., Kropachev, A.P., Heaman, L.M., Sukhorukov, V.I., 1998. U–Pb geochronology of Riphean sandstone and gabbro from southeast Siberia and its bearing on the Laurentia–Siberia connection. Earth and Planetary Science Letters 164, 409-420.
Reeve, J.S., Cross, K.C., Smith, R.N., Oreskes, N., 1990. Olympic Dam copper-uranium-gold-silver deposit, in: Hughes, F.E. (Ed.), Geology of the mineral deposits of Australia and Papua New Guinea. Australasian Institute of Mining and Metallurgy, Melbourne, pp. 1009-1035.
Reid, A., Hand, M., Jagodzinski, E., Kelsey, D., Pearson, N., 2008. Paleoproterozoic orogenesis in the southeastern Gawler Craton, South Australia. Australian Journal of Earth Sciences 55, 449-471.
Reid, A.J., Fabris, A., 2015. Influence of Preexisting Low Metamorphic Grade Sedimentary Successions on the Distribution of Iron Oxide Copper-Gold Mineralization in the Olympic Cu-Au Province, Gawler Craton. Economic Geology 110, 2147-2157.
Reid, A.J., Hand, M., 2012. Mesoarchean to Mesoproterozoic evolution of the southern Gawler Craton, South Australia. Episodes-Newsmagazine of the InternationalUnion of Geological Sciences 35, 216.
Renne, P.R., Swisher, C.C., Deino, A.L., Karner, D.B., Owens, T.L., DePaolo, D.J., 1998. Intercalibration of standards, absolute ages and uncertainties in $^{40}Ar/^{39}Ar$ dating. Chemical Geology 145, 117-152.
Roberts, D.E., Hudson, G.R.T., 1983. The Olympic Dam copper-uranium-gold deposit, Roxby Downs, south Australia. Economic Geology 78, 799-822.
Rollinson, H.R., 1993. Using geochemical data: evaluation, presentation, interpretation. Longman Scientific & Technical Essex.
Ross, G.M., Parrish, R.R., Winston, D., 1992. Provenance and U-Pb geochronology of the Mesoproterozoic Belt Supergroup (northwestern United States): implications for age of deposition and pre-Panthalassa plate reconstructions. Earth and Planetary Science Letters 113, 57-76.
Sandeman, H.A., Ootes, L., Cousens, B., Kilian, T., 2014. Petrogenesis of Gunbarrel magmatic rocks: Homogeneous continental tholeiites associated with extension and rifting of Neoproterozoic Laurentia. Precambrian Research 252, 166-179.
Saunders, A.D., Tarney, J., 1984. Geochemical characteristics of basaltic volcanism within back-arc basins. Geological Society, London, Special Publications 16, 59-76.
Schlegel, T.U., Heinrich, C.A., 2015. Lithology and Hydrothermal Alteration Control the Distribution of Copper Grade in the Prominent Hill Iron Oxide-Copper-Gold Deposit (Gawler Craton, South Australia). Economic Geology 110, 1953-1994.
Schoene, B., Crowley, J.L., Condon, D.J., Schmitz, M.D., Bowring, S.A., 2006. Reassessing the uranium decay constants for geochronology using ID-TIMS U–Pb data. Geochimica Et Cosmochimica Acta 70, 426-445.
Skirrow, R.G., 2010. "Hematite-group" IOCG ± U systems: Tectonic settings, hydrothermal characteristics, and Cu-Au and U mineralizing processes, in: Corriveau, L., Mumin, H. (Eds.), Exploring for Iron Oxide Copper-Gold Deposits: Canada and Global Analogues, Geological Association of Canada Short Course Notes 20, pp. 39-58.
Skirrow, R.G., Bastrakov, E., Davidson, G., Raymond, O.L., Heithersay, P., 2002. The geological framework, distribution and controls of Fe-oxide Cu-Au mineralisation in the Gawler Craton, South Australia: Part II: Alteration and mineralisation, in: Porter,

T.M. (Ed.), Hydrothermal Iron Oxide Copper-Gold & Related Deposits: A Global Perspective, Volume 2. PGC Publishing, Adelaide, pp. 33-47.
Skirrow, R.G., Bastrakov, E.N., Barovich, K., Fraser, G.L., Creaser, R.A., Fanning, C.M., Raymond, O.L., Davidson, G.J., 2007. Timing of iron oxide Cu-Au-(U) hydrothermal activity and Nd isotope constraints on metal sources in the Gawler craton, south Australia. Economic Geology 102, 1441-1470.
Spell, T.L., McDougall, I., 2003. Characterization and calibration of $^{40}Ar/^{39}Ar$ dating standards. Chemical Geology 198, 189-211.
Stacey, J.S., Kramers, J.D., 1975. Approximation of terrestrial lead isotope evolution by a two-stage model. Earth and Planetary Science Letters 26, 207-221.
Stewart, K., 1994. High temperature felsic volcanism and the role of mantle magmas in Proterozoic crustal growth: the Gawler Range Volcanic Province. University of Adelaide, Department of Geology and Geophysics.
Sun, S.S., McDonough, W.F., 1989. Chemical and isotopic systematics of oceanic basalts: implications for mantle composition and processes. Geological Society, London, Special Publications 42, 313-345.
Swain, G., Barovich, K., Hand, M., Ferris, G., Schwarz, M., 2008. Petrogenesis of the St Peter Suite, southern Australia: Arc magmatism and Proterozoic crustal growth of the South Australian Craton. Precambrian Research 166, 283-296.
Swain, G., Woodhouse, A., Hand, M., Barovich, K., Schwarz, M., Fanning, C.M., 2005. Provenance and tectonic development of the late Archaean Gawler Craton, Australia; U–Pb zircon, geochemical and Sm–Nd isotopic implications. Precambrian Research 141, 106-136.
Symington, N.J., Weinberg, R.F., Hasalová, P., Wolfram, L.C., Raveggi, M., Armstrong, R.A., 2014. Multiple intrusions and remelting-remobilization events in a magmatic arc: The St. Peter Suite, South Australia. Geological Society of America Bulletin, 1200-1218.
Taylor, B., Martinez, F., 2003. Back-arc basin basalt systematics. Earth and Planetary Science Letters 210, 481-497.
Thomas, J.L., Direen, N.G., Hand, M., 2008. Blind orogen: Integrated appraisal of multiple episodes of Mesoproterozoic deformation and reworking in the Fowler Domain, western Gawler Craton, Australia. Precambrian Research 166, 263-282.
Townsend, A.T., Yu, Z., McGoldrick, P., Hutton, J.A., 1998. Precise lead isotope ratios in Australian galena samples by high resolution inductively coupled plasma mass spectrometry. Journal of Analytical Atomic Spectrometry 13, 809-813.
Trueman, N.A., 1986. Lead-uranium systematics of the Olympic Dam deposit and Stuart shelf mineralization: Summary report of U-REE mineralization, Adelaide, Australia. Western Mining Corporation, unpublished group memo.
Vanderkluysen, L., Mahoney, J.J., Hooper, P.R., Sheth, H.C., Ray, R., 2011. The feeder system of the Deccan Traps (India): insights from dike geochemistry. Journal of Petrology 52, 315-343.
Veevers, J.J., 2004. Gondwanaland from 650–500 Ma assembly through 320 Ma merger in Pangea to 185–100 Ma breakup: supercontinental tectonics via stratigraphy and radiometric dating. Earth-Science Reviews 68, 1-132.
Wade, B., Hand, M., 2005. Geochemistry and Provenance of a Mesoproterozoic (1.4 Ga) eastern Musgrave Block basin: Buddying up to the Belt-Purcell Basin, Supercontinents and Earth Evolution Symposium (2005: Maritime Museum, WA).
Wade, B.P., Barovich, K.M., Hand, M., Scrimgeour, I.R., Close, D.F., 2006. Evidence for Early Mesoproterozoic Arc Magmatism in the Musgrave Block, Central Australia:

Implications for Proterozoic Crustal Growth and Tectonic Reconstructions of Australia. The Journal of Geology 114, 43-63.
Wade, C.E., McAvaney, S.O., Gordon, G.A., 2014. The Beda Basalt: new geochemistry, isotopic data and its definition. MESA Journal 73.
Waight, T., Baker, J., Willigers, B., 2002. Rb isotope dilution analyses by MC-ICPMS using Zr to correct for mass fractionation: towards improved Rb–Sr geochronology? Chemical Geology 186, 99-116.
Walter, M., Veevers, J., Calver, C., Grey, K., 1995. Neoproterozoic stratigraphy of the Centralian Superbasin, Australia. Precambrian Research 73, 173-195.
Wang, X., Li, X., Li, W., Li, Z., Liu, Y., Yang, Y., Liang, X., Tu, X., 2008. The Bikou basalts in the northwestern Yangtze block, South China: Remnants of 820–810 Ma continental flood basalts? Geological Society of America Bulletin 120, 1478-1492.
Wang, X., Li, X., Li, Z., Liu, Y., Yang, Y., 2010. The Willouran basic province of South Australia: Its relation to the Guibei large igneous province in South China and the breakup of Rodinia. Lithos 119, 569-584.
Webb, A., Coats, R., Fanning, C., Flint, R., 1983. Geochronological framework of the Adelaide Geosyncline, Geological Society of Australia Abstracts, pp. 7-9.
Webb, A.W., Coats, R.P., 1980. A reassessment of the age of the Beda Volcanics on the Stuart Shelf. South Australia, South Australia. Department of Mines and Energy. Report Book.
Werner, M., Dutch, R., Pawley, M., Krapf, C., 2014. Mafic intrusions in the East Musgraves: New geochemical data set available now, Unlocking SA's Technical Wealth-South Australian Resources and Energy Investment Conference, Adelaide.
White, Clarke, Nelson, 1999. SHRIMP U–Pb zircon dating of Grenville-age events in the western part of the Musgrave Block, central Australia. Journal of Metamorphic Geology 17, 465-481.
Wingate, M.T.D., Campbell, I.H., Compston, W., Gibson, G.M., 1998. Ion microprobe U–Pb ages for Neoproterozoic basaltic magmatism in south-central Australia and implications for the breakup of Rodinia. Precambrian Research 87, 135-159.
Wingate, M.T.D., Pirajno, F., Morris, P.A., 2004. Warakurna large igneous province: A new Mesoproterozoic large igneous province in west-central Australia. Geology 32, 105-108.
Woodget, A.L., 1987. The petrology, geochemistry and tectonic setting of basic volcanics on the Stuart Shelf and in the Adelaide Geosyncline, South Australia, School of Earth and Environmental Sciences, Geology & Geophysics. University of Adelaide. Unpublished B.Sc.(Hons) thesis. .
Woodhead, J., Pickering, R., 2012. Beyond 500 ka: Progress and prospects in the UPb chronology of speleothems, and their application to studies in palaeoclimate, human evolution, biodiversity and tectonics. Chemical Geology 322–323, 290-299.
Yang, D.-B., Xu, W.-L., Pei, F.-P., Yang, C.-H., Wang, Q.-H., 2012. Spatial extent of the influence of the deeply subducted South China Block on the southeastern North China Block: Constraints from Sr–Nd–Pb isotopes in Mesozoic mafic igneous rocks. Lithos 136–139, 246-260.
Yang, Y., Wu, F., Xie, L., Zhang, Y., 2009. High-Precision Measurements of the 143Nd/144Nd Isotope Ratio in Certified Reference Materials without Nd and Sm Separation by Multiple Collector Inductively Coupled Plasma Mass Spectrometry. Analytical Letters 43, 142-150.
Yeates, G., 1990. Middleback Range iron ore deposits. Geology of the mineral deposits of Australia and Papua New Guinea 2, 1045-1048.

Zhao, J., McCulloch, M.T., 1993. Sm-Nd mineral isochron ages of Late Proterozoic dyke swarms in Australia: evidence for two distinctive events of mafic magmatism and crustal extension. Chemical Geology 109, 341-354.
Zhao, J., McCulloch, M.T., Korsch, R.J., 1994. Characterisation of a plume-related ~ 800 Ma magmatic event and its implications for basin formation in central-southern Australia. Earth and Planetary Science Letters 121, 349-367.

Supplementary materials

Table S1 Primary and secondary standards for apatite and titanite U-Pb LA-ICPMS dating

	^{207}cor ^{206}Pb/^{238} age[a]	+/-1 ster	^{238}U/^{206}Pb ratio	+/-1 ster	^{207}Pb/^{206}Pb ratio	+/-1 ster	^{204}Pb ppm	^{206}Pb ppm	^{207}Pb ppm	^{208}Pb ppm	^{232}Th ppm	^{238}U ppm
Apatite standards:												
Primary Standards:												
OD306	1562	29	3.61	0.07	0.1054	0.0030	0.00	2.8	0.3	2.9	40	12
OD306	1568	22	3.60	0.05	0.1049	0.0023	0.01	4.3	0.4	6.1	85	18
OD306	1585	49	3.50	0.11	0.1176	0.0066	0.00	1.9	0.2	2.2	31	8
OD306	1591	41	3.50	0.09	0.1158	0.0051	0.00	1.2	0.1	1.1	15	5
OD306	1594	30	3.49	0.07	0.1157	0.0034	0.01	2.2	0.2	3.2	43	9
OD306	1595	21	3.55	0.05	0.1018	0.0018	0.01	5.4	0.5	6.6	92	22
OD306	1603	23	3.49	0.05	0.1112	0.0022	0.01	5.8	0.6	6.9	94	23
OD306	1607	32	3.52	0.07	0.1035	0.0040	0.00	1.9	0.2	2.3	32	8
OD306	1611	29	3.43	0.06	0.1220	0.0029	0.00	3.5	0.4	3.4	45	14
OD306	1632	58	3.46	0.12	0.1040	0.0070	0.00	1.4	0.1	2.1	27	5
NIST610			3.82	0.04	0.9198	0.0042	5.85	100.5	92.3	218.8	448	453
NIST610			4.02	0.04	0.9103	0.0034	5.94	100.4	91.1	217.8	447	453
NIST610			4.00	0.04	0.9101	0.0034	6.32	108.0	98.0	233.7	478	482

Mean = 1591±18 [1.1%] 95% conf.
Wtd by data-pt errs only, 0 of 10 rej.
MSWD = 0.41, probability = 0.93

Acropolis OD306 apatite
Concordia intercept age=1595.9±5.9 Ma
MC-ICP-MS analysis by Roland Maas in 2012

NIST610			3.95	0.04	0.9118	0.0035		5.95	101.0	92.2	219.9	452	458
NIST610			3.99	0.04	0.9088	0.0037		6.35	106.9	96.9	231.3	473	476
NIST610			3.97	0.04	0.9091	0.0035		6.04	101.9	92.5	220.5	449	453
NIST610			3.90	0.04	0.9112	0.0035		6.19	103.6	94.5	225.4	460	465
NIST610			3.96	0.04	0.9079	0.0035		5.95	101.0	91.6	218.3	447	450
NIST610			3.92	0.04	0.9084	0.0035		6.25	107.2	97.5	232.3	476	480
NIST610			3.94	0.04	0.9073	0.0035		5.86	99.2	90.1	214.9	441	443

Secondary standards- treated as unknowns:

Mean = 384±15 [3.9%] 95% conf.
Wtd by data-pt errs only, 0 of 6 rej.
MSWD = 1.7, probability = 0.14

Kovdor apatite
Recommended age Mean = 377.5±3.5 Ma
Amelin and Zaitsev (2002)

Kovdor	365	10	12.43	0.28	0.2788	0.0092		0.01	1.3	0.4	34.4	2060	18
Kovdor	380	11	11.47	0.27	0.3029	0.0084		0.01	1.2	0.4	34.0	1986	16
Kovdor	385	20	10.67	0.44	0.3358	0.0184		0.00	0.8	0.3	24.6	1453	8
Kovdor	386	8	13.69	0.27	0.1810	0.0053		0.02	1.6	0.3	39.7	2361	25
Kovdor	397	9	11.90	0.24	0.2541	0.0070		0.03	1.3	0.3	35.5	2085	18
Kovdor	435	33	8.48	0.49	0.3946	0.0244		0.00	0.7	0.3	23.7	1235	7

Mean = 927±13 [1.4%] 95% conf.
Wtd by data-pt errs only, 0 of 9 rej.
MSWD = 2.7, probability = 0.005

Otter Lake apatite
Recommended age Mean = 913±7 Ma
Barfod et al. (2005)

OtterLake	889	13	5.83	0.09	0.1840	0.0038		0.17	18.2	3.4	43.7	933	115
OtterLake	908	9	5.98	0.06	0.1490	0.0015		0.11	17.0	2.5	40.3	919	114

OtterLake	912	10	5.95	0.07	0.1491	0.0013	0.09	17.4	2.6	41.3	932	115
OtterLake	931	10	5.87	0.06	0.1432	0.0014	0.09	18.2	2.6	43.6	999	123
OtterLake	932	9	5.89	0.06	0.1407	0.0013	0.08	17.8	2.5	42.6	964	118
OtterLake	933	10	5.88	0.06	0.1407	0.0013	0.09	18.2	2.5	43.2	976	120
OtterLake	938	10	5.72	0.06	0.1575	0.0015	0.11	17.3	2.7	40.9	891	111
OtterLake	939	17	5.47	0.10	0.1915	0.0047	0.14	18.2	3.5	43.7	878	109
OtterLake	950	10	5.70	0.06	0.1507	0.0015	0.08	17.3	2.6	41.0	901	112
OtterLake			0.00	0.00	0.9200	0.0088						

Titanite Standards:

Primary Standards:

Mean = 431.5±4.5 [1.0%] 95% conf.
Wtd by data-pt errs only, 0 of 20 rej.
MSWD = 0.18, probability = 1.000

AUR100606
TIMS age 432.02 ± 0.64 Ma
Best et al. 2012

100606	424	8	13.66	0.25	0.1121	0.0037	0.05	6.8	0.8	9.5	406	101
100606	426	11	13.46	0.34	0.1210	0.0050	0.03	3.4	0.4	3.5	132	49
100606	426	18	13.33	0.56	0.1279	0.0079	0.01	2.6	0.3	2.6	107	36
100606	427	14	13.79	0.46	0.1015	0.0061	0.02	3.2	0.3	4.2	189	50
100606	427	13	13.83	0.41	0.0980	0.0048	0.00	4.4	0.4	6.5	301	69
100606	427	13	13.66	0.43	0.1073	0.0057	0.04	2.6	0.3	3.3	138	38
100606	428	10	12.62	0.29	0.1635	0.0057	0.07	4.3	0.7	4.8	175	59
100606	429	10	13.39	0.31	0.1191	0.0042	0.00	4.6	0.5	5.8	249	67
100606	430	11	13.76	0.34	0.0973	0.0048	0.00	3.9	0.4	4.5	189	59
100606	430	13	12.18	0.34	0.1856	0.0085	0.10	8.7	1.8	9.0	275	117
100606	431	12	13.62	0.36	0.1030	0.0050	0.03	3.0	0.3	3.5	152	44
100606	432	10	13.77	0.31	0.0927	0.0040	0.03	4.4	0.4	6.0	269	64

100606	432	8	13.66	0.26	0.0981	0.0032	0.00	9.7	1.0	10.8	463	146
100606	432	8	13.90	0.24	0.0844	0.0025	0.07	9.6	0.8	10.2	455	145
100606	435	9	13.89	0.28	0.0805	0.0030	0.01	7.1	0.6	7.9	355	108
100606	435	11	13.70	0.33	0.0913	0.0044	0.00	4.3	0.4	6.1	269	63
100606	435	11	13.59	0.34	0.0966	0.0051	0.03	3.8	0.4	3.2	128	56
100606	436	8	13.89	0.27	0.0784	0.0030	0.00	8.0	0.6	5.0	213	121
100606	439	11	13.54	0.35	0.0929	0.0046	0.02	3.7	0.3	4.9	212	54
100606	439	10	13.72	0.31	0.0818	0.0033	0.01	5.4	0.4	6.8	303	81
NIST610			4.21	0.06	0.9146	0.0053	5.79	101.1	92.8	222.0	453	460
NIST610			4.15	0.06	0.9136	0.0053	6.14	103.4	94.5	225.0	461	464
NIST610			4.11	0.05	0.9118	0.0051	6.16	104.3	95.2	227.2	464	468
NIST610			4.12	0.05	0.9074	0.0052	6.00	101.1	92.1	218.5	450	455
NIST610			4.10	0.06	0.9001	0.0054	5.96	103.3	93.2	223.6	455	461

Seconday Standards - treated as unknowns:

Mean = 28.6±2.7 [9.5%] 95% conf.
Wtd by data-pt errs only, 0 of 10 rej.
MSWD = 0.32, probability = 0.97

Fish Canyon Titanite 28.13+/-0.48 Ma
Daze et al 2003 Chem Geol 199, 111-127

FISH CANYON 3	24	9	106.61	7.79	0.5251	0.1193	0.01	0.5	0.3	0.9	260	55
FISH CANYON 3	25	4	114.86	7.26	0.4797	0.0516	0.01	0.5	0.2	1.0	293	56
FISH CANYON 3	26	5	79.21	4.34	0.5832	0.0455	0.03	0.5	0.3	0.9	238	44
FISH CANYON 3	27	5	82.30	5.03	0.5614	0.0474	0.03	0.5	0.3	1.0	210	44
FISH CANYON 3	28	3	115.24	6.66	0.4446	0.0370	0.02	0.5	0.2	0.8	284	58
FISH CANYON 3	29	5	71.20	5.34	0.5851	0.0402	0.04	0.4	0.2	0.8	167	29
FISH CANYON 3	30	3	118.21	7.26	0.4065	0.0390	0.01	0.4	0.2	0.9	272	58

FISH CANYON 3	30	5	114.25	7.09	0.4182	0.0588	0.02	0.5	0.2	0.9	283	57
FISH CANYON 3	33	4	108.22	7.23	0.4057	0.0422	0.00	0.5	0.2	0.9	298	56
FISH CANYON 3	36	13	86.92	5.27	0.4489	0.1340	0.00	0.5	0.2	0.8	233	50

Mean = 2014±16 [0.79%] 95% conf.
Wtd by data-pt errs only, 0 of 10 rej.
MSWD = 1.00, probability = 0.44

LIMPOPO	1998	23	2.74	0.03	0.1263	0.0013	0.05	101.9	12.8	21.3	214	305
LIMPOPO	1999	26	2.75	0.04	0.1242	0.0015	0.05	69.9	8.7	17.8	170	209
LIMPOPO	1999	23	2.72	0.03	0.1324	0.0013	0.02	80.0	10.6	23.2	218	238
LIMPOPO	2002	27	2.73	0.04	0.1275	0.0015	0.02	67.4	8.7	14.6	142	209
LIMPOPO	2004	24	2.74	0.03	0.1257	0.0012	0.01	91.0	11.4	20.8	204	271
LIMPOPO	2011	25	2.73	0.03	0.1246	0.0013	0.03	107.1	13.4	26.5	256	323
LIMPOPO	2011	25	2.72	0.03	0.1272	0.0012	0.03	91.0	11.7	26.4	247	268
LIMPOPO	2016	30	2.72	0.04	0.1245	0.0017	0.00	105.3	13.2	25.0	249	326
LIMPOPO	2039	27	2.67	0.03	0.1316	0.0019	0.05	43.7	5.7	17.1	159	130
LIMPOPO	2087	29	2.62	0.04	0.1288	0.0015	0.02	68.5	8.8	23.3	219	196

Mean = 99.1±2.1 [2.1%] 95% conf.
Wtd by data-pt errs only, 0 of 10 rej.
MSWD = 0.82, probability = 0.59

Mt Dromadery
98.7 ± 0.6 Ma Khon et al, 1990 Journal of Geology

MT DROMADERY	92	4	57.81	2.11	0.1813	0.0111	0.00	1.5	0.3	3.1	558	95

MT DROMADERY	96	3	58.56	1.96	0.1437	0.0084	0.00	1.8	0.3	2.7	490	111
MT DROMADERY	98	4	56.29	1.91	0.1562	0.0083	0.02	1.8	0.3	2.7	485	109
MT DROMADERY	99	3	54.12	1.76	0.1804	0.0092	0.02	2.1	0.4	4.1	739	127
MT DROMADERY	99	3	59.73	1.55	0.1064	0.0063	0.04	2.3	0.3	2.7	493	154
MT DROMADERY	100	3	57.48	1.88	0.1298	0.0083	0.04	1.9	0.2	3.8	729	117
MT DROMADERY	100	3	61.51	1.50	0.0752	0.0046	0.00	4.4	0.3	2.7	512	300
MT DROMADERY	101	7	50.99	2.96	0.2031	0.0209	0.00	0.6	0.1	0.3	17	32
MT DROMADERY	101	3	57.56	1.79	0.1173	0.0067	0.00	2.4	0.3	4.1	779	156
MT DROMADERY	104	4	55.43	1.91	0.1237	0.0071	0.01	2.0	0.2	3.1	560	118

[a]The 207-correction is based on common Pb composition of Stacey and Kramers (1975) at 820 Ma. ster, standard error.

Table S2 Drill core (RU65-7938) assays of the Olympic Dam dolerite

Sample No.	RX 8152	RX 8155	RX 8156	RX 8157	RX 8158	RX 8159	RX 8160	RX 8161	RX 8163	RX 8164	RX 8168	RX 8169	RX 8170
SiO_2	40.3	49.1	50.1	50.2	51.5	49.7	51.9	47.1	48.2	45.9	48.0	50.6	50.2
TiO_2	2.1	2.4	2.4	2.4	2.4	2.1	1.6	2.1	2.9	2.8	2.9	2.9	3.1
Al_2O_3	13.1	12.6	12.8	12.8	13.4	13.8	16.2	14.0	14.8	14.5	13.1	14.7	14.4
FeO_t	18.9	14.6	13.9	15.1	13.7	13.9	6.0	16.5	15.6	14.7	20.5	15.3	16.1
MnO	0.8	0.2	0.2	0.2	0.2	0.3	0.2	0.2	0.2	0.2	0.2	0.2	0.2
MgO	3.6	5.0	5.5	5.2	5.4	5.9	9.8	5.2	3.9	3.4	3.8	2.8	3.7
CaO	4.3	8.0	7.8	7.3	7.0	9.0	3.4	5.6	5.4	5.5	1.4	6.5	4.8
Na_2O	1.2	2.2	2.0	2.3	2.4	2.5	2.9	2.7	3.0	3.4	3.0	2.7	2.7
K_2O	3.2	0.3	0.2	0.3	0.4	0.7	1.6	0.8	1.3	1.5	1.6	0.8	0.9
P_2O_5	0.2	0.2	0.2	0.2	0.2	0.2	0.1	0.2	0.2	0.3	0.3	0.3	0.3
S	25	808	257	231	205	25	25	157	363	160	175	90	244
Li	34.5	17.0	26.7	24.9	24.0	20.5	122.4	43.9	21.6	24.6	32.0	23.0	24.3
Be	7.2	0.9	0.7	0.8	0.8	0.9	1.0	1.4	1.2	1.4	2.0	1.3	0.9
Sc	40	39	39	39	41	40	44	41	34	34	35	35	36
Ti	12373	14134	14634	14504	14614	12573	9392	12703	17175	17005	17595	17435	18455
V	386	412	437	419	413	406	361	450	509	421	375	402	413
Cr	157	97	93	85	121	182	289	138	32	38	23	24	23
Co	22.4	74.5	58.2	58.8	60.6	54.6	58.4	59.6	57.9	54.8	46.5	50.7	57.9
Ni	62	72	74	70	75	91	93	64	51	46	34	43	40
Cu	47	394	260	284	216	104	11	142	162	99	30	258	306
Zn	183	169	182	151	159	191	427	320	280	238	224	178	243

Ga	20.9	21.3	21.4	22.0	21.9	20.9	20.1	21.8	25.9	25.5	28.1	24.9	25.0
As	1.2	2.8	<0.5	1.9	2.4	1.5	1.7	4.4	7.5	4.6	0.6	1.4	0.8
Rb	185.4	8.8	5.2	7.0	14.5	24.1	44.0	32.8	51.6	65.0	58.5	32.2	33.3
Sr	44	170	157	163	170	159	100	142	163	94	66	194	182
Y	30.4	34.5	31.9	34.3	31.4	28.9	19.8	28.2	37.6	38.9	38.4	39.6	37.2
Zr	135	134	137	140	140	122	87	117	156	166	198	179	181
Nb	12.2	13.0	12.9	12.1	14.0	10.5	8.4	9.6	12.4	13.1	13.9	13.3	13.2
Mo	8.4	1.5	0.5	4.7	0.8	0.6	0.1	0.9	0.5	1.2	0.5	0.7	0.5
Ag	0.1	0.2	0.1	0.1	0.1	0.1	<0.05	0.1	0.1	0.2	<0.05	0.1	0.1
Cd	0.1	0.1	0.1	0.1	0.1	0.2	0.1	0.2	0.1	0.2	0.1	0.1	0.1
Sn	3.0	2.0	2.0	2.0	1.0	1.0	<1	1.0	2.0	2.0	2.0	2.0	2.0
Sb	1.7	<0.5	<0.5	<0.5	<0.5	<0.5	<0.5	<0.5	<0.5	<0.5	<0.5	<0.5	<0.5
Te	0.1	0.1	0.1	0.1	0.1	0.1	0.1	0.1	0.1	0.1	0.1	0.1	0.1
Cs	1.6	1.3	0.6	0.6	0.6	0.7	1.6	0.9	0.6	0.7	1.0	0.7	0.6
Ba	496	88	75	88	95	104	395	102	176	138	243	98	107
La	16.7	24.6	13.9	13.6	11.7	10.2	6.4	11.0	14.9	13.9	15.5	14.3	15.2
Ce	39.3	54.5	33.5	32.7	29.3	25.7	17.0	35.1	36.2	34.7	39.8	36.8	38.0
Pr	5.0	7.1	4.6	4.6	4.2	3.7	2.5	3.8	5.0	5.0	5.4	5.4	5.4
Nd	20.3	29.7	21.0	20.8	19.4	17.3	11.7	17.5	23.3	24.0	25.4	25.5	24.3
Sm	4.9	6.6	5.7	5.7	5.1	4.7	3.2	4.9	6.4	6.8	6.4	7.0	6.5
Eu	0.9	2.1	1.8	1.9	1.8	1.6	1.1	1.6	2.2	2.2	1.6	2.3	2.2
Gd	5.3	6.9	6.3	6.4	6.0	5.2	3.8	5.6	7.3	7.6	7.6	7.6	7.2
Tb	0.8	1.0	1.0	1.0	1.0	0.9	0.6	0.9	1.1	1.2	1.2	1.2	1.1
Dy	5.4	6.5	5.9	6.3	5.9	5.2	3.6	5.3	6.7	7.3	7.3	7.0	6.9
Ho	1.1	1.3	1.2	1.3	1.2	1.1	0.8	1.1	1.4	1.5	1.5	1.5	1.4

Er	3.2	3.7	3.4	3.5	3.2	3.1	2.2	3.0	3.6	3.9	4.2	4.0	4.0
Tm	0.5	0.5	0.5	0.5	0.5	0.4	0.3	0.4	0.6	0.6	0.6	0.6	0.6
Yb	3.0	3.1	3.0	3.1	3.0	2.8	2.1	2.6	3.3	3.6	3.6	3.6	3.6
Lu	0.4	0.4	0.4	0.3	0.4	0.3	0.2	0.3	0.4	0.4	0.5	0.4	0.4
Hf	3.7	3.8	4.0	4.0	3.9	3.5	2.4	3.4	4.2	4.7	5.3	5.0	5.1
Ta	0.8	0.9	0.8	0.8	0.8	0.6	0.4	0.7	0.8	0.9	2.4	0.9	0.9
W	28	113	52	60	83	60	30	45	52	32	35	58	75
Tl	0.6	0.2	0.1	0.1	0.1	0.1	0.2	0.2	0.2	0.2	0.3	0.2	0.2
Pb	16	11	10	12	14	17	11	19	25	84	17	19	16
Bi	0.1	0.1	0.0	0.0	0.0	0.0	0.0	0.1	0.1	0.1	0.0	0.1	0.1
Th	2.1	2.9	1.9	1.9	1.8	1.5	1.1	2.0	2.1	2.5	2.9	2.6	2.7
U	1.0	3.0	0.9	0.6	0.5	0.4	b.d.	b.d.	0.4	0.5	0.8	0.6	0.5

(Table S2 continued)

Sample No.	RX 8171	RX 8172	RX 8173	RX 8174	RX 8175	RX 8176	RX 8177	RX 8178	RX 8179	RX 8180	RX 8181	RX 8182	RX 8183
SiO_2	49.8	51.5	50.2	49.3	50.7	49.6	49.4	49.4	49.6	49.7	49.7	49.7	47.5
TiO_2	2.9	2.9	2.7	2.9	2.8	2.9	2.9	2.7	2.7	3.0	2.8	2.9	2.8
Al_2O_3	14.8	14.8	14.6	14.5	15.1	14.8	15.2	14.7	15.2	14.8	15.1	15.0	15.2
FeO_t	15.3	14.9	15.3	13.6	14.8	15.4	13.7	15.8	14.1	15.3	15.4	13.7	15.5
MnO	0.2	0.2	0.2	0.2	0.2	0.2	0.3	0.2	0.2	0.2	0.2	0.2	0.7
MgO	3.6	3.1	3.3	3.1	3.0	3.3	3.8	3.4	3.7	3.0	3.1	3.0	3.2
CaO	5.0	5.8	5.2	6.5	6.5	6.3	5.8	5.6	5.4	5.1	5.2	7.0	5.8
Na_2O	2.9	2.6	2.7	2.5	2.5	2.5	2.6	2.7	2.8	2.7	3.0	2.7	2.8

K_2O	1.1	0.7	1.0	0.9	0.9	1.1	0.9	1.0	1.0	1.2	1.2	1.0	1.2
P_2O_5	0.3	0.3	0.3	0.3	0.2	0.3	0.3	0.3	0.3	0.3	0.3	0.3	0.3
S	518	277	616	136	279	340	258	375	307	368	211	898	339
Li	22.3	20.8	21.0	16.0	14.9	13.3	16.1	15.2	15.0	15.8	15.2	15.3	11.7
Be	1.1	1.0	1.1	1.1	0.8	1.0	1.1	1.0	1.1	1.1	1.1	0.9	1.1
Sc	32	34	33	32	31	33	31	33	30	30	31	31	30
Ti	17455	17595	16484	17205	16604	17605	17175	15944	16114	17865	16984	17345	17065
V	402	376	347	382	373	418	364	372	401	362	347	355	349
Cr	29	22	20	<20	<20	<20	<20	20	21	<20	<20	<20	<20
Co	57.6	59.3	61.1	56.6	56.6	52.6	58.7	56.1	56.0	53.4	47.5	51.6	48.5
Ni	40	38	38	39	35	38	36	39	35	33	30	35	33
Cu	240	356	429	377	328	398	357	348	349	337	160	235	384
Zn	244	234	260	253	287	199	283	362	255	236	228	250	372
Ga	25.7	25.5	25.9	24.7	25.4	25.4	26.9	26.4	26.6	26.2	25.6	29.2	26.0
As	2.4	1.6	3.0	2.3	6.4	4.7	5.2	6.9	5.8	5.5	6.1	6.4	2.5
Rb	34.7	18.7	29.5	25.8	27.4	31.9	28.6	28.8	28.4	36.5	40.0	28.7	33.9
Sr	195	211	198	195	201	200	188	194	188	201	228	340	182
Y	38.2	41.4	41.7	39.8	39.4	39.7	37.6	40.6	40.1	42.0	40.0	38.7	41.0
Zr	180	187	191	170	185	183	179	200	181	196	188	185	183
Nb	12.8	14.0	14.5	13.4	13.1	13.1	13.5	13.1	13.1	14.1	13.4	13.4	13.4
Mo	0.7	0.5	1.1	0.3	0.5	0.3	0.7	0.8	0.7	0.5	0.5	0.2	<0.1
Ag	0.1	0.2	0.2	0.2	0.2	0.1	0.1	0.3	0.2	0.2	0.1	0.1	0.2
Cd	0.1	0.2	0.2	0.2	0.3	0.2	0.6	0.4	0.2	0.2	0.1	0.1	0.3
Sn	1.0	2.0	2.0	1.0	2.0	3.0	2.0	3.0	2.0	3.0	2.0	2.0	4.0
Sb	<0.5	<0.5	<0.5	<0.5	<0.5	<0.5	<0.5	<0.5	<0.5	<0.5	<0.5	0.5	<0.5

Te	0.1	0.1	0.1	0.1	0.1	0.1	0.1	0.1	0.1	0.1	0.1	0.1	0.1
Cs	0.5	0.4	0.5	0.3	0.3	0.3	0.3	0.3	0.3	0.4	0.4	0.3	0.3
Ba	143	128	154	134	126	137	144	153	137	164	140	139	160
La	16.0	14.6	18.2	12.4	15.0	15.1	16.5	19.4	17.9	16.3	14.5	16.3	17.8
Ce	38.7	34.8	43.0	33.5	37.4	36.9	41.0	46.5	43.4	40.7	39.1	41.4	47.0
Pr	5.3	5.1	6.2	4.8	5.3	5.1	5.8	6.5	6.1	5.8	5.2	5.7	5.9
Nd	24.8	23.9	28.3	23.8	24.8	24.9	26.2	29.6	28.7	26.9	25.0	26.6	28.1
Sm	6.7	6.5	7.5	6.5	6.9	6.7	6.7	7.5	7.4	7.3	6.6	6.6	7.2
Eu	2.2	2.3	2.5	2.4	2.3	2.3	2.4	2.3	2.3	2.4	2.3	2.3	2.3
Gd	7.3	7.3	7.9	7.6	7.4	7.4	7.4	8.2	7.9	8.0	7.7	7.5	8.1
Tb	1.1	1.2	1.3	1.2	1.2	1.2	1.1	1.3	1.2	1.3	1.2	1.2	1.3
Dy	6.8	7.1	7.7	7.1	7.2	7.5	6.9	7.4	7.2	7.7	7.4	7.2	7.8
Ho	1.4	1.5	1.5	1.5	1.5	1.5	1.5	1.5	1.5	1.6	1.5	1.5	1.5
Er	3.8	4.3	4.2	3.9	4.0	4.1	4.1	4.3	4.0	4.4	4.1	3.9	4.3
Tm	0.5	0.6	0.6	0.6	0.6	0.6	0.6	0.6	0.6	0.6	0.6	0.6	0.6
Yb	3.7	3.8	3.9	3.5	3.4	3.6	3.3	3.7	3.7	3.8	3.8	3.7	3.8
Lu	0.4	0.5	0.5	0.4	0.5	0.5	0.5	0.5	0.4	0.5	0.4	0.5	0.4
Hf	4.8	5.3	5.6	4.7	5.2	5.1	5.0	5.3	5.1	5.3	5.3	5.1	5.3
Ta	0.9	1.0	0.9	0.8	0.9	0.9	1.0	1.0	0.9	1.0	1.0	1.0	0.9
W	79	125	115	99	94	83	73	74	68	61	50	63	44
Tl	0.2	0.1	0.1	0.1	0.1	0.2	0.1	0.2	0.2	0.2	0.2	0.2	0.2
Pb	16	13	20	24	45	28	28	85	27	61	20	30	65
Bi	0.1	0.0	0.0	0.0	0.1	0.1	0.0	0.1	0.1	0.1	0.0	0.1	0.0
Th	2.5	2.7	2.9	2.4	2.8	2.5	2.8	2.8	2.6	2.9	3.0	2.7	2.8
U	0.5	0.5	0.6	0.5	0.5	0.5	0.4	0.5	0.6	0.5	0.5	0.6	0.6

(Table S2 continued)

Sample No.	RX 8211	RX 8212	RX 8213	RX 8214	RX 8215	RX 8216	RX 8217	RX 8218	RX 8219	RX 8220	RX 8221	RX 8222	RX 8223
SiO_2	49.0	48.0	48.8	48.3	47.9	47.3	48.5	46.4	47.6	46.4	48.8	48.8	49.5
TiO_2	2.7	2.8	2.7	2.8	3.1	3.1	2.6	3.1	3.1	2.7	2.8	2.7	2.8
Al_2O_3	15.1	15.0	15.1	14.5	14.2	14.4	14.7	15.0	14.2	14.4	14.5	14.8	14.7
FeO_t	13.8	13.8	13.5	15.0	15.1	14.5	14.0	15.5	15.5	15.7	14.6	15.0	14.6
MnO	0.3	0.3	0.3	0.3	0.3	0.2	0.3	0.2	0.3	0.2	0.3	0.2	0.2
MgO	2.4	2.6	2.9	3.3	3.1	3.2	3.1	4.3	3.4	3.3	3.2	3.3	3.2
CaO	9.7	9.7	9.7	9.4	9.5	9.7	9.8	5.1	9.9	9.9	9.4	9.4	9.8
Na_2O	2.3	2.3	2.3	2.2	2.2	2.2	2.4	2.4	2.2	2.0	2.3	2.4	2.3
K_2O	0.6	0.6	0.4	0.5	0.5	0.4	0.5	0.4	0.4	0.4	0.5	0.5	0.5
P_2O_5	0.3	0.3	0.3	0.3	0.2	0.3	0.3	0.2	0.3	0.3	0.3	0.3	0.3
S	400	254	205	105	196	149	119	150	135	180	325	159	271
Li	9.0	7.9	7.5	7.2	8.1	11.8	9.3	29.0	12.4	16.1	8.2	9.2	8.0
Be	1.5	1.4	1.2	1.2	1.5	1.6	1.4	1.4	1.4	1.1	1.2	1.3	1.0
Sc	28	28	29	32	31	31	29	33	33	32	30	32	31
Ti	16384	16754	16354	16614	18465	18645	15824	18795	18845	16344	16844	16404	16524
V	249	257	341	368	430	400	343	416	429	369	369	390	359
Cr	<20	<20	<20	<20	<20	<20	<20	27	24	22	20	27	24
Co	35.9	37.5	39.8	50.9	50.4	37.6	44.0	49.4	45.0	52.4	51.7	42.5	47.9
Ni	19	21	30	37	38	35	33	37	38	37	35	38	36
Cu	359	345	346	299	329	326	303	200	288	269	333	307	307
Zn	482	357	246	159	321	255	205	258	154	402	344	201	160

Ga	27.2	25.5	25.0	26.0	25.5	25.3	25.3	25.9	25.7	25.0	25.9	25.8	24.8
As	4.0	2.5	4.2	2.7	8.6	9.7	3.8	5.5	5.2	10.9	3.8	3.2	3.5
Rb	14.1	14.9	10.1	12.3	12.0	8.5	12.4	9.4	9.1	8.2	12.9	11.2	11.8
Sr	209	204	202	192	193	176	195	110	192	160	196	199	204
Y	46.6	41.4	39.5	38.0	39.6	39.7	36.9	38.4	38.0	40.1	40.2	37.2	39.4
Zr	223	201	186	178	178	173	175	189	174	180	177	174	180
Nb	14.5	14.0	12.9	12.0	12.3	12.6	11.8	12.9	12.0	12.1	12.6	11.5	12.2
Mo	0.9	0.9	0.9	0.7	0.9	1.0	0.7	1.1	0.8	1.5	0.9	0.8	0.8
Ag	0.2	0.2	0.3	0.2	0.3	0.3	0.3	0.2	0.2	0.5	0.3	0.2	0.2
Cd	0.9	0.7	0.4	0.3	0.7	0.6	0.4	0.3	0.2	1.1	1.0	0.4	0.3
Sn	3.0	3.0	2.0	2.0	4.0	3.0	2.0	2.0	2.0	2.0	2.0	1.0	2.0
Sb	<0.5	<0.5	<0.5	<0.5	<0.5	<0.5	<0.5	<0.5	<0.5	<0.5	<0.5	<0.5	0.6
Te	0.1	0.1	0.1	0.1	0.1	0.1	0.1	0.1	0.1	0.2	0.1	0.1	0.1
Cs	0.5	0.5	0.6	0.6	0.5	0.4	0.4	0.4	0.3	0.3	0.4	0.4	0.4
Ba	126	136	131	107	107	102	114	91	108	84	125	132	144
La	22.9	19.8	14.8	14.3	17.1	17.9	15.3	13.9	15.9	11.9	24.3	17.6	18.0
Ce	56.4	51.2	36.9	35.8	41.3	43.0	37.0	35.1	38.9	30.4	52.2	41.5	42.7
Pr	7.8	6.5	5.3	5.1	5.8	6.0	5.5	5.2	5.5	4.7	7.0	5.9	6.0
Nd	35.3	30.1	25.4	24.3	26.4	27.3	24.9	25.0	25.5	22.9	31.9	26.8	26.9
Sm	8.9	7.8	7.0	6.3	6.8	7.3	6.6	7.0	6.5	6.6	8.1	7.1	7.0
Eu	2.9	2.5	2.2	2.2	2.6	2.4	2.4	1.8	2.3	2.0	2.4	2.7	2.3
Gd	9.4	8.5	7.3	7.4	7.4	8.0	7.2	7.5	7.2	7.3	8.4	7.2	7.6
Tb	1.5	1.4	1.2	1.2	1.1	1.2	1.1	1.2	1.2	1.2	1.3	1.2	1.2
Dy	8.7	7.9	7.1	7.1	7.1	7.5	6.8	7.2	6.8	7.5	7.6	6.9	7.1
Ho	1.8	1.6	1.5	1.5	1.5	1.6	1.5	1.5	1.4	1.5	1.5	1.4	1.5

Er	4.9	4.5	4.1	3.9	4.0	4.1	3.9	4.0	3.9	4.2	4.2	4.0	4.2
Tm	0.7	0.6	0.6	0.5	0.6	0.6	0.6	0.6	0.6	0.6	0.6	0.5	0.6
Yb	4.3	3.9	3.6	3.5	3.4	3.6	3.5	3.6	3.5	3.6	3.6	3.5	3.5
Lu	0.6	0.5	0.5	0.5	0.4	0.4	0.5	0.4	0.5	0.5	0.5	0.5	0.5
Hf	6.2	5.4	5.2	5.0	4.9	5.0	5.0	5.4	4.9	5.0	5.0	4.8	5.2
Ta	2.0	1.0	0.9	0.9	0.9	1.0	0.9	0.9	0.9	0.8	0.8	0.9	0.8
W	32	34	35	38	32	24	60	22	30	22	56	44	48
Tl	0.1	0.1	0.1	0.1	0.1	0.1	0.1	0.1	0.1	0.1	0.1	0.1	0.1
Pb	42	77	89	70	122	91	64	58	38	162	70	24	19
Bi	0.1	0.1	0.1	0.0	0.1	0.0	0.0	0.0	0.0	0.1	0.1	0.0	0.0
Th	3.2	3.2	2.8	2.7	2.6	2.6	2.6	2.6	2.4	2.7	2.7	2.4	2.6
U	0.8	0.8	0.5	0.5	0.7	0.5	0.5	0.5	0.5	0.5	0.5	0.4	0.5

(Table S2 continued)

Sample No.	RX 8224	RX 8225	RX 8226	RX 8227	RX 8228	RX 8229	RX 8230	RX 8231	RX 8232	RX 8233	RX 8234	RX 8235	RX 8236
SiO_2	48.6	48.5	49.0	48.8	47.2	48.4	49.6	47.4	49.0	49.3	48.7	50.1	49.8
TiO_2	2.8	2.7	2.9	2.4	2.8	2.8	2.8	2.6	2.8	2.6	2.6	2.6	2.3
Al_2O_3	14.5	14.7	14.4	13.9	14.6	14.9	14.5	14.3	14.7	14.9	14.7	14.9	15.3
FeO_t	15.3	14.8	15.5	15.4	16.2	15.1	15.6	15.6	15.4	14.9	16.0	15.2	13.5
MnO	0.2	0.2	0.3	0.2	0.2	0.2	0.2	0.3	0.2	0.2	0.2	0.2	0.2
MgO	3.3	3.4	3.5	3.4	3.5	3.6	3.8	3.3	3.4	3.8	4.0	3.8	4.0
CaO	9.8	9.7	9.3	8.3	7.5	9.7	8.4	10.1	7.9	8.8	8.3	8.4	9.3
Na_2O	2.3	2.3	2.3	2.1	2.3	2.4	2.3	2.1	2.5	2.4	2.4	2.5	2.4

K_2O	0.5	0.5	0.5	0.3	0.5	0.6	0.6	0.7	0.7	0.5	0.7	0.7	0.4
P_2O_5	0.3	0.3	0.2	0.2	0.3	0.3	0.2	0.3	0.3	0.2	0.3	0.3	0.2
S	242	273	344	688	276	173	185	793	660	256	512	141	55
Li	8.2	9.2	8.5	10.9	12.6	9.3	9.4	8.8	9.5	8.6	9.7	9.0	8.1
Be	1.0	1.2	0.9	0.8	1.5	1.3	1.0	1.0	0.9	1.0	0.7	0.8	0.7
Sc	31	31	33	29	32	32	33	31	35	31	33	34	33
Ti	16544	15944	17595	14554	17075	16564	16744	15674	16504	15724	15884	15844	13684
V	376	377	417	369	388	380	403	367	400	382	385	390	375
Cr	27	39	34	24	33	29	33	<20	30	30	37	43	60
Co	49.5	50.2	55.7	55.1	46.9	51.0	53.1	48.9	52.9	51.0	53.0	52.0	48.1
Ni	36	36	39	41	37	38	39	40	40	37	42	45	53
Cu	281	281	325	212	302	285	299	252	294	254	234	308	237
Zn	167	272	192	239	402	156	226	143	122	225	153	145	141
Ga	25.5	25.0	25.2	24.5	25.7	26.2	24.6	27.0	26.5	25.4	25.8	25.0	24.8
As	4.9	4.4	2.7	3.7	6.5	0.9	3.3	4.2	3.7	2.2	3.0	1.4	2.6
Rb	10.9	11.9	11.5	6.9	11.0	13.9	16.0	18.1	20.5	14.4	18.0	18.2	11.3
Sr	199	192	191	159	172	213	172	452	226	204	198	188	188
Y	36.4	38.5	37.9	37.1	37.9	37.8	37.2	38.9	38.2	35.9	38.0	34.9	32.2
Zr	169	191	169	167	171	169	170	166	170	168	166	160	143
Nb	11.6	11.6	11.9	11.2	15.4	11.5	12.2	11.4	11.1	11.0	10.9	10.8	9.0
Mo	0.8	0.8	0.8	0.9	1.1	0.7	0.8	0.8	0.8	0.8	0.7	0.7	0.5
Ag	0.2	0.2	0.2	0.2	0.2	0.1	0.2	0.1	0.1	0.2	0.1	0.1	0.2
Cd	0.4	0.6	0.4	0.4	0.8	0.2	0.4	0.2	0.2	0.8	0.3	0.2	0.3
Sn	2.0	1.0	2.0	2.0	3.0	2.0	2.0	2.0	2.0	2.0	2.0	3.0	1.0
Sb	<0.5	<0.5	<0.5	<0.5	<0.5	<0.5	<0.5	<0.5	<0.5	<0.5	<0.5	<0.5	<0.5

Te	0.1	0.1	0.1	0.1	0.1	0.1	0.1	0.1	0.1	0.1	0.1	0.1	0.1
Cs	0.4	0.4	0.4	0.4	0.4	0.4	0.3	0.3	0.3	0.4	0.4	0.4	0.3
Ba	110	114	118	84	113	114	105	103	118	128	113	129	89
La	19.3	15.7	15.9	11.4	15.0	15.0	14.7	16.0	15.9	14.7	13.9	14.9	12.1
Ce	53.8	38.3	37.7	29.6	38.2	37.8	36.2	38.2	37.3	36.1	34.3	35.9	30.5
Pr	6.3	5.4	5.3	4.5	5.4	5.3	5.1	5.4	5.5	5.2	4.8	5.0	4.2
Nd	29.0	24.9	25.7	21.4	25.5	25.7	23.9	26.2	25.9	24.2	23.7	23.8	20.4
Sm	7.1	6.6	6.5	6.3	6.8	6.9	6.9	6.9	6.9	6.4	6.4	6.2	5.5
Eu	2.2	2.3	2.2	1.9	2.1	2.4	2.1	2.5	2.2	2.1	2.2	2.0	1.9
Gd	7.4	7.4	7.3	7.0	7.5	7.5	7.2	7.5	7.4	6.9	6.8	6.8	5.9
Tb	1.1	1.2	1.1	1.1	1.2	1.2	1.1	1.2	1.2	1.1	1.1	1.1	1.0
Dy	6.9	6.9	6.9	6.8	7.2	7.0	6.8	7.2	7.0	6.5	6.7	6.4	5.7
Ho	1.4	1.4	1.4	1.3	1.5	1.5	1.4	1.5	1.4	1.4	1.4	1.3	1.2
Er	3.8	4.0	3.8	3.9	3.8	4.0	3.8	3.9	3.9	3.8	3.8	3.7	3.3
Tm	0.5	0.5	0.6	0.6	0.6	0.6	0.6	0.6	0.6	0.6	0.6	0.6	0.5
Yb	3.4	3.3	3.4	3.3	3.4	3.6	3.5	3.3	3.5	3.3	3.4	3.4	2.9
Lu	0.4	0.4	0.4	0.4	0.6	0.5	0.4	0.4	0.4	0.4	0.4	0.4	0.4
Hf	4.6	5.2	4.7	4.7	4.8	4.9	4.8	4.8	4.5	4.5	4.5	4.6	3.9
Ta	0.8	0.9	0.9	0.7	0.9	0.9	0.8	0.9	1.1	0.9	0.8	0.7	0.7
W	36	34	37	22	22	55	35	40	51	48	39	48	47
Tl	0.1	0.1	0.1	0.1	0.1	0.1	0.1	0.1	0.1	0.1	0.1	0.1	0.1
Pb	40	63	42	36	32	47	36	15	12	51	15	18	16
Bi	0.1	0.1	0.1	0.1	0.1	0.1	0.1	0.1	0.0	0.1	0.0	0.1	0.1
Th	3.2	2.7	2.4	2.4	2.5	2.4	2.5	2.4	2.4	2.3	2.2	2.3	2.2
U	0.4	0.7	0.4	0.4	0.7	0.5	0.4	0.4	0.4	0.6	b.d.	b.d.	0.4

(Table S2 continued)

Sample No.	RX 8237	RX 8238	RX 8239	RX 8240	RX 8241	RX 8242	RX 8243	RX 8244	RX 8245	RX 8246	RX 8247	RX 8248
SiO_2	48.6	48.9	50.2	50.2	50.4	50.1	49.8	49.8	49.4	48.5	48.5	40.4
TiO_2	2.8	2.9	1.9	2.1	1.8	1.7	2.0	2.4	2.3	2.3	2.4	2.4
Al_2O_3	13.9	13.5	14.8	13.7	13.9	14.1	13.4	12.8	12.6	12.1	12.4	12.9
FeO_t	15.8	15.5	12.7	13.4	12.8	11.8	13.8	15.1	15.3	15.4	15.0	13.3
MnO	0.2	0.3	0.2	0.2	0.2	0.2	0.2	0.2	0.2	0.3	0.3	1.8
MgO	4.5	4.4	5.1	5.6	6.2	6.8	5.7	5.8	6.0	5.9	5.9	3.2
CaO	8.9	8.8	10.5	10.0	10.3	7.1	9.8	9.0	9.2	10.1	9.4	8.8
Na_2O	2.2	2.2	2.3	2.1	2.1	2.7	2.1	2.0	2.0	1.9	2.0	3.0
K_2O	0.4	0.5	0.3	0.2	0.2	0.2	0.3	0.3	0.3	0.2	0.3	1.1
P_2O_5	0.3	0.3	0.2	0.2	0.2	0.1	0.2	0.2	0.2	0.2	0.2	0.3
S	95	419	136	99	25	25	25	150	119	25	213	396
Li	9.1	9.7	7.1	7.8	8.9	24.0	10.1	11.5	11.5	20.1	8.4	38.2
Be	0.8	1.0	0.6	0.8	0.8	1.0	0.9	0.7	0.9	1.1	1.0	2.4
Sc	36	36	35	38	39	36	37	38	38	38	38	39
Ti	16824	17365	11673	12543	11073	10293	12033	14114	13904	13614	14194	14414
V	493	421	359	396	361	362	356	421	417	391	422	424
Cr	55	30	123	113	172	155	137	106	105	86	100	106
Co	53.5	51.9	47.6	54.1	51.7	48.3	58.6	60.0	58.6	53.2	60.1	23.1
Ni	54	46	57	60	76	93	81	76	70	64	69	64
Cu	271	327	205	256	176	66	217	268	215	191	262	451
Zn	145	120	250	133	100	141	145	129	143	124	168	153

Ga	24.3	25.6	22.6	22.1	21.5	20.5	21.4	22.3	22.0	21.2	22.0	22.3
As	1.9	1.6	2.1	0.6	<0.5	<0.5	<0.5	<0.5	<0.5	<0.5	2.5	3.8
Rb	8.5	11.8	7.9	7.3	6.5	8.2	8.3	10.6	8.5	6.8	10.4	58.5
Sr	171	189	182	167	164	115	161	161	156	156	169	126
Y	33.7	39.6	26.5	28.3	25.8	26.6	30.0	32.2	32.2	38.8	32.4	42.1
Zr	153	176	120	125	108	92	124	138	137	137	141	146
Nb	10.0	11.3	7.8	8.1	7.3	7.0	8.8	9.1	9.2	9.4	10.1	11.5
Mo	0.4	0.9	0.5	0.4	0.5	0.3	0.7	0.6	1.9	0.8	0.9	2.3
Ag	0.1	0.2	0.1	0.1	0.1	0.1	0.2	0.1	0.1	0.1	0.1	0.1
Cd	0.2	0.2	0.6	0.3	0.2	0.1	0.2	0.2	0.2	0.3	0.2	0.1
Sn	2.0	2.0	1.0	1.0	<1	1.0	2.0	2.0	<1	2.0	1.0	2.0
Sb	<0.5	<0.5	<0.5	<0.5	<0.5	<0.5	<0.5	<0.5	<0.5	<0.5	<0.5	<0.5
Te	0.1	0.1	0.1	0.1	0.1	<0.05	0.1	0.1	0.1	0.1	0.1	0.1
Cs	0.3	0.5	0.4	0.7	0.5	0.4	0.3	0.9	0.8	1.6	1.1	0.8
Ba	87	107	78	72	79	42	109	93	78	80	84	148
La	12.3	14.9	9.4	10.4	9.2	15.2	11.0	11.7	11.7	19.4	12.7	33.1
Ce	35.0	36.8	23.7	25.4	22.4	42.8	27.3	28.7	29.0	48.8	30.9	71.4
Pr	4.4	5.3	3.4	3.7	3.2	5.7	3.8	4.2	4.0	6.5	4.4	9.1
Nd	21.7	25.1	16.1	17.5	15.5	23.2	18.8	20.5	19.4	27.6	21.0	37.4
Sm	5.9	6.9	4.5	4.6	4.2	5.3	5.1	5.5	5.4	7.1	5.7	7.9
Eu	2.0	2.3	1.6	1.6	1.5	1.6	1.7	1.9	1.9	1.9	1.8	1.8
Gd	6.7	7.6	5.1	5.3	4.8	5.2	5.9	6.2	6.1	7.1	6.3	7.9
Tb	1.0	1.2	0.8	0.8	0.8	0.8	0.9	1.0	1.0	1.1	1.0	1.2
Dy	6.3	7.0	4.8	5.2	4.7	5.0	5.6	6.1	5.9	7.1	6.0	7.5
Ho	1.2	1.5	1.0	1.1	1.0	1.0	1.2	1.2	1.2	1.4	1.2	1.5

Er	3.5	4.0	2.7	2.9	2.7	2.8	3.0	3.4	3.3	4.0	3.3	4.1
Tm	0.5	0.6	0.4	0.4	0.4	0.4	0.4	0.5	0.5	0.6	0.5	0.6
Yb	3.2	3.6	2.4	2.7	2.4	2.6	2.7	2.9	3.0	3.8	3.1	3.7
Lu	0.4	0.4	0.3	0.3	0.3	0.3	0.4	0.3	0.3	0.5	0.4	0.4
Hf	4.3	4.8	3.2	3.4	3.0	2.6	3.6	3.8	4.0	3.9	3.9	3.9
Ta	1.0	0.9	1.1	0.6	0.6	0.5	0.6	0.6	0.6	0.8	0.6	1.0
W	40	29	41	35	32	16	48	34	28	22	20	8
Tl	0.1	0.1	0.1	0.0	0.0	0.0	0.0	0.1	0.1	0.0	0.1	0.2
Pb	11	12	53	11	9	9	53	7	13	19	11	14
Bi	0.0	0.0	0.1	0.0	0.0	0.0	0.1	0.0	0.1	0.1	0.0	0.1
Th	2.3	2.4	1.5	1.7	1.6	1.3	1.6	1.7	1.8	2.2	1.8	2.7
U	0.4	0.6	b.d.	b.d.	b.d.	1.0	b.d.	b.d.	0.4	2.1	0.4	1.3

Major element (oxides) compostions are in wt%, trace element in ppm. b.d. - below detection limits. See Ehrig et al. (2012) for detailed assay methods.

Table S3 Compositions of Cr-spinel inclusions from Wirrda Well, Olympic Dam and Mount Gunson.

Location	SiO_2	TiO_2	Al_2O_3	Cr_2O_3	FeO_{tot}	MnO	MgO	NiO	ZnO	Total	Fe_2O_3	FeO	Mg#	Cr#	Inferred Fo number of host olivine
Wirrda Well															
1	0.09	3.08	10.30	38.30	36.50	0.20	8.70	0.31	0.11	99.16	15.93	22.17	41	71	Fo<80
2	0.07	2.76	10.29	38.81	36.24	0.21	8.55	0.30	0.11	98.92	15.82	22.00	41	72	Fo<80
3	0.06	2.92	8.01	41.95	36.20	0.21	8.14	0.23	0.11	99.35	15.10	22.61	39	78	Fo<80
4	0.07	2.81	9.91	38.94	37.20	0.21	8.21	0.22	0.12	99.31	16.12	22.69	39	72	Fo<80
5	0.08	3.09	9.67	38.41	37.81	0.22	8.05	0.25	0.11	99.31	16.31	23.14	38	73	Fo<80
6	0.09	2.59	10.53	39.72	35.97	0.23	8.56	0.24	0.13	99.60	15.37	22.14	41	72	Fo<80
7	0.05	3.09	9.51	38.14	38.45	0.23	7.82	0.25	0.15	99.36	16.74	23.38	37	73	Fo<80
8	0.06	3.17	9.27	38.15	38.34	0.24	7.79	0.25	0.12	99.04	16.60	23.40	37	73	Fo<80
9	0.02	3.51	9.58	37.16	39.15	0.25	7.77	0.28	0.13	99.56	17.02	23.83	37	72	Fo<80
10	0.06	2.73	10.00	39.59	37.33	0.26	7.69	0.23	0.15	99.58	15.45	23.43	37	73	Fo<80
11	0.06	3.01	9.41	38.45	38.85	0.26	7.03	0.22	0.17	99.06	16.04	24.41	34	73	Fo<80
12	0.08	2.71	9.64	39.40	37.47	0.27	7.44	0.24	0.14	98.93	15.47	23.54	36	73	Fo<80
13	0.06	2.73	10.13	39.91	37.78	0.27	7.46	0.22	0.18	100.27	15.32	24.00	36	73	Fo<80
14	0.08	3.27	9.42	37.53	39.06	0.28	7.42	0.26	0.12	99.09	16.66	24.07	35	73	Fo<80
15	0.08	2.80	9.95	38.68	38.20	0.28	7.39	0.20	0.13	99.30	15.89	23.90	36	72	Fo<80
16	0.08	2.81	9.87	39.49	37.79	0.28	7.58	0.23	0.14	99.83	15.61	23.74	36	73	Fo<80
17	0.04	3.07	9.24	38.25	39.00	0.28	6.96	0.22	0.15	98.83	16.18	24.44	34	74	Fo<80
18	0.15	3.36	9.60	37.25	37.39	0.29	8.54	0.25	0.14	98.64	16.66	22.40	40	72	Fo<80
19	0.07	2.80	9.67	39.06	38.62	0.29	7.33	0.21	0.15	99.83	16.18	24.06	35	73	Fo<80
20	0.30	3.89	9.49	34.44	38.51	0.30	8.73	0.29	0.14	97.87	17.86	22.43	41	71	Fo<80
21	0.19	3.57	9.16	36.82	37.90	0.31	8.48	0.26	0.13	98.52	17.00	22.60	40	73	Fo<80
22	0.05	2.98	8.68	38.07	40.44	0.31	6.64	0.22	0.19	99.31	17.33	24.85	32	75	Fo<80

23	0.05	3.03	8.41	36.73	41.73	0.32	6.34	0.20	0.16	98.81	18.40	25.17	31	75	Fo<80
24	0.10	2.70	10.40	39.43	35.78	0.32	8.48	0.23	0.17	99.13	15.22	22.08	41	72	Fo<80
25	0.20	4.01	8.43	35.60	40.90	0.32	5.79	0.23	0.09	97.15	15.85	26.64	28	74	Fo<80
26	0.10	2.97	9.76	39.44	36.96	0.34	8.48	0.22	0.17	100.05	16.06	22.51	40	73	Fo<80
27	0.08	3.39	8.60	35.36	41.53	0.35	6.33	0.26	0.18	97.89	18.17	25.18	31	73	Fo<80
28	0.23	3.83	9.01	34.28	39.87	0.36	8.18	0.24	0.17	98.05	18.68	23.05	39	72	Fo<80
29	0.08	3.28	9.37	37.43	40.37	0.37	6.35	0.18	0.26	99.34	16.37	25.63	31	73	Fo<80
30	0.07	3.31	9.46	37.46	39.38	0.38	7.42	0.22	0.20	99.58	16.96	24.12	35	73	Fo<80
31	0.23	3.92	8.91	34.35	39.50	0.38	8.08	0.25	0.18	97.61	18.21	23.11	38	72	Fo<80
32	0.23	3.84	8.95	35.19	40.37	0.38	6.02	0.26	0.12	96.94	15.90	26.06	29	73	Fo<80
33	0.13	2.79	9.47	38.21	38.28	0.39	7.64	0.18	0.20	98.97	16.74	23.22	37	73	Fo<80
34	0.14	2.82	9.53	38.41	38.07	0.39	7.61	0.18	0.21	98.99	16.38	23.32	37	73	Fo<80
35	0.32	3.87	8.82	33.73	40.89	0.46	7.39	0.26	0.21	97.80	18.57	24.17	35	72	Fo<80
36	0.13	3.45	8.58	35.06	42.74	0.46	5.98	0.17	0.25	98.68	18.63	25.98	29	73	Fo<80
37	0.15	3.52	8.20	36.14	42.22	0.53	6.31	0.14	0.29	99.33	18.42	25.65	30	75	Fo<80
38	0.13	3.33	8.71	35.44	42.18	0.56	6.08	0.21	0.26	98.75	18.40	25.62	30	73	Fo<80
39	0.05	1.92	14.97	40.45	30.51	0.17	10.65	0.25	0.11	100.32	12.42	19.33	50	64	80<Fo<85
40	0.11	1.87	14.59	40.98	30.26	0.18	10.30	0.25	0.13	99.84	11.77	19.67	48	65	80<Fo<85
41	0.09	1.86	15.53	40.57	28.76	0.19	11.18	0.24	0.14	99.72	11.53	18.38	52	64	80<Fo<85
42	0.03	2.05	14.73	39.92	30.67	0.19	10.40	0.27	0.14	99.64	12.43	19.48	49	65	80<Fo<85
43	0.09	2.76	11.18	39.76	33.99	0.20	9.58	0.31	0.08	99.42	14.66	20.79	45	70	80<Fo<85
44	0.08	2.84	10.57	39.11	34.84	0.20	8.98	0.32	0.11	98.53	14.99	21.35	43	71	80<Fo<85
45	0.07	1.80	15.94	41.15	28.35	0.20	11.28	0.28	0.14	100.32	11.09	18.37	52	63	80<Fo<85
46	0.07	2.99	10.89	38.60	35.31	0.21	9.12	0.31	0.11	99.14	15.35	21.50	43	70	80<Fo<85
47	0.27	1.83	15.48	40.86	26.99	0.23	11.37	0.36	0.09	98.52	10.21	17.81	53	64	80<Fo<85
48	0.09	2.70	12.21	40.60	31.91	0.25	10.37	0.33	0.09	99.90	13.47	19.79	48	69	80<Fo<85
49	0.17	3.37	9.83	37.96	36.27	0.26	9.38	0.34	0.14	99.38	16.57	21.35	44	72	80<Fo<85

50	0.19	3.52	9.56	37.17	36.91	0.27	9.16	0.29	0.12	98.88	16.91	21.69	43	72	80<Fo<85
51	0.17	3.03	11.01	38.23	34.15	0.27	9.55	0.32	0.16	98.39	14.98	20.67	45	70	80<Fo<85
52	0.19	3.37	11.25	37.24	35.52	0.28	9.44	0.29	0.14	99.28	15.57	21.51	44	69	80<Fo<85
53	0.12	3.49	9.91	37.15	37.12	0.28	9.18	0.29	0.10	99.36	17.08	21.75	43	72	80<Fo<85
54	0.16	2.92	11.01	38.62	34.59	0.29	9.68	0.31	0.11	99.22	15.48	20.65	46	70	80<Fo<85
55	0.26	3.16	10.66	37.78	35.19	0.29	8.96	0.33	0.12	98.25	14.99	21.70	42	70	80<Fo<85
56	0.15	2.87	10.40	39.04	36.24	0.31	8.76	0.25	0.23	99.82	15.80	22.02	41	72	80<Fo<85
57	0.36	3.24	10.32	37.02	35.92	0.32	8.91	0.29	0.14	98.08	15.62	21.86	42	71	80<Fo<85
Olympic Dam															
1	0.08	0.98	19.66	35.88	32.21	0.17	10.05	0.08	0.13	100.76	13.07	20.45	47	55	Fo<80
2	0.43	0.40	9.55	51.36	27.06	0.18	7.34	0.08	0.11	97.08	5.74	21.90	37	78	Fo<80
3	0.08	0.67	22.41	35.50	29.71	0.18	10.45	0.12	0.09	100.46	10.88	19.92	48	52	Fo<80
4	0.12	0.31	6.53	53.11	31.27	0.19	6.48	0.03	0.11	99.09	9.32	22.89	34	85	Fo<80
5	0.18	0.22	9.18	53.74	26.46	0.19	7.40	0.08	0.16	98.15	5.45	21.55	38	80	Fo<80
6	0.97	1.03	19.70	34.29	30.80	0.19	10.23	0.15	0.26	97.63	11.37	20.57	47	54	Fo<80
7	0.22	0.24	8.95	53.75	27.54	0.19	7.12	0.06	0.12	98.78	5.87	22.26	36	80	Fo<80
8	0.18	0.25	9.61	53.53	26.53	0.20	7.50	0.08	0.15	98.58	5.46	21.62	38	79	Fo<80
9	0.19	0.38	10.28	51.26	27.30	0.20	7.56	0.08	0.08	97.95	6.31	21.61	38	77	Fo<80
10	0.16	0.26	8.84	52.91	29.47	0.20	6.00	0.03	0.17	98.67	6.26	23.83	31	80	Fo<80
11	0.07	1.09	19.68	36.18	32.12	0.20	9.96	0.09	0.12	100.95	12.67	20.71	46	55	Fo<80
12	0.17	0.38	8.37	53.71	27.49	0.20	7.42	0.04	0.11	98.54	6.44	21.70	38	81	Fo<80
13	0.17	0.30	9.12	53.76	27.67	0.20	7.36	0.06	0.15	99.40	6.23	22.07	37	80	Fo<80
14	0.60	1.01	18.53	34.82	29.30	0.20	9.52	0.22	0.17	94.37	10.42	19.92	46	56	Fo<80
15	0.21	0.30	8.79	53.23	28.18	0.20	6.84	0.04	0.14	98.56	6.19	22.61	35	80	Fo<80
16	0.17	1.79	9.02	53.13	27.83	0.20	6.27	0.05	0.17	98.95	3.21	24.95	31	80	Fo<80
17	0.06	1.02	18.83	37.63	31.63	0.20	9.74	0.10	0.14	99.37	12.13	20.72	46	57	Fo<80
18	0.22	0.30	9.45	52.48	26.99	0.20	7.36	0.07	0.11	97.76	5.89	21.69	38	79	Fo<80

19	0.22	0.38	9.59	52.03	28.10	0.20	7.20	0.08	0.10	98.53	6.48	22.27	37	78	Fo<80
20	0.08	1.00	18.86	36.54	31.31	0.21	9.78	0.08	0.15	99.37	12.27	20.27	46	57	Fo<80
21	0.08	1.40	13.63	35.47	37.54	0.21	9.15	<0.02	0.08	99.42	18.56	20.84	44	64	Fo<80
22	0.08	1.40	13.63	35.47	37.54	0.21	9.15	<0.02	0.08	99.42	18.56	20.84	44	64	Fo<80
23	0.16	0.29	8.78	53.14	29.06	0.21	6.14	0.03	0.18	98.60	6.08	23.59	32	80	Fo<80
24	0.05	0.92	19.17	37.41	31.34	0.21	9.70	0.10	0.10	100.36	11.84	20.68	46	57	Fo<80
25	0.17	0.24	9.38	54.77	27.58	0.22	6.69	0.05	0.18	99.76	4.88	23.19	34	80	Fo<80
26	0.14	0.26	9.15	54.15	27.52	0.22	7.00	0.04	0.16	99.20	5.61	22.48	36	80	Fo<80
27	0.07	1.17	17.93	36.68	32.71	0.22	9.77	0.11	0.13	98.79	13.60	20.47	46	58	Fo<80
28	0.10	0.75	22.21	35.37	30.15	0.22	10.50	0.11	0.18	100.84	11.38	19.91	48	52	Fo<80
29	0.14	0.48	11.89	49.63	29.10	0.22	7.08	0.05	0.11	99.37	6.71	23.06	35	74	Fo<80
30	0.19	0.26	6.57	52.97	30.90	0.22	6.65	0.06	0.12	98.87	9.29	22.54	34	84	Fo<80
31	0.24	0.27	4.77	55.64	26.82	0.22	6.28	0.09	0.08	94.40	5.69	21.70	34	89	Fo<80
32	0.09	0.87	19.70	37.85	30.19	0.22	9.96	0.07	0.14	100.32	10.93	20.35	47	56	Fo<80
33	0.08	0.83	19.98	37.94	30.20	0.22	10.05	0.12	0.11	100.79	10.96	20.34	47	56	Fo<80
34	0.16	0.18	7.65	58.18	22.44	0.23	6.82	0.05	0.15	95.86	1.05	21.50	36	84	Fo<80
35	0.05	1.10	18.36	36.27	32.54	0.23	9.81	0.12	0.11	98.59	13.55	20.35	46	57	Fo<80
36	0.06	0.86	21.56	35.85	30.57	0.23	10.39	0.09	0.10	101.00	11.55	20.17	48	53	Fo<80
37	0.09	0.89	19.04	37.11	31.15	0.23	9.66	0.10	0.08	99.66	11.81	20.52	46	57	Fo<80
38	0.07	1.10	18.11	37.19	32.10	0.23	9.75	0.08	0.15	98.78	12.93	20.47	46	58	Fo<80
39	0.52	0.48	9.92	48.22	30.88	0.23	6.66	0.04	0.19	97.98	8.36	23.35	34	77	Fo<80
40	0.06	1.01	20.81	35.71	30.87	0.23	10.21	0.10	0.16	100.53	11.83	20.23	47	54	Fo<80
41	0.07	0.95	20.26	36.22	30.98	0.23	10.03	0.10	0.16	100.33	11.86	20.31	47	55	Fo<80
42	0.11	1.15	18.48	35.63	32.67	0.24	9.57	0.11	0.11	99.56	13.25	20.75	45	56	Fo<80
43	0.07	1.01	17.68	36.91	32.55	0.24	9.50	0.08	0.11	99.70	13.28	20.59	45	58	Fo<80
44	0.21	0.34	9.22	52.07	29.14	0.24	6.14	0.05	0.15	98.18	6.14	23.61	32	79	Fo<80
45	0.04	1.19	17.37	36.09	33.45	0.24	9.37	0.08	0.14	97.98	14.12	20.75	45	58	Fo<80

46	0.08	1.27	17.58	36.03	33.32	0.24	9.38	0.07	0.10	99.63	13.70	21.00	44	58	Fo<80
47	0.09	1.16	17.81	37.26	32.74	0.24	9.75	0.13	0.08	99.25	13.40	20.67	46	58	Fo<80
48	0.07	1.13	19.10	35.57	31.89	0.24	9.67	0.09	0.16	99.39	12.64	20.52	46	56	Fo<80
49	0.09	0.95	19.24	36.80	31.57	0.24	9.80	0.12	0.07	100.32	12.21	20.58	46	56	Fo<80
50	0.07	0.99	20.53	36.08	31.63	0.24	10.20	0.11	0.12	101.40	12.38	20.49	47	54	Fo<80
51	0.08	1.16	17.44	36.62	33.21	0.24	9.64	0.09	0.12	98.61	14.04	20.58	46	58	Fo<80
52	0.07	1.01	18.47	37.19	31.44	0.24	9.65	0.11	0.12	99.73	12.17	20.49	46	57	Fo<80
53	0.13	1.41	13.64	35.32	37.59	0.25	9.15	<0.02	0.10	99.46	18.58	20.87	44	63	Fo<80
54	0.13	1.41	13.64	35.32	37.59	0.25	9.15	<0.02	0.10	99.46	18.58	20.87	44	63	Fo<80
55	0.06	0.75	19.91	37.91	30.46	0.25	9.90	0.10	0.10	100.65	11.17	20.41	46	56	Fo<80
56	0.25	0.33	6.02	53.67	28.44	0.25	6.16	0.06	0.16	95.36	6.72	22.39	33	86	Fo<80
57	0.07	1.35	17.37	34.96	35.50	0.25	8.83	0.09	0.09	98.51	15.03	21.97	42	57	Fo<80
58	0.10	1.30	18.68	35.31	32.63	0.25	10.03	0.15	0.11	98.57	13.77	20.24	47	56	Fo<80
59	0.07	1.13	17.80	36.83	32.76	0.25	9.52	0.09	0.07	100.04	13.27	20.82	45	58	Fo<80
60	0.10	0.99	18.68	37.82	31.76	0.25	9.75	0.09	0.17	100.97	12.23	20.75	46	58	Fo<80
61	0.08	0.75	20.85	37.45	29.88	0.26	10.07	0.08	0.12	100.71	10.59	20.35	47	55	Fo<80
62	0.03	1.13	18.28	35.50	33.01	0.26	9.63	0.08	0.10	99.58	13.90	20.49	46	57	Fo<80
63	0.08	2.60	17.73	37.55	30.69	0.26	8.66	0.12	0.08	97.76	8.51	23.03	40	59	Fo<80
64	0.14	1.52	13.65	35.58	37.23	0.26	9.19	<0.02	0.08	99.45	18.12	20.93	44	64	Fo<80
65	0.14	1.52	13.65	35.58	37.23	0.26	9.19	<0.02	0.08	99.45	18.12	20.93	44	64	Fo<80
66	0.04	0.73	21.24	37.66	29.74	0.26	10.15	0.10	0.15	101.27	10.42	20.36	47	54	Fo<80
67	0.07	0.17	6.12	52.06	30.69	0.26	6.44	0.06	0.14	96.99	9.79	21.88	34	85	Fo<80
68	0.10	1.40	17.84	34.68	33.62	0.26	9.48	0.09	0.13	99.25	14.20	20.84	45	57	Fo<80
69	0.04	1.60	11.67	29.35	46.22	0.26	7.33	0.30	0.07	96.83	25.83	22.97	36	63	Fo<80
70	2.61	1.14	11.22	29.16	44.48	0.26	6.59	0.30	0.08	95.84	19.91	26.56	31	64	Fo<80
71	0.04	1.62	18.29	28.96	40.14	0.27	9.48	0.13	0.13	101.37	20.62	21.58	44	52	Fo<80
72	0.08	1.21	17.43	36.66	33.61	0.27	9.64	0.14	0.13	99.16	14.34	20.70	45	59	Fo<80

73	0.02	1.06	19.31	35.48	32.45	0.27	9.83	0.15	0.12	100.22	13.37	20.41	46	55	Fo<80
74	0.06	1.65	17.84	36.30	33.13	0.27	9.18	0.10	0.11	100.10	12.61	21.78	43	58	Fo<80
75	0.06	1.30	18.00	36.40	32.60	0.27	9.58	0.06	0.07	99.85	13.02	20.88	45	58	Fo<80
76	0.12	1.63	17.02	27.71	41.41	0.27	8.75	0.14	0.15	99.61	21.58	21.99	41	52	Fo<80
77	0.06	1.15	17.55	36.12	33.36	0.27	9.46	0.08	0.13	99.78	14.05	20.72	45	58	Fo<80
78	0.08	0.84	19.22	37.04	31.10	0.27	9.89	0.08	0.15	100.07	12.13	20.18	47	56	Fo<80
79	0.29	1.72	19.75	26.72	38.98	0.27	9.86	0.18	0.18	100.19	19.80	21.16	45	48	Fo<80
80	0.08	0.72	20.40	38.19	30.50	0.28	9.80	0.12	0.14	101.44	10.76	20.82	46	56	Fo<80
81	0.07	1.05	19.67	36.08	31.92	0.28	9.90	0.10	0.13	100.65	12.61	20.57	46	55	Fo<80
82	0.06	0.96	18.97	37.84	31.31	0.28	9.62	0.08	0.18	100.64	11.69	20.79	45	57	Fo<80
83	0.10	3.10	15.87	37.75	33.07	0.28	7.59	0.09	0.11	97.96	9.06	24.91	35	61	Fo<80
84	0.04	0.83	21.74	35.89	30.28	0.28	10.31	0.15	0.15	100.92	11.32	20.10	48	53	Fo<80
85	0.08	0.42	5.74	49.58	34.58	0.28	6.90	0.08	0.26	99.35	14.12	21.87	36	85	Fo<80
86	0.04	1.36	19.13	29.68	36.77	0.29	10.41	0.24	0.06	100.13	19.08	19.61	49	51	Fo<80
87	0.09	2.76	16.38	37.20	33.05	0.29	7.56	0.14	0.06	97.52	9.40	24.59	35	60	Fo<80
88	0.13	0.28	5.04	55.19	27.76	0.30	5.06	0.07	0.17	94.00	5.06	23.20	28	88	Fo<80
89	0.09	0.81	19.88	37.84	30.24	0.30	9.90	0.11	0.16	100.57	10.98	20.35	46	56	Fo<80
90	0.08	1.30	17.88	36.80	32.59	0.30	9.33	0.09	0.07	99.87	12.66	21.19	44	58	Fo<80
91	0.16	1.46	13.23	35.25	36.91	0.31	8.99	<0.02	0.08	98.20	18.02	20.69	44	64	Fo<80
92	0.16	1.46	13.23	35.25	36.91	0.31	8.99	<0.02	0.08	98.20	18.02	20.69	44	64	Fo<80
93	0.06	0.70	7.95	32.91	46.45	0.32	7.27	0.28	0.11	98.87	27.80	21.43	38	74	Fo<80
94	0.05	0.42	4.87	52.29	33.87	0.32	6.80	0.07	0.16	98.87	12.96	22.21	35	88	Fo<80
95	0.28	0.16	7.22	50.29	30.10	0.34	5.97	0.13	0.22	94.70	8.58	22.38	32	82	Fo<80
96	0.09	1.56	17.80	28.03	41.81	0.34	7.93	0.16	0.26	100.27	20.56	23.30	38	51	Fo<80
97	0.19	1.11	7.51	35.65	43.96	0.34	7.00	0.14	0.28	98.59	24.14	22.23	36	76	Fo<80
98	0.06	0.91	11.02	42.83	35.56	0.35	6.79	0.09	0.15	99.28	13.60	23.32	34	72	Fo<80
99	0.05	3.73	12.95	37.95	34.95	0.35	6.67	0.13	0.14	96.91	10.04	25.91	31	66	Fo<80

100	0.18	0.51	10.02	51.91	28.98	0.36	6.20	0.12	0.12	98.96	5.68	23.87	32	78	Fo<80
101	0.12	0.38	6.22	51.51	32.92	0.36	6.57	0.06	0.21	98.35	11.50	22.57	34	85	Fo<80
102	0.08	0.84	9.55	45.83	32.98	0.37	7.27	0.07	0.18	98.54	12.16	22.04	37	76	Fo<80
103	0.02	1.01	10.18	32.05	43.71	0.37	8.28	0.29	0.12	96.04	25.96	20.34	42	68	Fo<80
104	0.09	0.88	11.03	42.34	35.62	0.37	6.79	0.05	0.17	98.88	13.80	23.20	34	72	Fo<80
105	0.09	0.44	11.53	46.72	30.50	0.38	7.12	0.13	0.15	98.06	9.33	22.11	36	73	Fo<80
106	0.03	0.64	6.59	50.39	33.78	0.39	6.96	0.06	0.23	99.08	12.72	22.34	36	84	Fo<80
107	0.07	0.91	9.73	46.38	35.07	0.40	6.40	0.06	0.13	100.52	12.16	24.12	32	76	Fo<80
108	0.13	0.24	5.15	53.07	33.19	0.40	6.22	0.07	0.19	98.65	11.47	22.87	33	87	Fo<80
109	0.01	0.69	7.57	40.74	41.29	0.40	6.68	0.13	0.22	97.73	20.79	22.58	35	78	Fo<80
110	0.00	1.02	10.81	31.28	45.10	0.40	6.73	0.25	0.13	95.72	24.90	22.68	35	66	Fo<80
111	0.03	0.65	6.56	44.78	37.69	0.41	7.02	0.09	0.22	97.43	17.69	21.77	36	82	Fo<80
112	0.10	0.18	5.81	56.75	25.85	0.41	5.87	0.09	0.20	95.28	4.08	22.18	32	87	Fo<80
113	0.22	0.38	9.59	52.03	28.10	0.41	7.20	0.08	0.10	98.09	6.64	22.12	37	78	Fo<80
114	0.07	0.94	10.49	43.23	34.92	0.41	7.51	0.11	0.23	99.51	14.27	22.08	38	73	Fo<80
115	0.03	0.88	8.15	35.98	44.36	0.42	6.12	0.19	0.21	96.34	23.45	23.25	32	75	Fo<80
116	0.03	0.92	7.16	41.53	41.69	0.42	6.03	0.15	0.29	98.22	19.90	23.78	31	80	Fo<80
117	1.04	0.59	7.13	47.37	35.79	0.42	6.68	0.07	0.28	99.37	12.96	24.13	33	82	Fo<80
118	0.52	0.48	9.92	48.22	30.88	0.43	6.66	0.04	0.19	97.35	8.52	23.22	34	77	Fo<80
119	0.07	0.48	5.08	49.12	36.62	0.44	5.41	0.04	0.22	97.48	14.15	23.89	29	87	Fo<80
120	0.15	0.29	8.60	52.88	30.40	0.44	5.20	0.03	0.16	98.16	6.18	24.84	27	80	Fo<80
121	0.04	0.47	4.94	50.44	34.38	0.45	6.22	0.06	0.24	97.24	13.27	22.43	33	87	Fo<80
122	0.17	0.39	9.18	52.11	30.11	0.46	5.75	0.04	0.15	98.35	6.51	24.26	30	79	Fo<80
123	0.92	0.18	5.92	52.10	29.06	0.47	6.22	0.10	0.19	95.17	7.10	22.68	33	86	Fo<80
124	0.04	0.76	12.44	42.84	34.89	0.48	6.62	0.12	0.13	99.73	12.47	23.67	33	70	Fo<80
125	0.10	0.21	6.12	55.54	30.41	0.48	5.57	0.05	0.25	98.73	7.36	23.79	29	86	Fo<80
126	0.22	0.29	8.76	52.20	30.67	0.48	5.09	0.02	0.15	97.87	6.28	25.01	27	80	Fo<80

127	0.17	1.15	5.36	44.54	39.74	0.48	5.25	0.06	0.23	96.98	16.70	24.70	27	85	Fo<80
128	0.22	0.27	8.35	54.08	29.74	0.48	5.18	0.04	0.18	98.54	5.33	24.94	27	81	Fo<80
129	0.09	0.44	11.33	43.01	34.51	0.53	6.25	0.09	0.22	97.87	12.66	23.11	33	72	Fo<80
130	0.07	0.58	5.14	49.00	35.59	0.55	5.85	0.07	0.29	97.13	14.01	22.98	31	86	Fo<80
131	0.08	0.39	16.71	44.68	25.48	0.29	8.38	0.10	0.17	96.29	5.31	20.69	42	64	Fo<80
132	0.13	0.32	14.88	50.06	25.93	0.33	5.98	0.07	0.17	97.87	1.55	24.53	30	69	Fo<80
133	0.12	0.30	14.02	48.77	29.03	0.51	5.83	0.06	0.22	98.85	4.75	24.75	30	70	Fo<80
134	0.23	0.19	8.98	58.97	15.90	0.11	14.12	0.15	0.06	99.16	4.65	11.71	68	82	Fo > 85
135	0.28	0.21	9.07	59.20	14.77	0.11	14.87	0.18	0.03	99.18	4.58	10.65	71	81	Fo > 85
136	0.17	0.22	9.10	58.88	16.17	0.12	14.05	0.18	0.06	99.42	4.83	11.82	68	81	Fo > 85
137	0.62	0.21	9.08	58.61	14.77	0.12	14.77	0.18	0.05	98.82	4.05	11.13	70	81	Fo > 85
138	0.20	0.23	10.47	56.59	16.58	0.12	13.60	0.15	0.08	98.48	4.57	12.47	66	78	Fo > 85
139	0.23	0.19	9.96	57.74	17.13	0.13	13.02	0.14	0.07	99.02	4.04	13.49	63	80	Fo > 85
140	0.19	0.19	10.08	58.39	14.92	0.13	14.45	0.16	0.04	98.95	4.06	11.26	70	80	Fo > 85
141	0.49	0.18	9.02	56.66	18.87	0.14	12.26	0.14	0.20	98.45	4.85	14.50	60	81	Fo > 85
142	0.13	0.19	9.03	59.09	14.57	0.14	14.50	0.15	0.16	98.40	4.37	10.64	71	81	Fo > 85
143	0.29	0.24	9.51	55.82	19.60	0.14	12.09	0.10	0.05	98.38	5.35	14.78	59	80	Fo > 85
144	0.23	0.29	9.49	55.47	21.36	0.15	10.81	0.11	0.05	98.48	5.15	16.72	54	80	Fo > 85
145	0.19	0.22	9.00	56.18	20.53	0.15	11.99	0.13	0.07	99.09	6.30	14.86	59	81	Fo > 85
146	0.21	0.19	8.66	57.20	20.77	0.15	10.78	0.09	0.06	98.58	4.66	16.58	54	82	Fo > 85
147	0.26	0.20	9.10	56.45	20.69	0.15	10.98	0.10	0.07	98.48	4.80	16.36	54	81	Fo > 85
148	0.16	0.20	9.04	57.80	19.16	0.16	11.66	0.14	0.05	98.80	4.32	15.27	58	81	Fo > 85
149	0.13	0.39	13.92	48.72	23.75	0.17	10.58	0.20	0.09	98.63	6.82	17.61	52	70	Fo > 85
150	0.15	0.25	9.64	55.64	22.85	0.17	9.87	0.14	0.10	99.31	5.14	18.22	49	79	Fo > 85
151	0.13	0.19	9.01	58.97	14.82	0.17	14.23	0.16	0.18	98.29	4.30	10.95	70	81	Fo > 85
152	0.24	0.26	8.85	55.52	22.34	0.17	10.59	0.04	0.09	98.70	5.91	17.02	53	81	Fo > 85
153	0.61	0.13	5.43	57.42	20.69	0.17	13.21	0.16	0.23	98.94	8.96	12.62	65	88	Fo > 85

154	0.13	0.37	7.37	51.90	27.23	0.17	9.85	0.15	0.15	98.41	10.78	17.52	50	83	Fo > 85
155	0.19	0.18	9.05	58.07	17.11	0.18	12.41	0.14	0.20	97.53	3.79	13.69	62	81	Fo > 85
156	0.22	0.31	9.64	53.81	24.13	0.18	9.63	0.08	0.10	98.70	6.17	18.58	48	79	Fo > 85
157	0.17	0.23	8.59	57.54	22.40	0.18	9.54	0.14	0.09	99.29	4.26	18.57	48	82	Fo > 85
158	0.39	0.34	10.10	52.04	24.27	0.18	9.74	0.09	0.08	97.88	6.46	18.46	48	78	Fo > 85
159	0.22	0.24	9.37	54.50	22.96	0.18	9.91	0.06	0.09	98.10	5.66	17.87	50	80	Fo > 85
160	0.17	0.35	9.79	54.60	22.90	0.19	9.94	0.11	0.07	98.65	5.37	18.07	50	79	Fo > 85
161	0.29	0.14	6.45	56.11	24.57	0.19	9.79	0.13	0.24	98.70	7.80	17.55	50	85	Fo > 85
162	0.18	0.22	8.99	57.41	22.53	0.19	9.74	0.12	0.10	99.92	4.44	18.54	48	81	Fo > 85
163	0.19	0.18	8.54	58.19	19.05	0.19	11.77	0.10	0.25	98.46	4.63	14.88	59	82	Fo > 85
164	0.24	0.20	7.85	58.05	18.35	0.19	10.75	0.11	0.14	95.88	3.00	15.65	55	83	Fo > 85
165	0.15	0.17	7.52	56.82	22.30	0.21	10.54	0.10	0.11	97.93	6.44	16.51	53	84	Fo > 85
166	0.19	0.20	8.52	57.55	18.83	0.21	11.57	0.13	0.26	97.46	4.45	14.83	58	82	Fo > 85
167	0.22	0.16	8.58	58.47	17.91	0.21	12.62	0.12	0.28	98.58	4.79	13.59	62	82	Fo > 85
168	0.16	0.18	8.62	58.19	19.89	0.21	11.54	0.11	0.22	99.13	4.96	15.42	57	82	Fo > 85
169	0.22	0.51	9.62	45.76	30.37	0.22	9.89	0.20	0.12	98.31	13.84	17.92	50	76	Fo > 85
170	0.08	0.22	5.09	54.15	25.96	0.22	9.97	0.13	0.12	95.93	10.68	16.35	52	88	Fo > 85
171	0.24	0.17	8.89	57.40	17.90	0.22	13.12	0.12	0.16	98.23	5.54	12.92	64	81	Fo > 85
172	0.21	0.24	4.00	53.35	29.86	0.23	8.73	0.11	0.10	96.83	12.50	18.61	46	90	Fo > 85
173	0.18	0.17	7.26	56.96	21.62	0.24	10.97	0.13	0.15	97.69	6.59	15.69	55	84	Fo > 85
174	0.09	0.13	6.22	45.14	34.53	0.24	9.73	0.17	0.11	98.30	19.42	17.05	50	83	Fo > 85
175	0.19	0.19	9.23	57.96	16.28	0.24	13.17	0.12	0.21	97.59	4.15	12.54	65	81	Fo > 85
176	0.20	0.18	7.03	55.66	24.01	0.25	9.38	0.11	0.15	96.97	6.79	17.90	48	84	Fo > 85
177	0.31	0.24	4.50	46.58	35.65	0.26	9.10	0.16	0.10	98.83	19.26	18.32	47	87	Fo > 85
178	0.17	0.22	9.10	58.88	16.17	0.26	14.05	0.18	0.06	99.09	4.94	11.72	68	81	Fo > 85
179	0.18	0.16	7.84	56.73	21.73	0.27	10.63	0.09	0.17	97.81	6.01	16.32	54	83	Fo > 85
180	0.07	0.14	5.98	50.88	27.58	0.27	12.03	0.22	0.05	98.82	15.44	13.68	61	85	Fo > 85

181	0.15	0.18	5.20	53.83	26.95	0.27	9.87	0.15	0.07	96.67	11.27	16.80	51	87	Fo > 85
182	0.12	0.20	6.45	56.21	22.82	0.28	12.47	0.16	0.06	99.83	10.19	13.65	62	85	Fo > 85
183	0.10	0.20	6.97	49.72	27.74	0.28	10.75	0.19	0.15	97.53	13.68	15.43	55	83	Fo > 85
184	0.06	0.11	6.32	54.37	24.90	0.28	12.17	0.19	0.07	99.80	12.29	13.84	61	85	Fo > 85
185	0.20	0.20	7.30	56.07	22.49	0.28	10.91	0.12	0.09	97.67	7.36	15.87	55	84	Fo > 85
186	0.06	0.26	4.80	43.37	38.93	0.29	8.95	0.19	0.10	99.24	22.91	18.30	47	86	Fo > 85
187	0.10	0.15	6.26	53.89	25.32	0.29	11.74	0.13	0.14	99.24	12.15	14.38	59	85	Fo > 85
188	0.06	0.10	6.06	54.79	24.56	0.30	12.25	0.14	0.06	99.59	12.12	13.64	62	86	Fo > 85
189	0.08	0.06	6.26	54.10	25.06	0.30	11.87	0.16	0.13	99.35	12.20	14.08	60	85	Fo > 85
190	0.17	0.08	4.95	50.56	30.39	0.31	10.83	0.12	0.10	99.23	16.48	15.55	55	87	Fo > 85
191	0.29	0.19	4.69	47.13	33.66	0.31	10.45	0.19	0.09	98.93	19.45	16.15	54	87	Fo > 85
192	0.49	0.18	9.02	56.66	18.87	0.31	12.26	0.14	0.20	98.13	4.98	14.39	60	81	Fo > 85
193	0.12	0.14	6.39	49.86	28.58	0.31	11.93	0.23	0.07	99.31	16.15	14.05	60	84	Fo > 85
194	0.11	0.13	4.94	57.07	25.24	0.32	11.68	0.13	0.07	100.91	11.55	14.85	58	89	Fo > 85
195	0.28	0.18	7.47	55.86	23.74	0.32	9.48	0.08	0.17	98.22	6.32	18.05	48	83	Fo > 85
196	0.23	0.10	6.10	52.59	25.88	0.34	11.92	0.18	0.06	98.77	13.17	14.02	60	85	Fo > 85
197	0.18	0.18	7.29	50.09	27.57	0.34	11.78	0.22	0.15	99.29	14.58	14.45	59	82	Fo > 85
198	0.21	0.20	9.09	57.87	15.32	0.34	13.96	0.11	0.29	97.40	4.68	11.11	69	81	Fo > 85
199	0.04	0.11	5.78	51.04	29.14	0.34	11.33	0.20	0.11	99.73	15.90	14.83	58	86	Fo > 85
200	0.12	0.21	6.30	43.25	35.75	0.35	11.00	0.20	0.12	99.61	22.53	15.47	56	82	Fo > 85
201	0.14	0.14	5.68	58.09	21.99	0.36	12.50	0.16	0.04	100.05	9.48	13.46	62	87	Fo > 85
202	0.09	0.12	6.38	53.30	26.46	0.36	11.34	0.20	0.09	99.63	12.73	15.00	57	85	Fo > 85
203	1.48	0.21	7.47	47.03	29.25	0.36	10.98	0.22	0.20	98.61	13.44	17.16	53	81	Fo > 85
204	0.07	0.19	6.89	47.94	29.54	0.36	11.28	0.26	0.05	98.23	16.51	14.68	58	82	Fo > 85
205	0.07	0.14	5.77	41.96	37.86	0.37	10.66	0.22	0.09	99.66	24.58	15.74	55	83	Fo > 85
206	0.04	0.18	4.28	53.12	29.03	0.38	10.82	0.20	0.12	99.74	15.15	15.40	56	89	Fo > 85
207	0.38	0.20	7.09	49.60	27.83	0.39	10.82	0.20	0.21	98.12	13.46	15.72	55	82	Fo > 85

208	0.16	0.22	4.33	52.19	29.82	0.40	10.69	0.14	0.12	99.64	15.56	15.82	55	89	Fo > 85
209	0.17	0.35	9.79	54.60	22.90	0.40	9.94	0.11	0.07	98.32	5.53	17.93	50	79	Fo > 85
210	0.15	0.19	6.31	48.86	30.43	0.40	11.68	0.18	0.09	100.13	17.50	14.68	59	84	Fo > 85
211	0.09	0.10	3.79	55.88	27.00	0.41	10.68	0.12	0.11	99.46	12.74	15.54	55	91	Fo > 85
212	0.05	0.13	5.44	40.94	38.44	0.41	10.50	0.27	0.24	98.96	25.56	15.44	55	83	Fo > 85
213	0.06	0.09	3.96	55.59	26.93	0.41	10.86	0.17	0.08	99.46	13.03	15.21	56	90	Fo > 85
214	0.29	0.14	6.45	56.11	24.57	0.41	9.79	0.13	0.24	98.15	7.96	17.40	50	85	Fo > 85
215	0.09	0.10	5.26	53.55	28.25	0.41	10.79	0.15	0.13	100.11	13.89	15.75	55	87	Fo > 85
216	0.22	0.12	5.95	57.51	22.25	0.42	12.24	0.13	0.08	99.87	9.31	13.87	61	87	Fo > 85
217	0.00	0.44	6.07	44.63	35.40	0.43	10.70	0.23	0.17	100.25	21.56	15.99	54	83	Fo > 85
218	0.17	0.36	5.13	42.46	37.76	0.43	9.73	0.28	0.20	98.89	23.14	16.93	51	85	Fo > 85
219	0.08	0.18	5.02	48.08	32.35	0.43	10.37	0.26	0.04	98.72	18.34	15.84	54	87	Fo > 85
220	0.27	0.11	3.59	54.16	28.53	0.43	10.31	0.17	0.13	99.07	13.82	16.09	53	91	Fo > 85
221	0.11	0.10	3.48	57.15	26.64	0.43	10.85	0.17	0.10	100.28	12.42	15.46	56	92	Fo > 85
222	0.19	0.09	5.13	55.74	25.46	0.44	11.45	0.15	0.11	99.94	11.86	14.79	58	88	Fo > 85
223	0.08	0.13	4.88	55.65	24.16	0.44	11.77	0.19	0.10	98.56	11.60	13.71	60	88	Fo > 85
224	0.09	0.16	3.80	51.25	32.00	0.45	10.15	0.14	0.09	99.86	17.31	16.43	52	90	Fo > 85
225	0.50	0.17	3.71	53.31	29.52	0.45	9.81	0.10	0.18	99.11	13.65	17.24	50	91	Fo > 85
226	0.08	0.34	5.86	47.39	32.96	0.46	10.34	0.20	0.14	99.65	18.41	16.40	53	84	Fo > 85
227	0.17	0.21	6.66	41.00	38.02	0.47	10.39	0.25	0.17	99.81	24.08	16.35	53	81	Fo > 85
228	0.05	0.12	5.15	48.64	33.13	0.48	10.56	0.17	0.11	100.31	19.08	15.96	54	86	Fo > 85
229	0.07	0.11	4.94	54.32	26.74	0.51	10.54	0.16	0.09	98.72	12.43	15.56	55	88	Fo > 85
230	0.17	0.19	3.17	55.45	30.53	0.52	9.06	0.08	0.14	100.68	13.50	18.39	47	92	Fo > 85
231	0.35	0.07	5.01	39.06	40.86	0.55	8.75	0.26	0.27	97.78	25.59	17.83	47	84	Fo > 85
232	0.16	0.15	7.49	49.55	27.56	0.57	11.16	0.22	0.05	98.39	14.01	14.95	57	82	Fo > 85
233	0.17	0.22	4.79	52.22	30.71	0.27	8.44	0.11	0.10	97.04	12.85	19.14	44	88	Fo > 85
234	0.11	0.32	19.51	44.27	19.72	0.24	13.80	0.15	0.09	98.21	6.86	13.55	64	60	Fo > 85

235	0.12	0.30	16.37	49.81	18.30	0.20	13.69	0.18	0.09	99.07	5.37	13.47	64	67	Fo > 85
236	0.11	0.31	19.34	44.55	20.07	0.30	13.51	0.16	0.11	98.47	6.80	13.95	63	61	Fo > 85
237	0.13	0.32	15.93	49.75	19.32	0.21	13.16	0.11	0.06	98.98	5.57	14.31	62	68	Fo > 85
238	0.03	0.29	15.57	50.66	19.12	0.24	13.01	0.15	0.06	99.13	5.35	14.31	62	69	Fo > 85
239	0.15	0.26	15.99	49.79	18.56	0.50	12.76	0.15	0.30	98.45	4.90	14.14	62	68	Fo > 85
240	0.11	0.28	16.04	48.82	19.72	0.42	12.63	0.16	0.14	98.32	5.77	14.53	61	67	Fo > 85
241	0.08	0.32	16.61	46.62	21.48	0.17	12.74	0.14	0.10	98.27	7.46	14.76	61	65	Fo > 85
242	0.09	0.36	18.14	46.50	20.59	0.22	12.92	0.14	0.05	99.02	6.22	14.99	61	63	Fo > 85
243	0.14	0.28	15.21	49.81	19.80	0.27	12.27	0.13	0.10	98.02	5.23	15.09	59	69	Fo > 85
244	0.12	0.34	18.44	45.94	20.29	0.31	11.44	0.15	0.12	97.14	4.18	16.53	55	63	Fo > 85
245	0.15	0.29	14.82	50.62	22.38	0.29	10.14	0.09	0.15	98.93	4.24	18.56	49	70	80<Fo<85
246	0.38	0.23	9.08	54.22	23.19	0.16	8.81	0.14	0.27	96.94	4.51	19.13	45	80	80<Fo<85
247	0.17	0.26	8.56	56.37	24.54	0.17	7.63	0.07	0.19	98.32	3.70	21.21	39	82	80<Fo<85
248	0.56	0.22	8.37	55.26	24.75	0.17	7.76	0.12	0.28	97.88	3.98	21.17	40	82	80<Fo<85
249	0.06	0.53	18.36	43.60	26.51	0.17	10.15	0.12	0.12	100.51	7.64	19.64	48	61	80<Fo<85
250	0.08	0.78	21.29	37.64	28.28	0.17	11.01	0.16	0.11	100.69	10.27	19.03	51	54	80<Fo<85
251	0.18	0.82	8.39	56.85	24.60	0.18	8.26	0.03	0.19	99.86	3.71	21.26	41	82	80<Fo<85
252	0.20	0.42	10.79	51.29	25.72	0.18	9.67	0.05	0.12	99.20	7.58	18.91	48	76	80<Fo<85
253	0.05	1.36	13.69	35.93	36.70	0.18	9.38	<0.02	0.07	99.17	18.12	20.39	45	64	80<Fo<85
254	0.05	1.36	13.69	35.93	36.70	0.18	9.38	<0.02	0.07	99.17	18.12	20.39	45	64	80<Fo<85
255	0.24	0.54	6.95	52.59	27.96	0.18	8.00	0.14	0.17	97.61	8.43	20.38	41	84	80<Fo<85
256	0.07	1.13	20.07	37.25	28.85	0.18	11.14	0.17	0.15	99.02	11.29	18.69	52	55	80<Fo<85
257	0.23	0.61	8.41	56.78	24.41	0.18	8.62	0.05	0.14	99.86	4.25	20.58	43	82	80<Fo<85
258	0.26	0.23	8.68	55.88	23.43	0.18	9.13	0.10	0.08	98.45	4.82	19.09	46	81	80<Fo<85
259	0.06	1.05	19.66	36.73	29.59	0.19	10.78	0.18	0.12	98.36	11.88	18.89	50	56	80<Fo<85
260	0.07	0.82	21.65	36.34	30.18	0.19	10.51	0.11	0.19	101.34	11.27	20.04	48	53	80<Fo<85
261	0.17	0.28	9.51	54.80	26.10	0.19	7.72	0.07	0.14	99.47	4.97	21.62	39	79	80<Fo<85

262	0.08	0.80	20.95	37.66	28.50	0.19	11.06	0.16	0.13	100.77	10.69	18.88	51	55	80<Fo<85
263	0.10	1.12	19.82	37.55	28.94	0.19	11.19	0.16	0.12	99.19	11.39	18.69	52	56	80<Fo<85
264	0.22	0.28	9.52	54.44	23.71	0.19	9.37	0.10	0.10	98.45	5.43	18.82	47	79	80<Fo<85
265	0.19	0.26	8.60	54.42	25.70	0.19	7.82	0.05	0.10	97.86	5.39	20.85	40	81	80<Fo<85
266	0.10	1.27	19.62	36.72	30.06	0.19	11.08	0.15	0.13	99.31	12.28	19.01	51	56	80<Fo<85
267	0.26	0.47	10.94	50.90	24.79	0.19	9.47	0.08	0.09	97.83	6.51	18.94	47	76	80<Fo<85
268	0.15	0.27	8.60	55.38	25.05	0.19	8.50	0.04	0.13	98.85	5.52	20.08	43	81	80<Fo<85
269	0.18	0.23	9.21	55.11	26.33	0.19	7.70	0.11	0.14	99.72	5.27	21.59	39	80	80<Fo<85
270	0.40	0.32	9.10	53.53	24.29	0.19	9.16	0.05	0.10	97.72	5.71	19.15	46	80	80<Fo<85
271	0.05	1.09	19.13	36.84	30.40	0.19	10.59	0.13	0.11	98.53	12.40	19.24	50	56	80<Fo<85
272	0.09	1.05	18.27	36.75	32.34	0.19	10.03	0.15	0.17	99.04	13.62	20.09	47	57	80<Fo<85
273	0.26	0.27	9.14	54.83	23.78	0.19	9.25	0.05	0.08	98.37	5.27	19.03	46	80	80<Fo<85
274	0.10	1.08	20.49	36.89	29.19	0.19	11.21	0.19	0.11	99.44	11.56	18.78	52	55	80<Fo<85
275	0.06	0.73	21.36	37.09	28.09	0.19	11.19	0.18	0.09	100.26	10.65	18.51	52	54	80<Fo<85
276	0.21	0.35	9.80	53.24	26.41	0.19	7.76	0.08	0.13	98.73	5.50	21.46	39	78	80<Fo<85
277	0.27	0.29	9.31	52.59	25.86	0.20	8.50	0.06	0.09	97.82	6.50	20.01	43	79	80<Fo<85
278	0.05	1.03	19.67	37.38	30.38	0.20	10.78	0.16	0.16	99.83	12.29	19.32	50	56	80<Fo<85
279	0.24	0.24	9.63	53.53	25.77	0.20	7.86	0.07	0.11	98.16	5.23	21.06	40	79	80<Fo<85
280	0.22	1.05	18.24	36.48	31.32	0.20	9.83	0.16	0.14	97.65	12.44	20.12	47	57	80<Fo<85
281	0.11	1.10	19.88	37.97	28.81	0.20	11.30	0.18	0.07	99.62	11.27	18.67	52	56	80<Fo<85
282	0.06	0.61	18.48	42.26	27.43	0.20	9.88	0.10	0.12	100.12	8.25	20.00	47	61	80<Fo<85
283	0.09	0.85	20.38	37.56	27.96	0.20	11.29	0.19	0.11	99.88	10.84	18.21	53	55	80<Fo<85
284	0.05	1.03	19.67	37.58	29.00	0.20	11.13	0.18	0.19	99.02	11.71	18.46	52	56	80<Fo<85
285	0.14	1.21	19.82	36.70	29.79	0.20	10.98	0.16	0.12	99.12	11.85	19.12	51	55	80<Fo<85
286	0.09	1.03	19.53	37.51	30.80	0.20	10.63	0.13	0.12	100.04	12.33	19.70	49	56	80<Fo<85
287	0.12	0.32	11.16	51.52	25.88	0.20	8.47	0.07	0.14	98.50	6.16	20.34	43	76	80<Fo<85
288	0.12	0.29	8.74	54.72	25.82	0.20	8.24	0.04	0.11	98.88	5.93	20.48	42	81	80<Fo<85

289	0.17	0.74	9.13	56.75	24.11	0.20	8.62	0.15	0.24	100.47	3.73	20.75	43	81	80<Fo<85
290	0.10	0.92	20.26	37.25	29.03	0.21	11.02	0.15	0.12	100.34	11.33	18.83	51	55	80<Fo<85
291	0.08	1.03	19.74	37.14	29.12	0.21	10.99	0.17	0.13	98.62	11.62	18.67	51	56	80<Fo<85
292	0.04	1.20	18.78	36.17	31.32	0.21	10.56	0.14	0.14	98.56	13.35	19.30	49	56	80<Fo<85
293	0.11	1.14	19.53	37.74	29.45	0.21	11.04	0.18	0.17	99.56	11.67	18.94	51	56	80<Fo<85
294	0.07	0.97	20.30	37.46	28.67	0.21	11.22	0.19	0.14	99.23	11.30	18.50	52	55	80<Fo<85
295	0.19	0.96	11.43	34.87	39.33	0.21	9.06	0.29	0.09	98.60	21.74	19.77	45	67	80<Fo<85
296	0.13	0.25	11.51	52.26	25.22	0.21	8.15	0.11	0.15	98.48	4.92	20.79	41	75	80<Fo<85
297	0.14	0.19	6.77	56.06	22.85	0.21	7.85	0.14	0.19	94.42	4.01	19.25	42	85	80<Fo<85
298	0.06	0.90	20.61	37.00	28.88	0.21	11.04	0.17	0.12	100.25	11.27	18.74	51	55	80<Fo<85
299	0.00	0.87	18.04	39.39	30.03	0.21	9.65	0.06	0.13	99.66	10.84	20.28	46	59	80<Fo<85
300	0.21	0.22	8.82	56.03	25.07	0.21	7.90	0.11	0.12	99.14	4.45	21.07	40	81	80<Fo<85
301	0.06	0.82	22.01	35.90	29.98	0.21	10.54	0.12	0.18	101.09	11.18	19.91	49	52	80<Fo<85
302	0.18	0.24	8.87	54.70	25.84	0.21	7.78	0.03	0.09	98.49	5.25	21.12	40	81	80<Fo<85
303	0.21	0.32	11.66	52.74	22.87	0.21	8.43	0.11	0.13	97.00	3.06	20.12	43	75	80<Fo<85
304	0.07	0.98	20.09	37.56	29.20	0.21	11.02	0.19	0.12	99.44	11.48	18.87	51	56	80<Fo<85
305	0.13	0.24	9.88	54.52	23.56	0.22	8.98	0.10	0.21	98.34	4.89	19.15	46	79	80<Fo<85
306	0.08	1.01	20.67	35.71	29.11	0.22	11.20	0.18	0.10	98.28	11.94	18.37	52	54	80<Fo<85
307	0.09	0.99	14.63	37.06	34.39	0.22	10.96	0.20	0.13	100.60	18.21	18.00	52	63	80<Fo<85
308	0.04	1.09	19.88	35.80	31.17	0.22	10.73	0.14	0.09	99.14	13.17	19.32	50	55	80<Fo<85
309	0.30	0.54	10.80	48.36	27.52	0.22	8.48	0.05	0.11	97.18	8.05	20.28	43	75	80<Fo<85
310	0.06	1.09	20.36	37.02	28.71	0.22	11.07	0.19	0.12	100.13	11.07	18.75	51	55	80<Fo<85
311	0.07	0.93	20.37	37.25	29.16	0.22	11.06	0.16	0.13	100.63	11.48	18.83	51	55	80<Fo<85
312	0.09	0.89	20.37	37.61	28.20	0.22	11.09	0.19	0.15	100.06	10.72	18.56	52	55	80<Fo<85
313	0.06	1.25	18.82	37.13	30.99	0.22	10.48	0.13	0.14	99.22	12.56	19.69	49	57	80<Fo<85
314	0.10	1.11	20.14	36.40	29.40	0.22	10.90	0.16	0.14	98.56	11.63	18.93	51	55	80<Fo<85
315	0.07	1.04	20.00	37.25	29.35	0.22	11.07	0.17	0.10	99.27	11.74	18.79	51	56	80<Fo<85

316	0.15	0.20	7.36	57.35	22.23	0.22	8.50	0.11	0.27	96.39	3.67	18.93	44	84	80<Fo<85
317	0.09	0.88	20.74	37.78	28.64	0.22	10.99	0.15	0.16	100.85	10.67	19.03	51	55	80<Fo<85
318	0.07	0.98	20.10	37.13	29.42	0.22	10.78	0.16	0.11	100.28	11.40	19.16	50	55	80<Fo<85
319	0.07	1.08	18.55	37.94	31.14	0.22	10.28	0.06	0.13	99.47	12.41	19.97	48	58	80<Fo<85
320	0.09	1.11	18.16	36.13	32.57	0.22	10.15	0.11	0.17	98.72	14.13	19.86	48	57	80<Fo<85
321	0.11	1.06	19.30	38.21	29.47	0.23	10.79	0.19	0.11	99.46	11.39	19.21	50	57	80<Fo<85
322	0.09	1.21	19.76	36.57	30.54	0.23	10.86	0.14	0.10	99.49	12.42	19.36	50	55	80<Fo<85
323	0.12	1.37	13.93	36.06	36.31	0.23	9.47	<0.02	0.07	99.34	17.69	20.39	45	63	80<Fo<85
324	0.12	1.37	13.93	36.06	36.31	0.23	9.47	<0.02	0.07	99.34	17.69	20.39	45	63	80<Fo<85
325	0.06	0.97	19.79	37.35	30.09	0.23	10.75	0.13	0.13	100.85	11.98	19.31	50	56	80<Fo<85
326	0.12	1.07	19.81	35.74	29.48	0.23	10.82	0.17	0.15	98.93	11.97	18.71	51	55	80<Fo<85
327	0.07	0.72	20.98	38.03	28.28	0.23	11.17	0.21	0.10	101.01	10.68	18.67	52	55	80<Fo<85
328	0.09	0.95	20.22	38.20	28.67	0.23	11.36	0.16	0.10	99.99	11.24	18.55	52	56	80<Fo<85
329	0.07	0.49	18.87	43.08	26.53	0.23	10.44	0.19	0.13	100.98	8.08	19.26	49	61	80<Fo<85
330	0.07	0.84	20.74	37.89	28.45	0.23	11.09	0.18	0.12	100.87	10.72	18.81	51	55	80<Fo<85
331	0.19	0.15	7.27	58.56	19.51	0.23	7.86	0.12	0.22	94.12	0.40	19.14	42	84	80<Fo<85
332	0.05	1.03	18.59	36.55	31.83	0.23	9.95	0.09	0.12	98.44	13.07	20.07	47	57	80<Fo<85
333	0.04	1.11	18.14	37.08	31.76	0.23	10.11	0.11	0.09	98.67	13.20	19.88	48	58	80<Fo<85
334	0.08	0.81	20.97	37.46	28.03	0.23	11.08	0.15	0.11	100.13	10.40	18.67	51	55	80<Fo<85
335	0.09	1.03	20.21	37.40	28.98	0.23	10.98	0.12	0.08	99.12	11.12	18.98	51	55	80<Fo<85
336	0.17	0.18	6.35	57.29	23.31	0.23	7.28	0.12	0.19	95.13	3.35	20.30	39	86	80<Fo<85
337	0.21	0.31	6.52	52.45	28.80	0.23	8.25	0.09	0.12	97.98	10.01	19.79	43	84	80<Fo<85
338	0.03	1.12	18.91	36.67	31.79	0.23	10.31	0.13	0.08	99.28	13.24	19.88	48	57	80<Fo<85
339	0.18	1.22	19.43	36.07	30.52	0.24	10.85	0.17	0.12	98.80	12.59	19.19	50	55	80<Fo<85
340	0.08	1.00	20.08	36.69	28.81	0.24	11.05	0.17	0.14	99.58	11.45	18.50	52	55	80<Fo<85
341	0.28	0.17	7.11	57.71	22.57	0.24	8.65	0.08	0.21	97.01	3.87	19.09	45	84	80<Fo<85
342	0.15	0.36	9.38	53.87	24.95	0.24	7.95	0.11	0.10	97.59	4.80	20.63	41	79	80<Fo<85

343	0.05	1.17	18.27	36.78	31.88	0.24	10.13	0.13	0.13	98.78	13.28	19.93	48	57	80<Fo<85
344	0.19	0.23	8.56	56.51	24.59	0.24	8.29	0.05	0.14	99.25	4.58	20.47	42	82	80<Fo<85
345	0.07	0.89	20.63	37.48	28.89	0.24	11.12	0.19	0.11	100.88	11.22	18.79	51	55	80<Fo<85
346	0.07	0.74	21.30	37.08	28.24	0.24	11.28	0.19	0.13	100.53	10.95	18.39	52	54	80<Fo<85
347	0.07	0.87	20.57	37.12	28.84	0.24	11.08	0.19	0.17	100.52	11.31	18.66	51	55	80<Fo<85
348	0.06	0.80	19.95	37.91	30.14	0.24	10.08	0.09	0.13	100.73	11.04	20.20	47	56	80<Fo<85
349	0.04	1.29	18.48	36.25	31.72	0.24	10.32	0.11	0.09	98.57	13.31	19.74	48	57	80<Fo<85
350	0.16	0.38	5.69	49.10	34.32	0.24	7.08	0.10	0.19	98.67	14.20	21.54	37	85	80<Fo<85
351	0.05	0.90	19.19	37.57	31.16	0.24	10.00	0.09	0.14	100.71	12.11	20.27	47	57	80<Fo<85
352	0.09	1.32	13.82	35.81	36.51	0.24	9.36	<0.02	0.11	99.07	17.99	20.32	45	63	80<Fo<85
353	0.09	1.32	13.82	35.81	36.51	0.24	9.36	<0.02	0.11	99.07	17.99	20.32	45	63	80<Fo<85
354	0.09	1.50	13.27	35.93	36.91	0.24	9.16	<0.02	0.04	98.94	17.98	20.73	44	64	80<Fo<85
355	0.09	1.50	13.27	35.93	36.91	0.24	9.16	<0.02	0.04	98.94	17.98	20.73	44	64	80<Fo<85
356	0.09	1.15	18.27	36.67	31.74	0.25	10.00	0.13	0.06	98.37	12.96	20.07	47	57	80<Fo<85
357	0.04	0.72	21.11	37.44	29.68	0.25	10.29	0.13	0.16	101.02	10.74	20.01	48	54	80<Fo<85
358	0.08	1.35	13.84	35.98	36.88	0.25	9.34	<0.02	0.11	99.64	18.15	20.54	45	64	80<Fo<85
359	0.08	1.35	13.84	35.98	36.88	0.25	9.34	<0.02	0.11	99.64	18.15	20.54	45	64	80<Fo<85
360	0.06	1.08	19.94	36.61	30.17	0.25	10.89	0.18	0.15	99.34	12.36	19.05	50	55	80<Fo<85
361	0.07	0.85	21.03	37.63	28.65	0.25	11.23	0.16	0.13	101.24	10.99	18.76	52	55	80<Fo<85
362	0.05	0.78	20.74	37.73	29.97	0.25	10.21	0.10	0.11	101.15	10.79	20.25	47	55	80<Fo<85
363	0.08	0.99	20.31	30.07	35.68	0.25	10.62	0.16	0.09	100.28	18.15	19.34	49	50	80<Fo<85
364	0.11	0.80	20.92	37.42	28.41	0.25	11.17	0.20	0.12	100.64	10.87	18.63	52	55	80<Fo<85
365	0.20	0.48	9.40	45.97	31.85	0.25	8.41	0.15	0.15	98.15	13.10	20.06	43	77	80<Fo<85
366	0.19	0.29	9.14	55.50	23.89	0.25	8.66	0.11	0.10	98.57	4.54	19.80	44	80	80<Fo<85
367	0.14	1.35	13.91	36.11	36.40	0.26	9.33	<0.02	0.14	99.40	17.62	20.54	45	64	80<Fo<85
368	0.14	1.35	13.91	36.11	36.40	0.26	9.33	<0.02	0.14	99.40	17.62	20.54	45	64	80<Fo<85
369	0.06	1.05	18.81	36.76	31.10	0.26	10.36	0.15	0.12	98.66	12.90	19.49	49	57	80<Fo<85

370	0.09	0.46	18.64	43.53	25.89	0.26	10.34	0.14	0.11	100.33	7.41	19.22	49	61	80<Fo<85
371	0.46	0.52	6.70	45.40	34.42	0.26	7.59	0.10	0.17	97.13	15.02	20.91	39	82	80<Fo<85
372	0.09	0.94	19.52	36.67	30.92	0.26	10.10	0.14	0.15	100.17	12.14	19.99	47	56	80<Fo<85
373	0.02	0.68	18.86	32.41	35.39	0.26	10.40	0.18	0.12	100.34	18.14	19.07	49	54	80<Fo<85
374	0.10	0.72	20.57	38.98	28.36	0.27	10.57	0.18	0.12	101.01	9.81	19.53	49	56	80<Fo<85
375	0.10	0.55	18.28	44.06	25.78	0.27	10.26	0.19	0.10	100.38	7.13	19.36	49	62	80<Fo<85
376	0.06	0.20	5.95	53.44	29.20	0.27	7.14	0.05	0.27	97.51	9.27	20.86	38	86	80<Fo<85
377	0.29	0.20	8.10	55.00	24.48	0.27	9.06	0.08	0.23	97.70	6.24	18.87	46	82	80<Fo<85
378	0.24	0.81	9.62	37.90	38.06	0.28	8.93	0.21	0.11	98.21	20.62	19.50	45	73	80<Fo<85
379	0.22	0.17	7.17	55.32	25.86	0.28	7.89	0.07	0.15	97.12	6.20	20.28	41	84	80<Fo<85
380	0.21	0.42	6.67	45.76	35.03	0.28	7.97	0.15	0.14	98.28	16.45	20.23	41	82	80<Fo<85
381	0.03	0.52	18.32	44.24	26.49	0.28	10.12	0.15	0.08	101.13	7.49	19.74	48	62	80<Fo<85
382	0.09	1.02	19.46	37.12	30.11	0.28	10.50	0.17	0.07	100.18	11.80	19.48	49	56	80<Fo<85
383	0.23	0.23	5.52	54.12	28.77	0.28	7.23	0.06	0.27	96.71	8.75	20.89	38	87	80<Fo<85
384	0.11	1.01	19.11	37.67	29.61	0.29	10.43	0.11	0.08	99.74	11.29	19.45	49	57	80<Fo<85
385	0.05	0.61	10.51	38.72	37.12	0.29	9.51	0.24	0.12	97.17	20.59	18.59	48	71	80<Fo<85
386	0.11	1.32	13.30	36.17	36.85	0.30	9.24	<0.02	0.11	99.23	18.23	20.44	45	65	80<Fo<85
387	0.11	1.32	13.30	36.17	36.85	0.30	9.24	<0.02	0.11	99.23	18.23	20.44	45	65	80<Fo<85
388	0.09	0.44	4.64	48.64	35.78	0.30	7.04	0.13	0.23	98.91	16.07	21.32	37	88	80<Fo<85
389	0.05	0.83	19.59	37.65	30.61	0.30	10.01	0.10	0.11	100.53	11.63	20.15	47	56	80<Fo<85
390	0.08	0.56	19.20	42.25	26.90	0.31	10.31	0.15	0.08	100.76	8.21	19.52	48	60	80<Fo<85
391	0.03	1.17	8.32	39.99	37.80	0.31	9.45	0.18	0.16	99.65	20.95	18.95	47	76	80<Fo<85
392	0.10	1.33	13.28	36.21	36.50	0.31	9.14	<0.02	0.12	98.78	17.87	20.41	44	65	80<Fo<85
393	0.10	1.33	13.28	36.21	36.50	0.31	9.14	<0.02	0.12	98.78	17.87	20.41	44	65	80<Fo<85
394	0.04	1.40	12.19	32.07	41.36	0.32	9.93	0.33	0.03	97.66	24.73	19.10	48	64	80<Fo<85
395	0.00	1.00	10.02	44.07	33.52	0.32	9.00	0.16	0.21	98.30	15.21	19.83	45	75	80<Fo<85
396	0.03	1.18	12.35	35.70	38.21	0.32	9.25	0.24	0.13	97.41	20.47	19.79	45	66	80<Fo<85

397	0.01	0.39	4.74	44.29	38.33	0.32	7.18	0.17	0.14	97.56	19.82	20.50	38	86	80<Fo<85
398	0.07	0.42	4.29	52.79	33.22	0.33	7.34	0.10	0.18	98.74	13.33	21.22	38	89	80<Fo<85
399	0.08	0.11	4.32	45.62	37.82	0.33	8.17	0.16	0.14	98.82	20.74	19.15	43	88	80<Fo<85
400	0.10	0.38	4.91	53.79	31.81	0.33	7.63	0.10	0.10	99.14	11.95	21.06	39	88	80<Fo<85
401	0.20	0.42	10.79	51.29	25.72	0.35	9.67	0.05	0.12	98.61	7.71	18.79	48	76	80<Fo<85
402	0.04	0.64	10.64	36.48	39.98	0.38	8.72	0.29	0.13	97.29	22.46	19.77	44	70	80<Fo<85
403	0.27	0.81	8.31	44.23	35.12	0.38	8.56	0.15	0.22	98.06	16.47	20.30	43	78	80<Fo<85
404	0.04	0.30	5.30	53.58	31.80	0.39	7.25	0.05	0.19	98.90	11.61	21.35	38	87	80<Fo<85
405	0.14	0.90	11.68	37.43	37.11	0.39	8.71	0.24	0.29	96.88	19.00	20.01	44	68	80<Fo<85
406	0.19	0.26	8.60	54.42	25.70	0.40	7.82	0.05	0.10	97.53	5.55	20.71	40	81	80<Fo<85
407	0.15	0.27	8.60	55.38	25.05	0.41	8.50	0.04	0.13	98.52	5.69	19.93	43	81	80<Fo<85
408	0.09	0.22	5.10	54.56	29.96	0.42	7.12	0.09	0.16	97.72	9.86	21.08	38	88	80<Fo<85
409	0.17	0.38	8.37	53.71	27.49	0.42	7.42	0.04	0.11	98.11	6.60	21.55	38	81	80<Fo<85
410	0.12	0.29	8.74	54.72	25.82	0.43	8.24	0.04	0.11	98.52	6.10	20.33	42	81	80<Fo<85
411	0.18	0.24	8.87	54.70	25.84	0.45	7.78	0.03	0.09	98.20	5.43	20.96	40	81	80<Fo<85
412	0.15	0.36	9.38	53.87	24.95	0.50	7.95	0.11	0.10	97.37	5.00	20.45	41	79	80<Fo<85
413	0.04	0.17	6.70	40.68	39.46	0.52	8.97	0.25	0.17	99.37	23.69	18.14	47	80	80<Fo<85
414	0.19	0.29	9.14	55.50	23.89	0.55	8.66	0.11	0.10	98.41	4.76	19.60	44	80	80<Fo<85
Mount Gunson															
1	0.14	0.78	9.41	45.40	35.22	0.42	6.14	0.12	0.19	97.81	12.62	23.86	31	76	Fo<80
2	0.14	0.73	9.85	46.64	33.58	0.43	6.53	0.16	0.21	98.26	11.38	23.34	33	76	Fo<80
3	0.05	1.03	9.43	43.12	37.92	0.44	6.27	0.07	0.15	98.48	15.36	24.09	32	75	Fo<80
4	0.15	0.75	9.71	47.13	33.77	0.45	6.61	0.12	0.17	98.86	11.44	23.47	33	77	Fo<80
5	0.05	3.35	7.15	33.59	47.60	0.48	5.45	0.13	0.10	97.89	22.95	26.94	27	76	Fo<80
6	0.10	0.88	10.33	43.29	37.68	0.51	5.77	0.10	0.14	98.79	14.20	24.90	29	74	Fo<80
7	0.15	0.73	8.13	44.06	34.47	0.54	5.41	0.13	0.22	93.83	12.41	23.30	29	78	Fo<80
8	0.19	0.46	8.99	48.61	28.61	0.42	7.65	0.13	0.19	95.24	9.17	20.36	40	78	80<Fo<85

9	0.09	0.43	9.59	48.45	28.07	0.43	7.93	0.14	0.17	95.32	9.09	19.89	42	77	80<Fo<85
10	0.21	0.49	9.28	47.58	29.25	0.43	7.70	0.18	0.19	95.31	9.88	20.36	40	77	80<Fo<85

Fe_{tot}, total Fe; Fo, forsterite; Mg# [Mg/(Mg + Fe^{2+}), mol. %]; Cr# [Cr/(Cr + Al), mol. %]

Table S4 LA-ICPMS apatite U-Pb dating results of mafic GRV at Mount Gunson, Wirrda Well and Olympic Dam

Mount Gunson olivine-phyric basalt	^{207}Pb cor $^{206}Pb/^{238}U$ age (Ma)	+/-1 ster	$^{238}U/^{206}Pb$ ratio	+/-1 ster	$^{207}Pb/^{206}Pb$ ratio	+/-1 ster	^{204}Pb (ppm)	^{206}Pb (ppm)	^{207}Pb (ppm)	^{208}Pb (ppm)	^{232}Th (ppm)	^{238}U (ppm)
1	1529	30	3.60	0.07	0.1270	0.0030	0.05	13.4	1.7	51.6	754.5	54.8
2	1530	21	3.61	0.05	0.1236	0.0018	0.05	23.7	2.9	90.8	1358.6	99.8
3	1595	204	3.05	0.37	0.2260	0.0377	0.00	0.1	0.0	0.1	0.4	0.4
4	1487	67	2.99	0.11	0.2924	0.0196	0.04	3.7	1.1	18.2	264.8	14.2
5	1673	81	3.04	0.14	0.1890	0.0130	0.02	1.1	0.2	5.8	74.9	4.2
6	1623	68	3.22	0.13	0.1674	0.0132	0.00	2.9	0.5	13.3	193.9	11.1
7	1441	117	2.73	0.20	0.3800	0.0275	0.03	1.7	0.6	9.3	133.3	6.0
8	1397	78	3.08	0.15	0.3175	0.0209	0.05	1.1	0.3	5.1	73.4	4.3
9	1535	47	3.59	0.11	0.1263	0.0055	0.05	12.2	1.5	19.5	282.2	49.8
10	1578	108	3.54	0.24	0.1140	0.0159	0.00	3.0	0.4	10.7	177.9	13.7
11	1619	41	3.35	0.09	0.1374	0.0043	0.00	11.1	1.5	36.9	527.2	46.3
12	1558	32	3.53	0.07	0.1263	0.0040	0.05	21.1	2.6	66.9	917.8	85.7
13	1593	22	3.50	0.05	0.1136	0.0016	0.00	31.2	3.5	113.0	1673.9	132.4
14	1654	31	3.29	0.06	0.1341	0.0037	0.07	14.5	1.9	54.4	805.1	59.4
15	1624	35	3.35	0.07	0.1357	0.0038	0.00	12.3	1.6	43.0	621.6	51.3
16	1677	55	3.27	0.11	0.1273	0.0059	0.02	8.0	1.0	29.8	430.3	33.1
17	1573	19	3.58	0.04	0.1052	0.0012	0.01	36.4	3.8	118.2	1746.6	153.7
18	1698	32	2.77	0.05	0.2514	0.0044	0.21	23.5	5.8	82.3	1088.5	80.8
19	1574	22	3.52	0.05	0.1211	0.0019	0.00	19.2	2.3	58.2	834.5	79.6
Wirrda Well olivine-phyric dyke												
1	2114	287	0.53	0.05	0.7880	0.0151	0.15	3.5	3.0	8.5	25.5	2.0
2	1774	173	1.03	0.07	0.6829	0.0195	0.05	1.2	0.8	3.3	19.5	1.7
3	1823	140	1.19	0.05	0.6288	0.0217	0.09	1.5	1.0	4.3	29.9	2.2
4	1617	147	1.34	0.07	0.6310	0.0243	0.02	1.1	0.7	3.0	20.6	1.7
5	1775	101	1.50	0.06	0.5555	0.0157	0.05	1.3	0.7	3.5	29.4	2.4
6	1579	99	1.87	0.09	0.5122	0.0192	0.03	1.0	0.5	3.1	26.1	2.2
7	1606	95	1.88	0.08	0.5013	0.0204	0.03	0.9	0.4	2.3	21.4	2.0
8	1589	112	1.92	0.09	0.4963	0.0246	0.04	0.9	0.4	2.3	21.4	2.0

9	1661	82	1.93	0.07	0.4720	0.0160	0.02	0.8	0.4	2.4	22.9	2.0
10	1514	82	1.98	0.07	0.5055	0.0184	0.04	0.7	0.4	2.3	21.4	1.8
11	1660	104	2.00	0.10	0.4555	0.0204	0.05	1.0	0.4	2.7	26.9	2.3
12	1752	90	2.02	0.09	0.4218	0.0162	0.05	0.9	0.4	2.7	26.2	2.1
13	1493	231	2.03	0.22	0.5023	0.0547	0.00	0.3	0.1	0.3	0.0	0.8
14	1416	130	2.03	0.12	0.5261	0.0321	0.00	0.3	0.1	0.2	0.0	0.7
15	1628	108	2.06	0.11	0.4519	0.0199	0.00	0.8	0.4	2.1	21.4	1.9
16	1697	169	2.07	0.15	0.4270	0.0391	0.00	0.3	0.1	0.3	0.0	0.7
17	1645	77	2.09	0.08	0.4384	0.0150	0.04	0.8	0.3	2.2	22.2	2.0
18	1640	73	2.09	0.08	0.4389	0.0144	0.02	0.7	0.3	2.2	21.0	1.8
19	1658	96	2.11	0.10	0.4283	0.0196	0.04	0.7	0.3	2.3	23.2	2.0
20	1659	110	2.25	0.12	0.3936	0.0237	0.04	0.3	0.1	0.2	0.2	0.8
21	1490	62	2.25	0.07	0.4524	0.0140	0.02	0.8	0.3	2.3	23.6	2.0
22	1579	73	2.27	0.09	0.4177	0.0152	0.01	0.7	0.3	2.0	20.4	1.8
23	1417	133	2.29	0.18	0.4703	0.0282	0.00	0.8	0.4	2.4	22.1	1.9
24	1570	58	2.36	0.07	0.3994	0.0110	0.00	0.9	0.3	2.9	31.6	2.5
25	1563	73	2.38	0.09	0.3971	0.0150	0.01	0.9	0.3	2.8	29.5	2.4
26	1617	71	2.45	0.09	0.3593	0.0156	0.03	1.0	0.3	2.8	29.9	2.8
27	1556	107	2.45	0.14	0.3824	0.0242	0.02	0.8	0.3	2.7	31.3	2.4
28	1734	176	2.45	0.21	0.3134	0.0391	0.00	0.2	0.1	0.1	0.1	0.6
29	1499	50	2.54	0.07	0.3827	0.0110	0.04	1.1	0.4	3.2	36.1	3.3
30	1524	82	2.56	0.12	0.3699	0.0177	0.00	0.9	0.3	3.2	37.5	2.7
31	1692	231	2.69	0.33	0.2688	0.0459	0.00	0.2	0.0	0.1	0.3	0.6
32	1652	33	2.79	0.05	0.2596	0.0051	0.07	3.5	0.9	6.7	73.1	11.3
33	1665	102	2.86	0.17	0.2370	0.0146	0.03	2.5	0.6	16.5	213.3	8.1
34	1588	94	2.90	0.15	0.2628	0.0220	0.02	0.3	0.1	0.1	0.2	1.0
35	1552	18	3.06	0.03	0.2395	0.0017	0.68	64.7	15.5	24.1	1.5	238.5
36	1623	37	3.07	0.07	0.2048	0.0050	0.03	2.6	0.5	5.7	70.5	9.5
37	1676	95	3.07	0.17	0.1789	0.0154	0.02	0.5	0.1	0.3	3.0	1.8
38	1626	124	3.12	0.22	0.1895	0.0258	0.00	0.3	0.1	0.1	0.6	1.1
39	1558	30	3.22	0.06	0.1992	0.0049	0.02	3.1	0.6	5.0	61.1	11.5
40	1521	36	3.37	0.08	0.1830	0.0055	0.00	2.7	0.5	5.5	71.1	10.2

41	1548	18	3.38	0.04	0.1674	0.0020	0.15	40.1	6.6	6.9	1.9	158.3
42	1628	27	3.43	0.06	0.1120	0.0026	0.01	3.8	0.4	10.5	146.9	15.4
43	1464	179	3.44	0.41	0.1978	0.0345	0.00	0.1	0.0	0.0	0.2	0.4
44	1617	29	3.45	0.06	0.1127	0.0031	0.04	4.8	0.5	11.3	154.4	18.9
45	1628	37	3.46	0.08	0.1057	0.0038	0.02	2.8	0.3	8.2	114.9	11.3
46	1477	137	3.48	0.31	0.1824	0.0252	0.02	0.4	0.1	0.1	0.9	1.8
47	1605	32	3.50	0.07	0.1082	0.0034	0.00	4.0	0.4	9.7	135.7	16.1
48	1606	50	3.50	0.11	0.1074	0.0054	0.03	2.7	0.3	8.8	117.9	10.8
49	1602	21	3.50	0.05	0.1092	0.0018	0.00	9.8	1.1	1.7	20.8	40.6
50	1595	27	3.54	0.06	0.1031	0.0027	0.00	5.8	0.6	6.4	87.7	23.2
51	1581	18	3.56	0.04	0.1069	0.0015	0.00	19.1	2.0	6.9	94.6	78.5
52	1568	26	3.59	0.06	0.1066	0.0027	0.01	4.9	0.5	11.2	158.4	20.1
53	1568	23	3.60	0.05	0.1057	0.0020	0.02	7.3	0.8	11.0	155.6	30.1
54	1572	27	3.60	0.06	0.1031	0.0025	0.00	4.7	0.5	5.4	74.8	19.3
55	1553	21	3.63	0.05	0.1064	0.0018	0.00	7.5	0.8	15.2	221.9	31.8
56	1700	25	3.31	0.05	0.1060	0.0021	0.02	8.0	0.8	11.3	153.5	31.3
57	1693	20	3.29	0.04	0.1146	0.0015	0.02	15.3	1.7	3.6	43.8	59.9
Olympic Dam High Zr/TiO_2 mafic dykes												
1	1277	60	3.43	0.06	0.1096	0.0030	0.01	2.3	0.4	7.4	138.7	11.9
2	1671	48	3.49	0.06	0.1189	0.0032	0.00	1.8	0.4	4.7	59.9	6.6
3	1492	116	1.71	0.06	0.4975	0.0137	0.04	1.5	0.5	3.5	69.6	5.6
4	1631	27	3.43	0.06	0.1110	0.0029	0.01	4.2	0.5	8.8	122.5	17.0
5	1611	28	1.77	0.06	0.4983	0.0149	0.01	3.4	0.4	8.6	120.9	14.0
6	1782	89	2.09	0.06	0.4094	0.0107	0.02	0.9	0.5	2.0	14.9	1.8
7	1710	74	3.12	0.06	0.1744	0.0046	0.03	1.2	0.4	3.0	32.8	3.4
8	1489	51	3.35	0.06	0.1189	0.0032	0.02	1.4	0.5	6.5	88.2	4.2
9	1743	127	3.48	0.06	0.1103	0.0031	0.04	1.0	0.4	2.2	19.1	2.1
10	1667	51	1.79	0.06	0.5698	0.0191	0.03	1.8	0.4	5.1	65.8	6.3
11	2233	201	3.43	0.06	0.1278	0.0040	0.08	2.1	1.4	6.3	51.0	2.0
12	1659	77	1.85	0.06	0.4839	0.0142	0.02	0.9	0.4	2.1	17.4	1.9
13	678	20	2.04	0.06	0.4618	0.0147	0.02	4.0	0.6	10.4	180.7	41.1
14	1191	109	1.84	0.06	0.5193	0.0176	0.02	0.9	0.4	2.0	19.7	2.7

15	1657	32	3.23	0.06	0.1726	0.0042	0.02	2.8	0.5	7.6	100.9	10.3
16	2434	180	1.93	0.06	0.4804	0.0141	0.04	1.3	0.6	2.9	23.6	1.9
17	1612	41	1.90	0.07	0.4706	0.0158	0.00	1.6	0.4	3.8	46.3	5.7
18	1584	60	1.98	0.07	0.4557	0.0141	0.02	1.3	0.3	1.9	22.1	4.8
19	1555	57	2.04	0.07	0.4971	0.0158	0.03	1.1	0.4	3.0	32.1	3.3
20	1670	54	2.17	0.07	0.4126	0.0111	0.02	1.2	0.4	3.1	35.3	3.4
21	1659	61	2.93	0.07	0.2224	0.0066	0.03	1.0	0.4	2.5	26.0	2.9
22	1662	67	1.83	0.07	0.4934	0.0149	0.03	1.1	0.4	2.8	27.8	3.0
23	1553	53	2.30	0.07	0.4035	0.0124	0.01	1.1	0.4	2.8	29.5	3.2
24	1609	53	3.01	0.07	0.2251	0.0073	0.02	1.1	0.4	2.7	28.2	3.5
25	2148	112	1.95	0.07	0.5004	0.0169	0.01	1.4	0.4	12.2	168.6	3.7
26	1711	59	2.44	0.07	0.3347	0.0102	0.04	1.1	0.4	3.4	34.5	2.8
27	1614	50	2.12	0.07	0.4309	0.0125	0.02	1.5	0.4	4.3	51.1	4.7
28	1636	61	2.24	0.07	0.3379	0.0115	0.02	1.3	0.5	4.1	44.0	3.4
29	1615	53	2.37	0.07	0.4063	0.0121	0.00	1.4	0.4	3.6	40.2	4.3
30	1311	30	1.87	0.07	0.4509	0.0144	0.02	4.4	0.7	9.5	153.5	20.8
31	1587	76	3.48	0.07	0.1297	0.0032	0.02	0.8	0.4	1.9	15.4	1.8
32	1679	66	2.93	0.07	0.2556	0.0071	0.03	1.1	0.4	2.6	26.3	3.1
33	1630	50	1.92	0.07	0.4842	0.0159	0.01	1.2	0.4	3.2	35.4	3.8
34	1627	51	2.28	0.07	0.3926	0.0124	0.01	1.3	0.4	3.4	37.5	4.0
35	2267	120	2.87	0.07	0.2993	0.0102	0.02	1.3	0.6	2.8	23.0	2.2
36	2192	105	1.92	0.07	0.5092	0.0169	0.03	1.2	0.5	2.8	23.3	2.1
37	1580	50	2.98	0.07	0.2281	0.0071	0.03	1.2	0.4	2.9	32.0	4.0
38	1601	39	2.03	0.07	0.4884	0.0166	0.00	1.7	0.4	4.1	52.4	6.3
39	1575	46	2.52	0.07	0.3386	0.0108	0.04	1.5	0.4	5.0	65.3	5.3
40	1661	51	2.48	0.07	0.3700	0.0109	0.03	1.3	0.4	3.6	41.8	4.2
41	1630	77	2.59	0.07	0.3025	0.0088	0.02	0.9	0.4	2.0	18.0	2.2
42	1616	61	2.01	0.07	0.4646	0.0147	0.01	1.0	0.4	2.8	26.7	2.9
43	1504	76	2.04	0.07	0.4830	0.0182	0.02	0.8	0.4	1.8	16.1	1.9
44	1666	80	1.97	0.07	0.4768	0.0145	0.03	0.8	0.4	1.9	15.6	1.8
45	1664	54	2.61	0.07	0.3094	0.0089	0.02	1.2	0.4	2.7	29.2	3.8
46	2024	88	2.35	0.07	0.3253	0.0116	0.04	1.8	0.7	3.5	30.0	3.7

47	1595	80	2.60	0.07	0.3118	0.0095	0.04	0.9	0.4	2.4	21.4	2.2
48	1539	84	2.24	0.07	0.3805	0.0126	0.04	0.9	0.5	2.2	18.2	2.1
49	1588	25	2.57	0.07	0.3234	0.0106	0.02	3.7	0.4	9.6	137.9	15.3
50	1599	30	2.17	0.07	0.4043	0.0117	0.02	3.3	0.4	9.3	130.8	13.8
51	1564	226	2.34	0.08	0.3647	0.0105	0.04	0.8	0.4	1.8	15.8	1.9
52	1756	83	2.46	0.08	0.3727	0.0119	0.04	0.8	0.4	1.9	15.5	1.9
53	1650	40	2.55	0.08	0.3095	0.0092	0.00	1.9	0.4	4.6	57.6	6.6
54	1605	33	2.70	0.08	0.3079	0.0101	0.01	3.5	0.6	8.6	118.3	13.3
55	1617	54	2.61	0.08	0.3654	0.0111	0.03	1.8	0.6	4.0	42.8	5.6
56	1581	69	2.36	0.08	0.3384	0.0118	0.03	0.9	0.4	2.1	18.5	2.1
57	1762	122	2.68	0.08	0.2975	0.0080	0.02	0.9	0.4	2.2	18.1	2.0
58	2173	108	1.72	0.08	0.4966	0.0152	0.00	1.2	0.5	2.3	18.9	2.1
59	1610	50	2.05	0.08	0.4431	0.0140	0.01	1.3	0.4	3.1	36.3	4.4
60	1511	43	2.57	0.08	0.3229	0.0097	0.01	1.2	0.4	2.9	33.4	4.2
61	1643	82	1.98	0.08	0.4553	0.0144	0.03	0.8	0.4	1.9	16.4	1.8
62	1762	71	2.91	0.08	0.2613	0.0083	0.04	1.5	0.4	3.6	38.1	4.5
63	1577	72	2.75	0.08	0.2833	0.0088	0.02	1.2	0.4	2.9	31.9	3.6
64	1899	133	2.95	0.08	0.2093	0.0079	0.04	1.1	0.5	2.3	18.7	2.6
65	1579	73	2.34	0.08	0.4254	0.0145	0.02	1.0	0.4	2.0	17.9	2.6
66	1766	78	2.25	0.08	0.4132	0.0157	0.03	1.5	0.5	3.8	43.9	4.5
67	1531	87	2.28	0.08	0.3616	0.0141	0.02	0.7	0.3	1.8	15.3	1.8
68	1514	81	3.03	0.08	0.2086	0.0054	0.01	0.8	0.4	1.8	14.9	1.8
69	1519	79	2.95	0.09	0.2094	0.0073	0.03	0.8	0.4	2.8	37.0	1.9
70	1487	66	1.95	0.09	0.4769	0.0187	0.02	0.9	0.4	2.1	19.9	2.6
71	1603	73	2.49	0.09	0.2883	0.0128	0.03	0.9	0.4	2.2	18.2	2.1
72	1572	31	2.39	0.09	0.3125	0.0142	0.02	3.6	0.5	10.6	157.3	15.2
73	1729	97	3.33	0.09	0.1599	0.0050	0.05	0.9	0.4	2.0	16.0	1.9
74	1523	56	1.82	0.10	0.4619	0.0206	0.03	1.1	0.4	3.3	34.4	3.3
75	1738	79	2.35	0.10	0.3648	0.0149	0.04	1.2	0.6	3.9	40.9	2.4
76	1597	75	1.84	0.10	0.4619	0.0230	0.00	0.9	0.4	2.2	19.3	2.1
77	1678	79	2.57	0.10	0.3387	0.0142	0.04	0.9	0.4	2.1	17.7	2.0
78	1512	79	2.06	0.11	0.4973	0.0271	0.01	0.8	0.4	1.9	16.5	2.1

79	1573	59	3.04	0.11	0.2276	0.0107	0.03	1.0	0.4	2.5	24.8	2.9
80	1395	87	1.80	0.11	0.4316	0.0185	0.02	0.8	0.4	2.1	15.7	1.8
81	1981	145	2.03	0.09	0.4787	0.0167	0.02	1.0	0.4	2.1	16.8	1.9

ster, standard error

Table S5 Drill core assays of the ca. 1590 Ma olivine-phyric basalt (flat-lying unit)

Sample No.	SR1394 059	SR1394 061	SR1394 064	SR1394 068	SR1394 069	SR1394 072	SR1394 081	SR932 943	SR1394 071	SR1394 023	SR1394 025	SR1394 027	SR1394 024	SR1394 026
Alteration type	Chl	Chl	Chl	Chl	Chl	Chl	Chl	Chl	Chl	Chl	Chl	Chl	Chl	Chl
Drill Hole No.	RD1687	RD1687	RD1687	RD1687	RD1687	RD1687	RD1687	RD1687	RD1687	RD1756	RD1756	RD1756	RD1756	RD1756
SiO_2	52.0	51.3	43.5	48.7	48.5	50.7	57.6	51.0	49.9	40.7	39.1	39.5	47.3	36.8
TiO_2	0.54	0.57	0.68	0.74	0.66	0.57	0.56	0.46	0.63	0.52	0.43	0.44	0.46	0.45
Al_2O_3	10.3	10.7	13.0	13.3	12.5	11.1	10.7	9.7	12.3	10.3	7.9	8.2	8.6	8.2
Fe_2O_3	16.4	14.8	15.4	22.9	17.3	15.2	13.4	23.2	18.7	13.5	14.4	13.2	14.6	15.8
MnO	0.26	0.41	0.76	0.10	0.10	0.89	0.15	0.31	0.28	1.06	1.24	1.30	0.81	1.23
MgO	4.3	4.1	5.7	4.5	3.7	4.4	2.6	2.1	4.5	7.1	10.8	10.1	7.8	10.7
CaO	4.1	5.1	5.0	0.8	5.9	3.9	6.3	2.3	2.0	8.0	8.6	9.0	5.9	8.7
Na_2O	0.16	0.19	0.20	0.12	0.15	0.07	0.18	0.09	0.08	0.15	0.07	0.08	0.09	0.11
K_2O	2.7	3.2	3.4	2.7	3.1	3.4	3.3	3.1	3.0	3.2	0.6	1.3	1.6	1.2
P_2O_5	0.23	0.21	0.41	0.34	0.41	0.27	0.37	0.23	0.41	0.27	0.25	0.25	0.27	0.21
CO_2	3.4	4.4	7.2	0.9	1.1	5.6	1.5	3.1	2.2	10.4	11.6	12.1	7.8	11.6
F	16239	18013	5133	4396	34475	4291	27141	5454	6465	3734	2900	2546	3027	2708
S	1300	900	1600	300	700	800	500	2800	1500	200	200	<100	400	200
Cl	140	130	110	70	60	40	70	20	50	40	40	40	80	60
Li	51	43	51	74	72	60	39	20	75	36	75	81	57	95
Be	4.2	4.3	5	5.1	4.1	5.2	3.9	3.9	4.7	6	3.3	4.6	3.7	4
Sc	27	30	42	32	32	34	26	26	30	29	21	21	21	22
V	169	186	232	228	200	181	178	156	213	172	134	141	138	143
Cr	2305	2392	3021	3213	2924	2388	2361	1549	2778	2223	1875	1967	1875	1965

Co	157.7	128.7	259.7	335.3	229.1	155.1	109.2	76.2	226.4	84	211.6	196.7	159.6	210.3
Ni	477	425	722	1390	893	552	464	339	866	407	853	589	846	594
Cu	847	551	711	377	439	463	685	1902	739	255	150	105	174	123
Zn	1355	1513	3948	9057	6371	3201	1833	1267	4814	422	310	508	353	354
Ga	9.7	11.3	14.7	12.4	13.6	10.1	9.1	11.3	12.5	10.8	8.5	8.6	8.4	8.6
As	56.1	35	37.1	35.7	28.7	61	67	71.5	31.4	60.9	15.6	20.3	29.4	25.2
Se	1.3	1.2	3.6	2	2.6	2.9	6.4	7.7	3.5	1.1	1	2.4	1.7	4
Rb	164.9	183.6	215.5	178.8	196.6	221.8	182.4	182.1	203.6	230.1	40.7	63.5	108.3	53
Sr	65	64	63	45	77	49	42	131	64	31	33	33	30	29
Y	109.7	88.7	96.9	138.6	120.5	90.3	93	86.9	101.8	58.2	49.2	53	59	53.2
Zr	134	151	154	167	150	132	146	134	144	117	92	96	110	98
Nb	100.2	103.4	119.6	136.8	112.3	101.4	94.4	69.9	112.8	97.9	80.7	82.2	83	83.4
Mo	21	6	6	5	6	7	7	25	9	4	2	2	4	13
Ag	0.16	0.025	0.025	0.025	0.025	0.05	0.06	0.37	0.08	0.025	0.025	0.025	0.025	0.07
Cd	0.11	0.11	0.13	0.05	0.06	0.1	0.05	0.06	0.08	0.13	0.04	0.16	0.06	0.08
Sn	22	20	22	25	23	20	20	16	22	19	14	14	15	15
Sb	9.0	7.9	8.6	10.2	8.8	13.0	9.3	18.0	11.5	13.5	5.4	5.7	8.2	7.9
Te	0.54	0.39	0.25	0.28	0.26	0.27	0.31	0.33	0.27	0.17	0.15	0.11	0.2	0.11
Cs	4.6	5.5	15.8	4.8	4.8	13.5	7.1	11.6	8.6	15.5	0.8	2.0	1.6	2.0
Ba	3443	2964	5182	303	316	1973	239	7523	3722	302	518	188	305	178
La	244	188	135	262	186	248	330	427	225	179	105	95	155	108
Ce	508	346	351	624	395	607	686	531	595	368	217	249	279	244
Pr	59.5	41.4	36.8	66.9	43.0	60.6	75.9	46.0	55.5	42.0	30.1	29.9	39.1	29.9
Nd	220	168	165	281	191	257	309	136	248	174	128	130	168	128
Sm	43.1	35.6	37.8	63.1	43.4	55.1	66.9	21.7	54.4	38.7	29.1	30.2	38.2	29.2
Eu	8.15	6.43	6.62	10.68	7.17	9.50	11.50	3.88	8.99	6.53	5.15	4.86	6.56	4.82

Gd	30.4	25.7	30.2	49.1	33.7	38.4	45.3	17.1	38.9	25.4	20.3	21.3	25.5	20.9
Tb	3.71	3.09	3.88	5.73	4.55	4.37	4.89	2.51	4.23	2.58	2.13	2.25	2.49	2.26
Dy	18.0	14.7	17.7	27.7	21.6	18.1	18.6	13.8	17.8	11.6	9.9	10.7	11.6	10.4
Ho	3.23	2.64	2.97	4.78	3.65	2.81	2.73	2.49	2.77	1.86	1.59	1.65	1.86	1.65
Er	7.97	6.58	6.21	10.77	8.52	5.77	5.7	6.22	6.28	4.13	3.44	3.46	4.08	3.46
Tm	0.96	0.82	0.90	1.57	1.19	0.71	0.79	0.76	0.73	0.55	0.45	0.46	0.59	0.45
Yb	5.79	4.93	5.08	8.74	6.95	4.07	4.72	4.69	4.39	3.36	2.54	2.55	3.13	2.60
Lu	0.79	0.73	0.66	1.21	0.85	0.50	0.58	0.64	0.64	0.46	0.32	0.34	0.40	0.33
Hf	4.5	5.1	5.2	6.0	5.5	4.4	5.2	4.3	5.1	4.1	3.3	3.3	3.7	3.4
Ta	4.6	4.7	5.9	6.5	5.4	4.7	4.5	3.3	5.3	4.7	3.9	3.9	3.9	3.9
W	10	9	9	12	9	12	7	25	11	25	6	5	10	7
Re	0.001	0.001	0.002	0.001	0.003	0.003	0.004	0.001	0.003	0.002	0.002	0.002	0.003	0.003
Au	0.036	0.02	0.116	0.027	0.022	0.12	0.055	0.095	0.064	0.009	0.036	0.179	0.018	0.418
Tl	1.12	1.32	1.86	1.54	1.62	1.94	1.41	1.41	1.66	2.33	0.27	0.45	0.95	0.43
Pb	51	41	48	70	67	59	60	65	64	61	37	46	52	79
Bi	1.2	0.52	0.51	0.34	0.38	0.48	0.44	1.21	0.5	0.68	0.46	0.43	0.51	1.38
Th	21.9	23.4	27.5	30.2	25.9	23.4	24.1	18.6	25.4	21.2	17.1	17.5	19.0	17.6
U	42.7	38.5	58.4	34.9	31.2	38.0	54.9	56.1	31.9	27.1	17.4	19.1	22.0	18.1

Table S5 continued

Sample No.	SR1118335	SR1118336	SR1118350	SR1394152	SR1394153	SR1394154	SR1394156	SR1394157	SR1394158	SR1394159	SR1394161	SR1394163	SR1394164	SR1393999
Alteration type	Chl	Chl	Chl	Chl	Chl	Chl	Chl	Chl	Chl	Chl	Chl	Chl	Chl	Chl
Drill Hole No.	RD3008	RD3008	RD3008	RD6	RD6	RD6	RD6	RD6	RD6	RD6	RD6	RD6	RD6	RD635
SiO_2	48.6	39.0	35.0	49.8	44.9	44.0	41.4	44.2	39.7	39.7	43.2	39.5	45.0	33.9
TiO_2	0.54	0.60	0.55	0.39	0.41	0.44	0.36	0.39	0.40	0.35	0.48	0.39	0.52	0.56
Al_2O_3	10.2	11.4	10.7	6.9	6.2	7.5	6.4	6.5	6.7	5.7	8.2	6.6	9.6	10.5
Fe_2O_3	15.4	14.0	19.2	18.9	22.6	18.4	20.6	20.2	21.9	23.6	17.3	20.5	13.4	17.0
MnO	0.52	0.88	0.94	0.52	0.62	0.65	0.88	0.71	0.77	0.79	0.74	0.88	0.66	0.99
MgO	6.1	6.4	6.2	5.2	5.3	6.1	6.4	5.6	6.4	6.1	6.7	7.2	6.9	9.5
CaO	4.3	7.3	7.6	5.2	5.3	7.0	7.8	6.9	7.2	7.5	6.7	8.3	7.1	7.4
Na_2O	0.15	0.15	0.22	0.04	0.04	0.04	0.04	0.04	0.04	0.04	0.04	0.05	0.03	0.12
K_2O	2.4	3.2	3.5	1.8	1.7	2.3	1.9	1.9	1.8	1.5	2.1	1.7	2.8	1.6
P_2O_5	0.30	0.32	0.30	0.16	0.14	0.27	0.16	0.21	0.21	0.11	0.27	0.18	0.25	0.25
CO_2	5.4	11.0	11.5	7.4	7.6	10.0	11.1	9.4	10.6	10.3	9.6	11.9	10.0	10.1
F	3263	3488	4275	2395	2319	2913	2744	2520	2734	2173	3187	2488	3630	3474
S	400	500	1600	1700	3600	1000	900	1200	900	3400	1400	600	400	100
Cl	40	50	50	50	60	40	30	60	80	80	40	60	140	70
Li	56	39	28	37	30	31	24	21	29	27	39	36	44	64
Be	5	6.2	4.6	3.4	3.4	4.2	4.1	4	3.6	3.3	4.1	3.9	5.2	4.2
Sc	23	29	24	14	14	18	15	15	16	15	19	17	22	26
V	156	177	156	79	128	101	129	110	118	136	119	130	121	180
Cr	2314	2617	2209	1308	1440	1721	1348	1436	1425	1192	1828	1403	2128	2502

Co	161.2	124.2	78.5	89.4	85.9	98.4	91.5	91.4	105.8	102.9	142.5	122.1	155.1	299
Ni	600	489	421	346	328	361	338	319	376	361	551	419	646	967
Cu	392	512	417	206	195	209	393	354	277	386	279	232	250	300
Zn	5758	4874	769	208	418	509	390	280	320	515	1301	964	1448	5133
Ga	11.1	13.1	12	9.3	7.1	9	7.8	7.4	8.1	6.4	9.2	7.1	10.4	11.3
As	37.1	39	86.6	73.6	120.8	86.8	69.6	86	67.9	114.4	86.3	90.3	63.3	16.4
Se	0.25	0.25	0.6	1.2	1.8	2	0.25	1.9	1.8	1.7	2.1	0.25	1.4	2.8
Rb	149.1	215	220.9	93.9	94.1	143.9	115.4	113.3	108	89.8	132.1	100.1	179.4	163.9
Sr	39	44	114	99	192	101	86	92	88	113	139	68	63	31
Y	66.1	67.2	82.4	42.3	37	51.1	43.5	39.2	45.1	46.2	48.2	51.7	71.9	59
Zr	120	129	133	154	134	143	95	108	106	120	130	122	126	119
Nb	97.6	107.2	109	57.8	61.5	71.7	58	63	68	55.2	76.1	66.4	89.1	106
Mo	7	4	31	44	20	25	15	14	17	27	16	12	17	4
Ag	0.12	0.3	0.17	0.22	0.1	0.21	0.14	0.17	0.16	0.12	0.19	0.14	0.17	0.26
Cd	0.14	0.21	0.14	0.25	0.31	0.32	0.26	0.18	0.33	0.46	0.26	0.31	0.28	0.08
Sn	21	20	27	13	15	16	15	13	16	15	16	14	18	19
Sb	10.2	11.0	16.0	14.2	21.2	13.6	16.9	18.4	17.5	20.4	15.5	17.4	12.7	3.8
Te	0.13	0.3	0.91	0.38	0.37	0.34	0.13	0.22	0.27	0.17	0.2	0.12	0.27	0.25
Cs	8.1	10.7	18.1	2.0	1.9	3.5	3.1	2.0	2.1	2.1	2.9	2.0	3.8	6.9
Ba	406	564	6120	6947	15507	3991	3218	4436	3387	6066	5639	2282	1737	223
La	176	161	505	66	102	99	70	131	105	106	133	106	149	156
Ce	386	330	794	116	173	183	135	230	170	170	215	191	368	305
Pr	48.1	44.0	79.6	15.3	21.7	24.7	18.6	26.8	23.4	26.2	26.7	25.5	33.4	40.0
Nd	207	181	269	69	87	105	82	110	96	107	107	107	145	169
Sm	49.5	39.6	47.2	17.5	20.4	25.7	21.1	23.4	22.0	23.3	25.0	25.6	34.1	39.1
Eu	7.59	6.41	8.65	3.07	3.39	4.31	3.44	3.75	3.86	4.15	4.01	4.21	5.59	6.31

Gd	34.1	26.7	32.2	12.6	14.0	17.0	15.0	14.8	15.5	17.7	17.2	17.8	23.2	26.3
Tb	3.36	2.79	3.34	1.63	1.63	2.06	1.84	1.73	1.93	2.02	2.05	2.24	2.65	2.82
Dy	15.1	13.6	15.9	7.7	7.4	9.4	8.2	7.8	8.9	8.7	9.5	10.0	12.8	12.3
Ho	2.27	2.09	2.63	1.31	1.16	1.58	1.33	1.25	1.36	1.36	1.48	1.58	2.07	1.89
Er	5.02	4.71	5.94	3.11	2.77	3.6	2.92	2.85	3.1	3.2	3.47	3.6	4.83	4.13
Tm	0.68	0.66	0.77	0.43	0.39	0.46	0.38	0.36	0.39	0.38	0.44	0.47	0.57	0.55
Yb	4.10	3.88	4.59	2.52	2.18	2.87	2.31	2.04	2.44	2.38	2.59	2.60	3.39	3.37
Lu	0.57	0.50	0.65	0.37	0.34	0.42	0.29	0.29	0.33	0.32	0.35	0.42	0.49	0.45
Hf	4.3	5.1	4.9	5.3	4.6	4.9	3.5	3.9	3.7	3.9	4.6	4.4	4.9	4.3
Ta	5.0	5.7	5.0	3.1	3.3	3.9	3.1	3.1	3.3	2.9	4.1	3.5	4.4	5.0
W	12	11	27	24	14	15	14	13	15	13	11	10	10	7
Re	0.001	0.001	0.001	0.003	0.004	0.003	0.002	0.003	0.003	0.003	0.003	0.003	0.003	0.002
Au	0.03	0.034	0.13	0.016	0.037	0.038	0.077	0.05	0.035	0.03	0.069	0.031	0.102	0.004
Tl	1.21	1.83	2.14	2.06	2.67	3.63	3.18	2.67	2.76	2.55	3.68	2.59	5.05	1.46
Pb	55	64	66	42	74	47	56	62	50	71	50	75	40	35
Bi	0.49	0.81	1.43	0.88	0.61	0.54	0.38	0.47	0.41	0.74	0.37	0.37	0.44	0.47
Th	22.7	24.9	24.7	15.7	14.8	18.7	15.0	15.0	15.8	13.3	18.9	14.9	20.8	22.8
U	23.4	29.9	48.9	16.5	18.2	18.3	23.0	22.9	18.4	15.7	19.2	25.9	24.7	30.6

Table S5 continued

Sample No.	SR1394001	SR1394002	SR1394003	SR1394004	SR1394005	SR1394007	SR1394008	SR1394009	SR1394010	SR1394012	SR1393968	SR1393970	SR1394018	SR1394019
Alteration type	Chl	Chl	Chl	Chl	Chl	Chl	Chl	Chl	Chl	Chl	Chl	Chl	Cb	Cb
Drill Hole No.	RD635	RD635	RD635	RD635	RD635	RD635	RD635	RD635	RD635	RD635	RD917A	RD917A	RD1756	RD1756
SiO_2	32.8	39.9	42.7	39.4	46.6	33.5	41.0	39.7	39.4	51.7	42.1	34.7	32.0	30.3
TiO_2	0.46	0.63	0.57	0.74	0.58	0.77	0.55	0.49	0.55	0.46	0.49	0.45	0.44	0.47
Al_2O_3	8.7	11.9	10.9	13.4	10.9	14.0	10.5	9.1	10.1	8.6	9.7	8.3	8.1	8.8
Fe_2O_3	14.4	17.2	16.4	18.6	15.5	19.8	15.4	10.3	13.4	13.6	17.5	20.7	8.7	10.2
MnO	1.27	0.75	0.72	0.61	0.68	0.59	0.94	1.10	1.02	0.67	1.28	1.73	1.73	1.59
MgO	9.0	7.1	6.2	6.0	5.8	7.9	6.8	7.9	7.4	5.2	4.6	6.4	9.4	9.5
CaO	10.3	5.6	5.7	4.4	4.7	5.2	6.7	10.3	8.0	5.4	6.8	9.5	13.5	13.1
Na_2O	0.12	0.16	0.19	0.16	0.18	0.15	0.16	0.13	0.13	0.16	0.08	0.07	0.13	0.15
K_2O	1.7	3.0	3.0	3.6	2.9	3.2	2.7	2.8	2.6	2.5	3.6	3.1	2.7	2.8
P_2O_5	0.21	0.34	0.23	0.32	0.27	0.39	0.32	0.27	0.30	0.25	0.23	0.23	0.21	0.27
CO_2	13.1	7.4	7.6	5.6	6.3	6.8	9.3	13.8	11.0	7.6	9.1	13.1	18.3	17.5
F	5835	4241	3543	4266	3423	4695	3625	2929	4549	3209	3389	2790	2507	3074
S	4300	100	100	200	200	400	300	100	100	400	2200	100	300	300
Cl	60	50	70	80	60	70	40	60	90	60	30	60	60	90
Li	44	55	44	51	49	70	44	25	40	33	9	8	22	25
Be	3.8	5.6	5.5	5.4	4.5	5.1	4.5	4.1	4.1	4.8	2.8	2.7	5	5.2
Sc	22	30	29	36	29	36	30	23	29	22	26	21	21	23
V	167	213	213	253	196	245	202	154	182	172	203	179	147	155
Cr	1996	2777	2508	3290	2593	3235	2443	2194	2412	2013	2210	1972	1851	2031

Co	218.1	227.6	165	233.4	178.1	325.1	174.6	95	193.8	107.8	64.2	50.4	76.1	79.8
Ni	590	724	610	938	718	1093	591	352	756	409	282	226	365	369
Cu	576	406	376	487	296	435	335	223	373	276	42	62	406	473
Zn	3955	4777	4298	6001	4269	5825	3607	2215	4400	2370	761	642	339	361
Ga	9.5	11.6	10.6	15	11.9	14.7	11.1	9	11.3	7.9	11	9.4	8.7	9.4
As	36	27.4	27.2	23.9	23.6	23.1	24.6	24.2	22.8	31	21.1	34.8	27.1	33.1
Se	2.6	3.4	5.3	2.2	2.6	2.4	3	3.1	2	2.6	1.2	1.4	1.7	1
Rb	159.9	233.3	210.1	239.1	196.1	219	188.9	182.3	178.5	180.4	226.8	194.8	178.2	190
Sr	108	40	39	58	48	38	34	43	46	41	131	30	39	34
Y	67.8	75.6	74.4	71.5	64.2	79.2	74.6	61.9	63	71.3	54.4	54.2	59.2	59.3
Zr	100	137	121	154	122	163	118	103	113	102	108	100	94	106
Nb	85.5	121.2	109.3	137.8	108.3	146	107.5	95.2	107.8	87.7	88.4	79.9	87.5	87
Mo	4	3	4	3	6	3	4	5	4	5	9	7	4	3
Ag	0.19	0.21	0.26	0.27	0.2	0.25	0.21	0.17	0.2	0.18	0.05	0.025	0.025	0.025
Cd	0.15	0.12	0.11	0.11	0.1	0.11	0.11	0.16	0.13	0.09	0.06	0.1	0.33	0.36
Sn	16	22	19	25	20	25	21	17	18	16	16	15	14	16
Sb	4.6	7.0	9.1	9.4	8.3	5.7	7.9	6.0	6.6	9.4	7.9	9.3	8.3	9.6
Te	0.34	0.37	0.21	0.22	0.14	0.26	0.19	0.22	0.17	0.22	0.05	0.005	0.17	0.15
Cs	9.8	12.4	15.4	7.3	7.3	9.4	11.7	6.7	6.8	11.0	3.0	3.1	10.4	18.0
Ba	8011	642	416	597	499	449	312	336	365	498	8663	561	506	260
La	105	234	187	155	148	227	138	130	137	188	85	62	109	112
Ce	230	483	376	334	312	463	283	271	271	373	238	186	224	250
Pr	30.6	58.8	49.3	44.8	40.7	59.9	37.4	35.5	36.0	48.8	36.4	27.9	28.4	31.9
Nd	128	239	203	185	176	244	157	147	155	201	167	131	123	134
Sm	29.8	53.7	46.4	43.3	40.7	55.9	37.8	34.1	36.7	45.9	43.4	34.9	28.7	31.6
Eu	5.03	8.44	7.72	6.88	6.71	9.06	6.08	5.49	5.96	7.27	8.14	7.21	5.22	5.37

Gd	24.0	33.8	31.0	29.2	27.2	38.4	26.5	23.7	25.5	29.2	26.7	23.5	22.6	22.6
Tb	2.80	3.60	3.42	3.21	3.06	4.02	3.21	2.70	2.82	3.13	2.64	2.47	2.42	2.50
Dy	13.3	15.7	15.3	14.9	14.1	16.7	14.9	12.4	12.7	14.5	11.2	11.2	11.9	11.6
Ho	2.08	2.32	2.3	2.29	2.09	2.45	2.27	1.92	1.84	2.16	1.64	1.64	1.84	1.78
Er	4.72	5.29	5.21	5.27	4.74	5.53	5.07	4.14	4.12	4.59	3.63	3.56	3.87	4.04
Tm	0.60	0.72	0.68	0.71	0.67	0.80	0.67	0.53	0.57	0.58	0.46	0.45	0.48	0.54
Yb	3.51	4.19	4.12	4.32	3.86	4.70	4.00	3.05	3.20	3.42	2.56	2.59	2.93	3.05
Lu	0.45	0.58	0.57	0.71	0.55	0.66	0.57	0.42	0.46	0.50	0.35	0.36	0.39	0.46
Hf	4.0	5.2	4.5	6.1	4.5	6.2	4.5	4.0	4.3	3.8	4.1	3.6	3.3	3.7
Ta	4.1	5.5	4.9	6.4	5.2	6.8	4.7	4.4	4.7	4.0	4.4	3.9	4.0	4.2
W	8	10	13	9	10	7	11	8	8	12	13	5	11	15
Re	0.004	0.001	0.001	0.001	0.002	0.003	0.001	0.001	0.001	0.001	0.002	0.003	0.002	0.002
Au	0.011	0.029	0.009	0.006	0.011	0.009	0.012	0.008	0.007	0.011	0.005	0.002	0.026	0.021
Tl	1.58	1.94	1.8	1.84	1.49	1.81	1.55	1.49	1.39	1.55	4.54	3.68	1.88	2.14
Pb	28	48	62	54	54	51	48	38	42	51	24	27	33	42
Bi	0.74	0.44	0.55	0.4	0.35	0.42	0.42	0.27	0.38	0.43	0.31	0.18	0.54	0.65
Th	18.4	25.0	22.4	29.7	23.0	31.0	21.8	20.3	22.0	19.1	18.1	17.1	17.4	19.1
U	47.4	38.6	36.8	43.7	35.5	39.8	33.8	32.1	32.2	31.3	12.7	14.2	22.6	24.6

Table S5 continued

Sample No.	SR1394020	SR1394021	SR1394022	SR1394028	SR1394030	SR1394031	SR1394032	SR1394033	SR1394034	SR1394035	SR1118333	SR1118334	SR1118338	SR1118339
Alteration type	Cb	Cb	Cb	Cb	Cb	Cb	Cb	Cb	Cb	Cb	Cb	Cb	Cb	Cb
Drill Hole No.	RD1756	RD1756	RD1756	RD1756	RD1756	RD1756	RD1756	RD1756	RD1756	RD1756	RD3008	RD3008	RD3008	RD3008
SiO_2	30.8	29.9	32.7	39.5	36.8	30.7	31.5	29.2	24.8	23.0	37.1	35.0	29.7	36.3
TiO_2	0.52	0.49	0.49	0.42	0.45	0.56	0.45	0.42	0.40	0.44	0.51	0.49	0.44	0.51
Al_2O_3	9.7	9.1	9.2	7.3	8.4	10.6	8.6	7.4	7.3	8.9	9.4	9.3	8.5	9.5
Fe_2O_3	15.6	16.2	16.3	8.8	11.9	16.5	17.1	12.2	8.3	12.8	12.0	13.4	12.6	13.6
MnO	1.54	1.65	1.54	1.47	1.39	1.32	1.25	1.68	1.82	2.08	1.36	1.43	1.61	1.19
MgO	7.9	8.0	7.6	9.4	8.3	8.0	8.1	9.4	11.0	10.0	8.1	7.9	9.7	7.4
CaO	10.7	11.3	10.4	11.8	11.1	10.6	11.1	14.0	16.6	14.8	9.7	10.2	13.1	9.9
Na_2O	0.19	0.18	0.18	0.09	0.15	0.15	0.12	0.12	0.12	0.19	0.11	0.11	0.16	0.16
K_2O	3.3	3.1	3.0	2.0	2.8	3.6	3.1	2.5	2.6	3.1	2.4	2.6	2.5	3.0
P_2O_5	0.25	0.27	0.37	0.16	0.32	0.23	0.23	0.25	0.21	0.25	0.25	0.25	0.25	0.27
CO_2	14.4	15.1	13.8	16.1	14.8	14.1	14.7	19.4	22.8	20.3	17.0	17.8	23.5	17.2
F	3422	3215	2716	2458	3668	2706	3715	2659	3085	3320	2880	3224	2630	3407
S	300	400	400	100	300	600	800	300	1600	400	500	1300	200	400
Cl	90	70	80	10	10	20	20	10	10	30	50	50	80	70
Li	31	27	27	34	29	25	25	16	16	21	33	28	43	24
Be	6.2	6.6	6.4	3.7	4.7	6.9	5	4.5	4.7	6.8	3.6	4.1	4.3	5.4
Sc	26	23	25	19	22	30	25	20	20	25	25	23	21	24
V	182	170	163	114	146	188	175	156	138	157	149	142	147	149
Cr	2166	2043	2100	1710	1871	2427	1898	1699	1624	1856	2182	2021	1938	2203

Co	81.9	68.6	66.4	124.9	97.4	86	68.3	69.2	74.4	70	130.5	100.6	87.1	65.3
Ni	416	373	364	541	481	407	319	328	279	286	466	410	490	324
Cu	443	349	404	232	434	411	521	264	374	221	811	1244	362	459
Zn	534	531	482	691	668	784	626	582	600	613	4507	3488	2471	2417
Ga	9.1	9	8.3	8	8.6	11.3	8.7	7.5	8.2	9.7	10.7	11.3	11.2	11.1
As	65.9	69.1	64.8	21.7	34.9	94.1	82.8	43	57	60.3	13.7	30.6	24.6	35.3
Se	0.8	1.6	1.4	1.2	1.6	0.6	1	1.7	2.5	2.3	0.25	0.25	0.25	0.25
Rb	234.4	206.8	220	107.9	187.3	250.9	221.4	163.7	169.7	220.3	166.4	161.2	159.9	191.7
Sr	33	33	32	37	41	38	47	40	50	38	57	91	37	45
Y	60.5	61	59.9	47.4	61.5	68.8	58.4	56.4	65.5	66.7	67.3	69.2	60.7	59.7
Zr	122	111	109	81	108	126	112	90	87	112	116	118	95	114
Nb	94.2	95.9	90.9	72.3	84.6	106.5	85.5	75.8	68.1	84.1	87.1	96.6	83.9	93.9
Mo	5	6	5	3	4	8	11	7	4	6	8	9	5	6
Ag	0.06	0.025	0.025	0.025	0.025	0.06	0.05	0.11	0.025	0.08	0.16	0.3	0.15	0.16
Cd	0.22	0.16	0.13	0.21	0.16	0.2	0.26	0.25	0.25	0.16	0.21	0.24	0.19	0.24
Sn	19	18	18	13	16	18	18	14	14	15	17	17	15	18
Sb	18.9	19.7	19.1	7.6	11.4	24.9	21.8	12.6	10.9	19.1	5.7	6.5	10.0	9.8
Te	0.26	0.25	0.25	0.13	0.15	0.17	0.29	0.22	0.13	0.17	0.1	0.3	0.005	0.17
Cs	22.1	20.3	20.3	2.7	5.6	29.0	12.8	9.9	13.7	23.9	4.5	4.1	6.7	8.9
Ba	283	328	395	514	881	473	797	613	622	525	1157	2136	413	581
La	207	184	203	82	164	146	178	116	110	118	139	221	107	190
Ce	422	366	354	235	364	289	426	236	305	317	304	355	256	404
Pr	51.7	44.1	46.1	24.9	37.0	38.2	43.9	31.9	31.1	36.0	38.6	45.6	31.0	45.7
Nd	213	184	194	108	157	166	187	138	138	159	161	174	134	185
Sm	45.8	40.1	42.2	24.8	35.1	37.4	41.7	31.0	31.9	37.0	36.5	37.2	31.4	41.4
Eu	7.75	7.29	7.12	4.07	6.06	6.16	7.25	5.25	5.64	7.11	5.92	6.38	4.95	6.47

Gd	29.6	28.6	28.3	17.8	25.1	26.6	27.7	22.2	23.4	27.2	26.3	26.8	23.9	28.4
Tb	2.94	2.87	2.81	1.94	2.65	2.97	2.73	2.35	2.54	2.87	2.93	2.95	2.63	2.80
Dy	12.5	12.9	13.0	9.2	12.4	13.7	12.5	10.9	12.4	13.5	13.9	14.3	12.6	13.4
Ho	1.92	1.97	1.92	1.44	1.88	2.12	1.93	1.68	1.94	2.12	2.24	2.24	1.89	2
Er	4.17	4.06	4.09	3.11	4	4.79	4.2	3.64	4.25	4.85	4.92	5.13	4.03	4.38
Tm	0.55	0.55	0.54	0.39	0.51	0.61	0.54	0.49	0.55	0.65	0.62	0.67	0.53	0.58
Yb	3.45	3.24	3.18	2.37	2.90	3.69	3.06	2.68	3.10	3.86	3.70	3.91	3.28	3.36
Lu	0.46	0.42	0.45	0.31	0.39	0.50	0.41	0.40	0.37	0.52	0.52	0.54	0.47	0.46
Hf	4.0	3.8	3.7	2.9	3.5	4.3	3.6	2.9	3.1	3.9	4.2	4.2	3.7	4.1
Ta	4.5	4.3	4.2	3.5	3.9	5.0	3.9	3.4	3.3	3.7	4.5	4.4	4.0	4.6
W	30	38	32	6	12	34	41	25	12	24	10	12	10	11
Re	0.002	0.002	0.003	0.004	0.004	0.002	0.003	0.002	0.002	0.001	0.003	0.003	0.001	0.001
Au	0.006	0.003	0.003	0.148	0.012	0.006	0.036	0.199	0.052	0.03	0.042	0.086	0.714	0.061
Tl	2.61	2.37	2.6	0.98	1.93	3.34	2.43	1.86	2.08	2.73	1.33	1.28	1.33	1.62
Pb	80	72	75	29	51	67	91	37	31	43	46	50	49	53
Bi	1.15	1.01	1.19	0.44	0.83	0.9	1.19	0.77	1.12	0.93	0.6	0.53	0.54	0.67
Th	21.0	20.4	20.1	15.6	18.3	23.2	19.3	16.0	15.3	19.2	20.8	21.5	18.2	21.1
U	34.6	32.9	36.1	14.3	23.3	28.7	28.7	27.6	20.5	29.5	24.9	45.3	20.9	25.2

Table S5 continued

Sample No.	SR1118340	SR1118341	SR1118342	SR1118343	SR1118344	SR1118345	SR1118346	SR1118349	SR1394155	SR1394162	SR215290	SR215291	SR215292	SR215293
Alteration type	Cb	Cb	Cb	Cb	Cb	Cb	Cb	Cb	Cb	Cb	Cb	Cb	Cb	Cb
Drill Hole No.	RD3008	RD3008	RD3008	RD3008	RD3008	RD3008	RD3008	RD3008	RD6	RD6	RD635	RD635	RD635	RD635
SiO_2	29.3	31.7	28.7	30.7	33.2	34.1	30.8	35.0	39.3	36.3	35.2	31.4	30.6	37.8
TiO_2	0.42	0.48	0.45	0.52	0.43	0.48	0.53	0.52	0.52	0.38	0.45	0.44	0.43	0.49
Al_2O_3	8.1	9.1	8.8	9.9	8.0	9.1	9.8	9.8	10.0	6.7	8.4	8.2	7.9	8.8
Fe_2O_3	10.5	11.6	10.7	11.1	11.9	14.4	10.5	13.3	10.0	17.0	12.1	11.3	9.6	9.7
MnO	1.68	1.51	1.65	1.55	1.23	1.28	1.69	1.28	0.97	1.11	1.15	1.24	1.63	1.41
MgO	9.9	9.1	9.5	8.8	8.6	8.3	9.0	7.7	8.1	7.7	8.9	8.9	9.1	7.9
CaO	14.1	12.4	13.1	12.3	10.8	10.8	12.8	10.5	9.9	10.5	10.9	13.1	14.0	11.3
Na_2O	0.13	0.16	0.16	0.19	0.22	0.28	0.19	0.20	0.04	0.05	0.09	0.11	0.11	0.12
K_2O	2.5	2.9	2.6	3.3	1.8	2.7	3.1	3.2	3.0	1.9	2.2	2.5	2.5	2.8
P_2O_5	0.23	0.23	0.21	0.30	0.23	0.23	0.27	0.23	0.23	0.16	0.23	0.23	0.23	0.27
CO_2	25.6	23.7	24.2	24.1	21.8	20.0	24.9	18.3	13.8	14.8	17.4	21.3	22.9	18.1
F	2715	3148	3014	3659	3224	3652	4023	5581	3709	4000	2874	2684	2661	2900
S	400	300	400	500	300	500	300	500	200	1300	400	400	900	100
Cl	70	10	70	60	60	50	50	80	50	70	10	30	50	10
Li	21	25	28	29	46	38	25	24	34	27	40	24	19	22
Be	3.8	5.2	4.1	4.4	3.6	4.1	4.3	4.8	5.4	3.5	3	2.6	2.7	2.9
Sc	22	24	23	26	19	22	26	24	25	17	21	19	20	22
V	132	145	157	165	144	147	162	176	125	98	141	132	124	144
Cr	1861	2149	1983	2245	1829	2074	2242	2103	2234	1406	2055	1897	1987	2268

Co	67.4	65.7	88.2	61.2	137.5	88.6	80.5	75.9	144.9	115.5	138.9	100.9	80.6	92.7
Ni	416	336	479	379	565	444	440	370	581	396	578	405	332	442
Cu	485	392	307	319	185	254	310	443	391	578	673	682	686	496
Zn	1443	1567	777	518	634	440	508	673	1012	952	2330	1070	1010	1555
Ga	10.5	10.9	11.1	11.8	10.2	10.8	12.3	11.4	11.3	8.4	10.8	11.7	11.1	11.1
As	30.6	30	25.3	28.7	20.2	39.6	31.8	60.7	26.8	69	29.9	35.3	32.1	32.8
Se	1.3	0.9	2.1	1.1	3.1	1	0.25	0.25	1.4	1.4	0.7	0.9	1.7	1.3
Rb	167.5	181.1	158.8	194.8	109.1	151.2	216.4	224.8	186	107.9	158.8	164.1	166.7	180.2
Sr	44	43	43	41	61	75	41	49	52	116	45	48	60	44
Y	58.7	62.8	60.9	69.3	53.3	62.7	70.6	67.8	58.3	54.5	61.4	59	54.8	55.8
Zr	93	115	98	115	101	115	117	121	113	104	105	100	98	111
Nb	76.5	88.9	87	94	74.2	91.4	98.9	96.1	84.9	63.4	85.7	74.7	81	90.6
Mo	4	4	5	3	6	12	3	9	3	14	5	8	5	6
Ag	0.33	0.16	0.14	0.14	0.2	0.12	0.11	0.15	0.14	0.14	0.1	0.34	0.14	0.18
Cd	0.21	0.2	0.22	0.19	0.22	0.21	0.19	0.18	0.31	0.32	0.14	0.16	0.16	0.12
Sn	15	17	16	18	16	19	18	20	14	13	15	15	15	18
Sb	8.0	8.2	6.9	7.9	4.5	8.5	7.6	10.3	7.1	17.4	7.3	6.9	9.3	5.2
Te	0.09	0.12	0.08	0.14	0.3	0.35	0.22	0.42	0.07	0.15	0.5	0.48	0.63	0.38
Cs	7.9	10.5	7.3	10.8	4.1	7.4	17.2	25.2	3.4	2.0	6.4	5.9	5.6	7.1
Ba	673	546	603	544	605	1512	1190	1091	713	5109	756	852	2169	543
La	131	166	147	225	149	301	178	315	65	66	147	160	110	141
Ce	270	336	279	416	264	494	327	483	156	141	321	269	266	261
Pr	33.0	43.0	37.4	50.4	36.2	55.0	41.9	58.2	23.6	19.6	39.9	40.1	36.2	33.2
Nd	141	177	151	207	143	208	167	220	106	87	155	159	141	132
Sm	31.8	39.7	34.6	44.9	31.4	42.2	37.2	45.4	28.5	23.2	34.3	34.3	32.2	30.3
Eu	5.06	6.23	5.39	7.32	5.04	7.38	5.95	7.71	4.29	4.03	6.76	7.44	6.93	5.88

Gd	25.3	28.4	26.5	31.9	23.4	30.5	27.3	31.4	20.1	17.6	24.5	24.4	22.3	21.5
Tb	2.75	3.03	2.75	3.24	2.47	3.03	3.02	3.19	2.45	2.24	2.74	2.65	2.40	2.39
Dy	12.6	13.9	12.4	14.7	11.7	14.1	14.3	14.5	11.4	10.3	12.3	12.6	10.8	11.0
Ho	1.87	2.08	1.89	2.22	1.78	2.01	2.25	2.16	1.77	1.59	2.01	2.05	1.73	1.77
Er	3.87	4.39	4.04	5.03	3.85	4.36	4.9	4.78	3.82	3.47	5.06	5.3	4.61	4.37
Tm	0.70	0.59	0.53	0.68	0.75	0.57	0.65	0.62	0.49	0.42	0.67	0.68	0.57	0.56
Yb	2.85	3.41	2.84	3.82	2.90	3.27	3.95	3.90	2.83	2.60	3.79	4.03	3.33	3.07
Lu	0.39	0.47	0.42	0.53	0.42	0.49	0.56	0.64	0.38	0.33	0.47	0.53	0.42	0.41
Hf	3.6	4.1	3.6	4.2	3.7	4.0	4.4	4.6	4.3	4.3	3.7	3.8	3.5	3.8
Ta	3.9	4.6	4.0	4.7	4.0	4.5	4.7	4.6	4.6	3.4	4.0	3.8	3.9	4.4
W	7	9	7	10	5	14	7	14	3	10	13	16	13	9
Re	0.001	0.001	0.001	0.001	0.001	0.001	0.001	0.001	0.001	0.002	0.001	0.001	0.001	0.001
Au	0.205	0.079	0.076	0.033	0.048	0.07	0.044	0.053	0.023	0.093	1.019	1.39	0.559	0.52
Tl	1.46	1.55	1.33	1.7	0.94	1.23	2.02	2.2	4.88	3.06	1.33	1.42	1.49	1.63
Pb	43	44	37	37	37	42	36	44	31	49	33	29	33	29
Bi	0.61	0.57	0.58	0.49	0.51	0.64	0.51	0.87	0.12	0.37	0.52	0.75	1.05	0.77
Th	17.8	21.0	18.4	22.2	18.1	21.0	21.8	22.8	20.4	14.8	19.3	18.9	17.3	19.8
U	22.3	26.8	29.6	32.0	27.8	36.6	32.6	39.6	16.5	19.0	27.5	35.5	28.0	24.8

Table S5 continued

Sample No.	SR1393986	SR1393987	SR1393988	SR1393989	SR1393990	SR1393991	SR1393992	SR1393993	SR1393994	SR1393995	SR1393996	SR1393997	SR1393998	SR1394013
Alteration type	Cb	Cb	Cb	Cb	Cb	Cb	Cb	Cb	Cb	Cb	Cb	Cb	Cb	Cb
Drill Hole No.	RD635	RD635	RD635	RD635	RD635	RD635	RD635	RD635	RD635	RD635	RD635	RD635	RD635	RD635
SiO_2	32.0	27.5	28.2	34.1	25.8	25.9	27.4	27.8	31.0	35.4	36.5	32.2	35.7	31.0
TiO_2	0.51	0.47	0.49	0.52	0.40	0.36	0.41	0.33	0.34	0.42	0.44	0.45	0.50	0.53
Al_2O_3	9.8	9.5	9.4	10.1	7.7	6.9	7.7	6.1	6.3	7.6	8.2	9.1	9.7	9.9
Fe_2O_3	10.5	11.4	11.9	11.7	9.9	9.6	9.0	9.2	8.9	8.4	11.2	11.6	13.2	13.3
MnO	1.59	1.65	1.67	1.43	2.13	2.08	2.08	2.04	2.04	1.60	1.24	1.59	1.19	1.52
MgO	9.2	10.3	10.0	8.5	10.8	11.1	10.6	11.1	9.9	9.2	9.8	8.9	9.5	8.6
CaO	12.1	13.6	13.0	10.8	15.6	16.0	15.1	15.9	14.9	12.9	11.4	12.0	9.7	11.5
Na_2O	0.15	0.13	0.12	0.18	0.09	0.12	0.11	0.09	0.08	0.11	0.11	0.16	0.12	0.11
K_2O	3.0	2.7	2.6	3.0	2.2	2.1	2.3	1.6	1.8	2.2	1.9	2.8	2.0	2.8
P_2O_5	0.27	0.34	0.21	0.27	0.16	0.18	0.21	0.16	0.14	0.23	0.27	0.23	0.21	0.30
CO_2	16.6	17.7	15.7	14.4	20.6	21.3	20.4	21.5	20.2	17.5	15.3	16.5	12.9	15.9
F	3210	3802	3944	3513	2650	3574	2664	2952	2363	2443	2876	3166	3344	5554
S	200	100	100	300	200	200	<100	300	200	200	300	200	<100	200
Cl	80	80	60	80	80	80	80	80	70	40	80	180	30	60
Li	27	28	31	25	20	22	20	21	16	21	34	21	46	29
Be	4.3	3.7	3.7	4.4	2.9	3.1	2.9	2.2	2	2.9	3.2	4.4	4.4	3.6
Sc	27	25	26	27	22	18	21	18	17	20	20	24	25	26
V	153	157	164	170	136	125	136	117	134	141	151	165	175	182
Cr	2163	2063	2094	2251	1779	1561	1803	1432	1468	1829	1954	2000	2196	2359

Co	100.2	130.4	141.9	116.5	100.6	78.7	94.2	98.5	79.2	99	143.2	90.5	213.9	146.4
Ni	335	518	586	368	415	314	454	400	280	385	559	298	715	582
Cu	545	597	629	325	449	485	251	450	251	270	274	259	301	489
Zn	1377	1542	2037	1635	1563	897	1501	1508	1308	1440	1549	1393	3468	3274
Ga	9.7	9.8	10	10.9	8.5	8.7	8.9	7.4	6.9	7.9	8.8	9.5	10.2	9.9
As	23.9	25.6	18.8	35	18.2	21.6	16.6	15.4	12.5	10.5	14.2	38.1	33.2	18.7
Se	2.4	2.3	1.5	1.7	2.8	1.7	2.7	2.4	3.3	2	1.8	2.6	2.2	2.9
Rb	210.8	191.3	185	204.9	145.4	149.3	145.9	100.1	111.1	127.1	114.6	190.4	170.4	181.1
Sr	36	37	34	43	48	35	38	35	42	47	36	32	32	54
Y	68.1	74.8	75.4	70.2	62.7	70.6	64.4	64.1	47.3	45.9	50.6	63.1	56.8	67.6
Zr	108	105	101	110	84	76	88	72	74	87	93	97	107	113
Nb	97.2	87.8	93.7	99.3	76.6	69	76.9	63	61.1	81.6	83.6	88.3	94.7	100.8
Mo	4	5	5	5	4	5	4	6	23	39	10	4	4	4
Ag	0.2	0.22	0.22	0.2	0.15	0.16	0.15	0.17	0.23	0.33	0.25	0.2	0.2	0.24
Cd	0.09	0.13	0.11	0.09	0.18	0.12	0.09	0.08	0.08	0.11	0.14	0.13	0.12	0.19
Sn	18	17	17	18	16	12	14	12	12	16	15	16	17	18
Sb	5.4	4.2	5.3	5.8	4.3	5.5	3.5	3.6	3.6	3.6	6.0	6.2	4.8	5.6
Te	0.35	0.37	0.25	0.28	0.18	0.14	0.17	0.16	0.18	0.16	0.14	0.23	0.19	0.19
Cs	18.3	7.7	8.3	17.6	5.9	5.5	4.0	4.3	2.4	3.4	2.7	12.8	8.7	3.8
Ba	668	481	500	1264	1181	584	521	797	623	668	399	365	276	539
La	143	183	142	118	113	66	94	81	92	94	89	116	125	147
Ce	264	328	287	250	237	141	191	165	178	199	192	239	272	313
Pr	37.3	46.0	37.2	32.8	32.4	19.6	26.0	21.9	22.6	27.2	26.0	31.3	35.5	40.6
Nd	150	179	158	136	138	86	109	96	95	118	109	130	146	170
Sm	33.1	39.6	36.6	32.1	31.7	23.8	26.7	23.7	23.2	27.7	26.4	30.5	33.7	40.4
Eu	6.17	7.27	6.52	5.43	5.34	4.23	4.61	4.15	3.84	4.43	4.32	4.89	5.17	6.59

Gd	22.9	27.3	26.6	23.5	22.3	20.6	21.0	19.8	17.2	19.4	19.2	22.3	22.3	28.7
Tb	2.72	3.13	3.12	2.92	2.59	2.72	2.63	2.47	2.06	2.09	2.23	2.72	2.46	3.15
Dy	13.1	14.4	14.7	13.5	12.4	13.2	12.7	12.1	9.3	9.8	10.5	12.4	10.8	14.1
Ho	2.07	2.21	2.23	2.08	1.85	2.03	1.9	1.8	1.39	1.44	1.61	1.95	1.71	2.03
Er	4.75	4.87	4.93	4.49	4.07	4.4	4.28	3.83	3.15	3.17	3.43	4.31	3.83	4.58
Tm	0.63	0.62	0.60	0.58	0.52	0.56	0.55	0.50	0.42	0.43	0.43	0.58	0.52	0.58
Yb	3.47	3.59	3.46	3.17	2.93	3.21	3.00	2.78	2.31	2.47	2.58	3.18	3.04	3.38
Lu	0.45	0.50	0.44	0.46	0.42	0.43	0.41	0.40	0.31	0.35	0.33	0.43	0.39	0.47
Hf	3.9	3.9	4.0	4.2	3.2	3.0	3.2	2.7	2.7	3.3	3.5	3.7	4.0	4.4
Ta	4.4	4.2	4.4	4.7	3.6	3.3	3.7	2.9	3.0	3.8	4.0	4.1	4.5	4.8
W	14	11	8	10	10	11	6	6	5	4	5	9	6	7
Re	0.002	0.003	0.002	0.003	0.002	0.001	0.001	0.001	0.001	0.003	0.002	0.001	0.001	0.001
Au	0.012	0.054	0.048	0.007	0.004	0.005	0.018	0.035	0.039	0.018	0.022	0.013	0.033	0.012
Tl	1.88	1.54	1.6	1.83	1.13	1	1.08	0.79	0.91	1.07	0.83	1.59	1.44	1.34
Pb	32	28	31	34	25	29	25	24	25	31	30	40	32	38
Bi	0.87	0.95	0.82	0.5	0.45	0.63	0.48	0.66	0.91	1.12	0.49	0.53	0.56	0.6
Th	20.4	19.3	20.1	20.4	15.6	14.5	16.2	13.2	13.6	16.9	17.4	19.1	20.0	21.5
U	25.1	26.9	25.4	24.8	20.9	24.6	23.7	20.9	21.0	23.9	22.7	28.6	27.7	38.2

Table S5 continued

Sample No.	SR1394014	SR1394015	SR1394016	SR1394017	SR215294	SR215295	SR215296	SR215297	SR215298	SR1393969	SR1394066	SR1394058	SR1394062	SR1394063
Alteration type	Cb	Cb	Cb	Cb	Cb	Cb	Cb	Cb	Cb	Cb	Ser	Ser	Ser	Ser
Drill Hole No.	RD635	RD635	RD635	RD635	RD635	RD635	RD635	RD635	RD635	RD917A	RD1687	RD1687	RD1687	RD1687
SiO_2	32.7	21.0	32.0	35.1	30.2	25.4	28.4	37.0	34.2	35.9	52.2	49.2	48.4	47.7
TiO_2	0.53	0.45	0.48	0.52	0.44	0.33	0.47	0.47	0.45	0.39	0.86	0.55	0.73	0.76
Al_2O_3	9.9	8.5	9.0	9.8	8.1	6.0	8.5	8.5	8.2	7.6	16.8	10.8	13.6	14.8
Fe_2O_3	11.5	8.8	9.3	9.1	8.3	9.3	11.0	9.7	7.6	14.0	14.8	12.6	16.7	16.4
MnO	1.73	2.49	1.83	1.73	2.00	2.16	1.85	1.55	1.81	2.13	0.06	0.17	0.36	0.28
MgO	8.6	10.9	8.9	8.2	9.6	9.7	8.5	7.8	8.7	7.2	2.5	2.2	4.2	4.2
CaO	11.3	16.7	13.0	11.5	14.5	17.1	13.9	11.7	13.3	11.2	1.0	10.7	3.5	2.2
Na_2O	0.16	0.15	0.16	0.18	0.15	0.08	0.12	0.13	0.11	0.05	0.19	0.20	0.24	0.26
K_2O	2.9	2.7	3.0	3.2	2.6	1.9	2.7	2.8	2.8	2.8	5.9	3.6	4.0	4.5
P_2O_5	0.27	0.21	0.27	0.32	0.21	0.14	0.23	0.25	0.23	0.21	0.53	0.27	0.50	0.44
CO_2	15.0	24.4	18.7	16.8	23.5	26.0	22.1	18.9	21.5	14.8	1.1	1.9	3.9	3.3
F	3600	3473	3281	3571	3480	10723	5165	3106	3177	2501	5527	57847	10436	5375
S	200	200	200	<100	<100	3800	2600	600	600	1600	200	4300	800	1100
Cl	70	80	40	80	60	10	10	10	10	40	100	120	180	120
Li	30	19	20	22	26	21	23	22	26	9	37	27	46	50
Be	3.8	3.7	4.1	4.8	3.1	2.1	2.7	2.9	2.9	2.7	7.7	5.1	5.4	5.5
Sc	29	27	24	24	21	16	23	22	21	20	39	21	36	38
V	187	150	164	168	150	118	148	149	148	137	260	171	236	230
Cr	2335	1951	2114	2315	2073	1564	2232	2254	2120	1717	3721	2385	3183	3184

Co	139.3	107.4	87.2	75.7	80.6	87.8	122.5	82.2	83.1	74	97	78.7	155.4	169.7
Ni	469	289	375	378	415	329	504	398	351	277	363	326	475	514
Cu	339	229	290	221	260	285	339	182	262	59	276	1578	698	623
Zn	2413	1211	800	504	457	509	1499	1291	1020	497	3184	1584	2180	2751
Ga	10.9	10.2	9.6	10.4	11.2	8.9	11.8	10.3	10.8	8.2	17.3	10.6	14.7	14.2
As	31.5	26.3	29.4	32	37.2	117.4	119.5	43.3	41.6	16.3	59.5	59.8	47.8	35.6
Se	3.8	5	3.9	3	1.8	2	1.3	1.8	2.3	2.4	0.25	2.8	2.8	2.8
Rb	171.8	156.8	180.2	187.4	160	112.1	176	181.4	183.2	165	371	224.8	240.2	273.3
Sr	37	41	48	36	37	315	177	39	44	142	32	125	52	65
Y	68.9	66.7	59.8	55.7	58.5	55.1	64.7	72.4	62.2	50.3	103.8	106.7	145.7	247.2
Zr	107	92	102	114	94	72	102	104	105	86	188	130	171	182
Nb	100.9	85.5	87.8	100.1	82.4	58.1	85.2	86.6	82.8	70.8	154.4	102.9	135.5	132.1
Mo	5	5	4	4	4	6	9	6	4	15	6	11	7	5
Ag	0.22	0.18	0.18	0.21	0.025	0.025	0.09	0.06	0.025	0.025	0.05	0.26	0.06	0.025
Cd	0.2	0.24	0.2	0.15	0.16	0.13	0.14	0.16	0.22	0.06	0.06	0.11	0.11	0.09
Sn	18	16	17	18	15	11	17	16	15	13	29	21	25	26
Sb	6.8	5.4	5.9	11.0	6.3	7.8	8.2	7.0	5.5	7.1	10.6	9.2	10.1	8.1
Te	0.23	0.2	0.16	0.16	0.19	0.16	0.2	0.15	0.19	0.005	0.23	0.6	0.34	0.33
Cs	9.0	6.8	6.5	6.9	6.5	4.2	6.5	7.8	4.9	2.6	18.4	11.3	10.1	15.4
Ba	991	1139	1030	455	264	14702	9253	627	349	6475	314	8137	2040	3474
La	129	128	138	138	111	95	124	147	124	55	228	246	215	273
Ce	274	252	279	2888	195	165	241	272	274	179	511	609	448	558
Pr	37.2	34.2	36.4	37.5	29.9	25.1	34.1	38.2	33.5	27.2	57.5	62.3	54.4	69.2
Nd	153	141	155	158	126	103	137	156	135	124	250	248	232	291
Sm	36.5	33.4	35.5	36.1	29.9	24.8	33.0	36.3	31.2	32.7	54.3	47.2	50.7	67.5
Eu	5.94	5.39	5.65	5.59	4.71	4.21	5.31	6.23	5.32	6.71	9.04	8.90	8.83	11.04

Gd	26.6	24.1	24.1	23.8	24.3	21.5	25.2	28.5	25.1	22.7	39.3	32.8	40.8	57.7
Tb	3.05	2.88	2.69	2.61	2.69	2.38	2.76	3.08	2.80	2.55	4.52	4.04	5.34	8.25
Dy	14.3	13.1	12.3	11.7	12.0	10.4	12.4	13.9	12.4	10.9	19.6	18.2	27.0	47.2
Ho	2.08	2.01	1.79	1.75	1.8	1.52	1.89	2.1	1.89	1.57	3.32	3.19	4.86	9.2
Er	4.64	4.27	3.84	3.92	3.98	3.46	4.49	4.62	4.47	3.39	7.43	7.59	11.08	21.8
Tm	0.64	0.57	0.49	0.49	0.50	0.44	0.62	0.55	0.52	0.43	1.06	1.08	1.65	3.31
Yb	3.58	3.20	2.85	2.87	2.78	2.28	3.27	3.03	2.83	2.40	6.37	6.54	9.00	18.03
Lu	0.49	0.45	0.39	0.37	0.38	0.29	0.45	0.40	0.36	0.34	0.81	0.83	1.12	2.31
Hf	4.4	3.6	3.9	4.2	3.6	2.7	4.2	3.7	3.8	3.0	6.5	4.6	6.0	6.2
Ta	4.7	3.9	4.2	4.6	4.0	3.0	4.4	4.2	4.0	3.6	7.3	4.5	6.4	6.6
W	9	7	7	7	4	4	6	6	4	4	12	11	10	9
Re	0.001	0.002	0.004	0.003	0.001	0.001	0.001	0.001	0.001	0.001	0.003	0.004	0.002	0.004
Au	0.034	0.063	0.036	0.017	0.131	0.082	0.083	0.019	0.068	0.023	0.029	0.03	0.01	0.028
Tl	1.37	1.21	1.34	1.4	1.11	0.83	1.49	1.54	1.31	3.28	2.65	1.84	1.85	2.15
Pb	39	30	27	30	23	23	34	30	30	22	53	66	58	64
Bi	0.55	0.45	0.58	0.56	0.33	0.4	0.55	0.5	0.48	0.79	0.43	1.3	0.55	0.46
Th	21.7	17.9	19.1	21.1	18.3	12.7	19.6	19.1	18.8	14.9	34.1	22.1	29.0	31.3
U	36.0	37.0	45.0	48.5	38.2	31.0	45.5	38.8	31.4	11.6	35.0	55.0	51.3	52.6

Table S5 continued

Sample No.	SR1394065	SR1394067	SR1394070	SR1394073	SR1394074	SR1394075	SR1394077	SR1394078	SR1394079	SR1394080	SR1394082	SR932941	SR932942	SR932944
Alteration type	Ser	Ser	Ser	Ser	Ser	Ser	Ser	Ser	Ser	Ser	Ser	Ser	Ser	Ser
Drill Hole No.	RD1687	RD1687	RD1687	RD1687	RD1687	RD1687	RD1687	RD1687	RD1687	RD1687	RD1687	RD1687	RD1687	RD1687
SiO_2	42.5	54.2	50.5	42.7	43.4	50.1	54.5	53.1	44.1	47.5	52.8	43.5	42.9	44.0
TiO_2	0.89	0.75	0.68	0.71	0.79	0.73	0.63	0.61	0.69	0.70	0.57	0.85	0.60	0.69
Al_2O_3	16.3	13.8	13.0	13.3	15.2	13.8	12.5	11.6	13.5	12.7	11.5	15.9	11.4	13.6
Fe_2O_3	20.5	16.5	18.1	20.5	15.9	13.7	13.4	15.9	19.1	20.2	15.8	22.4	21.1	27.8
MnO	0.27	0.19	0.19	0.58	0.32	0.52	0.39	0.53	0.76	0.46	0.19	0.14	0.66	0.05
MgO	3.6	4.2	4.5	3.6	3.3	3.2	3.0	3.2	3.8	3.6	2.7	3.0	3.6	1.3
CaO	2.4	1.4	2.2	3.3	6.4	3.8	3.0	3.2	3.9	3.3	3.6	1.6	4.1	1.4
Na_2O	0.18	0.16	0.09	0.13	0.12	0.23	0.16	0.16	0.18	0.16	0.12	0.15	0.11	0.11
K_2O	5.4	3.7	3.6	4.4	5.0	4.6	4.1	3.7	4.3	4.0	3.6	5.0	3.6	4.6
P_2O_5	0.37	0.44	0.44	0.34	0.48	0.46	0.41	0.37	0.39	0.48	0.37	0.37	0.27	0.41
CO_2	3.4	2.1	1.9	4.2	2.9	3.8	3.0	3.8	5.0	3.7	1.9	1.2	4.4	0.3
F	5759	4739	8971	4736	29108	10847	9118	7143	6449	8298	15180	5753	6037	7388
S	400	100	900	2100	700	1500	1700	1500	1200	500	3000	1300	3300	3200
Cl	50	70	30	70	10	100	70	90	60	50	50	10	50	10
Li	44	62	86	52	51	44	46	32	33	39	36	37	28	22
Be	8.5	5.7	4	7.1	6.6	6.4	6	5.2	5.5	5.7	4.7	4.3	3.5	6.3
Sc	43	36	36	43	40	36	30	29	35	36	28	43	36	30
V	297	222	215	274	241	232	207	188	206	215	176	253	210	216
Cr	3875	3375	3011	3160	3476	3231	2754	2639	2862	3017	2413	3951	2773	2940

Co	140.1	218.6	224	102.9	119	93.3	106.6	112.6	110.4	118	117.7	158.7	116.8	110.3
Ni	464	935	717	373	600	396	406	444	469	500	498	694	507	413
Cu	566	235	436	607	592	530	591	784	449	215	613	458	1056	4689
Zn	3489	5259	4477	3013	3376	2376	2420	2180	2163	2220	1879	3102	2206	1837
Ga	18.4	13.4	12.4	13.8	15.8	14.6	13	11.7	13.4	12.9	11.6	17.5	12.7	15.1
As	38.1	39.4	23.8	75.7	36.1	59.6	66.7	55	53.9	48.4	57.4	55.6	68.4	178.8
Se	2	0.9	3.1	5.4	5.8	10.1	9.8	9.3	3.7	2.3	7	3.9	7.2	9.6
Rb	368.7	238.5	229.6	303.7	306.8	268.7	244	213.3	237.2	238.7	210.3	310.1	211.9	263.6
Sr	32	34	63	99	103	67	48	60	54	41	82	59	98	158
Y	133.5	98.1	145.5	100	194.1	215.2	201.8	109.1	86.1	120.9	98.7	91.4	95.8	230.2
Zr	200	183	154	168	174	163	147	149	168	171	145	197	147	185
Nb	164.3	147.2	120.6	132.4	145	130.9	118.2	110.6	123.7	130	102.9	154.5	118.3	153.9
Mo	6	5	6	10	6	12	9	9	10	10	11	11	16	52
Ag	0.09	0.05	0.025	0.14	0.16	0.33	0.29	0.21	0.12	0.025	0.14	0.22	0.28	1.38
Cd	0.16	0.05	0.08	0.11	0.11	0.09	0.1	0.09	0.08	0.07	0.07	0.1	0.12	0.1
Sn	30	25	23	24	26	25	22	23	26	24	20	30	21	34
Sb	11.2	8.5	10.2	19.9	13.4	12.1	12.3	11.5	15.5	15.8	12.1	15.0	16.2	28.8
Te	0.25	0.2	0.24	0.31	0.22	0.29	0.36	0.49	0.5	0.38	0.47	0.58	0.24	0.9
Cs	36.4	8.0	5.2	35.1	20.1	14.9	12.4	13.5	14.3	17.7	10.4	21.5	14.0	14.5
Ba	406	210	2329	7134	1541	4357	3843	4781	3513	1685	9573	3654	11514	6111
La	193	252	252	181	246	241	201	302	414	282	276	230	172	729
Ce	471	573	524	505	480	551	440	676	781	653	542	500	341	1211
Pr	50.2	65.4	64.2	48.0	64.7	57.8	50.2	63.2	73.6	63.7	55.8	61.1	44.5	125.5
Nd	218	287	279	204	284	246	211	251	297	259	221	230	176	400
Sm	48.0	61.9	62.6	44.9	65.6	59.2	49.5	53.1	60.2	55.2	46.6	48.3	38.1	66.0
Eu	8.13	10.05	10.51	7.51	10.73	9.61	8.52	9.53	10.40	9.53	7.60	8.28	6.22	14.84

Gd	37.4	42.8	47.8	33.6	52.9	52.9	47.2	40.5	42.5	40.0	32.6	33.9	27.2	50.6
Tb	5.08	4.68	6.00	4.22	6.92	7.30	6.88	4.90	4.57	5.05	4.00	3.75	3.24	6.76
Dy	24.6	19.8	28.1	18.7	35.9	40.9	39.1	20.8	17.8	22.9	18.0	17.3	16.5	37.3
Ho	4.1	3.14	4.77	3.06	6.62	7.42	7.35	3.26	2.59	3.99	3.04	2.93	2.77	6.88
Er	8.54	6.83	10.29	6.62	15.07	18.03	17.18	7.12	5.8	9.05	7.01	7.28	6.72	17.13
Tm	1.17	0.97	1.50	0.88	2.20	2.72	2.62	0.95	0.82	1.35	0.99	0.88	0.80	1.99
Yb	6.59	5.73	8.60	5.23	12.88	14.98	14.71	5.43	4.64	7.80	6.12	5.73	4.99	12.06
Lu	0.85	0.71	1.06	0.69	1.54	1.88	1.86	0.72	0.63	1.00	0.75	0.80	0.65	1.55
Hf	7.1	6.6	5.3	5.9	6.6	5.8	5.2	5.0	5.6	5.9	4.9	7.4	5.3	7.0
Ta	7.6	7.4	6.0	6.1	6.8	6.2	5.5	5.1	5.8	6.0	4.8	7.7	5.4	6.1
W	16	8	11	22	14	10	9	10	14	14	11	14	16	47
Re	0.003	0.003	0.001	0.003	0.001	0.001	0.003	0.004	0.007	0.004	0.002	0.001	0.001	0.001
Au	0.049	0.01	0.024	0.069	0.038	0.046	0.05	0.067	0.092	0.067	0.075	0.083	0.082	0.244
Tl	3.19	1.62	1.78	3.11	2.49	2.27	2.08	1.72	1.86	1.95	1.77	2.63	1.81	2.12
Pb	98	65	63	90	95	84	82	66	69	66	67	84	70	98
Bi	0.63	0.31	0.35	0.53	0.51	0.7	0.62	0.64	0.56	0.35	0.64	0.41	0.67	3.28
Th	35.5	30.9	26.7	29.0	31.6	28.7	26.4	24.6	28.3	29.1	23.4	34.7	23.9	32.1
U	44.8	31.9	30.1	43.7	38.6	48.3	54.5	55.5	54.8	57.8	42.9	55.9	45.8	108.5

Table S5 continued

Sample No.	SR1394036	SR1394038	SR1394039	DA20612	DA20615	DA20616	SR1394006	SR215299	SR1393961	SR1393962	SR1393963	SR1393964	SR1393973	SR1393959
Alteration type	Ser	Ser	Ser	Ser	Ser	Ser	Ser	Ser	Ser	Ser	Ser	Ser	Ser	Ser
Drill Hole No.	RD1756	RD1756	RD1756	RD6	RD6	RD6	RD635	RD635	RD917A	RD917A	RD917A	RD917A	RD917A	RD917A
SiO_2	34.2	36.3	43.9	46.4	47.8	45.7	38.4	41.4	63.2	56.6	53.9	52.4	34.6	46.4
TiO_2	0.63	0.57	0.68	1.66	1.31	1.53	0.76	0.66	0.79	1.15	1.08	1.07	0.96	0.69
Al_2O_3	12.1	11.0	12.9	24.5	22.6	24.6	14.2	12.2	15.9	20.8	20.6	20.2	17.9	14.0
Fe_2O_3	16.1	20.3	26.1	8.9	11.3	11.0	19.9	12.6	5.5	5.0	5.0	5.2	31.1	25.3
MnO	1.02	0.94	0.18	0.04	0.04	0.05	0.50	0.79	0.04	0.04	0.03	0.03	0.04	0.03
MgO	6.7	6.0	2.8	1.4	1.3	1.2	5.7	5.5	1.5	2.0	2.1	2.0	1.6	1.3
CaO	8.5	7.1	1.8	0.6	0.6	0.6	4.0	7.6	0.7	1.0	0.8	0.8	0.7	0.7
Na_2O	0.19	0.16	0.15	0.27	0.30	0.23	0.24	0.16	0.03	0.03	0.11	0.15	0.15	0.01
K_2O	4.3	3.9	4.5	8.1	7.5	8.0	4.2	4.2	5.7	7.7	7.8	7.5	6.4	5.0
P_2O_5	0.32	0.32	0.30	0.44	0.48	0.46	0.39	0.37	0.39	0.48	0.60	0.48	0.39	0.34
CO_2	11.2	9.5	2.5	0.3	0.3	0.2	5.1	10.8	0.1	0.3	<0.05	<0.05	<0.05	0.2
F	4495	4965	5455	5370	5302	4982	5016	4171	4395	6309	6369	6563	5541	3825
S	200	200	700	1000	700	900	100	1500	2400	1400	5300	6800	800	5600
Cl	60	10	10	30	20	10	80	10	30	10	30	60	30	10
Li	30	33	34	23	20	20	52	30	16	19	18	18	17	14
Be	9	7.6	9.4	9	7.3	7.6	6.6	3.8	4.3	6.7	6.9	6.9	7.9	4.4
Sc	29	26	28	55	62	62	38	29	42	56	51	55	43	34
V	172	188	186	129	189	224	251	188	215	277	307	309	275	202
Cr	2708	2429	2308	5912	4822	5630	3156	3149	3401	4797	4455	4635	4121	2741

Co	63.4	63.1	48.2	138.1	137.6	121.4	195.2	74.8	84.6	110.7	106.3	95.2	68.3	77
Ni	354	342	286	304	281	240	728	372	435	570	604	600	384	346
Cu	184	145	220	570	115	62	387	315	56	60	25	29	47	83
Zn	919	743	772	1794	1754	1739	4393	1832	1856	2663	2424	2350	1870	1578
Ga	12.6	11.4	13	24.5	26.5	27.4	12.7	14.1	20.3	26.7	25.4	24.6	26	17.9
As	54.8	71.9	126.4	78.7	95.2	74.1	28.3	57.8	25	16.5	19.9	24.8	72.9	95.3
Se	1.1	1.2	1.3	0.25	5.1	0.25	2.3	1.1	1	1.4	2.1	1.1	3.1	1.2
Rb	288.4	269.4	314.9	350.2	348.2	334.5	277.2	258.9	359.7	481.6	458.9	476.5	371.5	295.5
Sr	37	39	70	123	115	137	39	41	137	101	287	479	67	335
Y	76.9	87.3	98.3	79.9	564.3	108.6	87.5	82.6	105.6	107.6	135.4	83.7	177.3	96.4
Zr	142	134	220	373	295	338	164	146	176	255	233	232	227	185
Nb	115.6	102.7	108.2	277	211.5	265.9	141.9	122.8	136.9	199.7	184.2	194.6	169.3	113.4
Mo	9	11	29	6	7	7	4	6	11	7	31	39	22	86
Ag	0.07	0.11	0.12	0.16	0.15	0.11	0.23	0.025	0.14	0.4	0.23	0.32	0.16	0.63
Cd	0.07	0.05	0.07	0.19	0.16	0.16	0.09	0.17	0.07	0.07	0.03	0.05	0.06	0.03
Sn	22	20	23	43	39	44	25	23	25	33	32	32	30	28
Sb	24.8	28.6	32.9	48.1	15.2	12.5	12.1	12.5	6.9	6.4	5.9	5.9	28.3	18.6
Te	0.29	0.6	0.71	0.72	0.28	0.36	0.26	0.34	0.14	0.11	0.09	0.08	0.22	0.63
Cs	29.8	25.3	33.7	10.6	9.9	8.3	24.4	12.0	8.1	12.4	13.0	14.6	21.2	7.2
Ba	699	940	1306	1753	1775	2157	459	841	9718	6011	22813	27429	3383	20728
La	170	165	330	230	244	309	259	231	127	147	142	128	110	353
Ce	491	489	604	542	567	535	558	494	299	405	393	342	231	539
Pr	53.3	55.0	65.0	53.7	75.1	80.0	68.6	60.5	44.4	60.6	59.0	52.0	29.8	58.4
Nd	234	233	253	196	330	309	277	236	194	279	275	231	131	206
Sm	52.6	51.1	49.9	29.5	73.5	44.5	64.5	49.3	50.6	75.8	75.3	60.4	37.6	45.3
Eu	10.14	10.44	9.96	8.94	26.72	10.44	10.01	8.95	13.06	18.51	18.51	11.72	10.49	11.86

Gd	33.9	35.8	31.7	27.2	101.4	32.3	43.0	34.9	46.6	57.0	59.4	41.0	41.7	34.7
Tb	3.47	3.81	3.62	3.00	15.41	3.86	4.49	3.65	5.07	5.81	6.52	4.18	6.21	3.90
Dy	15.8	18.0	18.8	15.0	82.4	19.1	19.4	16.1	21.2	23.5	28.1	18.4	33.2	18.3
Ho	2.48	2.91	3.25	2.6	15.18	3.38	2.86	2.63	3.22	3.42	4.22	2.66	5.54	2.84
Er	5.61	6.85	8.22	6.66	40.49	9.02	6.42	6.69	7	7.45	8.77	5.92	12.12	6.28
Tm	0.81	0.93	1.16	0.96	4.92	1.17	0.85	0.86	0.82	0.95	1.03	0.76	1.43	0.80
Yb	4.83	5.49	6.96	6.54	27.07	7.40	5.02	5.02	4.57	5.59	6.13	4.64	8.24	4.61
Lu	0.63	0.75	0.96	0.95	3.64	1.02	0.70	0.65	0.99	0.85	0.71	0.63	1.00	0.59
Hf	5.0	4.7	6.4	13.5	11.0	12.0	6.3	5.5	6.7	9.0	8.9	8.4	8.0	6.1
Ta	5.4	5.0	5.1	14.4	11.8	13.7	6.6	6.1	6.8	9.6	9.2	8.8	8.0	5.6
W	33	58	66	15	16	16	15	13	6	4	4	5	23	46
Re	0.003	0.003	0.004	0.001	0.001	0.001	0.002	0.001	0.001	0.002	0.001	0.001	0.001	0.005
Au	0.012	0.036	0.033	0.065	0.008	0.066	0.011	0.075	0.024	0.02	0.016	0.013	0.093	0.068
Tl	3.18	2.97	3.82	8.19	7.53	8.37	2.47	2.09	6.14	9.66	9.27	8.5	6.24	5.82
Pb	68	65	95	58	58	54	74	46	33	42	39	43	75	47
Bi	1.13	1.22	2.34	0.17	0.19	0.21	0.55	0.76	0.94	2.21	1.97	1.88	0.46	4.09
Th	25.8	23.1	33.4	59.5	50.6	54.0	29.9	27.5	30.3	40.8	38.8	38.8	38.2	25.9
U	40.0	39.3	52.1	37.2	41.5	40.5	50.0	37.1	15.2	19.2	19.4	20.3	40.9	21.5

Table S5 continued

Sample No.	SR1393965	SR1393966	SR1393967	SR1393971	DA20613	DA20608	DA20614	SR932946	SR1118351	SR215300	SR1393972	SR1393974	SR1393981
Alteration type	Ser	Ser	Ser	Ser	Hem	Hem	Hem	Hem	Hem	Hem	Hem	Hem	Hem
Drill Hole No.	RD917A	RD917A	RD917A	RD917A	RD6	RD6	RD6	RD1687	RD3008	RD635	RD917A	RD917A	RD917A
SiO_2	58.6	64.1	60.4	56.7	49.1	39.1	48.2	36.3	31.3	33.5	27.7	28.9	32.8
TiO_2	0.75	0.55	0.64	0.66	0.50	0.54	0.43	0.51	0.27	0.30	0.55	0.53	0.42
Al_2O_3	14.3	11.7	11.7	13.4	6.7	9.1	6.2	9.6	5.8	5.4	10.7	10.5	8.1
Fe_2O_3	3.8	8.6	11.4	9.7	31.6	30.9	30.2	39.1	38.7	38.7	49.8	50.2	47.7
MnO	0.03	0.04	0.28	0.48	0.08	0.30	0.05	0.17	0.56	0.50	0.09	0.06	0.01
MgO	1.4	1.2	2.1	2.7	0.8	3.2	0.6	1.2	3.5	3.1	1.2	0.9	0.5
CaO	0.6	0.6	1.9	2.9	0.8	3.3	0.6	1.6	5.4	4.6	0.8	0.5	0.1
Na_2O	0.09	0.08	0.08	0.11	0.09	0.12	0.11	0.11	0.15	0.08	0.16	0.04	0.04
K_2O	5.3	4.3	4.5	5.0	2.2	3.2	2.0	3.0	1.8	1.8	3.8	3.5	2.6
P_2O_5	0.34	0.32	0.23	0.32	0.30	0.25	0.32	0.48	0.30	0.27	0.16	0.34	0.23
CO_2	<0.05	<0.05	2.4	3.7	0.8	4.2	0.4	1.5	6.2	7.1	0.6	0.6	<0.05
F	5160	3386	4017	4304	2289	3796	2192	4007	7496	2209	3522	2677	1820
S	11100	10600	3100	4800	6200	1000	11900	4100	3600	4000	1700	2100	5400
Cl	60	60	30	10	10	10	10	30	20	10	50	10	10
Li	16	11	10	12	12	19	11	17	14	13	10	15	12
Be	4.6	3	3.2	4	3.2	5.9	3.1	5	3.5	2.2	4.3	4.9	2.7
Sc	39	26	26	33	13	21	14	20	10	12	26	15	10
V	224	209	218	200	59	163	85	129	91	110	260	122	75
Cr	3239	2446	2755	2903	1267	2011	1118	1863	989	1138	2430	1144	995

Co	74.8	55.8	58	62.6	31.5	84.3	30.4	54.3	38.7	36	46.6	32.4	10.4
Ni	472	414	357	388	92	366	107	155	192	140	305	160	56
Cu	22	18	29	28	155	268	77	1284	526	233	39	85	52
Zn	1828	1219	1212	1206	441	1140	389	962	331	733	1120	555	184
Ga	17.6	12.8	13.5	15	10.4	11.6	10.4	7.3	4.5	5.5	13.1	16.1	7.4
As	15.2	13.5	15.8	16.5	218.5	218.1	174.8	199.4	187.7	100.2	50.5	222.4	166.8
Se	0.8	1	0.25	2.1	0.25	1	0.7	3.1	1.8	0.9	1.2	3.3	4.6
Rb	362.1	268	278.1	310	105.6	217	104.7	147.5	122.6	114.4	245.2	189.2	132.4
Sr	778	674	152	278	438	103	495	445	323	183	90	227	450
Y	61.2	73.1	67.9	68.6	37.5	77.8	57.6	185.1	77.9	95.7	65	122.4	272.3
Zr	162	122	138	144	265	144	204	162	80	78	116	164	157
Nb	133.3	92.7	107.7	114	79	81.2	66.1	151.6	137.9	106.8	105.7	52.2	50.4
Mo	30	26	10	19	63	20	61	148	107	66	28	108	106
Ag	0.13	0.025	0.025	0.2	0.14	0.08	0.12	0.79	0.48	0.12	0.025	0.32	0.13
Cd	0.03	0.02	0.09	0.04	0.17	0.18	0.11	0.09	0.08	0.12	0.04	0.05	0.04
Sn	24	18	18	21	30	20	25	56	49	44	20	25	23
Sb	5.2	7.5	7.5	7.8	35.2	28.5	31.4	38.8	30.2	39.5	25.5	41.3	36.0
Te	0.07	0.07	0.07	0.06	1.14	0.31	0.92	3.38	2.96	2.18	0.06	0.88	0.81
Cs	7.6	4.2	4.1	7.2	3.7	11.6	3.7	10.1	13.2	5.7	11.3	11.1	4.9
Ba	41073	40938	12271	18035	21359	3148	42714	15082	14735	10038	6534	7933	23092
La	85	55	69	81	398	292	281	2041	1460	1291	66	793	608
Ce	225	180	210	245	692	462	419	2922	2105	1972	200	1067	854
Pr	34.1	27.1	31.3	37.4	54.5	47.5	48.7	223.2	183.3	155.2	32.5	85.5	70.8
Nd	159	126	146	171	170	168	161	547	524	447	154	218	196
Sm	42.4	33.6	38.4	47.1	20.3	31.7	22.7	51.5	63.3	59.8	44.0	20.0	24.2
Eu	8.41	6.53	7.89	9.19	4.74	6.16	5.86	13.61	15.00	14.37	9.61	6.35	10.82

Gd	27.3	23.5	25.6	31.2	11.5	25.8	15.9	37.2	38.1	37.5	30.5	20.1	48.4
Tb	2.76	2.64	2.74	3.17	1.17	2.86	1.78	4.76	3.79	3.98	3.20	3.51	8.53
Dy	12.4	13.1	12.8	13.6	6.6	14.0	9.8	26.3	16.8	17.1	13.8	20.7	45.1
Ho	1.92	2.18	2.09	2.06	1.18	2.21	1.69	5.36	2.57	2.79	2.08	3.63	8.14
Er	4.28	4.58	4.45	4.52	2.68	4.95	3.96	15.47	5.82	6.87	4.59	8.25	18.37
Tm	0.59	0.60	0.57	0.57	0.38	0.57	0.52	2.08	0.76	0.85	0.57	1.00	1.93
Yb	3.43	3.21	3.11	3.22	2.87	3.12	3.33	13.73	4.84	4.74	3.31	5.62	9.81
Lu	0.45	0.41	0.40	0.44	0.47	0.46	0.50	1.87	0.71	0.61	0.46	0.71	1.26
Hf	6.0	4.4	5.0	5.1	8.4	5.2	6.5	5.3	3.1	2.6	4.3	5.0	5.2
Ta	6.1	4.8	5.6	5.5	4.4	4.9	3.6	4.0	3.0	2.5	4.8	2.6	2.7
W	3	9	9	4	48	26	44	132	99	86	19	84	75
Re	0.001	0.001	0.003	0.004	0.001	0.001	0.001	0.003	0.003	0.002	0.002	0.007	0.008
Au	0.018	0.005	5.00E-04	0.014	0.159	0.038	0.021	0.665	0.76	0.316	0.012	0.609	0.156
Tl	6.61	4.89	5.32	5.55	2.76	6.09	3.03	1.44	1.22	1.04	4.07	2.79	1.07
Pb	39	32	27	27	86	114	55	84	73	61	49	92	47
Bi	1.59	1.19	0.45	1.17	0.76	0.34	0.94	3.49	2.06	2.07	0.46	1.66	0.96
Th	25.0	20.2	22.9	24.2	24.6	22.3	21.0	27.5	20.3	14.5	22.2	23.4	22.4
U	14.2	10.4	12.4	13.1	30.0	51.3	27.1	109.3	69.1	64.8	24.7	40.4	35.9

Oxides are in wt.%, and trace elements are in ppm. Total Fe as Fe_2O_3. Alteration type indicates the dominant secondary mineral in each analysis. Chl, chlorite; Cb, carbonate; Ser, sericite; Hem, hematite.

Table S6 LA-ICPMS apatite U-Pb dating results of secondary spongy apatite in the ca. 1590 Ma olivine-phyric basalt

No.	^{207}cor $^{206}Pb/^{238}U$ age (Ma)	+/-1 ster	$^{238}U/^{206}Pb$ ratio	+/-1 ster	$^{207}Pb/^{206}Pb$ ratio	+/-1 ster	^{204}Pb (ppm)	^{206}Pb (ppm)	^{207}Pb (ppm)	^{208}Pb (ppm)	^{232}Th (ppm)	^{238}U (ppm)
OD7-1	3037	127	1.28	0.03	0.4919	0.0070	0.31	12.3	5.2	12.2	11.5	24.1
OD7-2	1777	40	2.57	0.04	0.3009	0.0033	0.05	5.3	1.0	10.7	133.1	19.6
OD7-3	1886	56	2.19	0.04	0.3035	0.0040	0.05	5.3	1.0	10.5	129.9	18.9
OD7-4	2016	40	2.37	0.05	0.2883	0.0046	0.05	4.0	1.2	7.4	79.2	12.8
OD7-5	1652	32	3.10	0.05	0.1978	0.0030	0.08	16.9	2.6	8.1	80.6	67.3
OD7-6	3003	317	2.27	0.05	0.3684	0.0068	0.14	13.3	3.1	16.9	185.1	33.7
OD7-7	1715	26	3.00	0.05	0.1965	0.0031	0.12	17.8	2.9	17.0	259.1	66.9
OD7-8	1429	27	3.31	0.05	0.1579	0.0020	0.35	55.5	8.5	18.7	37.8	527.8
OD7-9	1873	58	2.74	0.05	0.1834	0.0038	0.03	6.0	1.1	10.5	132.8	21.9
OD7-10	1623	33	3.09	0.05	0.1873	0.0026	0.05	7.3	1.3	7.9	86.4	28.1
OD7-11	1602	43	3.18	0.05	0.1395	0.0026	0.27	37.8	8.5	19.0	51.6	134.7
OD7-12	1454	38	3.22	0.05	0.1816	0.0023	0.06	51.2	5.7	37.0	698.6	232.6
OD7-13	2311	91	2.08	0.05	0.2814	0.0050	0.06	13.3	2.4	12.0	131.8	42.3
OD7-14	1995	71	2.30	0.05	0.2783	0.0043	0.20	14.5	4.3	22.4	218.0	44.3
OD7-15	2688	99	3.07	0.06	0.2246	0.0061	0.15	13.0	3.4	17.8	193.5	35.6
OD7-16	1870	33	2.82	0.06	0.1868	0.0037	0.13	18.1	3.4	31.0	393.6	68.3
OD7-17	2546	82	3.05	0.06	0.1970	0.0053	0.45	19.9	6.1	15.4	45.0	53.7
OD7-18	2791	85	2.57	0.06	0.2856	0.0063	0.09	6.1	1.6	12.9	159.1	17.7
OD7-19	1587	30	3.22	0.07	0.1698	0.0023	0.87	59.4	17.0	51.0	372.3	230.6
OD7-20	3285	130	2.83	0.07	0.2794	0.0070	0.05	8.1	1.7	9.0	105.7	19.9
OD7-21	2555	68	3.08	0.08	0.2873	0.0055	0.32	12.3	5.2	12.1	9.6	29.9
OD024-1	1598	25	1.00	0.03	0.5795	0.0078	0.12	8.1	2.3	10.3	99.5	18.1
OD024-2	1898	38	1.30	0.04	0.5048	0.0117	0.20	5.8	3.3	10.4	46.6	7.1
OD024-3	1654	26	1.98	0.05	0.4260	0.0086	0.23	7.0	3.4	9.5	31.5	10.7
OD024-4	1680	26	1.62	0.06	0.4396	0.0096	0.17	9.3	3.5	11.3	67.5	15.6
OD024-5	1601	23	2.32	0.07	0.3137	0.0083	0.07	13.8	2.5	8.2	84.4	34.0
OD024-6	1808	36	2.30	0.08	0.2739	0.0098	0.05	3.4	0.9	3.1	22.5	8.5

ster, standard error

Table S7 Trace element compositions of chalcopyrite in sample OD1064

No.	Ti	Mn	Co	Ni	Cu	Zn	As	Se	Y	Zr	Nb	Mo
1	14561	102	5.3	7.6	375570	23.1	3.18	230	15.4	106	10.3	0.239
2	8645	203	7.2	7.4	374292	28.5	3.61	203	13.8	103	7.8	0.182
3	10868	136	7.7	7.2	372044	30.5	3.99	208	13.6	103	9.6	0.100
4	12721	142	7.9	8.5	353994	30.8	3.12	187	11.3	102	6.9	0.204
5	4542	441	5.1	2.8	347453	28.4	4.05	186	33.0	59	3.4	0.619
6	13844	173	10.0	10.7	342878	43.8	4.35	220	13.0	113	10.8	<0.5720
7	10188	174	10.3	8.1	341634	43.6	4.87	176	17.7	130	7.3	0.727
8	17673	117	6.1	7.6	339772	28.1	3.31	237	13.4	131	13.5	<0.2223
9	16489	247	11.0	8.9	339534	40.4	5.27	193	22.6	163	9.5	0.407
10	18527	153	9.2	12.2	335114	27.4	3.94	200	15.7	130	11.7	<0.2613
11	18244	138	9.2	8.8	334536	36.0	4.19	185	14.8	154	14.4	0.267
12	10859	167	3.6	3.3	324755	18.7	2.51	192	15.9	120	10.5	2.474
13	12907	104	6.0	5.1	324197	26.6	3.12	203	12.3	100	8.7	<0.4587
14	11934	102	6.2	5.5	322154	22.6	3.13	175	11.0	100	9.1	<0.2039
15	15523	237	7.3	7.0	320730	30.7	5.76	204	22.1	164	10.9	1.008
16	9798	311	8.2	8.4	318417	161.2	6.00	164	24.0	84	6.4	0.821
17	17310	158	10.5	12.0	316968	35.2	3.05	199	15.7	144	12.1	0.346
18	7849	313	9.5	8.7	316859	42.2	10.13	160	26.5	128	3.6	0.352
19	23106	406	27.5	29.7	311385	100.4	4.03	182	18.6	201	15.3	0.602
20	12386	420	8.0	5.7	311036	28.4	7.43	167	134.8	158	18.3	0.791
21	7523	201	16.4	17.6	310237	61.0	10.55	163	7.0	68	5.2	<0.1460
22	8122	79	3.7	4.5	307965	25.2	7.31	178	15.9	73	3.8	0.206
23	18621	563	19.5	27.0	307024	77.0	4.16	194	44.9	244	8.5	2.102
24	9319	326	15.7	16.8	305596	54.3	6.38	173	33.3	186	6.3	0.575
25	15427	305	15.7	16.1	304586	60.6	4.82	187	42.5	161	13.0	0.270
26	7693	78	5.8	3.2	301706	30.6	6.92	170	25.0	122	7.5	0.135
27	11900	193	10.6	9.1	300673	44.5	3.81	190	10.3	89	5.9	<0.3206

Table S7 continued

No.	Ag	Cd	Sn	Sb	Ce	Gd	Yb	Hf	Ta	W	Re	Au
1	5.16	3.56	1.17	1.07	21.6	5.23	1.40	1.75	0.635	0.94	<0.0979	0.143
2	5.21	1.86	1.14	1.32	14.7	2.15	1.39	1.73	0.282	1.13	<0.0701	0.250
3	4.33	3.08	1.05	2.92	16.5	2.35	0.78	3.22	0.383	0.86	<0.0819	0.195
4	5.03	2.51	1.25	1.01	15.8	3.82	<1.3441	1.99	0.756	1.00	<0.0716	0.164
5	8.79	3.58	1.56	1.72	30.7	3.60	5.60	1.88	0.149	0.63	<0.0382	0.428
6	4.68	1.71	1.08	1.50	17.2	4.26	1.72	2.06	0.738	1.22	<0.0860	0.241
7	3.56	3.25	1.18	2.49	10.6	2.17	2.24	3.69	0.491	1.03	<0.0904	0.243
8	5.49	2.08	1.41	1.24	20.2	6.13	1.70	2.45	0.872	1.59	<0.1658	0.239
9	7.21	1.74	1.31	2.18	19.1	4.57	4.35	2.33	0.829	1.45	<0.0598	0.399
10	5.91	2.15	1.96	1.26	19.9	6.21	1.76	1.89	0.802	1.39	<0.0787	0.298
11	5.03	4.24	1.45	1.87	21.0	2.86	1.33	3.08	0.758	1.75	<0.1093	0.277
12	5.85	2.34	0.98	1.04	19.6	2.99	1.19	2.52	0.476	2.32	0.0794828	0.139
13	5.70	2.43	1.12	1.48	17.1	4.14	1.53	2.70	0.489	0.87	0.0470936	0.142
14	5.02	2.20	0.99	1.63	13.1	3.94	1.42	1.74	0.550	0.83	<0.0442	0.184
15	6.52	1.68	9.56	2.53	21.9	4.89	2.36	3.30	0.737	2.09	<0.0491	0.196
16	3.82	4.37	1.11	1.94	27.4	4.66	2.34	1.67	0.434	1.78	<0.0662	0.567
17	4.15	3.44	1.57	1.67	20.7	3.35	1.68	2.85	0.898	1.25	0.0104077	0.095
18	6.98	1.38	1.73	4.27	27.3	3.99	2.93	3.35	0.386	0.86	<0.0768	0.377
19	4.36	1.35	2.42	1.97	24.7	4.12	1.88	4.35	0.749	2.31	<0.0834	0.291
20	6.68	3.51	18.65	3.27	95.3	25.24	10.39	4.03	0.510	2.17	<0.0461	0.620
21	5.34	4.97	1.60	4.84	8.9	2.11	0.93	1.53	0.308	0.46	<0.0620	0.272
22	5.33	2.97	2.02	3.05	21.9	4.04	1.78	2.20	0.326	1.68	<0.0333	<0.0990
23	5.67	1.76	2.18	1.60	44.6	6.35	5.48	5.66	0.651	1.60	0.097728	<0.2064
24	4.42	2.62	2.16	2.16	26.9	4.52	3.63	2.89	0.270	0.94	<0.1248	0.153
25	4.40	3.48	1.59	2.65	50.5	11.59	2.56	3.15	0.487	1.34	<0.1150	0.196
26	12.31	3.77	1.43	2.17	35.2	3.68	3.50	3.11	0.312	1.52	<0.0615	0.579
27	4.24	3.14	1.43	2.09	13.3	2.55	0.71	1.87	0.603	1.21	<0.0435	0.312

Table S7 continued

No.	Tl	Bi	Th	^{235}U	^{238}U	^{204}Pb	^{206}Pb	^{207}Pb	^{208}Pb	$^{204}Pb/^{206}Pb$	$^{207}Pb/^{206}Pb$
1	2.29	10.3	1.89	11.93	4.28	1.39	61.5	21.9	76.1	0.0226	0.357
2	1.86	12.4	1.25	<7.3757	2.46	1.52	58.8	24.0	81.3	0.0259	0.408
3	6.90	13.1	1.35	6.08	1.38	1.80	83.1	29.7	104.1	0.0216	0.358
4	1.03	9.5	1.55	<9.0455	2.54	1.16	50.9	19.6	67.9	0.0228	0.386
5	0.74	18.0	1.38	21.97	11.29	2.15	73.4	31.7	104.1	0.0292	0.432
6	1.74	11.5	1.75	<10.9281	3.61	1.54	66.2	25.7	88.7	0.0232	0.388
7	6.32	21.8	1.11	<8.0282	2.86	1.79	82.6	29.8	104.0	0.0217	0.361
8	5.06	11.4	2.47	8.85	5.61	1.44	77.4	25.3	89.4	0.0186	0.327
9	9.30	22.7	1.80	10.34	4.36	2.18	101.7	35.5	123.6	0.0214	0.349
10	5.07	8.7	2.73	15.36	6.17	1.29	67.6	22.9	80.6	0.0191	0.338
11	2.64	12.3	2.64	11.17	4.97	1.73	81.0	30.3	100.9	0.0214	0.374
12	1.91	9.2	1.43	8.41	1.98	1.16	50.8	20.3	68.0	0.0228	0.401
13	3.37	11.7	1.84	<14.2431	3.24	1.31	60.1	21.9	78.8	0.0219	0.364
14	1.74	12.3	1.51	<11.5772	3.08	1.54	58.9	23.2	79.2	0.0261	0.393
15	5.33	12.3	2.03	<18.6145	4.68	1.60	82.2	29.1	100.1	0.0194	0.354
16	3.92	9.3	1.34	43.28	19.83	3.81	143.6	61.5	194.6	0.0266	0.428
17	2.87	8.9	1.88	7.56	4.77	1.40	63.4	22.5	78.5	0.0221	0.355
18	3.58	19.4	1.61	7.50	5.26	2.44	99.8	41.4	140.5	0.0245	0.414
19	2.50	7.1	3.20	8.65	5.91	1.13	51.7	19.2	64.3	0.0218	0.371
20	4.57	22.0	2.17	32.18	14.17	1.81	84.2	33.9	110.4	0.0215	0.403
21	3.98	27.9	0.61	7.25	3.02	2.78	111.4	47.4	155.1	0.0249	0.425
22	3.22	29.4	0.95	12.93	7.77	2.72	110.4	46.4	151.1	0.0246	0.421
23	4.15	11.6	2.84	<20.2849	2.96	1.80	95.7	32.0	113.5	0.0188	0.334
24	3.01	10.0	1.81	10.50	4.72	1.22	58.4	22.2	75.4	0.0209	0.380
25	3.18	12.5	2.01	<10.2066	2.47	1.42	70.0	26.7	90.7	0.0203	0.382
26	3.03	32.0	1.70	46.99	22.41	2.97	121.0	52.2	171.8	0.0246	0.432
27	2.16	15.1	1.29	<10.0270	2.17	1.68	76.5	32.9	108.8	0.0220	0.431

Trace element compositions are in ppm.

Table S8 Pb isotope compositions of the Olympic Dam dolerite

	Pb (ppm)	$^{206}Pb/^{204}Pb$	Standard error (2σ)	$^{207}Pb/^{204}Pb$	Standard error (2σ)	$^{208}Pb/^{204}Pb$	Standard error (2σ)	$^{204}Pb/^{206}Pb$	$^{207}Pb/^{206}Pb$
OD80-1bas	87	34.3	0.0010	17.5	0.0004	49.0	0.0016	0.0292	0.510
OD80-2dol	161	34.4	0.0006	17.5	0.0003	49.0	0.0012	0.0291	0.509
OD82	10	30.5	0.0005	17.0	0.0003	47.9	0.0010	0.0327	0.558
OD84	6.3	32.1	0.0006	17.2	0.0003	48.8	0.0012	0.0311	0.535
OD850	3.0	34.5	0.0012	17.2	0.0006	49.3	0.0020	0.0290	0.500
OD198-1*	22	31.3	0.0006	17.2	0.0004	47.2	0.0015	0.0319	0.549
OD198-2*	201	32.8	0.0005	17.3	0.0003	48.0	0.0012	0.0305	0.529

*Pb concentrations of some (more altered) samples are from this study (Table 5.2) and the rest are from Chapter 3 (Table 3.2) (Huang et al., 2015).

Table S9 Pb isotope compositions of galena in the Olympic Dam dolerite sample OD852

No.	$^{207}Pb/^{206}Pb$	Standard error (1σ)	$^{208}Pb/^{206}Pb$	Standard error (1σ)	$^{206}Pb/^{204}Pb$	Standard error (1σ)	$^{207}Pb/^{204}Pb$	Standard error (1σ)	$^{208}Pb/^{204}Pb$	Standard error (1σ)	$^{204}Pb/^{206}Pb$
1	0.4243	0.001	1.2402	0.008	42.6618	0.316	18.1080	0.159	52.8801	0.515	0.0234
2	0.4246	0.001	1.2417	0.006	43.0451	0.089	18.2810	0.034	53.4199	0.216	0.0232
3	0.4213	0.001	1.2528	0.006	43.6901	0.253	18.4106	0.071	54.7050	0.423	0.0229
4	0.4235	0.001	1.2441	0.006	43.2327	0.067	18.3137	0.040	53.7544	0.233	0.0231
5	0.4250	0.000	1.2487	0.006	43.0503	0.100	18.3021	0.040	53.7281	0.232	0.0232
6	0.4250	0.000	1.2410	0.006	42.8855	0.066	18.2302	0.021	53.1897	0.222	0.0233
7	0.4257	0.000	1.2431	0.006	42.8766	0.147	18.2568	0.051	53.2706	0.250	0.0233
8	0.4384	0.001	1.2968	0.006	41.0259	0.130	17.9887	0.059	53.1709	0.246	0.0244
9	0.4372	0.001	1.2973	0.006	41.2244	0.132	18.0273	0.056	53.4525	0.241	0.0243
10	0.4378	0.003	1.2934	0.006	41.2290	0.460	18.0555	0.195	53.2946	0.586	0.0243
11	0.4289	0.001	1.2759	0.008	41.6329	0.781	17.8601	0.297	53.0919	0.771	0.0240
12	0.4349	0.001	1.2787	0.007	41.1783	0.355	17.9150	0.162	52.6240	0.420	0.0243
13	0.4379	0.002	1.2918	0.009	41.1901	0.379	18.0421	0.154	53.1798	0.630	0.0243
14	0.4254	0.002	1.2623	0.009	42.7814	0.211	18.2030	0.072	53.9717	0.329	0.0234
15	0.4246	0.003	1.2664	0.008	42.3546	0.329	17.9876	0.124	53.6068	0.521	0.0236
16	0.3882	0.001	1.1884	0.006	48.2423	0.206	18.7311	0.065	57.2999	0.272	0.0207
17	0.3749	0.002	1.1590	0.006	50.5344	0.342	18.9519	0.073	58.5369	0.346	0.0198
18	0.3526	0.004	1.1168	0.009	54.8102	0.900	19.3324	0.120	61.1793	0.732	0.0182
19	0.3530	0.003	1.1210	0.009	54.7578	0.702	19.3326	0.138	61.3508	0.494	0.0183
20	0.3918	0.003	1.1803	0.011	47.8978	1.367	18.7696	0.590	56.5020	1.643	0.0209
21	0.3797	0.004	1.1810	0.008	48.4361	1.206	18.3965	0.607	57.1730	1.351	0.0206

Table S10 Drill core (RD271) assays of the ca. 820 Ma Olympic Dam dolerite

SAMPLE ID	SAMPLE FROM	SAMPLE TO	SiO_2	TiO_2	Al_2O_3	Fe_2O_3	MnO	MgO	CaO	Na_2O	K_2O	P_2O_5	CO_2	F	S
SR1397496	647	648	49.54	2.04	11.54	14.17	0.50	7.13	3.65	1.67	0.37	0.14	4.94		100
SR1397497	648	649	53.54	2.23	12.01	12.45	0.41	5.66	3.60	2.86	0.20	0.21	4.28		200
SR1397498	649	650	49.46	2.15	11.75	14.14	0.36	6.40	4.02	1.99	0.07	0.21	4.33		600
SR1397499	650	651	49.97	2.22	11.71	13.53	0.30	6.55	3.89	2.12	0.06	0.11	3.9		300
SR1397501	**651**	**652**	**51.92**	**2.07**	**11.99**	**17.52**	**0.15**	**6.12**	**1.97**	**2.18**	**0.12**	**0.21**	**2.05**	**2004**	**400**
SR1397502	652	653	55.02	2.41	12.90	13.71	0.10	6.29	1.23	2.43	0.17	0.23	0.66		50
SR1397503	653	654	47.02	2.45	13.51	17.48	0.15	6.90	2.81	2.14	0.13	0.16	1.94		400
SR1397504	654	655	52.99	2.07	10.69	14.97	0.18	5.56	3.68	1.42	0.23	0.07	2.48		1800
SR1397505	655	656	51.04	2.61	13.66	15.14	0.10	6.83	1.54	2.37	0.06	0.18	0.79		400
SR1397506	**656**	**657**	**53.03**	**2.46**	**13.09**	**14.66**	**0.18**	**6.57**	**1.93**	**2.44**	**0.08**	**0.23**	**1.95**	**1717**	**600**
SR1397507	657	658	51.32	2.40	12.52	14.28	0.34	6.65	2.74	1.73	0.48	0.16	3.34		200
SR1397508	658	659	41.95	2.36	12.45	15.41	0.65	7.70	4.91	0.94	1.13	0.18	7.16		1400
SR1397509	659	660	46.38	2.86	14.22	17.75	0.15	7.23	1.23	0.80	1.55	0.25	0.87		2500
SR1397510	660	661	46.04	2.69	13.79	15.61	0.36	7.05	2.76	1.21	1.78	0.11	3.63		600
SR1397512	**661**	**662**	**44.67**	**2.49**	**13.62**	**18.07**	**0.27**	**7.60**	**2.11**	**0.57**	**1.48**	**0.27**	**3.24**	**1781**	**3500**
SR1397513	662	663	43.34	2.81	14.88	18.37	0.15	7.35	1.36	0.55	2.43	0.21	0.84		2800
SR1397514	663	664	38.16	2.38	12.75	17.35	0.68	8.64	5.48	0.63	1.61	0.21	7.91		1200
SR1397515	664	665	37.50	2.23	11.71	17.34	0.85	8.72	6.16	0.70	0.80	0.14	8.54		1500
SR1397516	665	666	40.62	2.29	11.84	16.64	0.81	8.29	5.89	1.01	0.94	0.21	8.28		200
SR1397517	**666**	**667**	**32.97**	**2.08**	**12.03**	**17.38**	**0.99**	**9.20**	**8.03**	**1.11**	**0.77**	**0.30**	**12.34**	**1582**	**<100**
SR1397518	667	668	45.48	2.69	13.34	15.64	0.43	6.80	3.41	1.87	0.90	0.18	4.18		1700

SR1397519	668	669	49.31	2.98	14.39	16.42	0.13	6.43	1.23	1.24	1.69	0.16	0.71		2100
SR1397520	669	670	44.43	2.85	13.88	14.21	0.53	6.47	3.95	2.39	1.37	0.18	5.14		900
SR1397521	670	671	39.38	2.75	13.90	15.74	0.72	7.65	5.23	2.21	1.16	0.16	7.43		100
SR1397522	**671**	**672**	**41.61**	**2.62**	**13.90**	**15.03**	**0.65**	**7.33**	**4.73**	**1.87**	**1.28**	**0.27**	**6.73**	**2122**	**<100**
SR1397523	672	673	46.33	2.69	14.02	16.47	0.31	6.68	3.19	2.24	0.57	0.23	3.13		100
SR1397524	673	674	46.06	2.67	14.24	13.68	0.30	5.19	4.97	3.32	0.65	0.16	4.3		50
SR1397525	674	675	46.25	2.54	12.96	16.01	0.15	6.19	4.52	1.97	0.82	0.18	2.56		400
SR1397526	675	676	45.03	2.55	13.07	17.11	0.15	7.48	4.58	1.86	0.28	0.11	1.83		400
SR1397527	**676**	**677**	**49.12**	**2.41**	**13.24**	**16.15**	**0.28**	**6.20**	**5.48**	**2.48**	**0.35**	**0.25**	**2.02**	**772**	**800**
SR1397528	677	678	49.80	2.63	13.43	14.38	0.27	7.71	3.13	2.64	0.40	0.25	0.57		500
SR1397530	678	679	50.49	2.43	12.49	14.43	0.22	6.90	4.13	2.14	0.46	0.11	0.7		1400
SR1397531	679	680	48.84	2.51	13.32	16.84	0.18	4.31	6.51	2.24	0.60	0.16	1.21		300
SR1397532	680	681	49.12	2.50	13.30	16.26	0.18	4.54	6.58	2.16	0.51	0.16	1.07		200
SR1397533	**681**	**682**	**49.82**	**2.41**	**13.60**	**17.29**	**0.19**	**4.73**	**6.28**	**2.28**	**0.60**	**0.27**	**1.2**	**636**	**200**
SR1397534	682	683	49.20	2.47	13.41	15.68	0.25	5.03	6.83	2.01	0.55	0.16	1		200
SR1397535	683	684	49.86	2.46	13.83	14.96	0.19	4.84	6.97	2.09	0.48	0.21	0.5		400
SR1397536	684	685	49.61	2.44	13.83	15.82	0.19	4.61	7.12	2.16	0.58	0.14	0.35		300
SR1397538	685	686	48.24	2.41	13.69	16.02	0.19	5.06	5.93	2.24	0.65	0.18	0.69		900
SR1397539	**686**	**687**	**51.43**	**2.44**	**13.73**	**17.35**	**0.15**	**4.69**	**4.60**	**2.43**	**0.87**	**0.32**	**0.33**	**805**	**900**
SR1397540	687	688	49.97	2.69	11.14	20.19	0.23	5.52	3.47	1.74	0.67	0.32	0.1		600
SR1397541	688	689	49.03	2.55	13.34	17.69	0.18	5.26	4.14	2.22	0.88	0.09	0.16		1200
SR1397542	689	690	49.63	2.44	14.79	15.51	0.14	4.28	4.66	2.84	1.04	0.14	0.41		400
SR1397543	690	691	49.59	2.38	14.77	15.52	0.13	4.30	4.56	2.99	0.99	0.18	0.32		300
SR1397544	**691**	**692**	**49.74**	**2.26**	**15.51**	**14.99**	**0.13**	**3.88**	**5.54**	**3.60**	**1.18**	**0.21**	**1.51**	**791**	**300**

SR1397545	692	693	48.94	2.36	14.96	15.09	0.14	4.00	5.71	2.72	1.01	0.21	0.68		200
SR1397546	693	694	49.16	2.37	15.13	15.24	0.13	3.83	5.74	2.83	1.00	0.16	0.68		300
SR1397548	694	695	48.05	2.34	15.04	15.85	0.15	3.90	6.10	2.61	0.86	0.18	0.85		200
SR1397549	695	696	49.44	2.40	15.36	16.09	0.12	3.30	5.83	2.76	0.99	0.18	0.54		100
SR1397550	**696**	**697**	**49.33**	**2.23**	**14.96**	**16.77**	**0.18**	**5.32**	**4.80**	**2.98**	**0.76**	**0.30**	**0.34**	**876**	**800**
SR1397551	697	698	47.23	2.28	15.13	15.48	0.21	5.72	4.38	2.88	0.69	0.16	0.14		900
SR1397552	698	699	50.59	2.40	15.81	14.21	0.13	3.80	4.48	3.32	1.08	0.25	0.09		400
SR1397553	699	700	48.94	2.39	15.68	16.03	0.17	4.11	4.86	2.97	0.89	0.07	0.07		300
SR1397554	700	701	50.14	2.50	16.38	10.56	0.25	6.22	4.62	3.13	0.81	0.23	0.07		200
SR1397555	**701**	**702**	**51.60**	**2.43**	**16.60**	**10.10**	**0.25**	**5.75**	**4.66**	**3.54**	**0.78**	**0.25**	**0.17**	**1117**	**300**
SR1397556	702	703	49.91	2.44	16.13	11.41	0.22	5.22	4.38	3.50	0.86	0.16	0.14		200
SR1397557	703	704	50.06	2.37	16.00	16.05	0.15	3.52	4.91	3.05	1.10	0.18	0.12		100
SR1397558	704	705	49.42	2.38	16.00	15.40	0.17	3.78	5.11	2.88	1.05	0.23	0.16		200
SR1397559	705	706	49.37	2.42	15.75	16.64	0.15	3.57	5.72	2.57	0.96	0.23	0.21		300
SR1397561	**706**	**707**	**49.99**	**2.34**	**15.36**	**17.48**	**0.15**	**3.37**	**5.41**	**2.83**	**0.89**	**0.27**	**0.22**	**857**	**300**
SR1397562	707	708	49.91	2.42	15.73	15.26	0.14	3.42	5.89	2.75	0.96	0.16	0.35		400
SR1397563	708	709	49.12	2.43	15.62	16.91	0.14	3.27	5.74	2.72	0.98	0.14	0.29		300
SR1397564	709	710	48.50	2.37	15.38	17.04	0.15	3.27	5.62	2.70	0.98	0.14	0.44		400
SR1397565	710	711	48.09	2.42	15.64	15.14	0.21	4.84	5.39	2.94	0.83	0.23	0.44		400
SR1397566	**711**	**712**	**50.81**	**2.39**	**15.73**	**13.87**	**0.18**	**4.06**	**5.16**	**3.46**	**1.07**	**0.25**	**0.87**	**858**	**200**
SR1397567	712	713	47.88	2.32	15.49	14.83	0.21	4.35	5.79	3.05	0.94	0.21	1.01		400
SR1397568	713	714	48.67	2.41	15.34	12.89	0.22	4.41	6.03	3.03	0.95	0.11	1.1		200
SR1397569	714	715	49.37	2.46	15.85	13.64	0.19	4.16	5.44	3.30	1.01	0.21	0.37		200
SR1397570	715	716	48.22	2.44	15.68	14.86	0.21	3.95	5.11	3.50	1.11	0.14	0.44		1000

SR1397571	**716**	**717**	**49.80**	**2.38**	**15.55**	**14.99**	**0.22**	**3.70**	**5.30**	**3.48**	**1.16**	**0.23**	**0.49**	**727**	**700**
SR1397572	717	718	48.77	2.38	15.41	15.33	0.21	3.78	5.60	2.99	1.26	0.16	0.32		400
SR1397573	718	719	48.37	2.40	15.60	13.06	0.26	4.63	5.90	3.23	1.12	0.14	0.67		100
SR1397574	719	720	48.45	2.40	15.36	16.37	0.21	3.33	5.81	2.97	1.57	0.09	0.23		400
SR1397575	720	721	48.69	2.39	15.24	15.59	0.22	3.50	6.32	2.87	1.43	0.25	0.31		300
SR1397577	**721**	**722**	**50.51**	**2.38**	**15.62**	**15.93**	**0.22**	**3.58**	**5.39**	**3.57**	**1.59**	**0.18**	**0.37**	**753**	**500**
SR1397578	722	723	49.84	2.46	16.04	15.78	0.15	2.64	4.88	3.41	1.99	0.23	0.21		1700
SR1397579	723	724	47.68	2.44	15.66	17.08	0.23	3.96	4.34	3.11	1.45	0.18	0.27		500
SR1397580	724	725	48.75	2.46	15.55	13.59	0.27	5.54	3.67	3.54	0.94	0.11	0.24		300
SR1397581	725	726	48.02	2.42	15.68	15.24	0.22	3.70	5.08	3.21	1.43	0.16	0.52		400
SR1397582	**726**	**727**	**48.65**	**2.39**	**16.00**	**14.05**	**0.30**	**4.98**	**4.97**	**3.68**	**0.82**	**0.25**	**1.34**	**800**	**200**
SR1397583	727	728	47.06	2.33	15.47	13.12	0.28	4.03	7.18	3.29	1.17	0.18	2.21		200
SR1397584	728	729	47.81	2.42	15.98	15.10	0.22	3.50	6.60	3.01	1.64	0.14	0.73		500
SR1397585	729	730	48.15	2.34	15.49	14.60	0.22	3.25	6.21	3.06	1.41	0.21	1.01		500
SR1397586	730	731	46.12	2.32	15.45	15.76	0.22	3.32	6.20	3.06	1.53	0.18	1.12		400
SR1397587	**731**	**732**	**48.88**	**2.29**	**15.77**	**14.63**	**0.22**	**3.52**	**6.86**	**3.09**	**1.54**	**0.27**	**0.93**	**581**	**600**
SR1397588	732	733	47.08	2.35	15.96	14.80	0.22	3.58	7.15	2.79	1.64	0.11	0.5		500
SR1397589	733	734	46.93	2.34	15.87	14.82	0.21	3.18	6.31	3.14	1.61	0.21	0.79		1500
SR1397590	734	735	49.22	2.40	16.15	12.54	0.21	3.47	5.90	3.50	1.41	0.25	0.47		200
SR1397591	735	736	48.65	2.71	15.89	12.92	0.22	3.91	6.39	3.37	1.23	0.16	0.24		400
SR1397592	**736**	**737**	**48.82**	**2.24**	**15.72**	**14.22**	**0.21**	**3.86**	**6.93**	**3.33**	**1.24**	**0.27**	**0.58**	**692**	**700**
SR1397593	737	738	47.28	2.27	15.11	14.94	0.22	4.33	5.53	3.30	0.89	0.14	0.62		600
SR1397594	738	739	44.88	2.05	14.24	19.26	0.25	5.57	3.69	2.78	0.41	0.16	0.63		500
SR1397595	739	740	47.40	2.34	16.07	16.77	0.21	4.69	4.55	3.22	0.58	0.11	0.18		1000

SR1397596	740	741	48.62	2.39	15.92	12.81	0.15	3.73	6.09	3.33	0.77	0.16	0.27		800
SR1397597	**741**	**742**	**49.35**	**2.38**	**15.90**	**14.70**	**0.17**	**4.11**	**6.00**	**3.42**	**0.77**	**0.23**	**0.25**	**819**	**800**
SR1397598	742	743	45.54	2.16	14.92	18.37	0.19	5.04	5.21	2.36	0.54	0.14	0.4		2300
SR1397599	743	744	48.88	2.49	16.38	13.77	0.19	3.80	8.37	2.88	1.01	0.18	0.27		300
SR1397601	744	745	47.64	2.37	15.28	14.35	0.25	3.52	8.86	2.52	0.92	0.09	0.3		500
SR1397602	745	746	48.45	2.47	15.49	15.03	0.26	3.60	8.48	2.56	1.11	0.21	0.16		600
SR1397603	**746**	**747**	**50.10**	**2.34**	**15.56**	**15.11**	**0.26**	**3.63**	**8.14**	**2.91**	**1.12**	**0.23**	**0.14**	**461**	**400**
SR1397604	747	748	48.60	2.37	15.60	14.63	0.23	3.63	7.91	2.64	1.22	0.14	0.2		100
SR1397605	748	749	48.20	2.35	15.89	14.92	0.21	3.68	9.07	2.49	0.87	0.18	0.39		700
SR1397606	749	750	48.39	2.36	15.60	15.06	0.25	3.93	8.83	2.44	0.81	0.11	0.22		200
SR1397607	750	751	47.21	2.44	14.96	14.84	0.22	3.81	9.33	2.28	0.61	0.16	0.9		1500
SR1397608	751	752	49.24	2.41	15.68	13.90	0.19	3.80	8.95	2.51	0.75	0.11	0.24		200

Table S10 continued

SAMPLE ID	SAMPLE FROM	SAMPLE TO	Cl	Li	Be	Sc	V	Cr	Co	Ni	Cu	Zn	Ga	As	Se
SR1397496	647	648				35	323	98	101	71	32	191		5	
SR1397497	648	649				33	283	99	78	57	149	158		5	
SR1397498	649	650				41	305	90	92	74	100	199		5	
SR1397499	650	651				42	305	98	85	71	36	192		5	
SR1397501	**651**	**652**	**800**	**71**	**1.8**	**35**	**363**	**100**	**81.4**	**71**	**69**	**179**	**19.9**	**8.5**	**<0.5**
SR1397502	652	653				31	347	105	84	73	70	189		5	
SR1397503	653	654				35	406	119	92	80	108	221		5	
SR1397504	654	655				30	351	87	72	66	31	189		5	
SR1397505	655	656				36	398	119	91	75	70	200		5	
SR1397506	**656**	**657**	**1500**	**53**	**1.5**	**37**	**427**	**109**	**79.8**	**61**	**91**	**169**	**23.7**	**3.3**	**<0.5**
SR1397507	657	658				39	370	98	79	60	38	181		5	
SR1397508	658	659				59	394	101	78	57	56	194		5	
SR1397509	659	660				29	452	115	96	72	39	222		5	
SR1397510	660	661				40	403	113	82	57	10	187		5	
SR1397512	**661**	**662**	**400**	**52**	**1.6**	**37**	**471**	**98**	**93**	**69**	**164**	**211**	**26.3**	**8**	**<0.5**
SR1397513	662	663				35	434	109	91	72	70	222		5	
SR1397514	663	664				49	383	109	76	57	33	187		5	
SR1397515	664	665				52	356	80	79	61	10	198		5	
SR1397516	665	666				43	342	84	74	59	10	190		5	
SR1397517	**666**	**667**	**300**	**50**	**1.9**	**48**	**392**	**89**	**79.9**	**56**	**23**	**167**	**21.6**	**<0.5**	**<0.5**
SR1397518	667	668				50	365	113	70	52	23	183		5	

SR1397519	668	669				35	462	115	65	51	33	174		5	
SR1397520	669	670				58	409	111	59	42	10	162		5	
SR1397521	670	671				58	421	107	65	44	10	170		5	
SR1397522	**671**	**672**	**<200**	**58**	**2.1**	**46**	**437**	**105**	**62.9**	**48**	**11**	**151**	**22.4**	**7.7**	**<0.5**
SR1397523	672	673				44	409	100	70	53	35	177		5	
SR1397524	673	674				43	408	107	54	52	155	161		5	
SR1397525	674	675				40	380	92	54	46	322	289		5	
SR1397526	675	676				41	396	101	54	50	309	277		5	
SR1397527	**676**	**677**	**<200**	**39**	**1.1**	**37**	**414**	**92**	**51.2**	**56**	**301**	**245**	**23.3**	**7.1**	**<0.5**
SR1397528	677	678				41	380	95	56	54	155	272		5	
SR1397530	678	679				39	346	95	51	52	216	248		5	
SR1397531	679	680				41	380	90	44	52	257	124		5	
SR1397532	680	681				41	386	87	49	53	272	134		5	
SR1397533	**681**	**682**	**400**	**25**	**1.1**	**37**	**417**	**89**	**49**	**54**	**183**	**131**	**23.2**	**6.6**	**<0.5**
SR1397534	682	683				39	360	79	45	44	203	140		5	
SR1397535	683	684				39	356	82	44	40	238	122		5	
SR1397536	684	685				39	373	84	39	37	285	115		5	
SR1397538	685	686				38	358	79	48	48	348	171		5	
SR1397539	**686**	**687**	**200**	**31**	**1.1**	**36**	**353**	**65**	**43.8**	**45**	**325**	**192**	**23.8**	**8.8**	**<0.5**
SR1397540	687	688				35	267	10	49	33	310	228		5	
SR1397541	688	689				37	340	57	46	39	463	203		5	
SR1397542	689	690				38	359	71	42	46	209	147		5	
SR1397543	690	691				35	339	62	42	44	141	147		5	
SR1397544	**691**	**692**	**<200**	**29**	**0.9**	**34**	**381**	**59**	**45.5**	**46**	**139**	**132**	**24.3**	**6.7**	**<0.5**

SR1397545	692	693				36	339	64	43	41	203	143		5	
SR1397546	693	694				36	339	67	41	41	205	130		5	
SR1397548	694	695				34	328	56	44	40	224	137		5	
SR1397549	695	696				34	331	71	37	38	177	110		5	
SR1397550	**696**	**697**	**300**	**31**	**1.5**	**32**	**371**	**56**	**57.8**	**43**	**104**	**183**	**25.7**	**5.7**	**<0.5**
SR1397551	697	698				33	312	47	54	42	102	233		5	
SR1397552	698	699				35	304	44	38	40	75	136		5	
SR1397553	699	700				34	325	47	37	38	101	175		5	
SR1397554	700	701				36	310	48	50	34	159	272		5	
SR1397555	**701**	**702**	**600**	**33**	**1.6**	**34**	**375**	**53**	**50.3**	**43**	**200**	**275**	**25.6**	**8.8**	**<0.5**
SR1397556	702	703				34	292	49	47	38	118	239		5	
SR1397557	703	704				32	315	55	32	36	129	155		5	
SR1397558	704	705				31	310	47	36	39	185	184		5	
SR1397559	705	706				33	298	47	34	36	178	165		5	
SR1397561	**706**	**707**	**500**	**21**	**1.2**	**31**	**350**	**45**	**36.5**	**41**	**180**	**165**	**23.9**	**5.2**	**<0.5**
SR1397562	707	708				33	313	42	33	37	283	149		5	
SR1397563	708	709				33	334	48	35	39	209	155		5	
SR1397564	709	710				33	316	47	33	37	252	148		5	
SR1397565	710	711				34	316	43	46	41	311	236		5	
SR1397566	**711**	**712**	**<200**	**21**	**1**	**31**	**344**	**37**	**43.5**	**43**	**247**	**182**	**24.8**	**7.9**	**<0.5**
SR1397567	712	713				33	334	45	43	40	312	201		5	
SR1397568	713	714				33	311	10	43	41	257	204		5	
SR1397569	714	715				32	322	46	42	41	242	195		5	
SR1397570	715	716				33	304	10	41	41	173	192		5	

SR1397571	**716**	**717**	**<200**	**17**	**0.9**	**30**	**354**	**41**	**41.6**	**45**	**196**	**180**	**25.2**	**7.4**	**<0.5**
SR1397572	717	718				34	284	38	36	35	189	176		5	
SR1397573	718	719				33	280	10	46	38	92	226		5	
SR1397574	719	720				33	298	10	32	37	63	140		5	
SR1397575	720	721				34	288	10	34	36	81	143		5	
SR1397577	**721**	**722**	**600**	**15**	**1.1**	**31**	**355**	**36**	**37.7**	**41**	**59**	**182**	**24.6**	**12.9**	**<0.5**
SR1397578	722	723				35	309	10	26	37	139	122		5	
SR1397579	723	724				32	286	10	39	41	98	222		5	
SR1397580	724	725				33	284	10	57	41	96	328		5	
SR1397581	725	726				34	280	38	37	39	135	219		5	
SR1397582	**726**	**727**	**400**	**26**	**1.2**	**30**	**365**	**42**	**55.5**	**45**	**262**	**257**	**26.2**	**5.8**	**<0.5**
SR1397583	727	728				33	268	10	42	39	336	226		5	
SR1397584	728	729				33	301	10	35	37	232	186		5	
SR1397585	729	730				31	276	10	38	39	991	181		5	
SR1397586	730	731				31	288	10	37	36	528	187		5	
SR1397587	**731**	**732**	**<200**	**15**	**1**	**30**	**353**	**39**	**40.2**	**43**	**466**	**186**	**25.5**	**2.7**	**<0.5**
SR1397588	732	733				31	282	10	32	31	470	179		5	
SR1397589	733	734				31	284	10	35	39	1070	173		5	
SR1397590	734	735				31	264	10	32	35	483	156		5	
SR1397591	735	736				34	315	10	30	27	258	145		5	
SR1397592	**736**	**737**	**<200**	**20**	**1.3**	**28**	**334**	**36**	**40.6**	**42**	**299**	**163**	**25.2**	**6.5**	**<0.5**
SR1397593	737	738				31	261	10	42	37	336	198		5	
SR1397594	738	739				28	248	10	54	46	199	273		5	
SR1397595	739	740				32	289	10	48	39	301	228		5	

SR1397596	740	741				33	264	10	31	29	352	201		5	
SR1397597	**741**	**742**	**400**	**26**	**1.5**	**30**	**346**	**34**	**37.9**	**39**	**263**	**191**	**24.7**	**5.4**	**<0.5**
SR1397598	742	743				27	260	26	64	41	188	255		5	
SR1397599	743	744				33	283	36	30	29	205	141		5	
SR1397601	744	745				32	269	10	30	24	317	133		5	
SR1397602	745	746				32	298	10	28	24	241	121		5	
SR1397603	**746**	**747**	**<200**	**13**	**0.9**	**30**	**353**	**40**	**35.6**	**41**	**259**	**140**	**24.6**	**<0.5**	**<0.5**
SR1397604	747	748				32	288	10	25	26	93	135		5	
SR1397605	748	749				32	273	10	34	26	319	142		5	
SR1397606	749	750				33	280	10	33	29	169	132		5	
SR1397607	750	751				33	280	38	41	27	317	151		5	
SR1397608	751	752				33	286	10	28	24	235	142		5	

Table S10 continued

SAMPLE ID	SAMPLE FROM	SAMPLE TO	Rb	Sr	Y	Zr	Nb	Mo	Pd	Ag	Cd	Sn	Sb	Te	Cs
SR1397496	647	648		38	17	160		11		0.5			0.7		
SR1397497	648	649		39	21	144		8		0.5			0.6		
SR1397498	649	650		79	20	136		9		0.5			0.25		
SR1397499	650	651		54	19	141		2		0.5			0.25		
SR1397501	**651**	**652**	**6.8**	**44**	**31.1**	**128**	**9.7**	**8**	**0.017**	**<0.05**	**0.02**	**2**	**1.3**	**0.05**	**0.66**
SR1397502	652	653		24	17	151		7		0.5			0.9		
SR1397503	653	654		54	26	155		6		0.5			0.6		
SR1397504	654	655		200	16	128		3		0.5			0.25		
SR1397505	655	656		45	21	161		3		0.5			0.25		
SR1397506	**656**	**657**	**5**	**60**	**27.3**	**152**	**10.7**	**3**	**0.021**	**<0.05**	**<0.02**	**3**	**1.2**	**<0.05**	**0.29**
SR1397507	657	658		28	16	152		2		0.5			0.25		
SR1397508	658	659		122	19	146		6		0.5			0.25		
SR1397509	659	660		171	28	186		6		0.5			0.25		
SR1397510	660	661		56	25	171		5		0.5			0.25		
SR1397512	**661**	**662**	**33.9**	**347**	**29.4**	**155**	**11.3**	**3**	**0.022**	**<0.05**	**<0.02**	**3**	**2.7**	**<0.05**	**0.79**
SR1397513	662	663		201	25	179		8		0.5			0.5		
SR1397514	663	664		87	23	147		3		0.5			0.6		
SR1397515	664	665		107	20	141		10		0.5			0.25		
SR1397516	665	666		43	18	152		6		0.5			0.25		
SR1397517	**666**	**667**	**26**	**42**	**32.9**	**131**	**9.2**	**2**	**0.018**	**<0.05**	**<0.02**	**3**	**0.7**	**<0.05**	**0.89**
SR1397518	667	668		83	16	167		11		0.5			0.25		

SR1397519	668	669		117	17	189		10		0.5			0.25		
SR1397520	669	670		114	17	184		4		0.5			0.7		
SR1397521	670	671		45	16	178		1		0.5			3		
SR1397522	**671**	**672**	**54.6**	**34**	**25.6**	**158**	**11.5**	**2**	**0.023**	**0.06**	**<0.02**	**3**	**0.9**	**<0.05**	**2.06**
SR1397523	672	673		40	25	171		13		0.5			0.25		
SR1397524	673	674		96	27	167		2		0.5			0.25		
SR1397525	674	675		83	23	165		2		0.5			0.25		
SR1397526	675	676		92	27	164		1		0.5			0.25		
SR1397527	**676**	**677**	**14.2**	**133**	**35.2**	**153**	**10.7**	**2**	**0.021**	**0.05**	**<0.02**	**4**	**0.6**	**<0.05**	**1.06**
SR1397528	677	678		110	23	160		10		0.5			0.25		
SR1397530	678	679		128	26	152		3		0.5			0.25		
SR1397531	679	680		168	28	153		1		0.5			0.25		
SR1397532	680	681		177	28	154		0.5		0.5			0.25		
SR1397533	**681**	**682**	**17.7**	**178**	**33.2**	**153**	**10.8**	**2**	**0.021**	**0.07**	**0.04**	**3**	**0.9**	**<0.05**	**0.65**
SR1397534	682	683		177	27	153		0.5		0.5			0.7		
SR1397535	683	684		188	26	146		0.5		0.5			0.25		
SR1397536	684	685		191	25	152		3		0.5			0.25		
SR1397538	685	686		168	25	152		8		0.5			0.25		
SR1397539	**686**	**687**	**27.7**	**174**	**39**	**172**	**12.5**	**4**	**0.019**	**0.12**	**0.05**	**2**	**0.7**	**<0.05**	**0.81**
SR1397540	687	688		151	42	280		4		0.5			0.25		
SR1397541	688	689		159	25	173		19		0.5			0.8		
SR1397542	689	690		175	24	144		1		0.5			0.25		
SR1397543	690	691		180	20	147		3		0.5			0.25		
SR1397544	**691**	**692**	**47**	**176**	**31.2**	**142**	**10.2**	**2**	**0.022**	**0.05**	**<0.02**	**3**	**0.7**	**<0.05**	**0.74**

SR1397545	692	693		187	22	145		1		0.5			0.25		
SR1397546	693	694		187	24	148		1		0.5			0.25		
SR1397548	694	695		188	21	144		3		0.5			1.7		
SR1397549	695	696		195	21	149		2		0.5			0.25		
SR1397550	**696**	**697**	**25.6**	**178**	**31.3**	**142**	**10.4**	**9**	**0.019**	**<0.05**	**<0.02**	**2**	**0.7**	**<0.05**	**0.62**
SR1397551	697	698		180	16	149		7		0.5			0.25		
SR1397552	698	699		196	19	150		0.5		0.5			0.25		
SR1397553	699	700		192	22	152		1		0.5			0.25		
SR1397554	700	701		170	26	160		1		0.5			0.25		
SR1397555	**701**	**702**	**21.9**	**183**	**34.1**	**157**	**11.2**	**11**	**0.021**	**<0.05**	**<0.02**	**2**	**0.6**	**<0.05**	**0.48**
SR1397556	702	703		180	22	151		1		0.5			0.25		
SR1397557	703	704		197	23	147		0.5		0.5			0.25		
SR1397558	704	705		192	17	149		1		0.5			0.25		
SR1397559	705	706		194	19	157		0.5		0.5			0.25		
SR1397561	**706**	**707**	**31.7**	**196**	**32**	**149**	**10.4**	**4**	**0.021**	**<0.05**	**0.02**	**3**	**0.7**	**<0.05**	**0.53**
SR1397562	707	708		204	21	155		0.5		0.5			0.25		
SR1397563	708	709		200	22	151		0.5		0.5			0.25		
SR1397564	709	710		199	16	148		0.5		0.5			0.25		
SR1397565	710	711		185	21	156		4		0.5			0.25		
SR1397566	**711**	**712**	**38.5**	**195**	**33.7**	**156**	**10.8**	**2**	**0.021**	**0.06**	**0.03**	**4**	**0.6**	**<0.05**	**0.49**
SR1397567	712	713		183	19	146		1		0.5			0.25		
SR1397568	713	714		183	20	151		1		0.5			0.25		
SR1397569	714	715		196	23	149		1		0.5			0.25		
SR1397570	715	716		205	28	142		0.5		0.5			0.25		

SR1397571	**716**	**717**	**44.4**	**212**	**33.3**	**150**	**10.7**	**2**	**0.021**	**0.06**	**0.05**	**3**	**0.6**	**<0.05**	**0.42**
SR1397572	717	718		203	26	142		1		0.5			0.25		
SR1397573	718	719		195	28	145		0.5		0.5			0.25		
SR1397574	719	720		202	25	141		0.5		0.5			0.25		
SR1397575	720	721		202	24	139		0.5		0.5			1		
SR1397577	**721**	**722**	**61.9**	**203**	**32.5**	**150**	**11.1**	**3**	**0.021**	**<0.05**	**<0.02**	**3**	**0.7**	**<0.05**	**0.44**
SR1397578	722	723		211	27	147		2		0.5			0.25		
SR1397579	723	724		193	22	139		2		0.5			0.25		
SR1397580	724	725		185	25	149		0.5		0.5			0.25		
SR1397581	725	726		203	23	144		2		0.5			0.25		
SR1397582	**726**	**727**	**32.3**	**188**	**32.3**	**150**	**10.9**	**3**	**0.02**	**0.08**	**0.04**	**2**	**0.5**	**<0.05**	**0.31**
SR1397583	727	728		191	23	140		35		0.5			0.25		
SR1397584	728	729		201	22	144		8		0.5			0.25		
SR1397585	729	730		191	22	136		1		0.5			0.25		
SR1397586	730	731		196	24	138		6		0.5			0.25		
SR1397587	**731**	**732**	**62.4**	**202**	**32.4**	**146**	**10.6**	**3**	**0.02**	**0.17**	**0.06**	**2**	**<0.5**	**<0.05**	**0.41**
SR1397588	732	733		201	20	139		0.5		0.5			0.25		
SR1397589	733	734		199	21	139		3		0.5			0.25		
SR1397590	734	735		213	22	144		0.5		0.5			0.25		
SR1397591	735	736		207	23	137		2		0.5			0.25		
SR1397592	**736**	**737**	**49.3**	**202**	**31.2**	**138**	**10.2**	**8**	**0.02**	**<0.05**	**0.16**	**2**	**0.6**	**<0.05**	**0.43**
SR1397593	737	738		175	22	133		13		0.5			0.25		
SR1397594	738	739		132	18	125		34		0.5			0.25		
SR1397595	739	740		173	21	140		116		0.5			0.8		

SR1397596	740	741		210	25	137		7		0.5			0.25		
SR1397597	**741**	**742**	**29.2**	**196**	**32.5**	**146**	**11.3**	**38**	**0.021**	**<0.05**	**0.65**	**2**	**0.7**	**<0.05**	**0.57**
SR1397598	742	743		154	19	127		611		1			0.8		
SR1397599	743	744		199	27	145		48		0.5			0.25		
SR1397601	744	745		205	23	135		11		0.5			0.25		
SR1397602	745	746		210	23	143		3		0.5			3.7		
SR1397603	**746**	**747**	**40.7**	**208**	**32.3**	**146**	**10.9**	**3**	**0.021**	**<0.05**	**0.1**	**3**	**0.7**	**<0.05**	**0.4**
SR1397604	747	748		204	26	142		9		0.5			0.25		
SR1397605	748	749		201	25	143		267		0.5			1.3		
SR1397606	749	750		205	22	143		1		0.5			0.25		
SR1397607	750	751		195	25	142		4		0.5			0.6		
SR1397608	751	752		208	23	141		0.5		0.5			0.25		

Table S10 continued

SAMPLE ID	SAMPLE FROM	SAMPLE TO	Ba	La	Ce	Pr	Nd	Sm	Eu	Gd	Tb	Dy	Ho	Er	Tm
SR1397496	647	648	81	25	50										
SR1397497	648	649	271	25	50										
SR1397498	649	650	2111	25	50										
SR1397499	650	651	584	25	50										
SR1397501	**651**	**652**	**829**	**16.6**	**37.4**	**4.85**	**21.1**	**5.48**	**1.6**	**5.72**	**1.04**	**5.93**	**1.2**	**3.38**	**0.49**
SR1397502	652	653	103	25	50										
SR1397503	653	654	1102	25	50										
SR1397504	654	655	7329	25	50										
SR1397505	655	656	967	25	50										
SR1397506	**656**	**657**	**1616**	**9.7**	**22.1**	**3.3**	**15.2**	**4.11**	**1.04**	**4.73**	**0.82**	**4.91**	**1.03**	**3.06**	**0.47**
SR1397507	657	658	182	25	50										
SR1397508	658	659	5133	25	50										
SR1397509	659	660	8493	25	50										
SR1397510	660	661	1733	25	50										
SR1397512	**661**	**662**	**13825**	**7.2**	**27.6**	**2.55**	**12.1**	**3.67**	**0.9**	**4.51**	**0.86**	**5.4**	**1.14**	**3.52**	**0.51**
SR1397513	662	663	10607	25	50										
SR1397514	663	664	3259	25	50										
SR1397515	664	665	4889	25	50										
SR1397516	665	666	150	25	50										
SR1397517	**666**	**667**	**258**	**8.6**	**20.3**	**3.07**	**15**	**4.49**	**1.36**	**5.79**	**1.06**	**6.35**	**1.3**	**3.66**	**0.55**
SR1397518	667	668	3323	25	50										

SR1397519	668	669	5080	25	50										
SR1397520	669	670	3193	25	50										
SR1397521	670	671	280	25	50										
SR1397522	**671**	**672**	**86**	**22.4**	**54.1**	**7.52**	**34.9**	**7.51**	**1.89**	**6.42**	**0.98**	**5.2**	**1.04**	**2.98**	**0.46**
SR1397523	672	673	274	25	50										
SR1397524	673	674	83	25	50										
SR1397525	674	675	535	25	50										
SR1397526	675	676	624	25	50										
SR1397527	**676**	**677**	**139**	**14.3**	**33.9**	**5.04**	**23**	**6.65**	**2.01**	**7.11**	**1.16**	**6.82**	**1.33**	**3.71**	**0.55**
SR1397528	677	678	52	25	50										
SR1397530	678	679	103	25	50										
SR1397531	679	680	76	25	50										
SR1397532	680	681	93	25	50										
SR1397533	**681**	**682**	**94**	**15.2**	**35**	**5.04**	**23.5**	**6.43**	**2.1**	**6.79**	**1.15**	**6.51**	**1.29**	**3.87**	**0.54**
SR1397534	682	683	71	25	50										
SR1397535	683	684	64	25	50										
SR1397536	684	685	89	25	50										
SR1397538	685	686	77	25	50										
SR1397539	**686**	**687**	**116**	**18.3**	**48.1**	**5.86**	**26.9**	**7.45**	**2.39**	**7.91**	**1.36**	**7.52**	**1.47**	**4.19**	**0.61**
SR1397540	687	688	106	25	50										
SR1397541	688	689	100	25	50										
SR1397542	689	690	105	25	50										
SR1397543	690	691	104	25	50										
SR1397544	**691**	**692**	**115**	**13.5**	**32.3**	**4.62**	**21.6**	**5.98**	**2.02**	**6.59**	**1.1**	**6.22**	**1.21**	**3.46**	**0.5**

SR1397545	692	693	100	25	50										
SR1397546	693	694	123	25	50										
SR1397548	694	695	79	25	50										
SR1397549	695	696	109	25	50										
SR1397550	**696**	**697**	**145**	**14**	**32.7**	**4.75**	**22**	**6.13**	**2.09**	**6.49**	**1.08**	**6.28**	**1.21**	**3.42**	**0.48**
SR1397551	697	698	80	25	50										
SR1397552	698	699	145	25	50										
SR1397553	699	700	136	25	50										
SR1397554	700	701	125	25	50										
SR1397555	**701**	**702**	**176**	**13.9**	**63.6**	**5.31**	**25.1**	**7.04**	**2.18**	**7.49**	**1.27**	**7**	**1.28**	**3.56**	**0.5**
SR1397556	702	703	143	25	50										
SR1397557	703	704	139	25	50										
SR1397558	704	705	129	25	50										
SR1397559	705	706	112	25	50										
SR1397561	**706**	**707**	**112**	**14.4**	**33.4**	**4.88**	**21.9**	**6.31**	**2.02**	**6.37**	**1.14**	**6.27**	**1.25**	**3.36**	**0.51**
SR1397562	707	708	86	25	50										
SR1397563	708	709	99	25	50										
SR1397564	709	710	116	25	50										
SR1397565	710	711	97	25	50										
SR1397566	**711**	**712**	**128**	**15.6**	**35.6**	**5.17**	**24**	**6.23**	**2.2**	**6.94**	**1.16**	**6.48**	**1.29**	**3.66**	**0.51**
SR1397567	712	713	111	25	50										
SR1397568	713	714	95	25	50										
SR1397569	714	715	106	25	50										
SR1397570	715	716	123	25	50										

SR1397571	**716**	**717**	**160**	**15.5**	**41**	**5.24**	**23.8**	**6.6**	**2.08**	**6.69**	**1.14**	**6.63**	**1.29**	**3.69**	**0.52**
SR1397572	717	718	151	25	50										
SR1397573	718	719	141	25	50										
SR1397574	719	720	170	25	50										
SR1397575	720	721	181	25	50										
SR1397577	**721**	**722**	**221**	**15.5**	**35.2**	**5**	**23**	**6.42**	**2.07**	**6.68**	**1.14**	**6.44**	**1.26**	**3.6**	**0.51**
SR1397578	722	723	217	25	50										
SR1397579	723	724	174	25	50										
SR1397580	724	725	164	25	50										
SR1397581	725	726	178	25	50										
SR1397582	**726**	**727**	**135**	**13.8**	**32.6**	**4.75**	**21.5**	**5.76**	**2.05**	**6.58**	**1.11**	**6.26**	**1.27**	**3.52**	**0.5**
SR1397583	727	728	142	25	50										
SR1397584	728	729	170	25	50										
SR1397585	729	730	151	25	50										
SR1397586	730	731	202	25	50										
SR1397587	**731**	**732**	**190**	**14.2**	**33.3**	**4.77**	**22.5**	**6.01**	**2.1**	**6.18**	**1.1**	**6.18**	**1.2**	**3.37**	**0.49**
SR1397588	732	733	185	25	50										
SR1397589	733	734	173	25	50										
SR1397590	734	735	175	25	50										
SR1397591	735	736	164	25	50										
SR1397592	**736**	**737**	**179**	**16.3**	**48.8**	**5.03**	**22.9**	**6.1**	**2.08**	**6.55**	**1.11**	**6.23**	**1.18**	**3.37**	**0.47**
SR1397593	737	738	156	25	50										
SR1397594	738	739	91	25	50										
SR1397595	739	740	157	25	50										

SR1397596	740	741	362	25	50										
SR1397597	**741**	**742**	**134**	**14.1**	**34.8**	**4.91**	**22.4**	**6.56**	**2.14**	**6.8**	**1.17**	**6.66**	**1.24**	**3.53**	**0.54**
SR1397598	742	743	103	25	50										
SR1397599	743	744	146	25	50										
SR1397601	744	745	131	25	50										
SR1397602	745	746	1950	25	50										
SR1397603	**746**	**747**	**168**	**16.3**	**35.6**	**5.03**	**23**	**6.38**	**2.02**	**6.8**	**1.11**	**6.26**	**1.27**	**3.56**	**0.53**
SR1397604	747	748	146	25	50										
SR1397605	748	749	130	25	50										
SR1397606	749	750	121	25	50										
SR1397607	750	751	91	25	50										
SR1397608	751	752	124	25	50										

Table S10 continued

SAMPLE ID	SAMPLE FROM	SAMPLE TO	Yb	Lu	Hf	Ta	W	Re	Pt	Au	Tl	Pb	Bi	Th	U
SR1397496	647	648								0.13		5	0.5		3.90
SR1397497	648	649								0.02		5	0.5		4.41
SR1397498	649	650								0.005		5	0.5		1.78
SR1397499	650	651								0.005		5	0.5		2.29
SR1397501	**651**	**652**	**3.04**	**0.43**	**3.8**	**0.7**	**2**	**0.01**	**0.009**	**0.007**	**0.05**	**12**	**0.3**	**2.05**	**5.94**
SR1397502	652	653								0.005		5	0.5		6.36
SR1397503	653	654								0.005		5	0.5		8.56
SR1397504	654	655								0.005		5	0.5		3.90
SR1397505	655	656								0.005		5	0.5		2.88
SR1397506	**656**	**657**	**2.91**	**0.41**	**4.5**	**0.8**	**1**	**0.038**	**0.01**	**0.01**	**0.04**	**9**	**0.12**	**2.11**	**3.22**
SR1397507	657	658								0.005		5	0.5		4.32
SR1397508	658	659								0.005		5	0.5		3.99
SR1397509	659	660								0.005		5	0.5		5.77
SR1397510	660	661								0.005		5	0.5		4.66
SR1397512	**661**	**662**	**3.12**	**0.44**	**4.7**	**0.8**	**1**	**0.101**	**0.01**	**0.005**	**0.18**	**6**	**0.06**	**2.26**	**4.92**
SR1397513	662	663								0.005		5	0.5		4.75
SR1397514	663	664								0.005		5	0.5		4.66
SR1397515	664	665								0.005		5	0.5		4.92
SR1397516	665	666								0.005		5	0.5		4.75
SR1397517	**666**	**667**	**3.39**	**0.46**	**3.9**	**0.7**	**<1**	**0.057**	**0.008**	**0.004**	**0.1**	**5**	**0.03**	**1.88**	**5.00**
SR1397518	667	668								0.01		5	0.5		4.32

SR1397519	668	669								0.005		5	0.5		3.90
SR1397520	669	670								0.005		5	0.5		2.46
SR1397521	670	671								0.02		5	0.5		2.29
SR1397522	**671**	**672**	**2.92**	**0.43**	**4.8**	**0.9**	**<1**	**0.007**	**0.011**	**0.003**	**0.2**	**5**	**0.02**	**2.34**	**2.29**
SR1397523	672	673								0.01		5	0.5		2.63
SR1397524	673	674								0.005		5	0.5		1.10
SR1397525	674	675								0.005		5	0.5		0.85
SR1397526	675	676								0.005		5	0.5		0.93
SR1397527	**676**	**677**	**3.27**	**0.45**	**4.3**	**0.8**	**<1**	**0.006**	**0.01**	**0.006**	**0.08**	**16**	**0.02**	**2.21**	**0.68**
SR1397528	677	678								0.005		5	0.5		0.85
SR1397530	678	679								0.005		5	0.5		2.54
SR1397531	679	680								0.005		5	0.5		0.68
SR1397532	680	681								0.005		5	0.5		0.59
SR1397533	**681**	**682**	**3.19**	**0.49**	**4.5**	**0.8**	**<1**	**0.004**	**0.01**	**0.006**	**0.11**	**13**	**0.02**	**2.19**	**0.76**
SR1397534	682	683								0.005		5	0.5		0.68
SR1397535	683	684								0.005		5	0.5		0.59
SR1397536	684	685								0.005		5	0.5		0.59
SR1397538	685	686								0.005		5	0.5		2.04
SR1397539	**686**	**687**	**3.67**	**0.54**	**5**	**0.9**	**<1**	**0.004**	**0.01**	**0.005**	**0.14**	**21**	**0.02**	**2.74**	**1.19**
SR1397540	687	688								0.005		5	0.5		2.04
SR1397541	688	689								0.01		5	0.5		2.80
SR1397542	689	690								0.005		5	0.5		0.76
SR1397543	690	691								0.005		5	0.5		0.85
SR1397544	**691**	**692**	**3.11**	**0.42**	**4.2**	**0.8**	**<1**	**0.005**	**0.009**	**0.005**	**0.19**	**11**	**0.02**	**2.15**	**0.85**

SR1397545	692	693								0.005		5	0.5		0.68
SR1397546	693	694								0.005		5	0.5		0.59
SR1397548	694	695								0.005		5	0.5		0.85
SR1397549	695	696								0.005		5	0.5		0.59
SR1397550	**696**	**697**	**3.07**	**0.43**	**4.2**	**0.8**	**<1**	**0.028**	**0.009**	**0.005**	**0.14**	**10**	**0.02**	**2.07**	**2.29**
SR1397551	697	698								0.005		5	0.5		3.22
SR1397552	698	699								0.005		5	0.5		1.10
SR1397553	699	700								0.005		5	0.5		2.54
SR1397554	700	701								0.005		5	0.5		4.49
SR1397555	**701**	**702**	**3.16**	**0.43**	**4.4**	**0.9**	**<1**	**0.008**	**0.01**	**0.009**	**0.13**	**19**	**0.02**	**2.59**	**2.88**
SR1397556	702	703								0.005		5	1		3.56
SR1397557	703	704								0.07		5	0.5		0.76
SR1397558	704	705								0.005		5	0.5		1.19
SR1397559	705	706								0.005		5	0.5		0.76
SR1397561	**706**	**707**	**3.17**	**0.43**	**4.3**	**0.8**	**<1**	**0.004**	**0.01**	**0.005**	**0.17**	**10**	**0.06**	**2.24**	**0.68**
SR1397562	707	708								0.005		5	0.5		0.68
SR1397563	708	709								0.005		5	0.5		1.10
SR1397564	709	710								0.005		5	0.5		0.85
SR1397565	710	711								0.02		5	0.5		1.44
SR1397566	**711**	**712**	**3.21**	**0.53**	**4.5**	**0.8**	**<1**	**0.008**	**0.01**	**0.005**	**0.19**	**14**	**0.09**	**2.37**	**0.85**
SR1397567	712	713								0.005		5	0.5		1.61
SR1397568	713	714								0.005		5	0.5		1.36
SR1397569	714	715								0.005		5	0.5		0.93
SR1397570	715	716								0.005		5	0.5		0.68

SR1397571	**716**	**717**	**3.1**	**0.47**	**4.3**	**0.8**	**<1**	**<0.002**	**0.01**	**0.006**	**0.21**	**10**	**0.04**	**2.32**	**0.68**
SR1397572	717	718								0.01		5	0.5		0.93
SR1397573	718	719								0.005		5	0.5		1.02
SR1397574	719	720								0.005		5	0.5		0.68
SR1397575	720	721								0.005		5	0.5		0.68
SR1397577	**721**	**722**	**3.22**	**0.44**	**4.5**	**0.8**	**<1**	**0.003**	**0.01**	**0.008**	**0.28**	**7**	**0.02**	**2.36**	**0.68**
SR1397578	722	723								0.005		5	0.5		0.76
SR1397579	723	724								0.005		5	0.5		1.36
SR1397580	724	725								0.005		5	0.5		3.73
SR1397581	725	726								0.005		5	0.5		1.87
SR1397582	**726**	**727**	**3.18**	**0.43**	**4.3**	**0.8**	**<1**	**0.037**	**0.01**	**0.006**	**0.17**	**11**	**<0.01**	**2.26**	**6.70**
SR1397583	727	728								0.005		5	0.5		5.94
SR1397584	728	729								0.005		5	0.5		1.27
SR1397585	729	730								0.005		5	0.5		1.53
SR1397586	730	731								0.005		5	0.5		2.88
SR1397587	**731**	**732**	**3.01**	**0.41**	**4.3**	**0.8**	**<1**	**0.032**	**0.01**	**0.004**	**0.29**	**9**	**<0.01**	**2.25**	**1.44**
SR1397588	732	733								0.005		5	0.5		0.68
SR1397589	733	734								0.08		5	0.5		0.68
SR1397590	734	735								0.005		5	0.5		0.68
SR1397591	735	736								0.005		5	0.5		0.59
SR1397592	**736**	**737**	**3.02**	**0.41**	**4.2**	**0.8**	**<1**	**0.011**	**0.01**	**0.002**	**0.25**	**35**	**<0.01**	**2.52**	**1.44**
SR1397593	737	738								0.005		50	0.5		2.80
SR1397594	738	739								0.005		40	0.5		3.82
SR1397595	739	740								0.01		42	0.5		3.56

SR1397596	740	741								0.005		26	0.5		1.10
SR1397597	**741**	**742**	**3.21**	**0.45**	**4.6**	**0.9**	**<1**	**0.283**	**0.011**	**0.002**	**0.35**	**23**	**<0.01**	**2.32**	**1.53**
SR1397598	742	743								0.005		51	0.5		4.49
SR1397599	743	744								0.005		5	0.5		0.68
SR1397601	744	745								0.005		5	0.5		0.68
SR1397602	745	746								0.005		5	0.5		0.59
SR1397603	**746**	**747**	**3.08**	**0.49**	**4.3**	**0.8**	**<1**	**0.006**	**0.01**	**0.004**	**0.22**	**7**	**<0.01**	**2.29**	**0.68**
SR1397604	747	748								0.005		5	0.5		0.93
SR1397605	748	749								0.005		5	0.5		0.93
SR1397606	749	750								0.005		5	0.5		0.68
SR1397607	750	751								0.005		5	0.5		0.59
SR1397608	751	752								0.005		5	0.5		0.68

There are two groups of assays displayed. Expanded assays (**bold**) include more elements than standard assays. Only the expanded assays are shown when both standard and expanded assays are available for certain interval. Standard assays sample at 1-m interval, and expanded assays sample every 5-m interval. Oxides are in wt.%, and trace elements are in ppm.

Appendix 1 Co-authors contributions for chapters 3 to 5 (in percentage)

Chapter 3 Neoproterozoic (ca. 820-830 Ma) mafic dykes at Olympic Dam, South Australia: Links with the Gairdner Large Igneous Province (published paper)

	Huang, Q	Kamenetsky, V.S.	McPhie, J.	Ehrig, K.	Meffre, S.	Maas, R.	Thompson, J.	Kamenetsky, M.	Chambefort, I.	Apukhtina, O.	Hu, Y.
Field work	50%	20%	10%	10%						10%	
Sample preparation	100%										
Sample analysis	60%				10%			10%			20%
Data interpretation	60%	20%		10%	5%		5%				
Figures and tables	100%										
Writing	95%	5%									
Proof read and discussions	50%	15%	10%	10%		10%			5%		

Chapter 4 Mafic magmas in the Mesoproterozoic Gawler silicic large igneous province, South Australia: evidence from olivine-phyric rocks at the Olympic Dam deposit and other localities (published paper)

	Huang, Q	Kamenetsky, V.S.	Ehrig, K.	McPhie, J.	Kamenetsky, M.	Cross, K.	Meffre, S.	Agangi, A.	Chambefort, I.	Direen, N.G.	Maas, R.	Apukhtina, O.
Field work	50%	20%	10%	5%		5%		5%				5%
Sample preparation	100%											
Sample analysis	60%	30%			10%							
Data interpretation	60%	20%	5%	10%			5%					
Figures and tables	100%											
Writing	95%	5%										
Proof read and discussions	40%	10%	10%	10%		5%	5%	5%	5%	5%	5%	

Chapter 5 Alterations of mafic lithologies at the Olympic Dam iron oxide Cu-U-Au-Ag deposit (unpublished)

	Huang, Q	Kamenetsky, V.S.	Ehrig, K.	McPhie, J.	Maas, R.	Kamenetsky, M.	Apukhtina, O.	Chambefort, I.
Field work	65%	20%	10%	5%				
Sample preparation	65%		15%		10%		10%	
Sample analysis	55%		15%		10%	10%	10%	
Data interpretation	60%	15%	10%		10%		5%	
Figures and tables	95%							5%
Writing	85%	5%			10%			
Proof read and discussions	45%	20%	15%	10%	5%			5%

Appendix 2 Selected drill core loggings

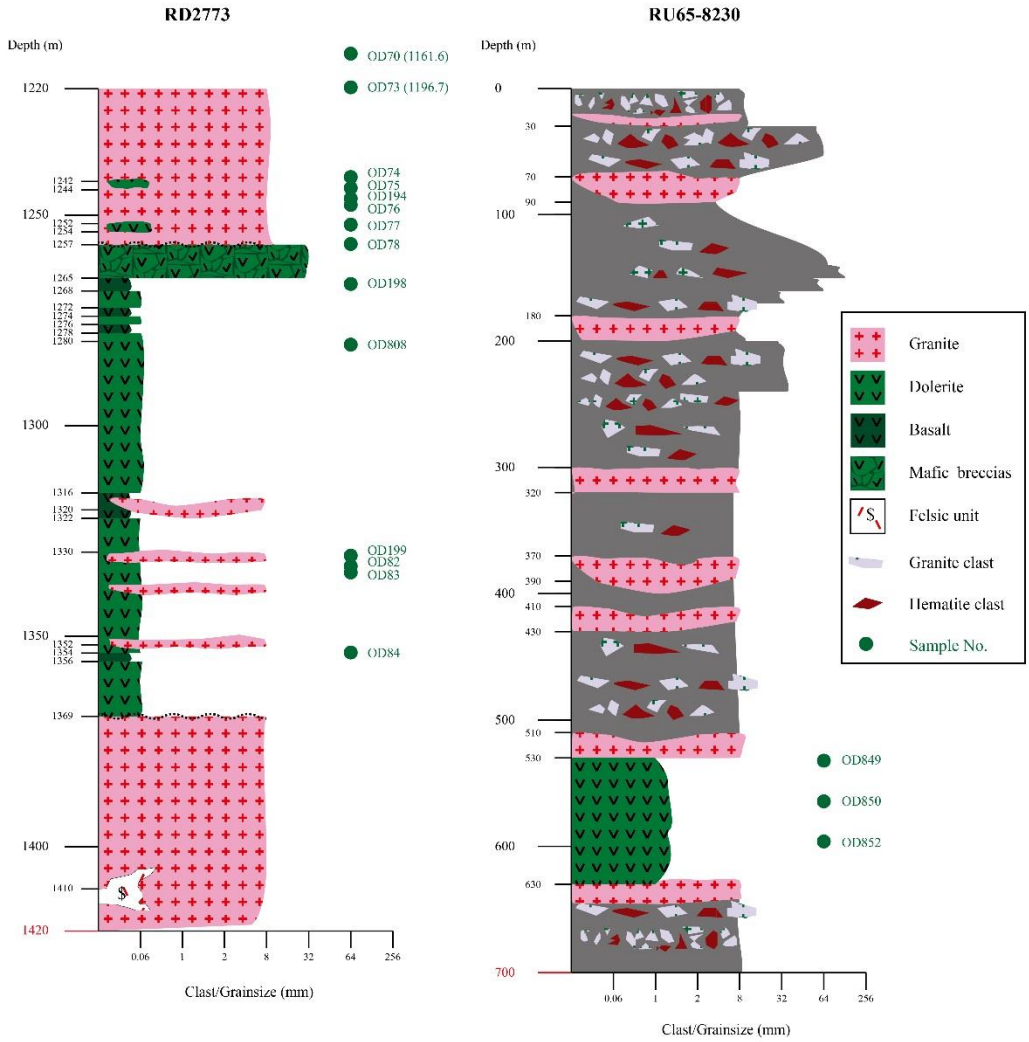

(Note: 'Granite' is the Roxby Downs Granite; 'Dolerite' and 'Basalt' are components of the ca. 820 Ma Olympic Dam dolerite; 'Mafic breccias' represents brecciated Olympic Dam dolerite; 'Felsic unit' is inferred to be a felsic pluton, see Chapter 2 and Ehrig et al. (2012) for further details.)

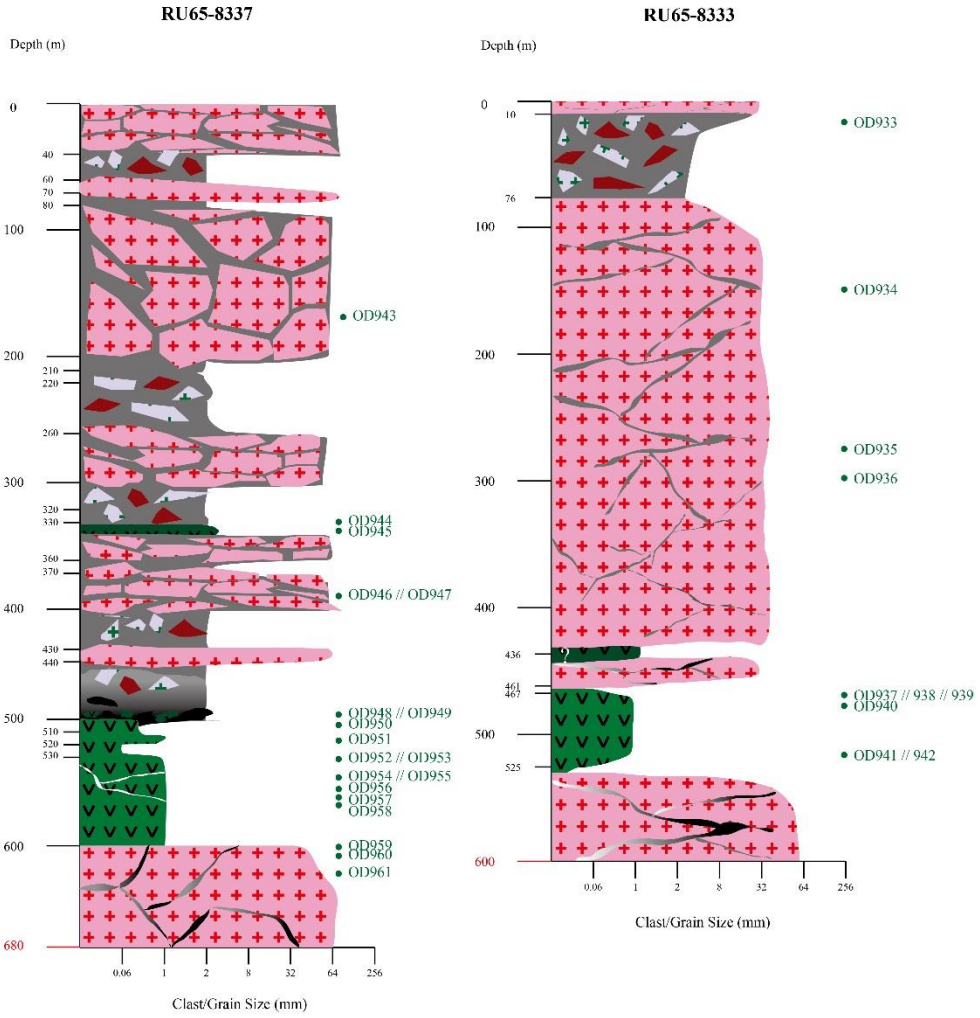
RU65-8337
Depth (m)
0
40
60
70
80
100
200
210
220
260
300
320
330
360
370
400
430
440
500
510
520
530
600
680
OD943
OD944
OD945
OD946 // OD947
OD948 // OD949
OD950
OD951
OD952 // OD953
OD954 // OD955
OD956
OD957
OD958
OD959
OD960
OD961
0.06
1
2
8
32
64
256
Clast/Grain Size (mm)
RU65-8333
Depth (m)
0
10
76
100
200
300
400
436
461
467
500
525
600
OD933
OD934
OD935
OD936
OD937 // 938 // 939
OD940
OD941 // 942
0.06
1
2
8
32
64
256
Clast/Grain Size (mm)

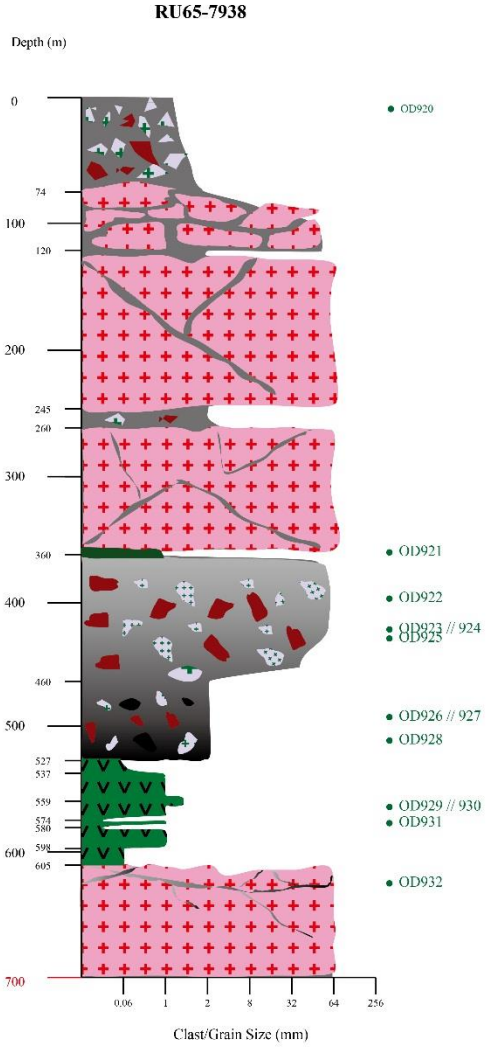
RU65-7938
Depth (m)
0
74
100
120
200
245
260
300
360
400
460
500
527
537
559
574
580
598
600
605
700
OD920
OD921
OD922
OD923 // 924
OD925
OD926 // 927
OD928
OD929 // 930
OD931
OD932
0.06
1
2
8
32
64
256
Clast/Grain Size (mm)

Appendix 3 Sample index

Sample No.	Location	Drill hole/Depth (m)	Unit	Complex	Petrography	WR comp.	Dating	Isotopes
OD118	Olympic Dam	RD271/682	Olympic Dam dolerite	Gairdner Dyke Swarm		√		
OD852	Olympic Dam	RU65-8230/596.1	Olympic Dam dolerite	Gairdner Dyke Swarm			Ap-U/Pb	
OD850	Olympic Dam	RU65-8230/544.1	Olympic Dam dolerite	Gairdner Dyke Swarm	√	√	Ap-U/Pb	Nd-Pb
OD849	Olympic Dam	RU65-8230/532.2	Olympic Dam dolerite	Gairdner Dyke Swarm		√		Nd
OD84	Olympic Dam	RD2773/1352.2	Olympic Dam dolerite	Gairdner Dyke Swarm		√		Nd-Pb
OD1	Olympic Dam	RU39-5426/237.1	Olympic Dam dolerite	Gairdner Dyke Swarm		√		
OD82	Olympic Dam	RD2773/1331.7	Olympic Dam dolerite	Gairdner Dyke Swarm	√	√		Nd-Pb
OD81-2	Olympic Dam	RD2773/1325.4	Olympic Dam dolerite	Gairdner Dyke Swarm		√		
OD80b	Olympic Dam	RD2773/1271.3	Olympic Dam dolerite	Gairdner Dyke Swarm		√		Nd-Pb
OD80d	Olympic Dam	RD2773/1271.3	Olympic Dam dolerite	Gairdner Dyke Swarm		√		Nd-Pb
OD79	Olympic Dam	RD2773/1270.6	Olympic Dam dolerite	Gairdner Dyke Swarm		√		
OD952	Olympic Dam	RU65-8337/531.8	Olympic Dam dolerite	Gairdner Dyke Swarm	√	√		
OD958	Olympic Dam	RU65-8337/565.2	Olympic Dam dolerite	Gairdner Dyke Swarm		√		
OD199	Olympic Dam	RD2773/1329.2	Olympic Dam dolerite	Gairdner Dyke Swarm	√		Tit-U/Pb	Nd
OD422	Olympic Dam	RD222/759	Olympic Dam dolerite	Gairdner Dyke Swarm				Nd
OD7	Olympic Dam	RD2570/764.4	olivine-phyric basalt	Mafic GRV	√		Ap-U/Pb	
OD862	Olympic Dam	RD1687/449.5	olivine-phyric basalt	Mafic GRV	√			
OD24	Olympic Dam	RD3008/406.2	olivine-phyric basalt	Mafic GRV		√	Ap-U/Pb	
GH80	Kokatha	outcrop	olivine-phyric basalt	Mafic GRV		√		
GH81	Kokatha	outcrop	outcrop	Mafic GRV		√		
EGC-13-06K	Kokatha	outcrop	outcrop	Mafic GRV	√			
OD395	Wirrda Well	WRD33/1121.4	olivine-phyric basalt	Mafic GRV		√		
OD398	Wirrda Well	WRD33/1206.4	olivine-phyric basalt	Mafic GRV		√		
RX3453	Mount Gunson	PY-1/939	olivine-phyric basalt	Mafic GRV	√	√	Ap-U/Pb	
RX3454	Mount Gunson	PY-1/939.5	olivine-phyric basalt	Mafic GRV		√		
RX3456	Mount Gunson	Py-1/946	olivine-phyric basalt	Mafic GRV	√	√		
OD906	Olympic Dam	RD2715/810.1	olivine-phyric basalt	Mafic GRV				Nd-Sr
OD914	Olympic Dam	RD2715/852.6	olivine-phyric basalt	Mafic GRV				Nd-Sr

OD968	Olympic Dam	RD635/371.6	olivine-phyric basalt	Mafic GRV				Nd-Sr
OD117	Olympic Dam	RD271/657.4	Olympic Dam dolerite	Gairdner Dyke Swarm		√		
OD73	Olympic Dam	RD2773/1196.7	Olympic Dam dolerite	Gairdner Dyke Swarm		√		
OD110	Olympic Dam	RD271/645.3	Olympic Dam dolerite	Gairdner Dyke Swarm		√		
OD113	Olympic Dam	RD271/650	Olympic Dam dolerite	Gairdner Dyke Swarm		√		
OD194	Olympic Dam	RD2773/1244.4	Olympic Dam dolerite	Gairdner Dyke Swarm		√		
OD4	Olympic Dam	RU39-5426/208.7	Olympic Dam dolerite	Gairdner Dyke Swarm		√		
OD74	Olympic Dam	RD2773/1239.3	Olympic Dam dolerite	Gairdner Dyke Swarm		√		
OD6	Olympic Dam	RU39-5426/195.6	Olympic Dam dolerite	Gairdner Dyke Swarm		√		
OD78	Olympic Dam	RD2773/1255.2	Olympic Dam dolerite	Gairdner Dyke Swarm		√		
OD3-2	Olympic Dam	RU39-5426/211.4	Olympic Dam dolerite	Gairdner Dyke Swarm		√		
OD112	Olympic Dam	RD271/649.2	Olympic Dam dolerite	Gairdner Dyke Swarm		√		
OD76	Olympic Dam	RD2773/1244.5	Olympic Dam dolerite	Gairdner Dyke Swarm		√		
OD116	Olympic Dam	RD271/652.7	Olympic Dam dolerite	Gairdner Dyke Swarm		√		
OD75	Olympic Dam	RD2773/1241.9	Olympic Dam dolerite	Gairdner Dyke Swarm		√		
OD114	Olympic Dam	RD271/650.5	Olympic Dam dolerite	Gairdner Dyke Swarm		√		
OD942	Olympic Dam	RU65-8333/517.7	Olympic Dam dolerite	Gairdner Dyke Swarm		√		
OD119	Olympic Dam	RD271/688.5	Olympic Dam dolerite	Gairdner Dyke Swarm		√		
OD198-2	Olympic Dam	RD2773/1264.7	Olympic Dam dolerite	Gairdner Dyke Swarm		√		Pb
OD120	Olympic Dam	RD271/725.4	Olympic Dam dolerite	Gairdner Dyke Swarm		√		
OD198-1	Olympic Dam	RD2773/1264.7	Olympic Dam dolerite	Gairdner Dyke Swarm		√		Pb
OD3-1	Olympic Dam	RU39-5426/211.4	Olympic Dam dolerite	Gairdner Dyke Swarm		√		
OD81-1	Olympic Dam	RD2773/1325.4	Olympic Dam dolerite	Gairdner Dyke Swarm		√		
OD83	Olympic Dam	RD2773/1333.2	Olympic Dam dolerite	Gairdner Dyke Swarm		√		
RX7913	Olympic Dam	RD2929/401.3	mafic dyke	Mafic GRV	√		Ap-U/Pb	
OD394	Wirrda Well	WRD33/1119.9	olivine-phyric basalt	Mafic GRV	√		Ap-U/Pb	
OD893	Wirrda Well	WRD33/1202.9	olivine-phyric basalt	Mafic GRV	√		Ap-U/Pb	
OD891	Wirrda Well	WRD33/1121.7	olivine-phyric basalt	Mafic GRV	√		Ap-U/Pb	
OD1064	Olympic Dam	RD222/781.5	Olympic Dam dolerite	Gairdner Dyke Swarm	√			
RX3653	Olympic Dam	underground	olivine-phyric basalt	Mafic GRV	√			
RX3656	Olympic Dam	underground	olivine-phyric basalt	Mafic GRV	√			
RX2229	Olympic Dam	RU3-739/60.5	olivine-phyric basalt	Mafic GRV	√			

RX3650	Olympic Dam	underground	olivine-phyric basalt	Mafic GRV	√
RX7919	Olympic Dam	RD2346/470.4	mafic dyke	Mafic GRV	√
RX7920	Olympic Dam	RD1914/452.5	mafic dyke	Mafic GRV	√
RX7922	Olympic Dam	RD1914/476	mafic dyke	Mafic GRV	√
RX7914	Olympic Dam	RD2929/411	mafic dyke	Mafic GRV	√
OD954	Olympic Dam	RU65-8337/546.3	Olympic Dam dolerite	Gairdner Dyke Swarm	√
OD950	Olympic Dam	RU65-8337/504.9	Olympic Dam dolerite	Gairdner Dyke Swarm	√
OD948	Olympic Dam	RU65-8337/495.6	Olympic Dam dolerite	Gairdner Dyke Swarm	√

WR Comp., whole-rock composition; Ap, Apatite; Tit, titanite